DEFENCE ACADEMY
OF THE UNITED KINGDOM

Cranfield UNIVERSITY

Defence College of Management and Technology

Power and Energy Management of Multiple Energy Storage Systems in Electric Vehicles

PhD Thesis

Leon C Rosario

June 2007

Department of Aerospace
Power & Sensors
Cranfield University, DCMT Shrivenham
Swindon, Wiltshire, SN6 8LA, United Kingdom

DEFENCE ACADEMY
OF THE UNITED KINGDOM
Cranfield UNIVERSITY
Defence College of Management and Technology

Power and Energy Management of Multiple Energy Storage Systems in Electric Vehicles

A dissertation by

LEON CHRISTOPHER ROSARIO

Submitted in partial fulfilment of the requirements
for the degree of

DOCTOR OF PHILOSOPHY

in

Electrical Engineering

Supervisor: Dr. Patrick Chi Kwong Luk

THESIS COMMITTEE

Dr. Patrick C. K. Luk
Dr. John T. Economou
Prof. Brian A. White

Department of Aerospace Power & Sensors
Cranfield University, DCMT Shrivenham
Swindon, Wiltshire, SN6 8LA, United Kingdom

Acknowledgements

This journey would not have been as interesting without the fascinating people I met along the way. I would first and foremost like to thank my supervisor, Dr. Patrick Luk for the opportunity to carry out this research project. I am indeed fortunate to have had him as my undergraduate lecturer and project supervisor many years ago and then the privilege of his insightful supervision for this work. The trust, support and 'the freedom to create' that he has provided throughout the project is very much appreciated. It is often said that in life, you will come across very few people that will take a chance on you and give you an opportunity to change your direction in life. Dr. Luk has taken such a chance, and I thank him for this.

A special thank you goes out to Dr. John Economou for the many brainstorming sessions as well as the leisurely chats we had. I am most grateful for the encouragement and support he gave me in writing my first conference paper. The subsequent intimidating experience of presenting that paper for a large military audience was somewhat lessened knowing that Dr. Economou was also there to back me up if the audience decided to use me as 'target practice'. I wish to also thank Professor Brian White for his many insightful recommendations and his continuous support throughout my research.

My sincere appreciation for the tremendous support provided by Cranfield University's technical staff. A special thanks to Barry Grey, Chris Ransom, Colin Offer, Stuart Carter, Stacey Paget, Barry Luffman, Alan Norris, Chris Bland, Tony Low and all workshop staff. Thanks to you folks, everything I build from now on has to be of a 'proper-job' calibre.

The postgraduate centre would not have been the same without Mr. John Reynolds to keep us all sane. I will certainly have fond memories of 'wind-up Wednesdays'. And where would we be without fellow student Michael Gibson to rescue us when our computers crash. It was also a pleasure to make the acquaintance of all the other research students at Heaviside Labs.

My heartfelt appreciation goes out to my parents, parents in-law, my two brothers, sister in-laws and my nephews, Jason and Kevin. A special thank you to my Mum for allowing me to experiment with electricity as a little boy even though she would have preferred if I had expressed an ounce of interest in biology, and to my Dad for fuelling my interest to understand how things work and for teaching me the art of transforming imagination into something real. I am an extension of both of them, and proud of it.

As an expression of my faith and appreciation of everything in my life,

El shaddai, El shaddai,
El-elyon na adonia
Erkamka na adonai

Finally,
To my loving wife Vanessa, for tolerating my eccentric ways the past three years, and for agreeing to stand by me till the end of time…

ABSTRACT

This dissertation contributes to the problem description of managing power and energy of multiple energy sources for electric vehicle power system architectures. The area of power and energy management in the application domain of electric vehicles is relatively new and encompasses several different disciplines. Primarily, the challenges in electric vehicles having multiple energy storage systems lies in managing the energy expenditure, determining the proportional power splits and establishing methods to interface between the energy systems so as to meet the demands of the vehicle propulsion and auxiliary load requirements.

In this work, an attempt has been made to provide a new perspective to the problem description of electric vehicle power and energy management. The overall approach to the problem borrows from the basic principles found in conventional management methodology. The analogy between well-known hierarchical management concepts and power and energy management under timing constraints in a general task-graph is exploited to form a well-defined modular power and energy management implementation structure. The proposed methodology permits this multidisciplinary problem to be approached systematically. The thesis introduces a modular power and energy management system (M-PEMS). Operation of the M-PEMS is structured as tri-level hierarchical process shells. An Energy Management Shell (EMS) handles the long-term decisions of energy usage in relation to the longitudinal dynamics of the vehicle while processes within a Power Management Shell (PMS) handles the fast decisions to determine power split ratios between multiple energy sources. Finally, a Power Electronics Shell (PES) encompasses the essential power interfacing circuitry as well as the generation of low-level switching functions.

This novel framework is demonstrated with the implementation of a power and energy management system for a dual-source electric vehicle powered by lead acid batteries and ultracapacitors. A series of macro simulations of the energy systems validated against practical tests were performed to establish salient operating parameters. These parameters were then applied to the M-PEMS design of a demonstrator vehicle to determine both the general effectiveness of a power and energy management scheme and to support the validity of the new framework. Implementation of the modular blocks that composes the entire system architecture is described with emphasis given to the power electronics shell infrastructure design. The modular structure approach is design-implementation oriented, with the objective of contributing towards a more unified description of the electric vehicle power and energy management problem.

Nomenclature

Notation	Description	Unit	
Ibatt	Battey current	ampere	[A]
Iuc	Ultracapacitor current	ampere	[A]
Iload	Load current	ampere	[A]
Ibattref	Battery reference current	ampere	[A]
Iucref	Ultracapacitor reference current	ampere	[A]
Vbatt	Battery voltage	volt	[V]
Vuc	Ultracapacitor volatge	volt	[V]
VDC	DC bus voltage	volt	[V]
Vbattref	Battery reference voltage	volt	[V]
Vucref	Ultracapacitor reference voltage	volt	[V]
Vbusref	DC bus reference voltage	volt	[V]
PLoad	Load power	watt	[W]
Pbatt	Battery power	watt	[W]
Puc	Ultracapacitor power	watt	[W]
Pbattmax	Maximum Battery discharge power	watt	[W]
Pbattmin	Maximum Battery charge power	watt	[W]
Pucmax	Maximum Ultracapacitor discharge power	watt	[W]
Pucmin	Maximum Ultracapacitor charge power	watt	[W]
Pavg	Average load power	watt	[W]
Pucchg	UC reference charging power	watt	[W]
Lbatt	Battey converter inductor	henry	[H]
Luc	Ultracapacitor converter inductor	henry	[H]
Cbatt	Battery parallel input capacitance	farad	[F]
Cuc	Ultracapacitor parallel input capacitance	farad	[F]
CDC	DC bus capacitance	farad	[F]
Voc	Open circuit voltage	volt	[V]
Ah	Ampere hour	amphour	[Ah]
η	Efficiency	-	[%]
fsw	Switching frequency	hertz	[Hz]
Gpbatt	Battery positive slew coefficient	watt/second	[W/s]
Gnbatt	Battery negative slew coefficient	watt/second	[W/s]
SoCbatt	Battery State of Charge	-	
SoCuc	Ultracapacitor State of Charge	-	
D	Duty cycle	-	

Notation	Description	Unit	
FTR	Tractive force	newton	[N]
Fla	Linear acceleration force	newton	[N]
FgxT	Gravitational force	newton	[N]
Froll	Rolling resistance force	newton	[N]
FAD	Aerodynamic Drag Force	newton	[N]
AF	Vehicle equivalent frontal area	square metre	[m^2]
β	Vehicle inclination angle	radians	[rad]
g	Gravitational acceleration constant	square metre	[m^2]
m	Mass	kilogram	[kg]
ρ	Air density	kilogram per cubic metre	[kg/m^3]
CD	Aerodynamic drag	-	
C0 ,C1	Rolling resistance coefficients	-	
E	Energy	watt hour (Joule)	[Wh] or [J]
P	Power	watt	[W]
I	Current	ampere	[A]
V	Voltage	volt	[V]
Vs	Vehicle speed	metre per second	[ms^{-1}]
t	Time	second	[s]
Euc	Ultracapacitor energy	joule	[J]
Ebatt	Battery energy	joule	[J]
Ekin	Vehicle kinetic energy	joule	[J]
k	Time step	-	
i	Index	-	
n	Index	-	

Abbreviations

Batt (batt)	Battery
DoD	Depth of Discharge
EMS	Energy Management Shell
EPR	Equivalent Parallel Resistance
ESR	Equivalent Series Resistance
EV	Electric Vehicle
HEV	Hybrid Electric Vehicle
KVL	Kirchoff's Voltage Law
LSB	Least Significant Bit
MOSFET	Metal Oxide Field Effect Transistor
M-PEMS	Modular Power and Energy Management Structure
MSB	Most Significant Bit
PES	Power Electronics Shell
PMS	Power Management Shell
PWM	Pulse Width Modulation
SLA	Sealed Lead Acid
SoC	State of Charge
SoD	State of Discharge
UC (uc)	Ultracapacitor
VHDL	Very high speed integrated circuit Hardware Description Language
VRLA	Valve Regulated Lead Acid

CONTENTS

List of Figures

List of Tables

CHAPTER 1

INTRODUCTION

"The reasonable man adapts himself to the world. The unreasonable one persists in trying to adapt the world to himself. Therefore, all progress depends on the unreasonable man" - ***George Bernard Shaw ,1856-1950.***

The primary design challenges in electric vehicles having multiple energy storage systems lies in managing the net energy expenditure, determining the proportional power split and establishing methods to interface between the energy systems so as to meet the demands of the vehicle propulsion and auxiliary load requirements. Combined usage of multiple energy storage systems in a synergistic arrangement permits key attributes of the individual systems to be exploited. However, to obtain high utilisation efficiencies, these energy storage systems require an intervention of their natural power sharing. As such, a power and energy management system is required to strategise and arbitrate power sharing between the multiple energy sources and the load. This thesis addresses the power and energy management problem in a systematic and holistic manner by adopting a new perspective approach and a functional implementation framework. To begin, this chapter provides an introduction to the applied research of power and energy management in electric vehicles.

1.1 Motivation

This research is motivated by the premise that electric vehicles represent an economical and technically feasibly option for future transportation systems. Environmental impacts, escalating prices of petroleum based fuels, emission restrictions and the depletion of natural resources provides compelling impetus towards the development of more eco-friendly solutions. In addition to sustaining EU policy objectives, as well as meeting the Kyoto obligations to reduce greenhouse gas emissions, innovations in electric vehicular technology contribute to the concept of sustainable development. A statement by Los Alamos Laboratories on alternative energy sources, accurately defines 'Sustainable Development' as, "meeting the needs of the present without compromising the ability of future generations to meet their own needs". This represents one of the greatest challenges of today, a challenge that calls for responsible development of technology. Meeting these challenges will require several areas of research to be investigated. One such area is advancements in electric vehicle technology.

Electric vehicles (EV)s have been in existence ever since the inception of the automobile [1]. However, in the early race for dominance, the internal combustion engine (ICE) quickly overtook the EV as the prime propulsion power system for road vehicles. Although the electric powertrain was superior in terms of performance and energy conversion efficiency, the restrictive factor remained the source of electrical energy. Battery powered vehicles simply could not match the high-energy density, abundant supply and logistical attributes of petroleum based propulsion [2]. Even with ICE energy conversion efficiency figures of below 20%, the energy density (Joules/kg) of petroleum far surpasses the energy density of any known battery technology. While economically recoverable petroleum deposits continue to diminish, the automobile population is ever increasing, causing cities to become congested with toxic hydrocarbons by-products. As a result, the ICE is increasingly becoming a target of environmental debates.

Assuming that personal transportation continues to be a vital link in the economic chain of modern societies, private automobile appears to be the system of choice. This would provide opportunities to rethink private transportation modes as we now see it. At present, after

more than a century since its introduction, and decades since it was forced into near oblivion, EVs have regained a strong global presence [3, 4]. Industry efforts, coupled with paradigm shifts in transportation perspectives provide substantial grounds for continuing EV research contributions. The viability of a purely electric vehicle as a future transportation solution is perhaps arguable. The single limitation of current EVs compared to an ICE-Hybrid EV is still the travel range. As a near future target, EVs will find definite niche applications where short commuting distances or predefined routes dictate the vehicles' range requirement [5].

Perhaps the EV or even the hybrid electric vehicle (HEV) is not the ultimate answer, it is surely not the optimum solution but rather an interim one. However, the very effort to diversify from the well-matured ICE based vehicles is a step forward towards sustainable development. Optimistically, several new ideas will spring from the collective efforts of many small but progressive research contributions.

1.2 The emerging area of Vehicle Power and Energy Management

As the future of electric and hybrid electric vehicles is evidently becoming promising [6, 7], significant research efforts worldwide have been directed towards improving propulsion systems and energy storage units [8]. In the course of vehicles becoming "More Electric" [9], with increasing number of onboard electrically powered subsystems for both commercial and military applications, the need to manage the vehicular power system is imperative.

Electrical loads for both traction and ancillary loads are expected to increase as the automotive power system architecture shifts towards a more silicon rich environment [10]. The complex demand profiles anticipated by these dynamic loads require accurate and optimised control of power flow and energy storage subsystems within the vehicle, thus presents a technical challenge and opportunity for vehicular power and energy management research.

In a broad sense, the term 'Electric Vehicle' can be identified with any vehicle with an electrical propulsion system. This should encompass land, sea and air vehicles but in fact it

has become generally accepted by both the scientific and industrial community that 'Electric Vehicles' are referenced exclusively to road vehicles unless otherwise specified. Under the term 'Electric Vehicle' (EV), subcategories exist. Hybrid Electric Vehicle (HEV), Fuel Cell Electric Vehicle (FCEV) and Battery Electric Vehicle (BEV) differ in specific design aspects but share the same core electrical technology. Apart from the abbreviations ZEV and ULEV, which refer to Zero Emission Vehicles and Ultra Low Emission Vehicles respectively, the prefixes to 'EV' identify the variations in the primary propulsion, primary energy storage units and drive train configurations.

In an EV, the energy resources are limited. However it is essential that the power requests from all loads be met. Conversely, with the limitation in energy systems, it is impractical and cost prohibitive to size a single energy storage unit to offer continuous power capacity many times higher than the average power demand, just to meet momentary peaks in power needs [11, 12]. For this reason, employing multiple onboard energy systems that are specialised for the various segments within a vehicular power demand bandwidth becomes a viable solution. The combination of energy storage devices with high-density specifications such as batteries with energy storage devices having high power density specifications such as ultracapacitors provides such a solution. The task of a power and energy management system then is to suitably coordinate the dynamics of the energy storage systems. This is to be done without compromising the vehicle target performance.

Energy storage systems on electric vehicles can be classified as either charge sustaining or charge depleting. The latter refers to a system with a declining state of charge (SoC) as the vehicle operates, thus limiting its operational range. In such systems, power and energy management is even more vital as it contributes to extending the operation range. In the context of this dissertation, the term Electric Vehicle (EV) shall refer to a land vehicle with at least one charge depleting energy storage unit and an electric propulsion system in a series drive train configuration. This baseline vehicle on which the research propositions will be built upon, forms the fundamental configuration of a purely electric vehicle. Where relative, references will be made to other types of vehicle systems applications to express the overlap in applicability. Figure 1.1 depicts the power train structure of a series EV.

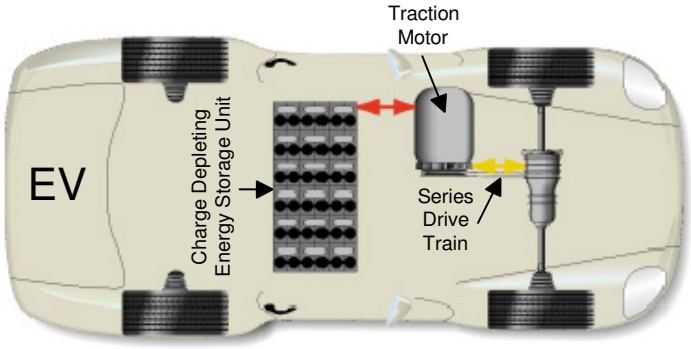

Figure 1.1 Electric Vehicle drive-train representation

1.3 Background on Electric Vehicles

The development process of the Electric Vehicle (EV) is interesting, as the first documented invention of an EV dates back to 1834 [1]. Due to the lack of technology, primarily for electrochemical storage units, the interest in EVs gradually diminished and ceased to receive any attention after 1920. In the early 1970s, circumstances changed in favour of the EV concept due to the dramatic increase in petroleum prices. Compelled by the Arab oil trade embargo of 1973, which resulted in an enormous energy crisis, exploration into alternate energy sources was initiated [3]. This eventually lead to the US Congress formation of the 'Electric and Hybrid Vehicle Research, Development and Demonstration Act' of 1976 (US Public Law 94-413) [2].

Since then, governments and research communities worldwide have embraced the importance of EV research. In 1997 for example, The United States Department of Energy and China's Ministry of Science and Technology signed a memorandum of understanding on electric vehicle research. Global transition towards eco-friendly vehicles will contribute to reduction in urban pollution caused by internal combustion engines (ICE) but the changeover will depend on the satisfactory performance of EVs. Although the ICE has significantly evolved over the years and toxic emissions of modern engines have greatly reduced, whenever there is an apparent fuel crisis, EV technology sees a renewed interest. Environmental awareness and energy concerns in the last decade have, for first time since the EV introduction, imposed a threat to ICE vehicles [3].

The reason for this new found interest in electric vehicles could be attributed to several causes. As stated, one reason is due to the increasing public awareness and media coverage of environmental issues. A technical reason for this increase of interest can be linked to the advent of new technology enablers such as efficient fuel cells, electrochemical double layer capacitors (EDLC) and high-speed composite flywheels. These devices contribute to a synergistic reintroduction of electric vehicle technology. For a long period, it was a widely excepted fact that electric vehicles were confined to limited applications due to the inherent power and energy density limits of battery technology. The advent of these enabling technologies has generated some new research activities that complement the resurrection of the EV.

From evidence of scientific and industrial efforts, government backing and present technology, EVs have a strong prospect of maintaining its presence this time around. However, the success rate in terms of public acceptance will primarily depend on two factors. Either the EVs' performance and cost will meet or beat the rival ICE vehicles or the depletion of natural resources will leave the public no other choice. Figure 1.2 shows an early version of an electric vehicle while Figure 1.3 highlights key historical events in the evolution of electric vehicle.

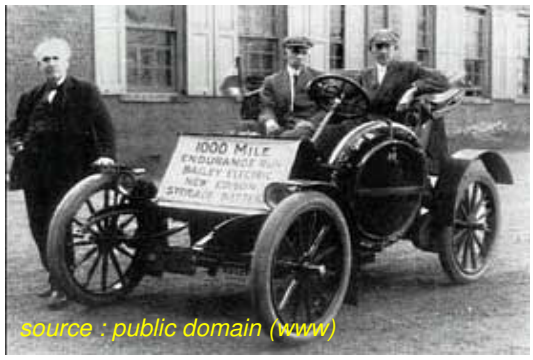

Figure 1.2 Thomas Edison with an early electric vehicle (Circa 1910)

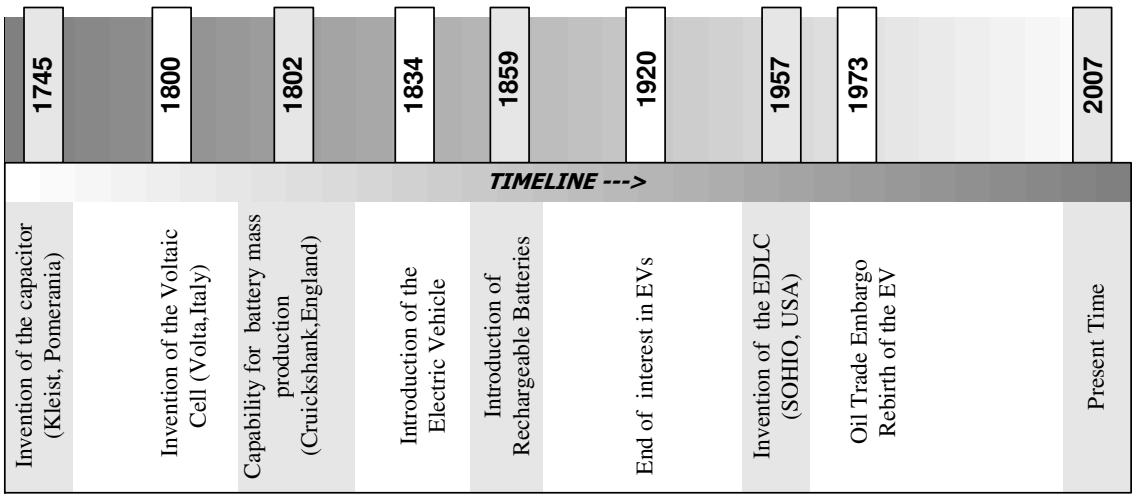

Figure 1.3 Key historical events in the evolution of EV technology

1.4 Research Rationale

Research efforts of this project is in line with specifications of the EU Joule III program, which stipulates the need of technical contributions in the area of vehicular energy storage technology, electrical management systems and energy management in electric vehicle drivelines [13]. The vehicular technology industry is currently going through a transition period with the introduction of multiple voltage systems to meet future electrical load requirements. As such, research contributions towards this field are timely.

Efficiency of electric vehicle energy storage systems is a system-level issue. Every aspect of the system has an impact on the energy efficiency, and the impact of a given subsystem is usually dependent on its interactions with other subsystems. The objective of a strategic power and energy management system for a charge depleting energy source (battery/ultracapacitor) powered electric vehicle is to meet the performance expectations of the vehicle operator and to maximise the overall system efficiency while the charge levels of the energy sources are depleting. This energy source integration has to be done with an objective of minimising the total mass and cost of the vehicle.

Considerable work in energy management in the past has focused on addressing energy savings options for portable battery operated devices. 'Energy-aware' computing and power save operating modes have been extremely successful in these consumer devices. It would appear that power management in electric vehicle technology is merely a scaled up implementation of the techniques used in managing power in these devices. However, directly relating vehicle power and energy management to portable consumer devices may not be entirely accurate as the primary and sometimes the only objective in portable systems is to maintain a high battery state of charge for as long as possible. This could be accomplished by basically turning off subsystems after a preset timeout. In the context of an electric vehicular application, the power and energy management issue encompasses more than just sustaining the energy levels. It includes the coordination of subsystem power flow, managing multiple energy storage devices and also ensuring power quality and stability is met.

An important feature of electric vehicles is the ability to recuperate energy during regenerative braking. This fundamentally differentiates the power and energy management requirement of an EV to other mobile battery powered equipment. Harnessing regenerative energy and transferring the energy back into the onboard storage systems is a demanding task. High power flows during rapid decelerations calls for the energy storage system to be receptive to the charging currents. Conversely, during accelerations, high power is demanded from the energy source. However, the chemical properties of batteries do not permit rapid charging or discharging without severe thermal rise, which eventually leads to premature failures. To mitigate battery high power stresses, an intermediate power buffer or peak power buffer is required. With today's technology, the 'Ultracapacitor' is a contending electrical peak power device. The challenge now is the hybridisation of batteries and ultracapacitors within the electric vehicle power systems architecture. To what extent the integration of these two energy storage systems can be exploited is of considerable research interest.

Owing to this requirement of a multiple energy sources, power and energy management of electric vehicles presents an even more challenging task. It requires the development of a higher-level control scheme that determines the proportional amount of power to be

generated, and split between the two sources. Predominately, how these sources are configured electrically within the vehicle power system and how the power flow and energy systems are coordinated is a power electronics intensive problem requiring a systems level supervisory control scheme [14].

Design methods for electric vehicle power systems management incorporating the use of batteries and ultracapacitors in synergistic operations are not well established. However, an increasing community of avid researchers are actively working towards the goal of achieving baseline concepts for vehicular power system architecture. Areas that are currently drawing focus are:

- Sizing of onboard charge sustaining and depleting energy storage units
- Regenerative energy recuperation.
- Peak power alleviation using ultracapacitors.
- Power blending of two or more energy sources of different power/energy specifications

1.5 Problem Scope

In the scope of this project, the specification of a Power and Energy Management for a dual energy system consisting of batteries as the primary 'energy' source and ultracapacitors as the primary 'power' source is as follows;

- The technique of power arbitration between batteries and ultracapacitors
- The power blending infrastructure for the battery- ultracapacitor system
- The energy management of the energy storage systems
- The assessment of regenerative energy receptivity
- The presentation and correlation of theoretical and empirical findings

The driveline architecture that will be investigated comprises of the two energy storage systems categorised as Type 1 and Type 2. As depicted in Figure 1.4, the scope of the power

and energy management problem encompasses the energy systems as well as the conversion and distribution of power. The vehicle load demand that is analysed in this dissertation is limited to the propulsion loads. Although the non-propulsion load demands have been investigated as part of this research project, the core of the work presented here will focus on addressing the system encapsulated as power and energy management.

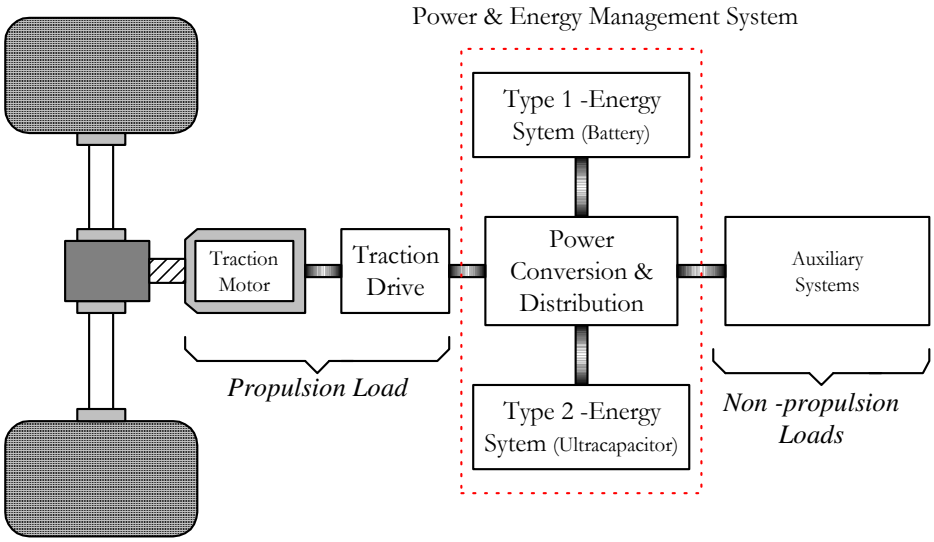

Figure 1.4 EV drive train and power system architecture

1.6 Methodology

An important aspect of this work that has a direct impact on the research methodology is the choice of the system under investigation. In order to gain and contribute implementation insights to the problem of managing power and energy in a vehicular environment, a pragmatic approach in this applied research project is adopted. The research begins from the general proposition of augmenting the main energy system of a vehicle with a high power capability power buffer system. Having identified the intended energy system technology to investigate, the research proceeds in reviewing past and current techniques to coordinate the operation of multiple energy systems in vehicle power system architectures.

In the past, many research works were targeted at overly ideal systems to theoretically demonstrate the general concept of power and energy management. Although detailed models have also been considered, the majority of previous work in this area involves non-causal approaches to achieve some closed-form analytical solution. Complete implementation and systematic procedures are rarely considered. The identification of this limitation in present literature leads to the investigation of more practical design methods. To form a structured systems level method that is able to encompass the complete implementation of a power and energy management system, general concepts and theory derived from traditional hierarchical management methodology are utilised. In addition, frameworks established from stochastic decision theory as well as intuitive reasoning of the general problem help create a structured modular process that presents a more systematic design methodology.

In this work, an attempt is made to include all relevant practical components and subsystems in order to produce results that are directly relevant to practical designs. It is expected that significant findings that are unattainable with purely theoretical approaches can be uncovered when practical systems are considered. To achieve this, a pure electric vehicle consisting of batteries as the main energy source and ultracapacitors as the peak power source is designed and constructed. The vehicle serves as a platform and experimental facility to demonstrate or even disprove the effectiveness of the hypothesized power and energy management implementation methodology. The hardware is developed based on the application requirements and constraints of the test vehicle and energy storage units.

The design process begins by identifying the physical and operating constraints of both battery and ultracapacitor technology. Subsequently, subsystem models and baseline design parameters are obtained through iterative simulations, experimental verifications and reference to literature. As the modelling platform, the Advanced Vehicle Simulator (ADVISOR) systems level simulation tool and the SIMPLORER simulation package are used extensively. Fuzzy logic theory is employed to implement the heuristic reasoning of energy management.

The research into power and energy management of hybrid battery-ultracapacitor energy storage systems is a challenge because both storage technologies are of different physical, electrical, and chemical characteristics resulting in very different power, energy, voltage and current characteristics. The interactions between these energy systems are not immediately obvious without reasonable exploration of both technologies and performing some empirical verification. This involves adopting a holistic research strategy, embracing all subsystems of an EV rather than narrowly focusing on specific frameworks adopted by other research work in this field. The approach provides a comprehensive perspective and adds value to this applied research topic. Figure 1.5 diagrammatically illustrates the research framework.

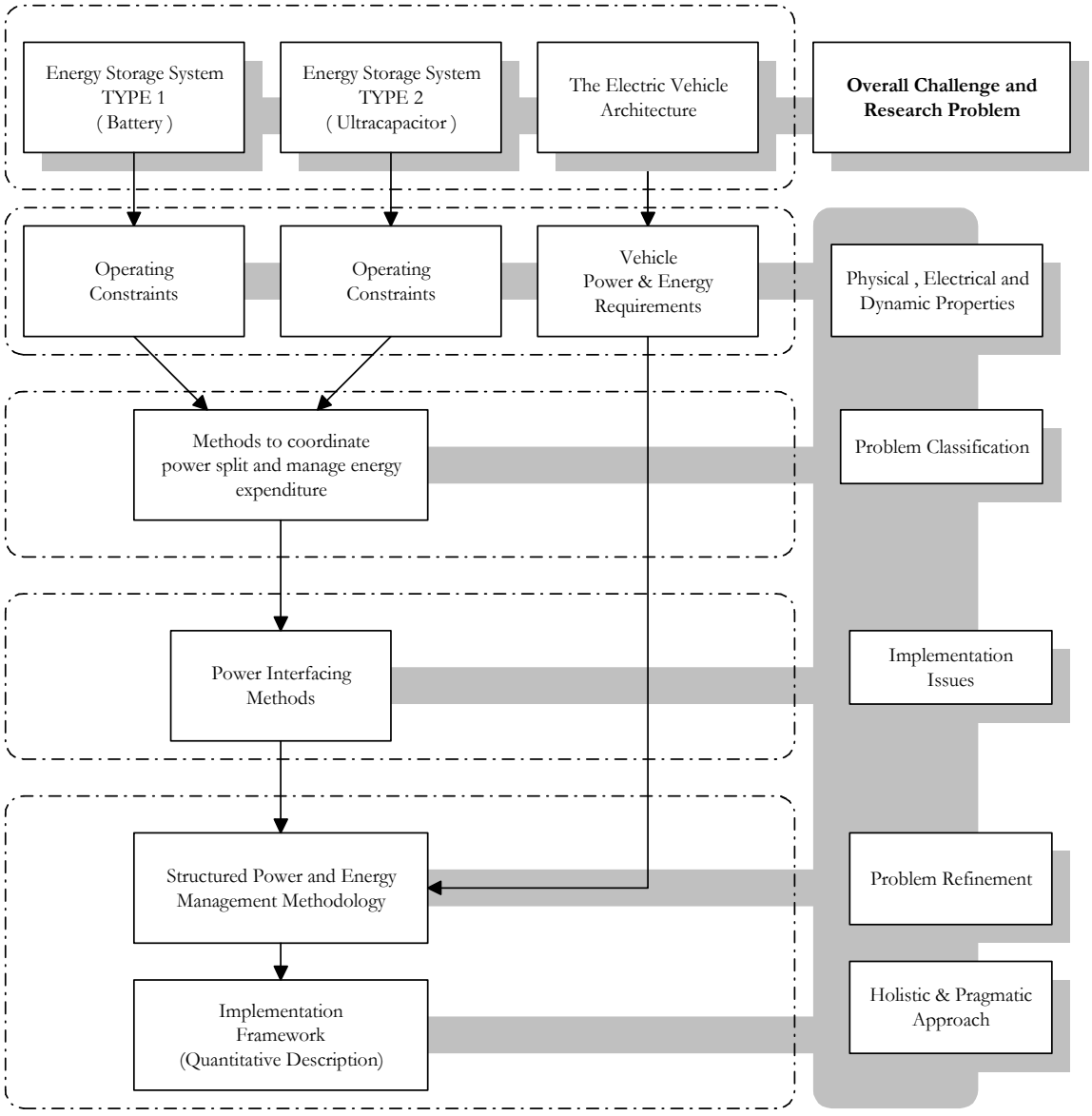

Figure 1.5 Research methodology

1.7 Contributions

This thesis deals with the concept, design and implementation a vehicular power and energy management system applicable to classes of electric vehicles that employ multiple energy storage units. In particular, the dissertation addresses the hybridisation of batteries and ultracapacitors as the reference vehicle model. The majority of published work mainly focus on offline computation and non-causal methods to obtain the reference power split trajectories of multiple energy systems. Minor considerations are generally given to the practical applicability and implementation methodology of power and energy management as a total working system. The majority of the previous works are limited to either obtaining optimum power split trajectories over a predefined load-mission profile or addressing the energy storage technology itself. As a result, the contradicting objectives that arise when power management, energy management, energy storage units and the associated power electronics infrastructure that facilitates the systems integration are often not addressed. As a total systems approach, this work contributes to describing and integrating the key processes involved in electric vehicle power and energy management.

As a novel approach, this work presents a modular concept in the design and implementation of a power and energy management system (PEMS) for Electric Vehicles (EV). The model EV developed for this work is powered by dual energy sources, consisting of batteries and ultracapacitors. Operation of the PEMS has been structured into modular hierarchical process shells. The Energy Management Shell (EMS) handles the longer-term decisions of energy usage in relation to the longitudinal dynamics of the vehicle. The process within the Power Management Shell (PMS) however handles the fast decisions to generate power split ratios between the batteries and ultracapacitors. Finally the Power Electronics Shell (PES) handles the ultra fast switching functions that facilitate the active power sharing between the two sources. The modular structure approach is design-implementation oriented, with the objective of contributing towards completeness of the EV power and energy management problem description.

The key contributions as a result of this work can be summarised as follows;

1. The work presents a fresh perspective to this research arena by introducing a novel approach that provides a method of decomposing the power and energy management problem into a modular structure with three distinct hierarchical processes.

2. It presents a clearly defined modular process and infrastructure in the form of structured building blocks for development, investigation and on-line optimisation of vehicular power and energy management systems.

3. The methods of determining power-split ratios are made using only measurement of power fluctuations at the DC-Bus rather than the conventional methods of monitoring the throttle input (driver input). This leads to the ability of including propulsion as well as non-propulsion loads in the implementation framework.

4. The thesis presents a formulation of the power management process based on sequential decision processes and the understanding of physical constraints of the energy storage technology.

5. This study identifies the overall system requirements and considers the power electronics constraints in order to implement and achieve the objectives of a power and energy management system. In addition to describing the requirements for active source sharing, the findings in the work identify designs that favour and designs that impede power sharing.

6. This work will clarify some of the specification of a relatively new energy storage device called ultracapacitors. In general literature it is common to find ultracapacitors specified as capable of being fully discharged at very high power levels. Although possible, the practicalities of doing so can be counter- productive in terms of energy efficiency. The reason for this is demonstrated.

7. As the hybridisation of multiple electric power sources requires an interfacing mechanism, a design philosophy of a power electronics interface architecture and the associated component-sizing methodology is presented in this work. The systematic approach and numerical design description of a purpose built test vehicle, provides a technical insight for researchers seeking information on experimental setup procedures. A variation in the standard form of designing the power electronics converter is presented in order to accommodate the process shell architecture concept.

8. The experimental effort carried out in this work provides experimental verification that ultracapacitors are more receptive to regenerative power compared to batteries specifically in the electric vehicle application domain.

1.8 Thesis Outline

Chapter 2 begins with a review of power and energy considerations in the context of electric vehicles. The trends in research activities in the context of publications in the area of electric vehicles are given as a chronological overview. The methods and propositions made by active researchers are investigated to gain an understanding of arising problems. This follows with a review of a specific technology-enabling device that has given the EV a significant boost in achieving its performance milestone. Various techniques that have been used to address the fundamental issue of managing vehicular power and energy are revisited to substantiate the above research rationale statements.

Chapter 3 discusses modelling and applications of the energy storage systems selected for this work. The chapter provides a theoretical background on batteries and ultracapacitors as well as the modelling of these energy systems for EV system studies. Focusing on the specifics of power delivery, usable energy content and the operating constraints of the two systems, the parameters required for a strategic power and energy management framework are presented. Simulations of the models developed are presented as a case to justify the hybridisation of batteries with ultracapacitors.

Chapter 4 presents the approach to analyse the power and energy requirements of a land based electric vehicle. Using fundamental vehicle kinematics equations and VHDL models of the energy systems, the development of an electric vehicle simulation model is presented. Following this, a case study is presented to accentuate the prospect of arbitrating the power delivery of battery and ultracapacitors for a set of mission profiles.

Chapter 5 introduces and describes a novel perspective of addressing power and energy management. The chapter begins by correlating standard management philosophy to the problem of managing power and energy. Subsequently, a decomposition of the problem into a structured and modular framework is presented. The framework is then demonstrated in the complete design of a power and energy management system for a dual source electric vehicle powered by lead acid batteries and ultracapacitors. An exemplification of the modular concept is discussed with simulation results.

Chapter 6 provides the hardware description of the experimental vehicle developed as the test platform and implementation framework.

Chapter 7 details the power electronics interface that facilitates the combination of power from multiple energy sources. The sizing methodology described in this chapter includes the actual design parameters used to develop a functional system. This serves as a design guide for researchers seeking technical information to carry out similar experimental work.

Chapter 8 contains procedures and results of experimental work. Validation of the energy system models as well as the vehicle model is presented here. Each experiment follows a standard format describing the purpose, procedure, results and discussion of the experiment.

Chapter 9 concludes this dissertation with a general summary of the contributions and offers some remarks and suggestions on the way forward. Key areas that require further investigations are also presented in this chapter.

The Appendix section provides detailed schematics, type-test and images of the experimental setup developed for this work.

1.9 Publications

The following papers have been published and presented at international conferences as progressive contributions of this research work. The publications are listed in chronological order of submission. Paper 1 presented a framework of managing pulse power requirements in tactical mission scenarios. The paper describes a concept of an adaptive ultracapacitor switching network as an intermediate energy storage system framework for an intelligent power and energy management system intended for vessel electrical power system designs.

Paper 2 extended the concept of switching ultracapacitors described in Paper 1 to the application domain of electric vehicles. With the aim of increasing the usable energy obtainable from the ultracapacitors, sequential switching of the ultracapacitor topology was investigated. Through parameter extraction, simulations demonstrated that peak power requests from vehicle propulsion loads could be mitigated from the battery to a bank of ultracapacitors.

Papers 3 and 4 discussed the non-propulsion load demands of electric and more-electric vehicles. Paper 3 suggested the non-propulsion loads be classified as Agents within the vehicle power distribution system and Paper 4 extended this idea into a negotiation framework of limited power resource allocation.

Paper 5 presented the demonstrator vehicle developed for the experimental part of this research project. A comparison between simulation and experimental data of the vehicle battery system was presented in this paper.

Paper 6 presented the concept and methodology of a modular power and energy management structure, while paper 7 extended this to implementation requirements.

Publications

1. *L.C. Rosario ,J T Economou, P C K Luk, T S El-Hasan,* '**Scenario Driven Intelligent Pulsed Power Management**', IEE- IMAREST 'Engine as a Weapon' Symposium, June 2004. Bristol, United Kingdom.

2. *L.C. Rosario, J.T Economou, P.C.K Luk,* '**Short Interval Supercapacitor Switching Networks for Electric Vehicles: A Parametric Approach'**, IEEE International Vehicular Power and Propulsion Conference - VPP 2004, October 2004. Paris, France.

3. *L.C. Rosario, J.T Economou, P.C.K Luk,* '**Multi-Agent Load Power Segregation for Electric Vehicles**', IEEE International Vehicular Power and Propulsion Conference - VPP 2005, September 2005. Illinois, USA.

4. *P.C.K Luk, L.C Rosario,* '**Towards a Negotiation-based Multi-Agent Power Management System for Electric Vehicles'**, IEEE International Conference on Machine Learning and Cybernetics, ICMLC 2005. August 2005. Guangzhou, China. (Invited Paper)

5. *L.C. Rosario, P.C.K Luk,* '**Power and Energy Management Policy Implementation of a Dual Energy Source Electric Vehicle'**, 3rd IEE International Conference – Power Electronics, Machines and Drives- PEMD 2006, April 2006. Dublin, Ireland.

6. *L.C. Rosario, P.C.K. Luk, J.T. Economou, B.A. White,* **'A Modular Power and Energy Management Structure for Dual-Energy Source Electric Vehicles'**, IEEE International Vehicular Power and Propulsion Conference - VPPC 2006, September 2006. Windsor, United Kingdom.

7. *L.C Rosario, P.C.K. Luk,* **'Implementation of a Modular Power and Energy Management Structure for Battery – Ultracapacitor Powered Electric Vehicles'**, IET Hybrid Vehicle Conference - Premium Automotive Research Programme (PARD), December 2006. Warwick, United Kingdom.

CHAPTER 2

LITERATURE REVIEW

" Many precede and many will follow " – ***anonymous***

In this chapter, a broad literature survey on electric vehicle research is first presented followed by a review on the specific topic of vehicular power and energy management. Subsequently, an introduction of an upcoming electric vehicle enabling technology, identified as the 'ultracapacitor' is presented. Ultracapacitor technology and ongoing research efforts in ultracapacitor hybridisation methods are then examined. Focusing on the prospects of augmenting battery system with ultracapacitor technology in electric vehicle power system architectures, the survey then directs emphasis to literature on hybridised systems having at least one component of its energy storage arrangement consisting of ultracapacitors. Power management, energy management as well as the power electronic interfacing issues involved in a battery-ultracapacitor system are discussed to draw attention to the research objectives and challenges of this work.

2.1 Overview

Published works on electric vehicle engineering dates back to the late 1970s, coinciding with the energy crises of that period. Since then, electric vehicles were considered the domain of automotive and mechanical engineers and hence not a popular topic of research for electrical engineers until the middle of the 1990s. The long held perception of electrical vehicles as simply vehicles with an electric propulsion system in replacement of an internal combustion engine has progressively changed. As depicted in the histogram of Figure 2.1, the last decade has shown an increase in publications by the electrical engineering community in this area of research. Although the figures for year 2006 would be incomplete at this time, it does however show that electric vehicles and the associated issue of managing power and energy is in fact gaining research interests.

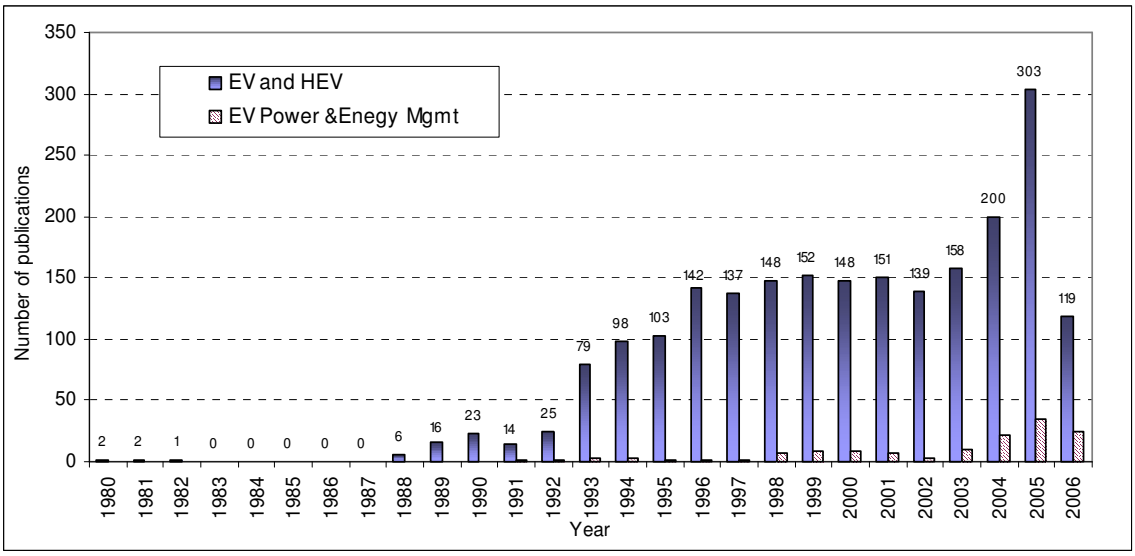

Figure 2.1 IET / IEEE Publications on Electric Vehicles - Extracted from IEEE Xplorer

(Search criteria included Electric and Hybrid Electric Vehicles)

Electric vehicles are now being classed as a new category of electrical equipment with unique features [4]. As such, there are various opportunities for research and development contributions in the scope of electrical engineering as there is a still some fluidity in industrial standards [15, 16]. Power and energy management of energy storage systems within the vehicle is one such area of growing interest. As shown in the histogram above, evident work

in the area or power and energy management only began in the late 1990's. Much of the work reported in the past has focused on the fundamental study of dividing power between multiple energy storage devices. The electric vehicle power and energy management problem has had a range of definitions. It has been described from the point of view as a purely mathematical optimisation problem to an electrical design, configuration and component problem. Consensus of opinions in recent reports indicates that it is a problem that is best approached at a systems level [17, 18]. The following section introduces the basis of having multiple energy storage systems in an EV. Subsequently, a summary of work conducted by research groups in the area of vehicular power and energy management as well as electric vehicle enabling technology is presented.

2.2 Multiple Energy Storage Systems in an EV

Combining multiple energy storage systems permits the main attributes of each source to be more efficiently utilised. Fundamentally this involves combining energy systems having high-energy capacity with systems having high power delivery capabilities. In general, energy storage systems capable of delivering continuous power with minimum reduction in their lifespan have greater energy storage capabilities when compared to the pulse power delivering devices. A combinational usage of these energy storage systems in a synergistic configuration exploits the effective use of power whenever necessary whilst maximising the storage devices operational lifespan. Energy storages systems can be further categorised according to their total energy storage capacity, energy density, and transient power deliverability, thus creating a multi-criteria selection depending upon the mission power demand profile.

In electric vehicles, rapid accelerations and decelerations require peak power to be delivered from and transferred to the energy storage system. For a battery sourced EV, augmenting the battery pack with a high power capacity system results in reduced high power stresses impressed on the battery [11]. A typical electric vehicle drive cycle requires short power burst to accelerate the vehicle. During rapid decelerations, kinetically produced energy via regenerative braking, generates currents of high magnitudes. As such, a peak power mitigation device is advantageous. Essentially, peak power can be generated and stored

electro-mechanically via a flywheel system, electro-chemically via capacitors or by other forms of peak power buffers. Having multiple energy storage systems in an EV necessitates a method to coordinate and arbitrate power sharing between the systems.

2.3 Power and Energy Management of Multiple Energy Storage Systems

The power split of different types of energy storage systems within an EV can be concisely described as follows. Considering the block diagram of Figure 2.2, the contribution of power to meet a particular load requirement is split between two energy storage types. W_1 and W_2 represent the weighing factors corresponding to the proportion of energy extracted from the two storage units. Due to the difference in Power to Energy ratios of Type 1 and Type 2 systems, a strategy to coordinate power flow by dynamically varying the weighting factors is required. For successful operation of the vehicle, the power availability must at least meet the power requirement. This has to be done with further consideration to the system constraints, for example the depletion level of the energy storage units. Figure 2.3 illustrates a typical power split of Type 1 and Type 2 Energy Storage Systems (ESS) to fulfil the load demands.

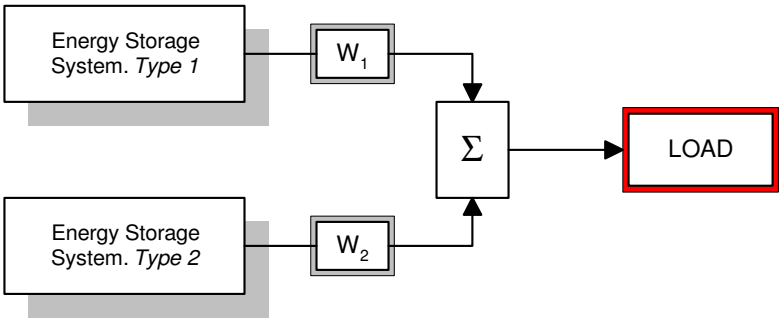

Figure 2.2 Power Split between two energy sources

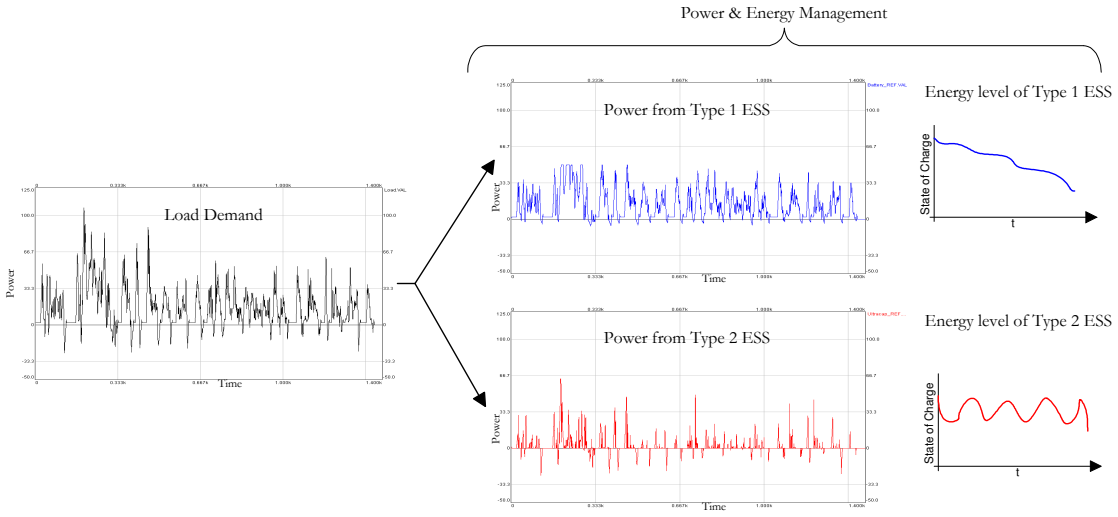

Figure 2.3 Power split and energy expenditure between two energy sources

This vexing issue of controlling the power flow of two or more sources has been addressed through various approaches. Jalil, Kher and Salman [19] suggested a rule-based framework for power split between a battery pack and an internal combustion engine. The proposed strategy ensured that both power sources operate at maximum efficiency whenever possible. The concept demonstrated an increase in efficiency in terms of fuel economy. Recognising that the battery energy expenditure as well as the system power split requires a controlled intervention, Caratozzolo, Sera and Riera [20] also suggested an energy management strategy derived from a heuristically composed rule-base. Due to the highly non-linear nature of EV and HEV drivelines, the authors suggested a rule-base approach to provide an employable scheme for arbitration of power flow under various operating modes of the vehicle.

Steinmauer and Del Rel [21] stated that techniques that use a fixed controller structure and then searches for optimal parameters to minimise a cost function yields only a solution that is a consequence of the selected structure. They proposed to tackle the dual source power split problem in terms of optimal control using statistical data of vehicle power demands for known drive cycles. Their procedure addressed the problem by deriving optimal solutions for a fixed set point, which was then extrapolated to various power demand profiles. The authors demonstrated optimal power split between a battery and generator. The analysis

showed that the battery State of Charge (SoC) at the beginning of the drive cycle equalled the SoC at the end of the cycle. However, the negative effects of rapid deep charge and discharge cycles imposed on the batteries were not considered.

According to Langari and Won [22], optimal control methods, due to its dependency on the drive cycles used to generate the control actions may not yield optimal power split for misclassified or arbitrary drive cycles. As an alternative, they proposed a concept of a fuzzy logic (FL) based energy management to capture driving situational awareness. Details of their study can be found in Won's Ph.D dissertation [23]. Similarly, Hellgren and Jonasson [24] conducted a comparison of a fuzzy logic approach and an analytical formula for a hybrid powertrain. Their findings showed that the FL method proved more flexible but required three times as many design variables.

The DC-Link voltage control method suggested by Lohner and Evers [25] uses a voltage reference as the power management control parameter. Given that multiple power delivery systems share a common DC-link in the vehicle power system architecture, the principle behind this method is to regulate the DC link voltage within a tolerance band around a set point reference voltage. Using band pass filters and proportional-integral (PI-type) loops to control the current drawn and delivered to several energy storage systems, the authors showed that the DC-link voltage control method limits the DC-link voltage dips that occur during vehicle acceleration and the voltage rises that occur during decelerations. In effect, the technique indirectly arbitrates the power sharing of several electrical power delivery systems.

West, Bingham and Schofield [26] introduced a Model Predictive Control (MPC) method to coordinate the power flow from two sources in a pure electric vehicle. Employing a constrained MPC with zone control, they demonstrated that the net energy expenditure of a battery bank in a battery-ultracapacitor system was significantly less compared to a DC-Link voltage control method. Also along the lines of predictive control, but for a HEV application, Salman, Chang and Chen [27] proposed a theoretical framework for a predictive energy management strategy. Although termed as 'predictive', the strategy still depends on

previewed information about the mission profile. However, the leaning energy management strategy [28], also by Chen and Salman, lends itself more of an implementable method.

Leading more towards the practical implementation of power split strategies, which require instantaneous management of power flow, Paganelli et al. [29] introduced a general supervisory control policy. Although the formulation of the policy was intended for charge-sustaining HEVs, the proposed power split algorithm is generic and may be adapted to pure electric vehicles with more than one energy storage type.

Moreno et al.[30] reported valuable experimental results for a test vehicle that incorporated optimal control methods with an artificial neutral network (ANN). The ANN was trained offline for a set of driving cycles followed by a series of field-testing. Compared to a fixed strategy to regulate the ultracapacitor SoC, the ANN strategy was reported to yield a 4.9% theoretical improvement in efficiency (km/kWh) when simulated and a 3.3% improvement during field-testing.

Also using ANNs, Papadimitropoulos et al. [31] evaluated their energy management concept on a test vehicle developed at the University of Patras. Their test vehicle, (the E-240) followed an energy management strategy to trace a maximum motor efficiency map regardless of the arbitrary driving patterns. The authors used a trained ANN to predict the battery state of charge and the motor temperature, which was then computed for maximum efficiency determination. In conclusion of their work, the authors commented that although energy economy of electric vehicles can be achieved by using more efficient energy storage systems, an energy management system could provide significant efficiency gains instead.

A strategy that uses knowledge of subsystem efficiency maps and then computes a reference power split following a minimisation function was proposed by Pisu and Rizzoni [32]. Based on a concept of Equivalent Consumption Minimization Strategy (ECMS), this generic strategy addresses the energy optimisation problem of multiple energy sources by replacing the global criteria of energy expenditure with a local criterion. The authors also drew attention to the fact that energy optimisation strategies that require priory information about the drive cycle cannot be readily implemented. The ECMS approach was also substantiated

by Guzzella and Sciarretta [18] for sub-optimal but implementable techniques due to the causal control nature of the method. In addition, the authors of [18] demonstrated that non-causal methods that strongly depend upon the precision of future power profile can lead to an energy management strategy that causes excessive deviation to energy storage system target state of charge.

Exploring several energy management strategies, Koot et at. [33] demonstrated that the general concept of energy management is warranted since even the most basic of strategies yields a reduction in net energy usage. For a fixed vehicle drive profile and subsystem architecture, the authors of [33] evaluated five energy management strategies. Since the outcome of their work also concurred that implementable strategies do not have the drive profile horizon as priory knowledge, they suggested a dynamic programming approach that uses a short horizon length rather than the complete driving cycle. Although dissimilar in implementation method, the strategy bares fundamental similarities to the ECMS proposed by Pisu and Rizzoni [32], which replaces a global criteria of energy expenditure with a local criterion.

Recognising the stochastic nature of the energy management problem, Lin, Peng and Grizzle [34] proposed a strategy using stochastic dynamic programming (SDP). Representing the vehicle power demand as transition probabilities over an unknown mission profile, the authors formulated the power split decision rules as a time-invariant infinite horizon SDP problem. Although the method was intended for a HEV application, the technique is transferable to EVs. The SDP technique was also examined by Min et.al [35]. Modelling the vehicle driver power demand as a Markov chain, the authors of [35] developed a strategy to split power delivery between a fuel cell and battery system. By constructing a transition probability function based on several driving scenarios, the SDP method was used to map the observed states to the control of power split decisions.

In a recent publication, Cacciatori et al.[36] provided a basic classification of energy management strategies. The authors categorised energy management strategies into two groups. Strategies that require a priori knowledge about the mission profile and those that have no or limited knowledge in that regard. For the first group, three approaches are

generally used. They are, optimal control theory, dynamic programming in which the control problem is recast into a multi criterion decision process and solved using Bellman's principal of optimality and a third approach that uses an optimal design technique. The second group of energy management strategies can be employed for real-time control. The general approaches used in this group are; heuristic rule-base control, fuzzy logic inference engines and cost-based suboptimal control. Similar to the ECMS for charge sustaining systems put forward by Pisu and Rizzoni [32] and also demonstrated Guzzella and Sciarretta [18], cost-based suboptimal techniques are based on representing the energy consumption as a cost function which is minimised in a very short period and can be implemented in real time controllers.

Miller et al.[37] suggested a method to determine power split ratios between batteries, ultracapacitors and ICE by means of power spectral decomposition and frequency banding. Using discrete wavelet transforms (DWT), the power splits are discerned simultaneously in time and frequency by utilising the DWT adaptive windowing characteristic. Decomposing the power spectrum into designated low, mid and high frequency bands correspondingly determine the power splits between the ICE, battery pack and ultracapacitors. A similar wavelet-based load sharing algorithm was later adopted by Uzunoglu and Alam [38] to determine the power split between fuel cells and ultracapacitors for a HEV application.

Gielniak and Shen [39] provided a very different perspective to the vehicular power management problem in suggesting a power split strategy based on game theory. Classifying the power sources and the load demands as game 'players', the authors explored the possibilities of adopting game theory to achieve high efficiency and performance payoffs, where the payoffs are represented by utility functions of each of the power sources. The general concept behind this approach is to assume that the energy systems are one set of players in a game and alters its strategy in order to place itself in a state that yields a high utility. The load demands, with its non-stationary fluctuating power demand and transients can be seen as the opposing player or the adversary in a two-player game.

Evidently there are various methods and approaches to manage multiple energy storage units in a vehicular propulsion system. Variations in approaches and methods provide interesting

insights to the problem description. As discussed, the problem is sometimes addressed solely as a 'power' management issue and sometimes as a topic of 'energy' management. Both problem descriptors are valid since energy is simply the time integral of power. However, when multiple energy storage systems that have very different specific power (kW/kg) to specific energy (kWh/kg) ratios and also different peak power handling capabilities are combined, the problem is best addressed jointly as power and energy management issue. The problem of designing a complete power and energy management system could be stated as a problem encompassing energy resource planning, power delivery and an effective architecture design for a real-time system

On a rather theoretical level, several researchers have developed energy management and power management techniques that apply priory information regarding the vehicle propulsion power demands. These methods do provide a means to identify the maximum obtainable improvements in terms of energy efficiency and performance benefits. The findings also clearly support the grounds for further research in this area. However, in spite of significant contributions, there have not been many attempts to address the complete implementation process of a working system.

2.4 EV Enabling Technology – The Ultracapacitor

Extensive development has been achieved in recent years in the field of high capacitance Electrochemical Double-Layer Capacitors (EDLC) [40]. More commonly refereed to as 'Supercapacitors' or 'Ultracapacitors', these devices are able to operate at power levels high above that of conventional batteries and can store a considerable amount of energy above the energy capacity of conventional capacitors. These devices represent one of the latest innovations in the field of electrical energy storage [41], and lends itself as a significant technology enabler for future electric and hybrid electric vehicles.

As a relatively new energy storage device, EDLC technology warrants a brief historical introduction. The first high capacity electrochemical capacitor device was patented in 1957 (US Patent 2800616) [42]. Developed by Howard Becker of General Electric Company, the device was of a basic construction consisting of porous carbon electrodes. Becker described

the large capacitive phenomena of the device but acknowledged that the exact reason for this exceptionally large capacitance was not fully known at the time. Subsequently, in 1966, Robert Rightmire of Standard Oil Company Cleveland Ohio (SOHIO) introduced a double layer capacitor utilising porous carbon in a non-aqueous electrolyte (US Patent 3288641).

Four years later, Donald Boos, also with SOHIO, patented another device that used a carbon paste soaked in an electrolyte (US Patent 3536963), which SOHIO later put into production. Thus making them the first company to market high capacitance devices. Between 1975 and 1980, Brian Conway carried out extensive fundamental work on EDLCs and also ruthenium oxide type electrochemical capacitors. A detailed account of this can be found in Conway's scientific monograph [43]. Conway was also the first to use the term 'supercapacitor'. However, in 1971, the Nippon Electric Company (NEC) produced the first commercially successful high capacitance device under the same name, 'supercapacitor' [44]. The NEC device was however primarily targeted for memory backup applications. Pinnacle Research Institute (PRI) began developing high power EDLCs in 1982, which they called 'ultracapacitors' [45]. Intended for critical military applications, the capacitors were designed for utilisation in electromagnetic launchers, missile guidance systems, laser weaponry, arming systems and power conditioners. It was more than a decade later that EDLC devices found presence in vehicular applications [46].

Interestingly enough, it is the advent of EDLCs in vehicle applications that has created a synergistic effect in terms of technology awareness of EDLCs and fuelled a popularity increase in hybrid and electric vehicle. Some conjectures can be made from Figure 2.1 to support the pervious statement. As the histogram shows, the increasing interests in EVs and HEVs coincide with the decade old introduction of EDLCs in vehicle applications. In retrospect, the increasing attention to EV power and energy management can also be linked to the introduction of this technology enabler to the vehicular application domain. Figure 2.4 illustrates the progress of EDLCs development since its inception in 1957.

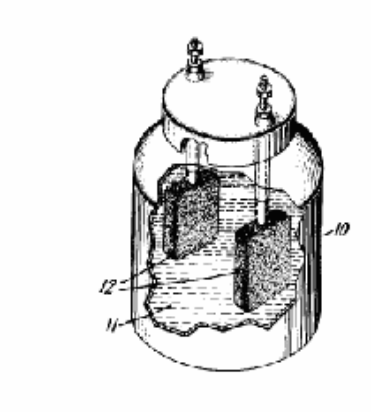

(a) From US Patent 2800616 (1957)

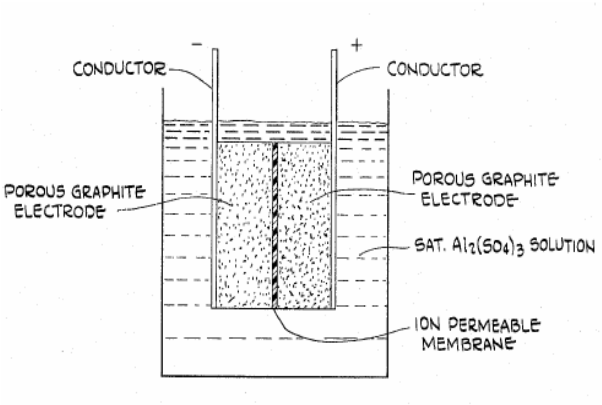

(b) From US Patent 3288641 (1966)

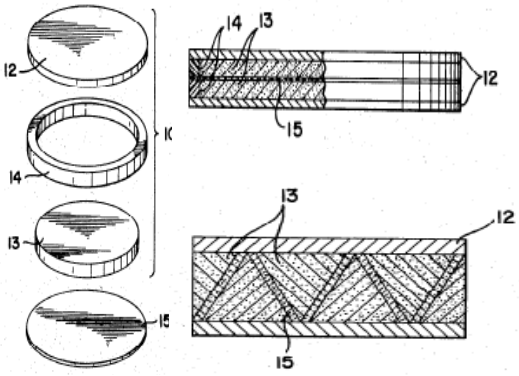

(c) From US Patent 3536963 (1970)

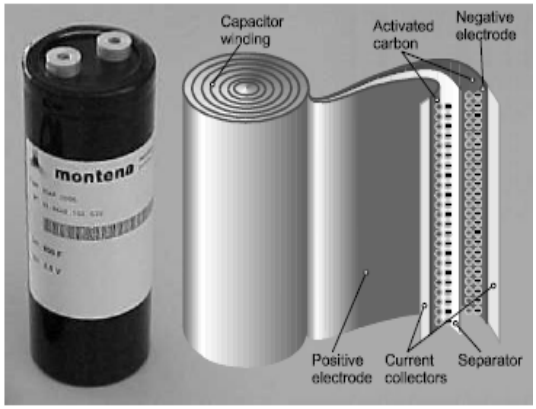

(d) Modern ultracapacitor construction (2002)

Figure 2.4 Evolution of the EDLC technology

(a) Patent by H.I Becker, (b) Patent by R. A. Rightmire, (c) Patent by D.L. Boos, (d) Modern ultracapacitor (Maxwell-Montena)

The terms 'Supercapacitor', 'Ultracapacitor' and 'Electrochemical Double Layer Capacitor' have been used indiscriminately in literature in reference to high capacitance devices. Huggins [47] identified this uncertainly in terminology and made a distinction between these type of capacitors in terms of their storage mechanisms and redox pseudo-capacitance. However, it is generally recognised that these terms are interchangeable depending on the

manufacturer. Throughout the rest of this dissertation, the term 'Ultracapacitor' will be adopted for the sole purpose of keeping with consistency when presenting the actual device used in the experimental part of the work. A listing of current manufacturers of these devices and their respective device names are shown in Table 2.1

MANUFACTURER	DEVICE NAME	CAPACITANCE (F)
AVX	Bestcap	0.022 - 0.56
Cap-XX	Supercapacitor	0.09 - 2.8
Cooper	PowerStor	0.47 - 50
ELNA	Dynacap	0.033- 100
ESMA	Capacitor modules	100 - 8000
Epcos	Ultracapacitor	5 - 5000
Evans	Capattery	0.01 - 1.5
Kold Ban	KAPower	1000
Maxwell	Ultracapacitor	1.8 -2600
NEC	Supercapacitor	0.01 - 6.5
Ness	EDLC	10 - 3500
Panasonic	Gold capacitor	0.1 - 2000
Tavirma	Supercapacitor	0.13 - 160

Table 2.1 Manufactures of High Capacitance devices

(Extracted from Namisnyk [48])

As one of the key technology enablers for electric vehicles, work on ultracapacitor systems and the associated power and energy management is being carried out worldwide. Research activities supported by the European Community Joule III [13] program specifically titled, 'Development of Supercapacitors for Electric Vehicles' began in 1996. In 2002, a worldwide consortium called KiloFarad International (kFi©) [49] was established as a regulatory body. One of the aims of kFi is to initiate working groups to drive forward the adaptation of ultracapacitor technology in automotive and other applications. The US DoE recognises ultracapacitors as one of the critical technology enablers for the future 'More Electric Vehicles' (MEVs), and stipulated the performance expectation of this technology in their 2003 annual report. An excerpt from the report is reproduced in Table 2.2.

PROPERTY	NEAR TERM TARGET	ADVANCED TARGET
Energy Stored (Wh)	500	750
Maximum Power (kW)	50	80
Weight (kg)	<100	<50
Volume (l)	<40	<20
Energy Density (Wh/kg)	>5	>15
Maximum usable power density (W/kg)	>500	>1600
Round trip efficiency (%)	>90	>90

Table 2.2 US DoE target performance specification for ultracapacitors
(Extracted from the FY2003 Progress report for Energy Storage Research and Development)

There is substantial evidence in literature to support further development in integration technology of ultracapacitors in electric vehicle power systems [50-54]. However, the obtainable efficiency enhancement has regularly been contested by a cost factor. In their 2002 report, Simpson and Walker [55] reported a lifecycle cost analysis of ultracapacitors in electric vehicles. They stipulated that efficiency gains are marginal compared to the lifecycle cost of ultracapacitors. Burke [56] however reported that due to the high prices of speciality carbons used in manufacturing ultracapacitors, a price reduction by a factor of ten (at 2000 prices) is necessary to justify capital costs. In 2002, Barker [57] stated that ultracapacitors are not ready from a cost perspective and requires a 2-3 cost reduction factor. Barker however concluded that the benefits of ultracapacitors as a leading contender in storage technology would very likely reduce the cost. Arguably, cost will always be an issue to debate. Prices have exponentially dropped since the year 2000, as manufacturers race to reduce the cost per farad. In fact, in 2004, both Miller [58] and Barrade [52] reported a significant cost reduction and projected a further fall towards more favourable cost targets.

2.5 Hybridisations of Batteries and Ultracapacitors in EV Power Systems

Although the high capacitance and high power density characteristics of ultracapacitors endorses its feasibility in electric vehicle applications, the energy capacity limitation dictates the need for a much higher energy sustainable source, namely a battery bank. The objective of integrating batteries and ultracapacitors is to create an energy storage system with the high

energy density attributes of a battery and the high power density of an ultracapacitor. In essence, the goal is to exploit the advantages of both the devices through ultracapacitor hybridisation of the two technologies in a vehicular power system architecture.

Ozatay et al. [59] concisely described this hybridisation as emulating a "non-existent super-device" by coordinated power transfer of batteries and ultracapacitors. An illustration of power density versus energy density of existing electrical storage devices is shown in Figure 2.5.

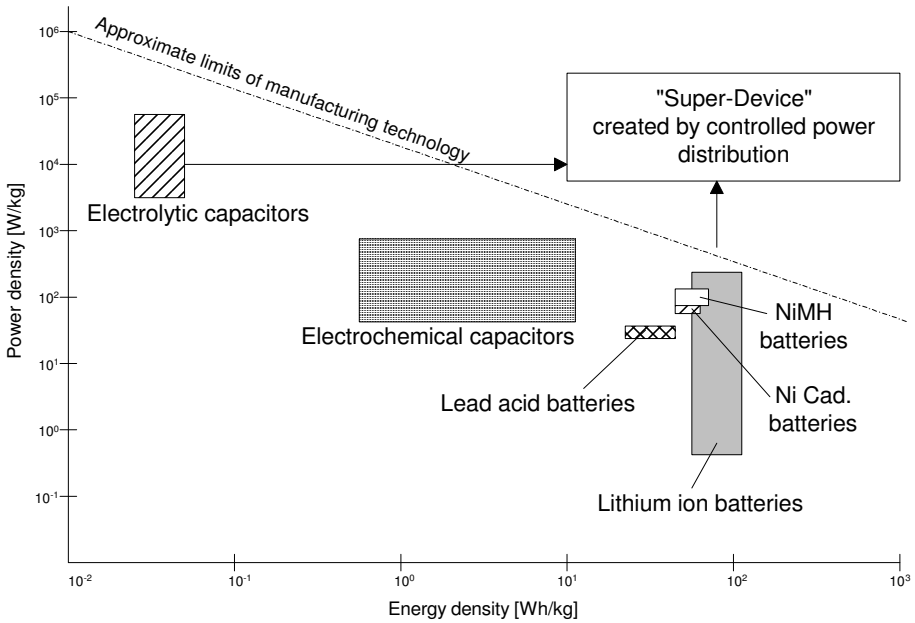

Figure 2.5 Power Density versus Energy Density of current energy storage technologies

(Reproduced from Ozatay et.al [59])

The proposition of combining high power density ultracapacitors with high energy density batteries was first claimed in 1992 by Michio Okamura [60]. However, the development of ultracapacitor systems specifically for vehicular applications only began in recent years. In 1996, Burke [46] produced a report on the prospective usage of ultracapacitors in electric and hybrid electric vehicles. Following this, various authors have examined the hybridisations of batteries and ultracapacitors in vehicle power systems.

The most basic method in combining an ultracapacitor system with a battery system as a power supplement device is to simply connect both systems in parallel. This has to be done with particular consideration to the maximum terminal voltage of the ultracapacitor system. Spyker and Nelms [61] looked at predicting the run-time of a ultracapacitor in a simplified model consisting of a battery and ultracapacitor connected in such a parallel configuration. For the arrangement shown in Figure 2.6, the authors concluded that the ultracapacitor is only suitable for low duty cycles, as the battery current will surpass the capacitor current during long pulse durations.

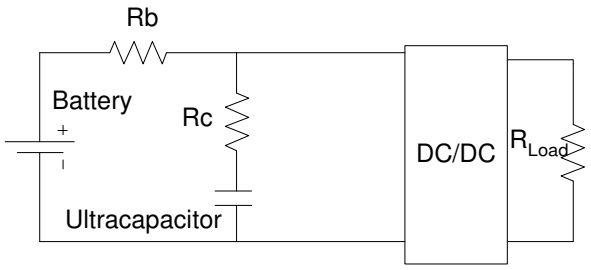

Figure 2.6 Battery and Ultracapacitor supplying a constant power load

(Extracted from [61])

In the topology shown in Figure 2.6, the battery potential determines the maximum discharge ability of the ultracapacitor. This direct interfacing of the battery and ultracapacitor is achieved by initially pre-charging the ultracapacitor to a terminal voltage of equal magnitude to the battery open circuit voltage prior to making the parallel connection. Following this, any current division between the battery and ultracapacitor is determined purely by the two branch resistances. Even though it would appear less efficient in terms of discharge capacity, the study provided a basic idea for other researchers to work on. For the same configuration, Miller [5] provides an analysis for the optimum sizing of the ultracapacitor and battery system for a 1610 kg mid-size passenger vehicle. The direct parallel connection of ultracapacitors and batteries are said to be in a passive configuration since there is no external intervention of power sharing between the devices.

Gao, Dougal and Liu [62, 63] produced comparison data of active and passive power sharing between ultracapacitors and batteries under varying load conditions. Figure 2.7 illustrates the circuit configurations. Using their Virtual Test Bed (VTB), the authors simulated and

experimentally verified an increase of power deliverability with the active configuration. In the passive system, the power sharing capabilities of the devices were dictated by the impedance of the components themselves.

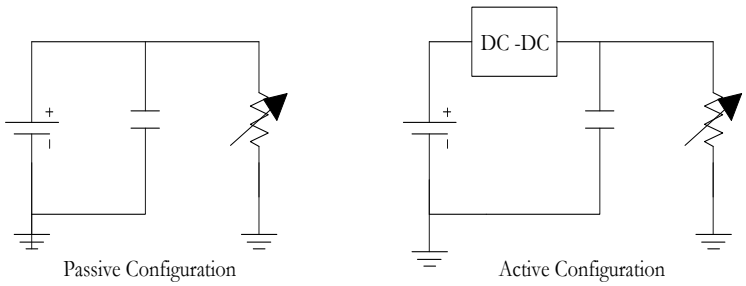

Figure 2.7 Ultracapacitor- Battery systems. Passive and Active Configurations

(Reproduced from Gao et al [63])

Patterson [64] classified the active configuration possibilities of batteries and ultracapacitors into two types. The first type has the ultracapacitor connected directly across the DC bus and the battery connected through a bi-directional DC-DC converter. The second configuration has the battery on the main DC bus instead. The two configurations are shown in Figure 2.8.

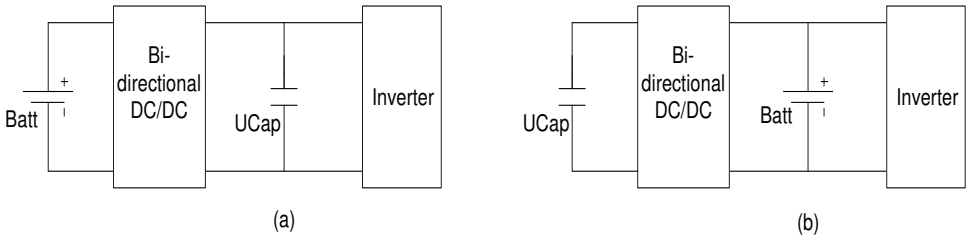

Figure 2.8 Connection configurations of ultracapacitors to an EV propulsion system

(Reproduced from Yan and Patterson [64])

Mellor, Schofield and Howe [65] also examined both these configurations and stated that having the ultracapacitors connected directly to the inverter as shown in Figure 2.8 (a) is likely to yield high efficiency. Notably, in the configuration of Figure 2.8 (a), the entire battery power has to be transferred through the DC-DC converter and hence lowering the total efficiency of the battery pack. Mellor et al. [65] concluded their report by suggesting the

need for precise energy management to ensure the effectiveness of system energy content. As an initial plan, the authors proposed the following as a simple idealised energy management scheme. Here the buffer unit refers to ultracapacitors.

- "The buffer unit normally supplies the peak power"
- "The battery supplies the average power"
- "If the DC link falls below a minimum set level, all further power requirement is drawn directly from the battery"
- "If the buffer unit is fully charged, any regenerative energy is diverted to the battery"

One of the key benefits of integrating ultracapacitors with batteries in an electric vehicle propulsion system is the extra ability to harness regenerative energy. Steiner and Scholten [66] demonstrated the potential of using ultracapacitors as an energy recovery system in larger DC fed applications. By harnessing regenerative energy in a railway vehicle application, the authors expected to increase energy savings by 30%. This gain is possible for vehicles with very large peak to average power ratios and extended regenerative braking events. For road vehicles, the figures are lower and are heavily influenced by vehicle drive cycles and overriding functions such as anti-lock braking, which pre-empts regenerative braking modes [5].

A simulation study of regenerative energy handling by Dixon, Ortuzar, and Wiechmann [67] was reported with very promising energy recovery results. The authors proposed connecting a series of ultracapacitors through a single Buck-Boost converter, which was then paralleled to a battery pack (see Figure 2.9). As a control scheme, they suggested a primary control loop to establish the ultracapacitor current reference and a secondary control loop to generate the required PWM signals for the Buck-Boost converter. Subsequently, Dixon's team constructed a prototype vehicle to implement their battery and ultracapacitor system for field-testing [68]. The authors reported an 87% energy efficiency with opportunity for improvement.

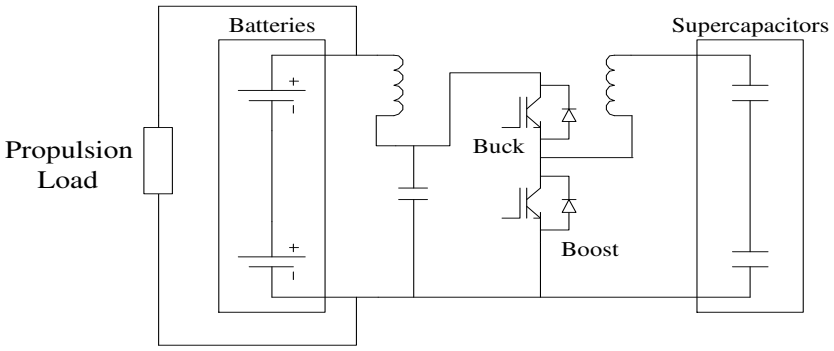

Figure 2.9 Ultracapacitor- Battery system with a Buck-Boost converter

(Extracted from Dixon et al. [68])

Also using cascaded proportional loops, Ozatay et at. [59] experimented on a frequency – based separation of battery and ultracapacitor currents in their test vehicle. In essence, the authors used a variable bandwidth low-pass filter for the battery current and a band-pass filter for the ultracapacitor current. Results of their drive cycle simulations showed a reduction in battery current stresses but not all peak currents were suppressed. The authors concluded that additional focus on energy management is required to achieve higher ultracapacitor efficiencies and battery life.

Baisden and Emadi [51] demonstrated a control strategy based on selecting three operating modes of a DC-DC converter to determine the power split between an ultracapacitor bank and battery pack. Referencing a dynamic variable to a look-up table, the approach showed that high current stresses experienced by the battery pack could be reduced by blending the power contribution with an ultracapacitor bank. During regenerative power cycles, the operation of the converter chargers the ultracapacitor bank to maximum state of charge and then diverts the access power to the battery pack. Using the Advanced Vehicle Simulator (ADVISOR)[69] package, the authors showed that the hybridisation of battery and ultracapacitors allowed the battery pack to be downsized to 70%. Although ultracapacitors were added to the energy storage system, the significant reduction in battery mass plus the increase in battery life justifies the addition of 35 ultracapacitor cells.

Arnet and Haines [70] designed a high power ultracapacitor interface-converter based on a high level view of energy flow. The authors developed a two-quadrant buck boost converter following an "intelligent" description of how the system should work. Flow of energy was represented by the following statements:

- "The primary source (battery or fuel cell) covers the average power consumption"
- "If more power is needed, energy is drawn from the ultracapacitors"
- "If less power is required, energy can be stored back into the ultracapacitors"

Along with the need to perform voltage and current regulation, the approach used by the authors provided a first estimation in describing the required tasks of the converter through high-level system definitions. A similar top- down approach has been adopted in the scope of this project to generate a strategic power and energy management system.

In a study supported by the U.S Department of Environment, Pay and Baghzouz [71] described the criteria for the coupling of batteries and ultracapacitors concisely. They stated that the battery current has to be maintained as constant as possible with slow transitions from current levels during load transients. In unison, the ultracapacitors have to charge as fast as possible during regenerative cycles and "discharge most of its stored energy during acceleration". In order to control the power throughput of the ultracapacitor bank, some form of regulation is necessary. This implies that any form of coupling that restricts the power transfer from the ultracapacitor system is not acceptable. This relates to the passive configuration described by Gao et al. [63] (Figure 2.7) since in the passive configuration, power flow in and out of the ultracapacitor is bounded by the battery terminal voltage. In their concluding remarks, the authors of [71] commented that, " The best control strategy is not fully developed due to challenging control issues ". The specifics of these issues and the techniques to integrate and manage the power flow and energy content are still a challenging research question.

In general, literature shows the need for an intermediate power electronics converter to regulate the power flow between the load, battery and ultracapacitor. Schupbach and Balda [72] produced a comparison study of three DC-DC converters for a hybrid electric vehicle

system. They compared the component design ratings of a Half bridge, Cuk and the SEPIC (single-ended primary inductance converter)/ Luo combined converter. Each topology had its advantages as well as disadvantages in terms of size, thermal constraints, conduction losses and isolation. Recognisably, the design of a converter to handle the wide operating voltage of an ultracapacitor bank will not be straightforward. In order to extract as much energy out of a series of ultracapacitors, the current handling capability of the converter will need to be very high.

Instead of a battery pack as a primary energy source, Drolia, Jose and Mohan [73] examined connecting ultracapacitors to fuel cells via a switched mode converter. Compared to other cited literature, the authors aimed at deep discharging the ultracapacitor bank. Their work can be extended to a battery-ultracapacitor configuration since both fuel cells and batteries have slow dynamic responses. In a fuel cell system, an inrush current can cause a total system shutdown whereas with batteries, a thermal rise and lifespan reduction can be expected.

Ohkawa's proposal [74] to augment its fuel cell vehicle (Honda- FCV) with ultracapacitors employs a DC-DC converter on the fuel cell inputs. Called the VCU (Voltage and current Control Unit), the interface controls power flow from the fuel cell to the propulsion system DC bus. The ultracapacitors were however connected directly to the bus via double-pole relays. Power flow control is established using two low pass filters that are used to regulate a single power electronic stage on the fuel cell side. Although this interface topology and control technique increases the system's receptivity to regenerative power, the useable energy of the capacitor is still restricted and bounded by the direct DC bus connection.

For a topology that provides galvanic isolation, Chiu and Lin [75] described an arrangement to interface a low voltage battery pack to a high voltage fuel cell and DC bus. Their topology offers the benefit of smaller power inductor values compared to conventional single stage designs, however two primary side inductors and an isolation transformer is required. The arrangement is directly applicable to ultracapacitor-battery hybrids with ultracapacitors operating on the low voltage side but requires the battery to be continuously connected to the DC bus. Also providing galvanic isolation, the wide input DC-DC

converter proposed by Todorovic et.al [76] uses cascaded boost converters to attain a possible 2:1 voltage variation on the primary energy source. Their design to interface a fuel cell stack with ultracapacitors provides a stiff and isolated output voltage while allowing a wide input voltage swing on fuel cell voltage. The ultracapacitor in this topology services the positive peak power demands. However, regenerative power handling capability is not inherent. The concepts of both these topologies are in fact derivations of the well established Weinberg converter [77], which dates back to 1974.

For a HEV application, Cegnar, Hess and Johnson [78] designed a mild hybrid system using only ultracapacitors as the energy storage system. The design relied on regenerative braking as the sole source for cyclically charging the ultracapacitor bank. No batteries were used in their design. To achieve voltage stiffness, they used a high and low voltage ultracapacitor bank coupled with a boost converter. Though not explicitly stated in their report, it is likely that such a design will require a very large inductor. This large inductor would be necessary to transfer power from the ultracapacitors to the load while maintaining the output voltage specification. However, their concept and simulation results interestingly show the capability of the ultracapacitors in recapturing large regenerative currents of magnitudes exceeding 200A. Early studies of using ultracapacitors as the sole energy storage device in HEVs in fact began during the early development of ultracapacitor technology itself. In 1994, Farkas and Bonert [79] examined the possibilities of replacing batteries with ultracapacitors if battery technology does not progress in terms of power deliverability.

Reports have shown convincing facts that the high power stress of a battery pack can be mitigated to a bank of ultracapacitors. Hence a method to determine the number of ultracapacitor cells, the capacity of each cell and the physical connections is needed. According to Schupbach et al [80], the sizing of a ultracapacitor bank was conventionally estimated by dividing the vehicle load energy and load power requirement by the power and energy coefficients of the ultracapacitor. Since these coefficients vary with respect to the load power levels, a more accurate sizing method was proposed. To capture this non-linearity and with the optimisation goal to minimize weight and volume, the authors implemented an iterative sizing procedure using the *gclsolve* optimisation routine developed by TOMLAB [81].

2.6 Ultracapacitor augmentation issues

In investigating the details of ultracapacitor based energy storage systems, several circuit implementation problems were found. The predominant limitation of ultracapacitor technology is the single cell voltage limitation, which is currently 2.5 Volts. Because of this limitation, multiple cells are connected in series to achieve a higher terminal voltage. Doing so introduces a cell equalisation or balancing issue that is critical for both component failure prevention and energy storage utilisation. On this subject, researchers investigated several cell-balancing techniques. Linzen et al. [82] investigated four different cell-balancing topologies. In essence, the authors of looked at both passive and active cell balancing techniques and reported that a DC-DC converter type topology would be a practically unattractive solution.

Barrade's et al. [83] voltage sharing device used an inductor, which was switched between adjacent cells via a pair of transistors. The configuration, based on buck-boost converter topology, demonstrated the achievability of voltage balancing through some form of active switching methods. Contrary to the conclusions of Linzen's et al. [82], Barrade's [83] DC-DC based cell equaliser showed a practical feasibility. Along the same subject, Barrade in [84] investigated the reduced energy storage capability of series connected ultracapacitor cells if the voltage levels are not shared equally. In a recent (patent pending) design [58], Miller and Everett [85], developed a non-dissipate charge equalisation circuit to address this voltage sharing problem. Also based on active switching techniques, Miller's circuit was designed for a 15V bank of ultracapacitors specifically for the automotive industry

2.7 Alternative ultracapacitor system configurations

Typically, ultracapacitor banks have been designed as a fixed series of cells to satisfy the terminal voltage demand. Multiple series strings can then be connected in parallel to increase the energy storage capacity of the ultracapacitor bank. The fixed bank of ultracapacitors is then coupled to a DC/DC converter that facilitates control of power flow. Moving away from the fixed configuration topologies, Okamura [60] stipulated that a bank switching topology is capable of achieving a 40% increase in usable energy of a ultracapacitor storage

system. Theoretically, the switching of the ultracapacitors to closely match the terminal voltage is similar to synthesising a current pump by controlling a voltage source. Based on this concept, Takara et al [86, 87] simulated series/parallel bank switching on the premise that the usable energy that the ultracapacitors are able to provide is increased. This was done without the use of a designated DC-DC converter. Following this, Rosario, Economou and Luk [88] reported that since the peak power demands of propulsion load in an electric vehicle are relatively of short intervals, sequential switching of ultracapacitors could be exploited. By coordinating the switching topology, the effective energy that can be extracted out of the ultracapacitor network showed an increase whilst the terminal voltage constraints were satisfied by sequentially changing the connections within the ultracapacitor network.

Miller and Everett [85] studied the effects of ultracapacitor time constant in relation to the specific demands of non-propulsion loads. They introduced the concept of distributing banks of ultracapacitors throughout the vehicle power network. By matching the capacitance to the load power and demand frequency, they demonstrated an increased utilisation of the energy content in smaller, matched capacity ultracapacitor banks. Further to this, distributing the ultracapacitors also eliminates the single point of failure that can occur in a single ultracapacitor bank configuration. The results of their report are of particular interest, since it supports the concept of adapting the capacitance of an ultracapacitor network to the load profile, this concept that was also investigated by Rosario, Economou, Luk and El-Hasan [89] in a publication on pulse power management.

2.8 Observations and Hypothesis

Observations

The fundamental task of a strategic power and energy management system in the context of electric vehicles is to control and coordinate the power generation, energy storage and subsystems power flow for maximum overall system efficiency. Although the generation and storage systems have their specific optimal operating ranges in terms of power and energy output efficiency, an overall systems approach to the coordinated operation is called for. The optimisation problem of power and energy management is in fact a global one [90]. Considering the problem on the basis that global optimality results from individual subsystem optimality may not be accurate.

A unified power and energy management system has the challenging mission of handling several tasks, which may be subdivide as follows: -

- Energy resource and power flow coordination
- Power generation and peak power handling
- Power availability for propulsion and safety critical loads
- Power quality and stability
- Regenerative power handling

Essentially, electric load management in a vehicle can be divided as shown in Figure 2.10

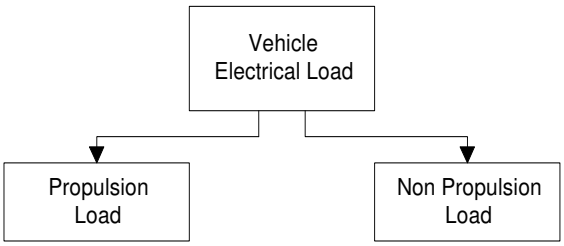

Figure 2.10 Vehicle electric load classification

For a multi energy storage system, the task of the vehicular power and energy management system is to coordinate the power sharing between multiple energy sources. Vehicle systems states have to be acquired and analysed in order to determine the operating modes of the energy storage units. Demands of non-propulsion loads are highly dynamic throughout the operation of the vehicle and hence place added stresses on the energy storage systems. At the same time, the propulsion power is bi-directional. In the combination of multiple energy storage systems, this then requires bi-directional energy exchanges between the systems. However, there is a penalty imposed in terms of losses when transfer of energy between storage devices takes place. The energy losses could then be expressed as a penalty function. Figure 2.11 illustrates the energy transfer between the loads and two energy storage systems that have different specific power and specific energy characteristics.

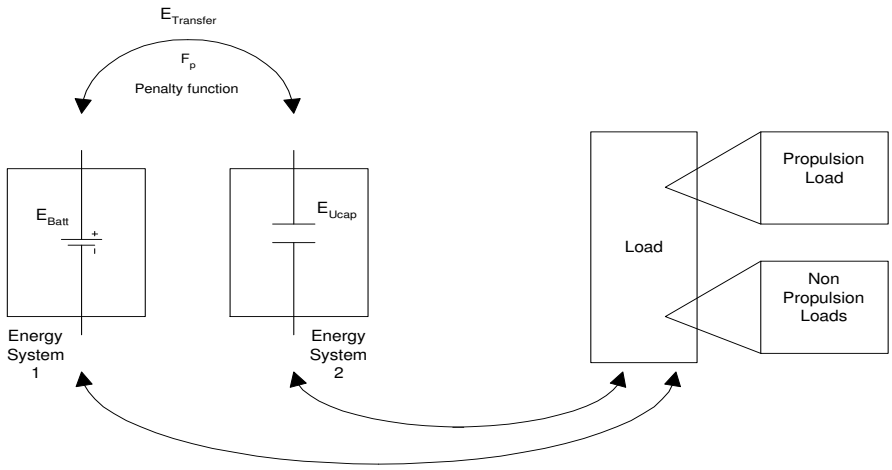

Figure 2.11 Energy Transfer between storage units and vehicle loads

As discussed in the literature review, power splitting between dual power sources for EVs and HEVs are often based on offline computation for known vehicle drive-cycles [19, 21, 22, 90]. These power trajectories are calculated to determine the proportioning ratios of power extracted from two or more power-producing units. The idea behind these forward simulation studies are to aid in the iterative design process of power pack sizing requirement for a given electric or hybrid electric vehicle. Reported works on managing vehicle system power throughout standard drive cycles are generally based on blending the power delivery of two sources, i.e. the battery/fuel cell and engine in HEVs or batteries and ultracapacitors in EVs.

Literature concerning vehicular power management cited thus far mainly proposes concepts to manage power splitting through optimisation of some objective function based on classifiable driving cycles. It is however recognised that dynamic optimisation algorithms are not readily applicable under uncertain or unknown vehicle drive cycle segments or conditions. Besides from being computationally intensive, these optimisations routines operate over a predefined time horizon rather that in a point in time, which is a requirement for real time power management systems. These methods however provide a good benchmarking for more intelligent control and estimation techniques such as rule based expert knowledge and fuzzy logic control.

Regenerative energy harnessing is one of the main attributes of electric vehicles and of particular interest in this research work. It is necessary that peak power buffers in the vehicle power system, namely a network of ultracapacitors be receptive to recover the regenerative energy while the vehicle is decelerating and rapidly release the energy during accelerations. This relates to the peak power buffer having a low SoC (state of charge) at high speeds and a high SoC at low or zero speed. It is the task of the power and energy management strategy to guarantee that these objectives are met. To do this, the system has to track the SoCs of the energy storage units and regulate net energy usage within efficient operating boundaries.

The application of an energy storage device can be categorised by two key factors. First being the maximum amount of energy that the device is able to store per unit volume. The second factor is the rate at which the energy can be transferred in-to and out-of the storage device. The latter defines the power rating of the device, which is critical to meet the requirement of electric vehicle loads. The characterisation of a particular energy storage device based on these two factors leads to the specification of Power to Energy ratio (P/E). For any application, a device having both a high energy storage capability as well as high power deliverability is desirable but at present, a single device specified to these requirements does not exist.

Batteries meet the high-energy content criteria but suffer from lack in high power capability. Chemical kinetics involved in the electricity production in batteries limits the operation at high power levels for a prolonged duration without reducing the battery life expectancy [91].

Rapid deep discharge cycles also contribute to frequent replacements of the battery pack. Ultracapacitors however are high power devices but with a much lower energy density compared to batteries. It is the hybridisation of these two technologies that enable the power and energy specifications of an electric vehicle to be met.

Literature shows that the power and energy management problem of energy storage systems within an electric vehicle is fundamentally a two-fold issue. The first being a control issue of how much and when power is to be split between the different energy storage units. The second concerned the interface mechanism in order to integrate and arbitrate multiple energy storage systems. While there is no consensus among researchers and industry as to the most efficient power electronics interface architecture between battery, ultracapacitors and the vehicle load bus, a number of recent studies[92] [93] have provided comparison data for several prospective approaches.

The power and energy management of a hybrid battery-ultracapacitor energy storage system is a challenge because each technology starts with different physical, electrical, and chemical characteristics that result in different power, energy, voltage characteristics, and charge-discharge methods. The interactions between these systems are not immediately obvious or predictable without a careful study and verification through hardware validation. The challenge lies in controlling the combination of both types systems so as to meet the demands of electric vehicles.

Hypothesis

In view of the various ways the electric vehicle power and energy management system has been approached, there is no consensus in development methodology nor is there a full implementation description of a complete working system in literature. This leads to the following propositions. Can the EV power and energy management problem be described and addressed in a way that encapsulates the various system requirements and limitations in a structured form in order to aid the design, development, implementation and testing stages of a complete system? Can this large multidisciplinary problem be modularised into more manageable and readily explainable sub-processes and hence contribute towards a more unified problem definition? Does the term 'management' itself indicate that some

philosophical concepts found in standard management methodology can be applied to the problem? A positive answer to the preceding questions leads to the following hypothesis;

> " The power and energy management of multiple energy sources in electric vehicles can be represented as a modular process that enables structured design and systematic implementation. By forming an analogy between classical management methodology and the underlying principles of managing power and energy, a more unified and more complete description of the EV power and energy management problem is attained "

To demonstrate or refute the hypothesis, a power and energy management system for a dual energy system electric vehicle sourced by batteries and ultracapacitors is chosen as the development framework. To begin with, the next chapter examines both these energy storage systems in the context of electric vehicle application.

CHAPTER 3

EV BATTERIES AND ULTRACAPACITORS - MODELLING AND APPLICATION

"Energy - The potential for causing changes" - ***anonymous***

Two factors fundamentally characterise the application of electrical energy storage systems. The first is the amount of energy that can be stored in the device and the second is the rate at which the energy can be extracted. The former refers to the energy capacity of the device and the latter refers to the device power rating. In order to design and implement a power and energy management system, the operating principles and factors that define the operating constraints or the energy storage systems must be considered. This chapter describes the fundamental operation, modelling and practical applications of a battery and ultracapacitor systems. Descriptions of the battery and ultracapacitor system parameters that are required to successfully implement a strategic power and energy management system is presented. For the simulation part of this work, extended Thevenin and VHDL models of the actual battery system used in the experimentation work were developed. Simulations and experimental results are presented to validate these models. For a power and energy management system to function, it is necessary that the operating parameters and constraints be observable by the controller. These parameters and the means of extracting these parameters via system variable measurements are presented.

3.1 EV Battery Systems

In EV applications, desirable attributes for the battery system are high specific power, high specific energy and a high number of cycle life as well as a long calendar life. Technical challenges exist to meet these performance requirements whilst adhering to the initial and replacement costs constraints. Battery systems for EVs need to be rechargeable and also handle the harsh operating environment that they are subjected to in an EV. There are basically two categories of battery systems that are accordingly termed as primary batteries and secondary batteries. Primary batteries are non-rechargeable and are discarded at the end of a single full discharge. These batteries are commonly found in consumable electronics. Secondary batteries however are rechargeable with the number charge-discharge cycles varying for different battery technology. It is the secondary battery that finds application in EVs.

3.2 Basic configuration of secondary batteries

A basic secondary battery cell consists of two electrodes immersed in an electrolyte. The anode is the electrode where oxidation occurs whereby electrons are transported out of the cell to the cathode via the load circuit. The cathode is the electrode where reduction takes place and where electrons from the external load return to the cell. The electrolyte however serves as a path for completing the electrical circuit inside the cell. Electrons are transported via ion migration from one electrode to the other through the electrolyte, thus creating a potential across the cell. During a battery cell charging operation, the process is reversed and the negative electrode becomes the cathode while the positive electrode becomes the anode. Electrons are externally injected into the negative electrode to perform reduction while oxidation takes place at the positive electrode. The reactions that take place during charge and discharge do not necessary occur at the same reaction rates. The unsymmetrical reaction rates are expressed as the charge acceptance rate during a charging process and a charge release rate during discharge. Generally, the charge release rate of a battery system is higher than the charge acceptance rate, which is why secondary batteries require a longer time to recharge. Figure 3.1 illustrates the basic battery cell construction and operating principle.

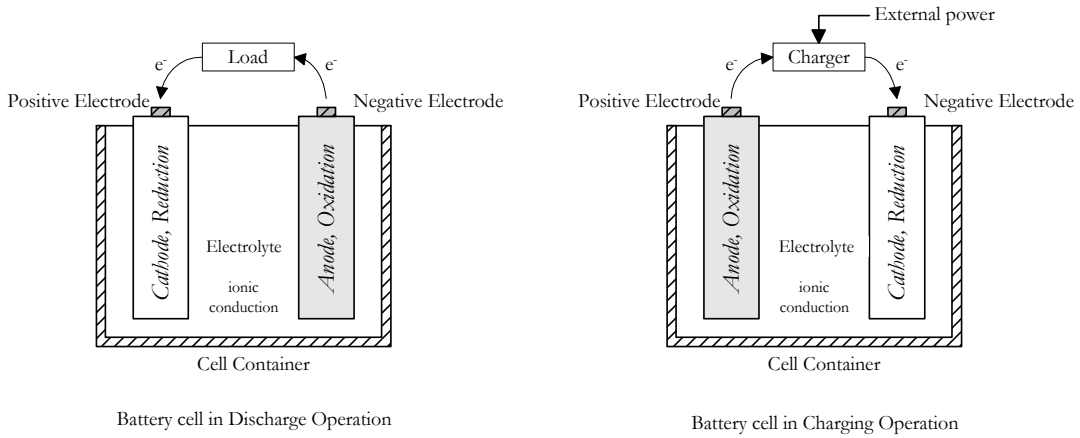

Figure 3.1 Operating principle of a secondary type battery cell

Only in an ideal battery cell do electrons only flow when the external circuit is completed. However, in all battery systems, a slow discharge does occur due to diffusion effects. This open circuit discharge is known as the self-discharge of the battery, and is a parameter that is used as one of the long-term performance descriptors of a particular battery type. Figure 3.2 illustrates the basic equivalent circuit model (Thevenin model) of a secondary battery, the corresponding voltage characteristic as a function of the battery stored charge capacity and the power characteristics. The battery is represented by an ideal open circuit voltage source (Voc) and a series internal resistance (Ri).

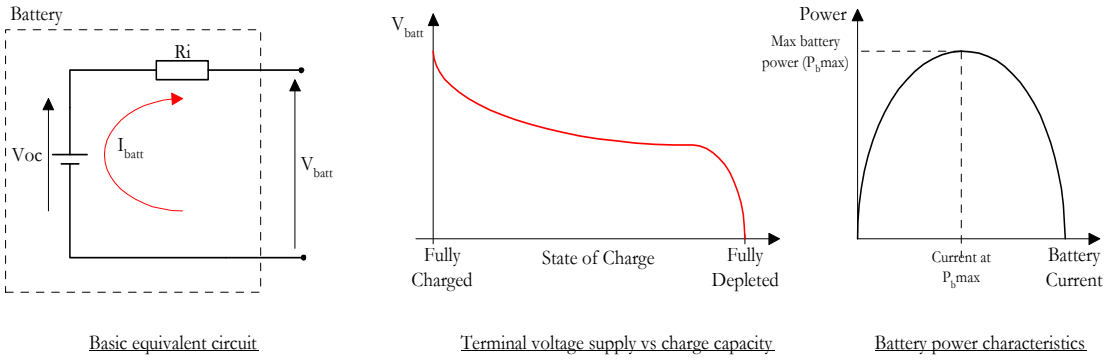

Figure 3.2 Battery basic equivalent circuit and voltage characteristic

The equivalent circuit loop holds true to Kirchhoff's voltage law to produce a terminal voltage expressed as,

$$V_{batt} = Voc - I_{batt} Ri \qquad (3\text{-}1)$$

where both Voc and Ri are dependent upon the battery instantaneous state of charge. The open circuit voltage Voc can be obtained from Nernst equations or by empirical methods [94]. The internal resistance Ri can be expressed as a function of the battery state of charge, operating temperature as well as the charge and discharge currents. Extensions to the basic circuit model can be made to account for the difference in charge acceptance and charge release rates. This will be addressed is a later section.

3.3 EV Battery systems

Several secondary battery technologies have been targeted for use in EV applications. Basically there are five main battery technologies, each having various attributes that are favourable for such an application. The description in Figure 3.3 shows the different battery technologies and the corresponding overall chemical reaction. A complete description of these battery types may be found in [94].

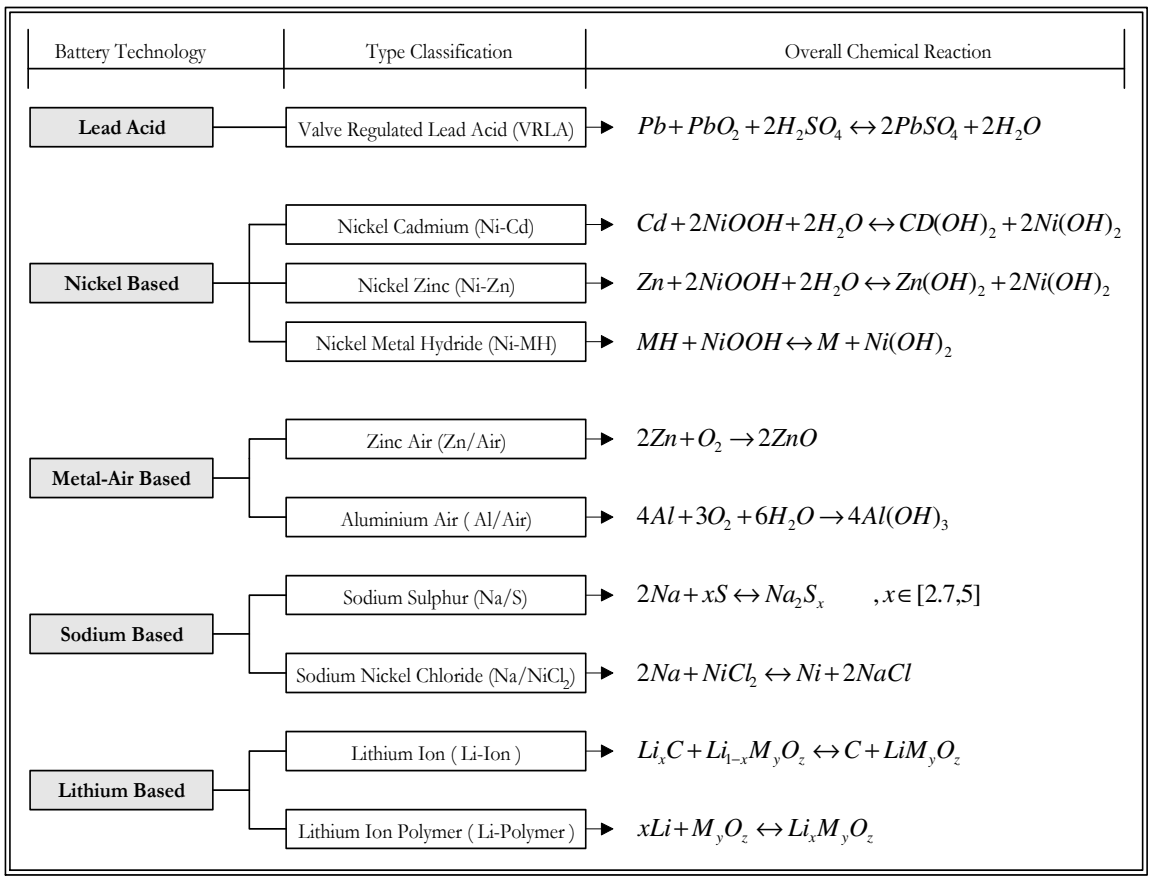

Figure 3.3 EV Battery Technology , Classification and Overal Reaction

Note the non-reversible reaction in the Aluminium Air and Zinc Air batteries indicating that these battery technologies do not permit electrical recharging. Considered as metal fuel cells, the electrodes in theses metal air batteries are continuously depleted during the discharge process. A comparison of the main attributes of the battery technology listed in Figure 3.3 are tabulated in Table 3.1. Note that the amphour efficiency for the Aluminium Air and Zinc Air batteries are not applicable since these battery types are charged by electrode replacement instead of an electrical charging process. Out of all the battery technologies, lithium based batteries are seeing the most rapid developments. Several additional lithium based systems are currently under extensive research worldwide. Variants of the Lithium Ion and Lithium Ion Polymer technology are Lithium Cobalt ($LiCoO_2$), Lithium Manganese ($LiMn_2O_4$), Lithium Nickel ($LiNiO_2$), Nickel Cobalt-Manganese ($Li(NiCoMn)O_2$), Lithium Iron Phosphate ($LiFePO_4$) and Lithium Sulphur (Li_2S_8). These technologies are at various stages of development and evaluation. Even with very high and favourable specific energy

merits, some of these technologies may not be accepted for EV applications due to safety and environmental issues. For example, the cobalt content in Lithium Cobalt batteries has been classified as an environmentally toxic hazard.

	Lead Acid	**Nickel metal hydride**	**Sodium Metal Chloride**
Specific Energy	20-35 Wh/kg	~65 Wh/kg	100 Wh/kg
Energy Density	54-95 Wh/l	~150 Wh/l	120 Wh/l
Specific Power	~250 W/kg	200 W/kg	150 W/kg
Nominal Cell Voltage	2V	1.2V	~2V (2.5 when fully charged)
Amphour efficiency	~80% (temp dependent)	>80%	>80%
Internal resistance	~0.022 ohm per cell @ 1Ah/cell	~0.06 ohm per cell @ 1Ah/cell	High at low SoC
Operating temperature	Ambient (poor in extreme cold)	Ambient (~25deg C)	300 - 350 deg C
Self-discharge	~2% per day	~5% per day	~10%
Number of Cycles	~800	~1000	>1000
Recharge time	8h (90% in 1 hour possible)	1hour rapid charge	2-3 hours

	Lithium Ion	**Aluminium Air**	**Zinc Air**
Specific Energy	180 Wh/kg	225 Wh/kg	230 Wh/kg
Energy Density	153 Wh/l	195 Wh/l	270 Wh/l
Specific Power	300 W/kg	10 W/kg	105 W/kg
Nominal Cell Voltage	3.5 V	1.4 V	1.2 V
Amphour efficiency	>80%	N/A	N/A
Internal resistance	Very Low	Very High	Medium
Operating temperature	Ambient (~25deg C)	Ambient (~25deg C)	Ambient (~25deg C)
Self-discharge	Very Low (~ 10% per month)	>10% per day	High
Number of Cycles	>1000	>1000	>2000
Recharge time	2 - 3h	10 mins (to replace electrode)	10 mins (to replace electrode)

Table 3.1 Comparison of current EV battery technology

3.4 Battery Specific Energy (SEbatt)

The amount of energy per unit of battery mass is termed as the specific energy of battery. This parameter is an intensive property of a battery system and is expressed in watt-hour per kilogram (Wh/kg). Although this parameter only serves as an approximation of the energy deliverable from a battery, it is commonly used as a reference quantifier between classes of battery technology. The actual energy that can be extracted from a battery system depends on several factors such as the temperature and discharge rate. As a general expression, the battery specific energy is,

$$SE_{batt} = \frac{\text{Discharge Energy}}{\text{Total Battery Mass}} = \frac{E_{dis}}{M_{batt}} \qquad (3\text{-}2)$$

Since the discharge energy varies with the discharge rate of the battery, the specific energy of the battery also varies accordingly.

3.5 Battery Specific Power (SPbatt)

The specific power of a battery system is the parameter that quantifies the magnitude of power obtainable per unit mass. Expressed in watt per kilogram (W/kg), this parameter also serves as an approximation of the power level available from a battery system.

$$SP_{batt} = \frac{\text{Discharge Power}}{\text{Total Battery Mass}} = \frac{P_{dis}}{M_{batt}} \qquad (3\text{-}3)$$

3.6 Battery Capacity

The capacity of a battery system is the measure of the amount of free charge generated by the active material at the negative electrode and consumed by the positive electrode. This parameter is measured in Coulombs (C) but is generally expressed in Ampere-hour (Ah),

where 1Ah = 3600C. The Ah of a battery system which is sometimes denoted by the letter 'C' corresponding to the coulometric capacity, is specified under constant current discharge. Ideally, the Ah rating for a specific battery would be the same for any discharge current. However, in all practical battery systems, the actual capacity is dependent on the magnitude of the discharge current. For example, a 20Ah battery could be rated to deliver 1A for 20 hours but instead would not be able to deliver 20A for a complete 1-hour duration. In general, for most battery types, the higher the discharge current, the less the resultant Ah measurement. This change is capacity is due to excess side reactions inside the battery cell. To take the discharge current magnitude into account when specifying battery capacity, a parameter termed as the '*C rate*' is included when expressing of battery capacity. The following equation provides a more complete definition of a battery capacity in relation to the discharge current.

$$I = kC_n \qquad (3\text{-}4)$$

where,

I is the charging or discharging current

C is the battery rated coulometric capacity in Ah

k is multiplication factor of C

n is the C rate (denoted as a subscript of the Capacity, C)

For instance, if a battery pack rated at 30Ah for 10hours is being discharged at a current of 15A, then following (3.4), this is expressed as $0.5C_{10.}$ Conversely, the C/10 rate of a battery that is rated for 10Ah indicates that the discharging current is 1. If a 20Ah battery is discharged at 4A, it is said to be discharging at 0.2C or at its C/5 or, " C by five " rate. Since the value of C generally decreases as the C-rate increases, the constant discharge current magnitude along with rated battery capacity must be stated together in order to accurately describe the actual battery capacity and hence its usable energy.

3.7 Self Discharge

When left unused, batteries exhibit various levels of self-discharge over time. This characteristic causes the energy stored in the battery to be wasted due to ion flow, which

continuously discharge the cell over a long period. The flow rate depends on the several factors, predominantly the temperature of the cell, where higher temperatures result in higher self-discharge rates. In lead acid batteries, self-discharge is caused by the release of hydrogen at the negative electrode whereas in nickel metal hydride batteries, self-discharge occurs due to slow decomposition of both positive and negative electrodes. The energy loss due to self-discharge of a battery, E_{SD} is expressed in percentage per 24 hour and is stated as,

$$E_{SD} = \alpha_{SD} E_{b\,Norm} \qquad (3\text{-}5)$$

where
α_{SD} is the battery 24 hour self discharge coefficient
E_{bNorm} is the battery nominal energy capacity in Wh.

3.8 Faradic Efficiency (Amphour Efficiency)

The Faradic efficiency or commonly termed as the Amphour efficiency or charge efficiency of a battery defines the ratio of discharge capacity (Ah) to the charge capacity (Ah). The parameter serves as an estimate of the maximum attainable charging efficiency of a particularly battery. Since this efficiency measurement is based on a constant current charge and a constant current discharge profile, it is less suitable for efficiency quantification in electric vehicle run-time applications where discharge currents vary significantly. It does however serve as a guide in comparing the efficiencies of various battery technologies. The amphour efficiency of a battery is expressed as,

$$\eta_{Ah} = \frac{Ah(\text{discharge})}{Ah(\text{complete recharge})} \qquad (3\text{-}6)$$

3.9 Battery Energy Efficiency

The battery energy efficiency is defined as the ratio of electrical energy delivered by a battery from a particular state of charge to the electrical energy required to return the battery to the

same state of charge. As mentioned in the preceding sections, the rate at which the battery is discharged and charged influences its efficiency. Under tests, two identical batteries starting from the same state of change can result in very different efficiency figures depending on how rapid the charge/discharge cycles are subjected to the batteries. Although the battery efficiency is not a straightforward parameter to quantify the performance of a battery, it is effective as a comparative measure of the various power and energy management strategies. If the use of power and energy management system operates the battery by limiting rapid high power discharges, a higher battery efficiency can be expected compared to a battery operation without a management system. In the case of a pure electric vehicle, the comparison must be made on the basis of the same battery charging profile.

As a general definition, the battery efficiency can be expressed under constant current tests (Peukert's Test) as follows. For a discharge time t_f, the battery discharge energy E_{dis} can be expressed as a function of its open circuit voltage V_{oc}, its internal resistance R_i and a constant discharge current I_b as,

$$E_{dis} = \int_0^{t_f} P_b(t)dt = t_f (V_{oc} - I_b R_i) I_b \qquad (3\text{-}7)$$

Charging the battery for the same duration as the discharge duration t_f with the same magnitude of charging current as the discharge current gives a charging energy E_{chg} as,

$$\left|E_{chg}\right| = \int_0^{t_f} \left|P_b\right|(t)dt = t_f (V_{oc} + \left|I_b\right|R_i)\left|I_b\right| \qquad (3\text{-}8)$$

Therefore, the battery efficiency expressed as a function of the battery current can be stated as,

$$\eta_{batt} = \frac{E_{dis}}{E_{chg}} = \frac{V_{oc} - R_i\left|I_b\right|}{V_{oc} + R_i\left|I_b\right|} \qquad (3\text{-}9)$$

3.10 Battery Modelling

The widely excepted empirical relation between capacity (Q), discharge current (I) and time (t) is Peukert's equation, formulated in 1897 by W. Peukert. The equation is used to develop fractional depletion models (FDM) of batteries. Peukert's equation under constant current discharge is

$$I^n \cdot t_{cut} = \lambda \qquad (3\text{-}10)$$

where I is the constant discharge current, t_{cut} is the time taken to reach the battery specified cut-off voltage, λ and n are curve fitting constants, with $n \to 1$ for small currents and $n \to 2$ for large currents. The Peukert exponent, n relates to the battery construction. If n equals 1, then the ideal condition where for example 1A current discharged for 100 hours is equal to 100 Ah is obtained (I = 1, n = 1, t = 100, SoC = 100 Ah.). However, practically, the exponent n is never equal to 1. n values of commercial batteries are 1.05 to 2, with about 1.2 being a common value [95]. A point to note is that the exponent varies with battery life thus making SoC estimation a more complicated process.

Using Peukert's equation (3.10), the relationship between the charge capacity Q and the current I can be established as

$$Q = I \cdot t_{cut} \qquad (3\text{-}11)$$

Eq.(3.11) into (3.10)

$$I^n \cdot \left(\frac{Q}{I}\right) = \lambda \qquad (3\text{-}12)$$

The state of charge (SoC) of a battery corresponds to the present battery capacity. It defines the remaining capacity throughout a discharge time. The SoC follows,

$$SoC(t) = Q - \int_o^t i(\tau) d\tau \qquad (3\text{-}13)$$

The state of discharge (SoD) , defined as the measure of charge drawn from the battery is represented as,

$$SoD(t) = \Delta q = \int_0^t i(\tau)d\tau \qquad (3\text{-}14)$$

The depth of discharge (DoD) of a battery is the percentage of capacity to which it is discharged and is given by [1],

$$DoD(t) = \frac{Q - SoC(t)}{Q} \cdot 100\%$$

$$= \frac{\int_0^t i(\tau)d\tau}{Q} \cdot 100\% \qquad (3\text{-}15)$$

For a small interval *dt*, assuming that the battery is fully charged at $t=t_0$, and with (3.14) and (3.15), it follows that;

$$d(DoD) = \frac{d(SoD)}{Q(i)}, \text{ where } d(SoD) = i(t)dt \qquad (3\text{-}16)$$

Referring to Peukert's equation, $0<n\text{-}1<1$, for $I>1$, Q decreases as I increases. From (3.12), $Q = \lambda / I^{n-1}$ for constant current discharge. Allowing for time varying currents, $Q = \lambda / i^{n-1}$ Therefore;

$$d(DoD) = \frac{idt}{\lambda / i^{n-1}} = \frac{i^n}{\lambda}dt \qquad (3\text{-}17)$$

Integrating both sides from t_0 to t,

$$\int_{t_0}^t d(DoD) = \int_{t_0}^t \frac{i^n}{\lambda}dt$$

$$\Rightarrow DoD(t) - DoD(t_0) = \int_{t_0}^t \frac{i^n}{\lambda}dt \qquad (3\text{-}18)$$

Since $DoD(t_0)= 0$ when the battery is fully charged at $t=t_0$, the factional depletion model (FDM) is given by

$$DoD(t) = \left[\int_{t_0}^{t} \frac{i^n}{\lambda} dt \right] \cdot 100\% \qquad (3\text{-}19)$$

To predict the workable range of an EV, either the SoC or DoD may be used. With (3.13) and (3.14), the SoC at time t is,

$$SoC(t) = Q_T - SoD(t) \qquad (3\text{-}20)$$

The accuracy of Q_T , which is a function of discharge current, temperature and environmental related parameters is important in the reliability of the SoC prediction. Since a predicting error in Q_T results in a incorrect SoC estimation, DoD measurement are sometimes used since it is expressed as a fraction of Q_T and can be expressed as,

$$DoD = \frac{SoD}{Q_T} \qquad (3\text{-}21)$$

3.11 Practical Application of Peukert's Equation

For practical applications, Peukert's equation can be expressed using the Peukert Capacity as,

$$C_p = I^n T \qquad (3\text{-}22)$$

where C_p is the Peukert capacity, I is the battery current, n is the Peukert exponent and T is the discharge time.

Although equation (3-22) may be rearranged to solve for the obtainable discharge time T (in hours) for different values of discharge current, it should be noted that the Peukert capacity also varies according to the discharge current. A variation can be made to (3-22) to use the fixed nominal capacity of the battery and the hour rating at that nominal capacity (data

provided by the battery manufacturer) to arrive at a more practical equation that can be expressed as,

$$T = \frac{C\left[\frac{C}{h}\right]^{n-1}}{I^n} \qquad (3\text{-}23)$$

where C is the nominal capacity of the battery and h is the hour rating at that capacity. (For example, a 100Ah battery rated for 20 hours translates to $C = 100$ and $h = 20$). With this, the estimated amphour of the battery can be evaluated by a multiplication of time T obtained from (3-23) with the discharge current I.

To demonstrate the effectiveness of the battery capacity estimation, a comparison using discharge profile data of a 27Ah – 10hour VRLA battery against the calculated capacity was performed. Figure 3.4 shows the comparison between the two. In the calculation, a Peukert coefficient of n=1.13 was used. As shown, the estimated Ah is in good agreement with most of the measured Ah points but shows a large error at very high currents. However, in a supervisory system that manages the power level exerted by the batteries and mitigates high power stresses to another device, the use of this capacity estimation method proves sufficient.

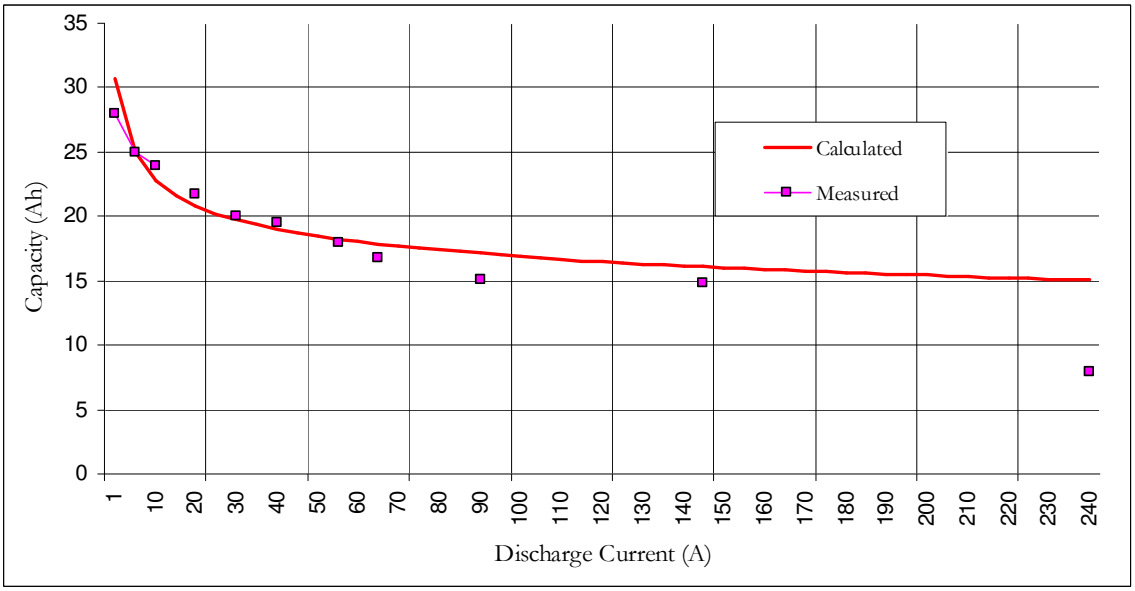

Figure 3.4 Comparison of a battery measured capacity and an estimated capacity using an adpatation of Peukert's equation

3.12 Battery State of Charge (SoC)

The battery state of charge is a dimensionless parameter that represents the present capacity in relation to the nominal capacity of the battery. As the battery is discharged and charged, the SoC indicates the relative amount of energy that has been removed or added into the battery Expressed in a normalised ratio, the SoC of a battery system is stated as,

$$SoC_{batt} = \frac{\text{actual battery charge}}{\text{total battery charge}} \qquad (3\text{-}24)$$

The accuracy in determining this parameter is important for successful implementation of any power and energy management scheme as well as for providing information regarding the amount of usable energy in the battery system. Various techniques have been used to estimate battery SoC such as fuzzy logic modelling [96] , analytical methods using Peukert's equation [97] and a combined approach using empirically obtained look-up table [2].

In most SoC determination methods, the battery current is integrated over time and related to battery nominal capacity. Current integration methods however are prone to integration errors caused by long-term drift in the calculation. A periodic resetting of the SoC is therefore required.

Discharging a battery system rated at Cn from t0 to t1 at discharge current I_b brings the battery state of charge at t1 to,

$$SoC_{batt}(t1) = SoC_{batt}(t0) + \frac{\int_{to}^{t1} I_b(t)}{C_n 3600} \qquad (3\text{-}25)$$

in real time control applications, the battery SoC can be calculated in discrete time steps as,

$$SoC_{batt}(k+1) = SoC_{batt}(k) + \left(\frac{I_b \Delta T}{C_n 3600} \right) \qquad (3\text{-}26)$$

with ΔT being the sampling period between k and $k+1$ and the sampling time is sufficiency small to assume that the battery current remains constant during the time step.

Figure 3.5 illustrates an implementation of a battery SoC estimation that combined Ah counting, Peukert's equation as well as the voltage and temperature parameters.

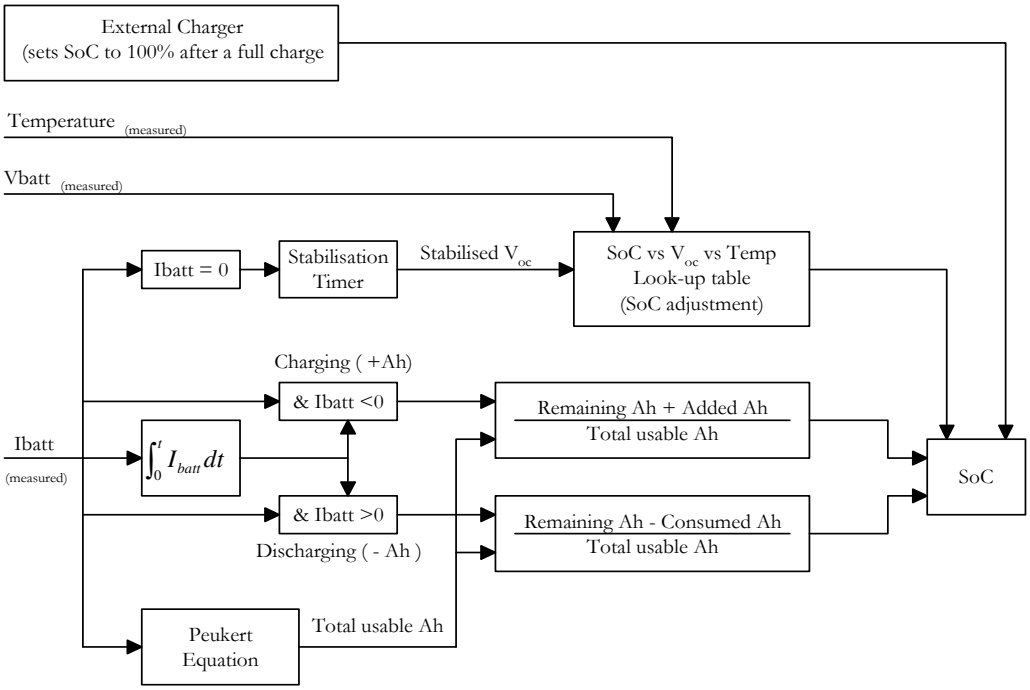

Figure 3.5 Combined method for practical implementation of SoC estimation

(Adapted from [2])

3.13 Battery Internal Resistance (Ri)

The DC internal resistance of a battery can be obtained experimentally using the test circuit shown in Figure 3.6. Subjecting the batteries to a change in load produces a corresponding change in voltage drop.

Accordingly, the internal resistance at DC is determined by,

$$Ri_{DC} = \frac{Vb_1 - Vb_2}{Ib_1 - Ib_2} \qquad (3\text{-}27)$$

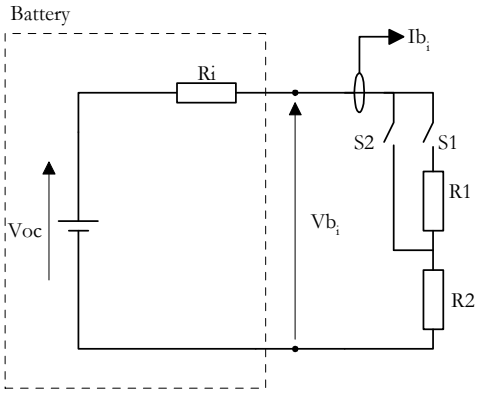

Test circuit to measure Ri_{DC}

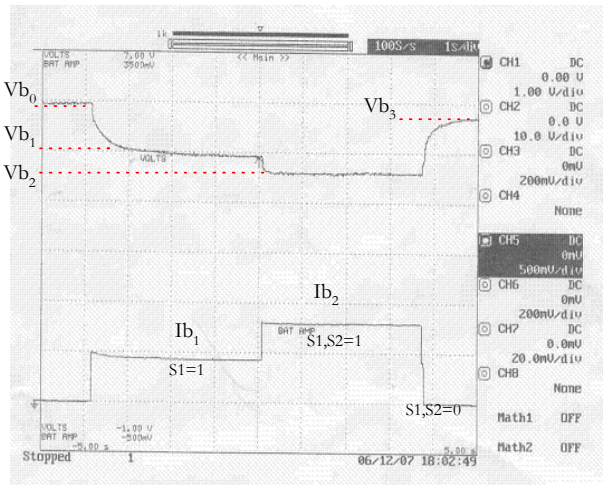

Voltage and current traces during an Ri measurement experiment

Figure 3.6 Tests to measure the DC internal resistance of a battery.

The exponential decay and rise of the voltage traces shown in the Figure 3.6 is due to the lead capacitance of the measuring instrumentation. This capacitance does not influence the DC resistance measurement, which is calculated based on voltage measurement points taken when the battery voltage trace is parallel to the horizontal axis.

3.14 Determining Battery Operating Constraints

Maximum Discharging Power

The maximum discharging power of a battery system is limited by the maximum allowable discharging current, minimum terminal voltage and temperature. Theoretically, the maximum current that the battery can deliver occurs when the battery is at full charge and the internal resistance is at its minimum value. However, in practice, specification of the maximum discharging current ($I_{batt}max$) is normally limited by mandatory safe operating conditions of the battery as well as the current handling capacity of the electrodes itself. The limitation in discharging power due to the current constraint can be expressed as,

$$Pb_{dis}\max = \left|I_{batt}\max\right|(Voc_{[SoC]}) - \left|I_{batt}\max\right|^2(Ri_{[SoC]}) \qquad (3\text{-}28)$$

where $Voc_{[SoC]}$ and $Ri_{[SoC]}$ are the battery state of charge dependent open circuit voltage and internal resistance respectively

The discharging power limit due to battery voltage constraint can be expressed as,

$$Pb_{dis}\max = Vb\min\left[\frac{Voc_{[SoC]} - Vb\min}{Ri_{[SoC]}}\right] \qquad (3\text{-}29)$$

where *Vbmin* is the minimum allowable battery voltage dictated by the lower operating voltage boundary of the device that the battery is sourcing.

Using experimentally obtained values of $Voc_{[SoC]}$ and $Ri_{[SoC]}$ and a manufacturer recommended value for *Vbmin* of 10.2V as well as a design value for $I_{batt}max$ of 350A, the maximum discharging power using (3-28) and (3-29) for an Odyssey 13.5V, 27Ah (1 hour) lead acid battery is shown in Figure 3.7. As the graph shows, the limit in of the maximum discharge power depends more upon the current constraint at high SoC and voltage constraint at lower SoC. In an EV application, it is the task of the power management systems controller to limit the available power that the battery can deliver based on these constraints.

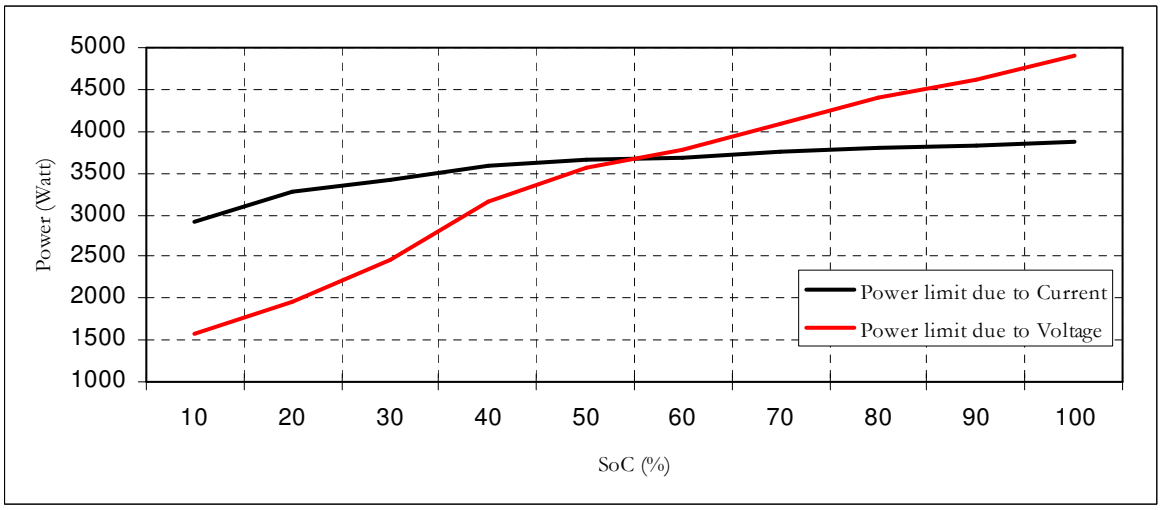

Figure 3.7 Maximum battery discharging power due to current and volatge limits

Maximum Charging Power

Similar to the maximum discharging power, the battery system is accordingly specified with a maximum charging power that also depends on the charging current and charging voltage. With all battery systems, the charge acceptance rate is always less than the charge release rate [5]. Therefore, for and efficient charging processes, the maximum charging current is significantly less than maximum discharging current. The maximum charging power constrained by the maximum charging current can be expressed as,

$$Pb_{chg}\max = \left|I_{batt}\max\right|(Voc_{[SoC]}) + \left|I_{batt}\max\right|^2 (Ri_{[SoC]}) \qquad (3\text{-}30)$$

The maximum charging power is also limited by the maximum charging voltage that can be safely applied across the battery electrodes. This voltage value and the sensitivity of exceeding this value vary for different battery technology. Lead acid batteries for example can handle an over voltage with less resultant damage compared to lithium ion batteries. The charging power limit due to maximum battery voltage can be expressed as,

$$Pb_{chg}\max = Vb\max\left[\frac{Vb\max - Voc_{[SoC]}}{Ri_{[SoC]}}\right] \qquad (3\text{-}31)$$

where $Vbmax$ is the maximum voltage that can be applied to the battery.

With the same experimentally obtained values of $Voc_{[SoC]}$ and $Ri_{[SoC]}$, a value for $Vbmax$ of 14.4V and the maximum charging current $I_{batt}max$ set to100A, the maximum charging power using (3-30) and (3-31) in shown in Figure 3.8. As can be seen, the maximum charging power due to the charging current limit is fairly constant across the SoC range. Instead, as the battery approaches full charge (100% SoC), the limiting factor of the charging power is the maximum battery voltage. Again, the power management system has to limit the battery charging power accordingly to ensure that the charging power is below both traces on the graph.

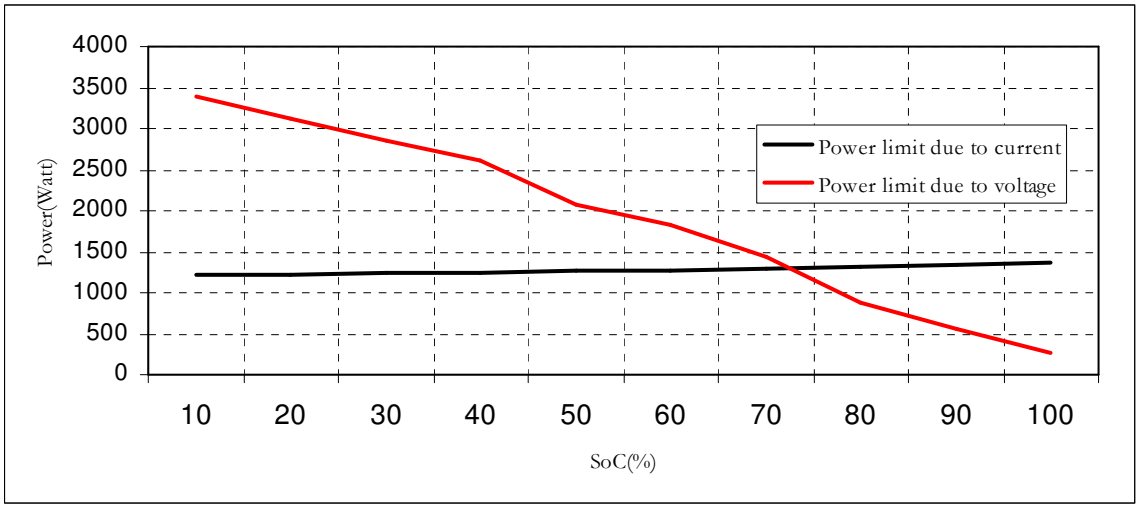

Figure 3.8 Maximum battery charging power due to current and voltage limits

3.15 EV Battery Management

EV battery systems are composed of a number of individual cells with a terminal voltage ranging from 1.2V to 4V depending on the specific battery technology. For an EV application, these cells are required to be connected in a series configuration in order to obtain a higher terminal voltage. For optimum performance, each cell should ideally operate at full capacity. In practice, this is does not always occur due to mismatch in the series string [98]. The battery system performance is degraded relative to the weakest cell. Furthermore, the weakest cell is then subjected to operation abuse by the rest of the batteries. As such, series connected battery packs in EVs require battery monitoring and management systems capable of measuring the voltages of individual battery modules in order to prevent damage and also to identify defective cells.

Excessively high or low voltages can damage virtually all types of batteries, and in some cases the results can be catastrophic. Lithium ion cells, for example, will ignite if they are overcharged, which occurs due to a high voltage across the cell. For all battery systems, the weakest cell in the series configuration causes an over-discharge imbalance problem while the strongest cell could cause an over-charge problem. Once high or low voltage cells have been identified, some equalisation process also must be used to re-balance the voltages. Imbalances are especially prevalent in EVs since the batteries are frequently subjected to

charge and discharge cycles. In Figure 3.10 and Figure 3.11, the terminal voltages and charging currents of 8 Li-Ion battery modules during an experimental charging process are shown. Each battery module consists of 4 Li-Ion cells, creating 16 cells in each series string and 32 cells in total. Each cell requires constant monitoring via a battery management system (BMS). This battery system topology is illustrated in Figure 3.9. In the experiment, Batt06 exhibits a rapid voltage rise compared to the other battery modules. As can bee seen in Figure 3.11, the higher voltage of Batt06 results in a decrease in charging current to its parallel branch (Batt05 to 08). In Figure 3.10 the terminal voltage of Batt06 rises above the maximum value of 14.4V. The BMS detects this and shuts down the charging process to allow the cells to enter a charge equalisation process. Once the BMS detects that the voltage variations between the cells are within the pre-programmed range, the charging process is then continued. As seen, this results in a succession of charging pulses.

The process of allowing the cells to equalise for a given time and then re-establishing the charging current occurs towards the end of the charging process when the batteries are almost at their maximum SoC. It is for this reason that the time required to fully charge (100%) the batteries is longer than the time taken to charge the batteries to nearly maximum SoC (~90%). Following this, a valid point to consider when designing a power and energy management scheme, is that at high SoC, the battery system will be less receptive to high current bursts that occur during regenerative braking events. Although in sensitive battery systems such as Li-Ion, an independent BMS would safeguard the batteries from such an event by means of disconnecting the battery system from the load, factoring this situation as one of the battery operating constraints in a power and energy management system is advantageous. To the power and energy management system, the operating conditions of the battery is not only limited by the battery itself but also by the operating conditions specified by the BMS.

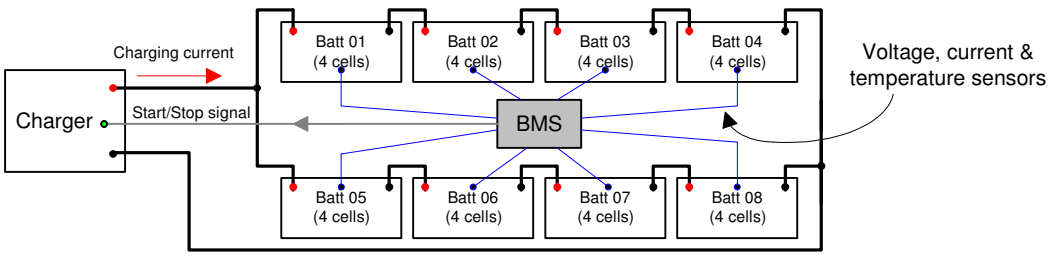

Figure 3.9 8 Li-Ion Battery modules connected to a BMS and charging system

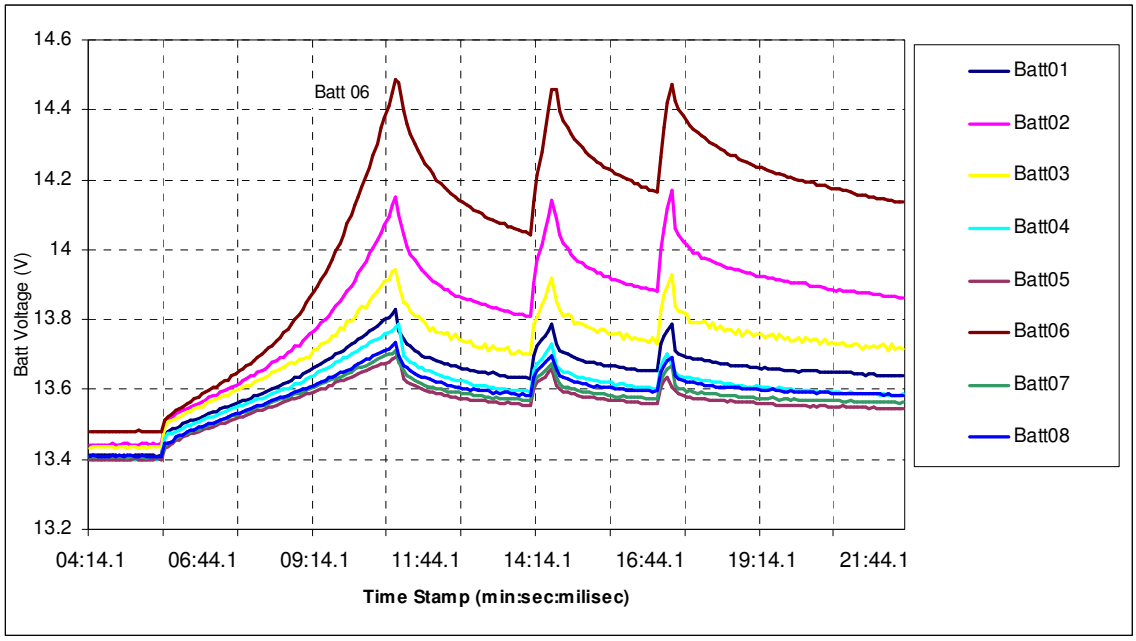

Figure 3.10 Voltage imbalance of 8 Li-Ion Battery modules during a charging process

(The voltage rise of Battery 6 is detected by the BMS, which then stops the charging process to allow cell equalisation)

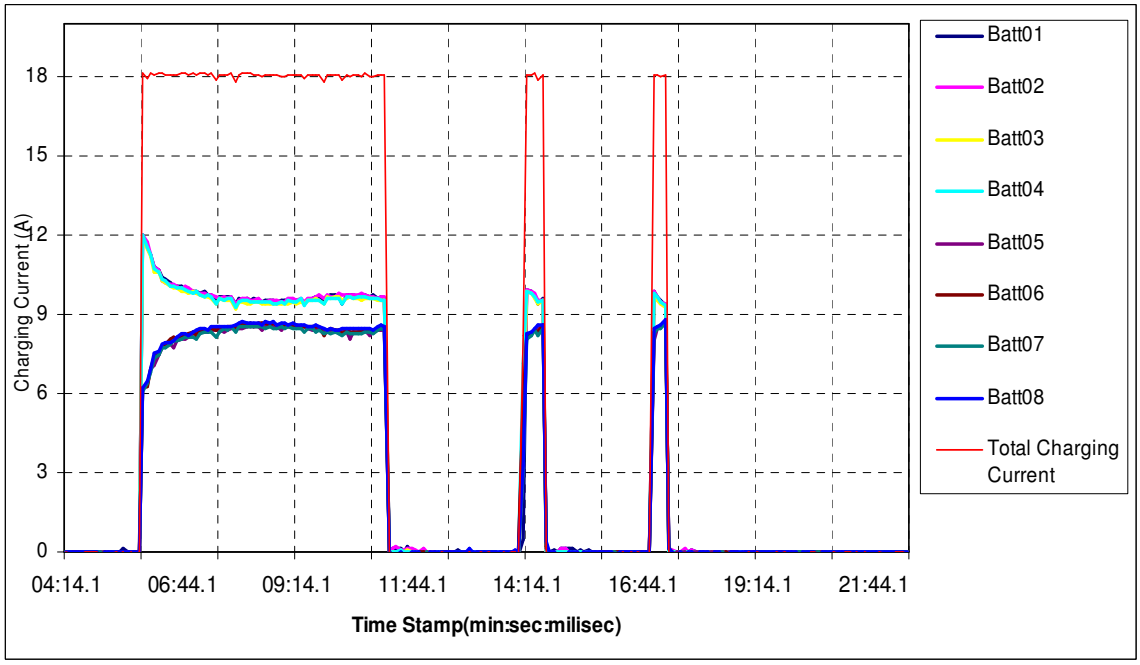

Figure 3.11 Charging current profile of 8 Li-Ion Battery modules

(Batteries 01 to 04 and batteries 05 to 08 are two series blocks connected in parallel to obtain a 4series-2parallel system)

3.16 Extended Battery equivalent circuit models

Depending on the required detail, the circuit model of batteries can represented by simple equivalent circuit consisting of a voltage source in series with an internal resistor or other more complete models based on impedance spectroscopy. Accurate modelling of the dynamical behaviour of electrochemical power sources is an important issue in the simulation of EV power systems. In addition, in practical applications the battery monitoring and battery management systems require some form of dynamic battery models, which are continuously adapted to the battery state. In all applications several issues need to be considered,

- Batteries are not static devices as energy is chemically converted during the discharge and charge process.
- Electrochemical systems are highly non-linear, and this nonlinearity is significant for most power sources under normal operating conditions.
- Their dynamical behaviour depends on many parameters such as temperature, state-of-charge, history of operation, and operating frequency.

Thevenin models

The basic Thevenin-based model shown in Figure 3.12 (a) uses two series resistors, each with a corresponding blocking diode to represent the variation in internal resistance during discharging and charging modes. In Figure 3.12 (b), replacing the voltage source with a bulk capacitor emulates the non-linear open circuit voltage as well as the charge depletion of the battery. Adding an additional series resistor as shown in Figure 3.12(c) to capture the losses during over charging and over discharging increases the accuracy of the battery model but may be excluded if such a condition is protected elsewhere in the system. The effect of self-discharge may be included into the model by adding a parallel resistance branch to the circuit. This is shown in Figure 3.12(d). The Thevenin model of batteries may be refined even further to include much more parameters including temperature effects to produce an even closer representation of the actual intended battery system.

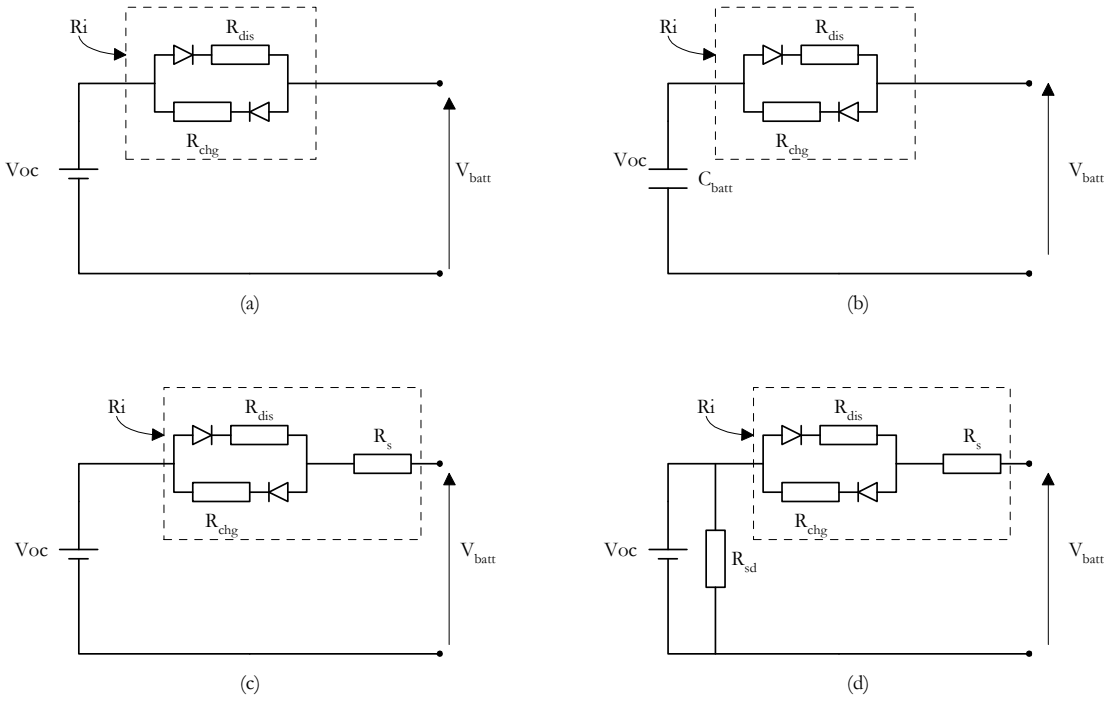

Figure 3.12 Variation of the Thevinin battery circuit model

Descriptions of the model parameters for Figure 3.12 are as follows;

V_{oc} and V_{batt} is the battery open circuit voltage and terminal voltage respectively

R_i is the lumped internal resistance

R_{dis} is the discharge resistance to account for the battery charge release rate

R_{chg} is the discharge resistance to account for the battery charge acceptance rate

R_s is the series resistance that accounts for over discharging and over charging (gassing)

R_{sd} is the parallel resistance that models the self-discharge of the battery

C_{batt} is the capacitor to model the bulk charge instead of a SoC dependent voltage source

Impedance spectroscopy model

Impedance-based models employ the method of electrochemical impedance spectroscopy to obtain an ac-equivalent impedance model in the frequency domain. The model uses complex R-L-C networks to fit the impedance spectra. By impedance spectroscopy measurements,

Surewaard et al.[99] produced an electric circuit representation of a battery model. In the circuit of Figure 3.13, R_i is the battery internal resistance, L_{batt} represents the battery inductance, V_{OC} is the open circuit voltage, R_{gas} and V_{ogas} represent the gassing reactions of the battery. The complex inductance of the model is represented by Z_{Arc1} and Z_{Arc2} and the impedance depression between the semicircles is approximated by the number of RC circuits. Depending on the number of depressions, additional RC circuits can be taken to approximate the battery impedance measurements. Impedance-based models however only work for a fixed SOC and temperature settings [100].

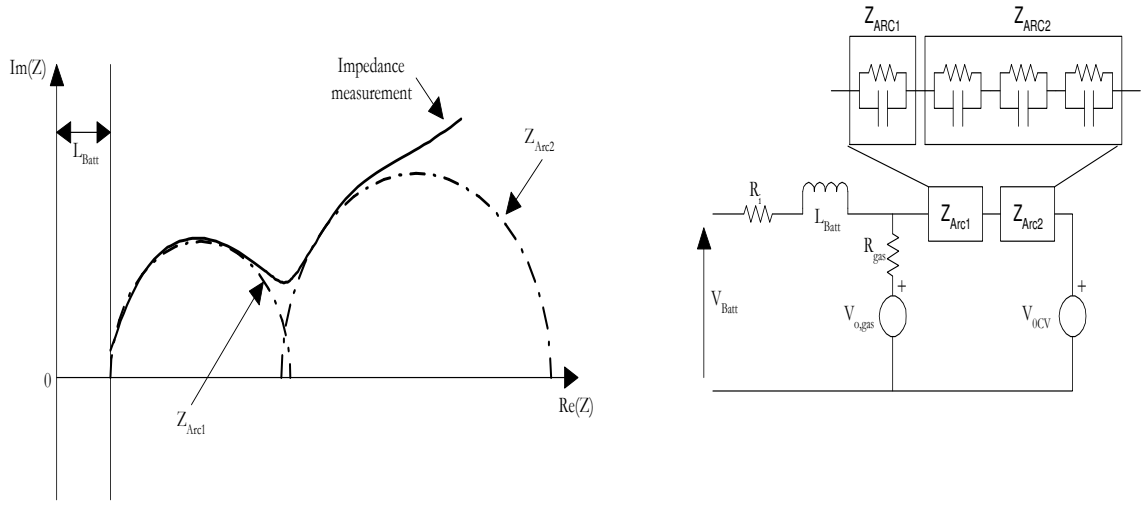

Figure 3.13 Approximation of measured impedance spectroscopy line by electrical elements

(Reproduced from Surewaard et al [101])

VHDL –AMS Model

Battery models can also be defined as a Very high-speed integrated circuit Hardware Description Language (VHDL) entity. The VHDL model permits both long and short term effects of the battery to be included during simulations of extended drive profiles and cycle life. The VHDL battery model used in this work is based on the standard VHDL-AMS (Analog Mixed Signal) entity in the SIMPLORER® [102] simulation package. Table 3-2 shows the VHDL input parameters and the corresponding values that was used to model four VRLA batteries in a series configuration.

Description [Unit]	Parameter ID	Value
Initial Acid Density [g/cm²]	ad0	1.27
Battery Temperature [°C]	temperature	30
Rated Capacity [Ah]	cap	500
Rated Discharge Current [A]	r_curr	250
Rated Discharge Time [h]	r_time	2
Internal Resistance at full charge and nominal temperature [Ω]	nom_res	40m
Number of Cells [/]	num_cells	24
Acid Density at Full Charge [g/cm³]	ad_full	1.28
Acid Density at Complete Discharge [g/cm³]	ad_disc	1.01
Nominal Temperature [°C]	nom_temp	25
Fraction of Capacity at Low Temperature [/]	f_low_cap	0.6
Gain Limit of Capacity at High Temperature [/]	f_hi_cap	1.02
Low Temperature where f_low_cap is Specified [°C]	low_temp	-20
Fraction of Capacity near plate [/]	f_plate_cap	0.3
Capacity Gain in the Slow Discharging Limit [/]	f_slow_cap	1.03
Self Discharge Rate per Day [%/day]	sdpd	0.25
Temperature Dependency of Self-Discharge [°C]	sd_t	16.37
Float Current [A/Ah]	flt_curr	2m
Cell Voltage where Float Current is Reached [V/cell]	flt_volt	2.3
Gassing Threshold Voltage at 25°C [V/cell]	gass_th	2.39
Scaling of Gassing Current with Terminal Voltage [V/cell]	gass_sl	0.2
Temperature Coefficient of OCV [V/cell/°C]	t_coeff_ocv	0.15m
Temperature Coefficient of Full Charge Internal Resistance [1/°C]	t_coeff_res	7.5m
Coefficient for Internal Resistance Variation with SOC	soc_coeff_res	0.5

Table 3-2 VHDL-AMS input parameters of a lead acid battery model

Simulation results of the battery VHDL model and an extended Thevenin model (Figure 3.11 -b) were compared with empirical measurements for model validation. Figure 3.14 presents the comparison of simulated and measured battery terminal voltages. The plots on the left show the comparison with the VHDL model while the plots on the right are the comparisons with the Thevinin model. Both these models produced very similar results and shows good agreement with the measured values. However, the VHDL model proves more accurate as the battery state of charge reduces. As the simulations and experiments were carried out sequentially, the VHDL model shows that it accounts for parameters not considered in the Thevenin model. This can be seen in the fourth comparison set of Figure 3.14. The highlighted region of the graph shows that the VHDL model produces a smaller no-load battery voltage error compared to the Thevenin model. Therefore for extended battery run times, the VHDL model is more accurate. Since the execution time for both

models are very similar (20 seconds in this case), adopting the VHDL model for the rest of this work proved viable.

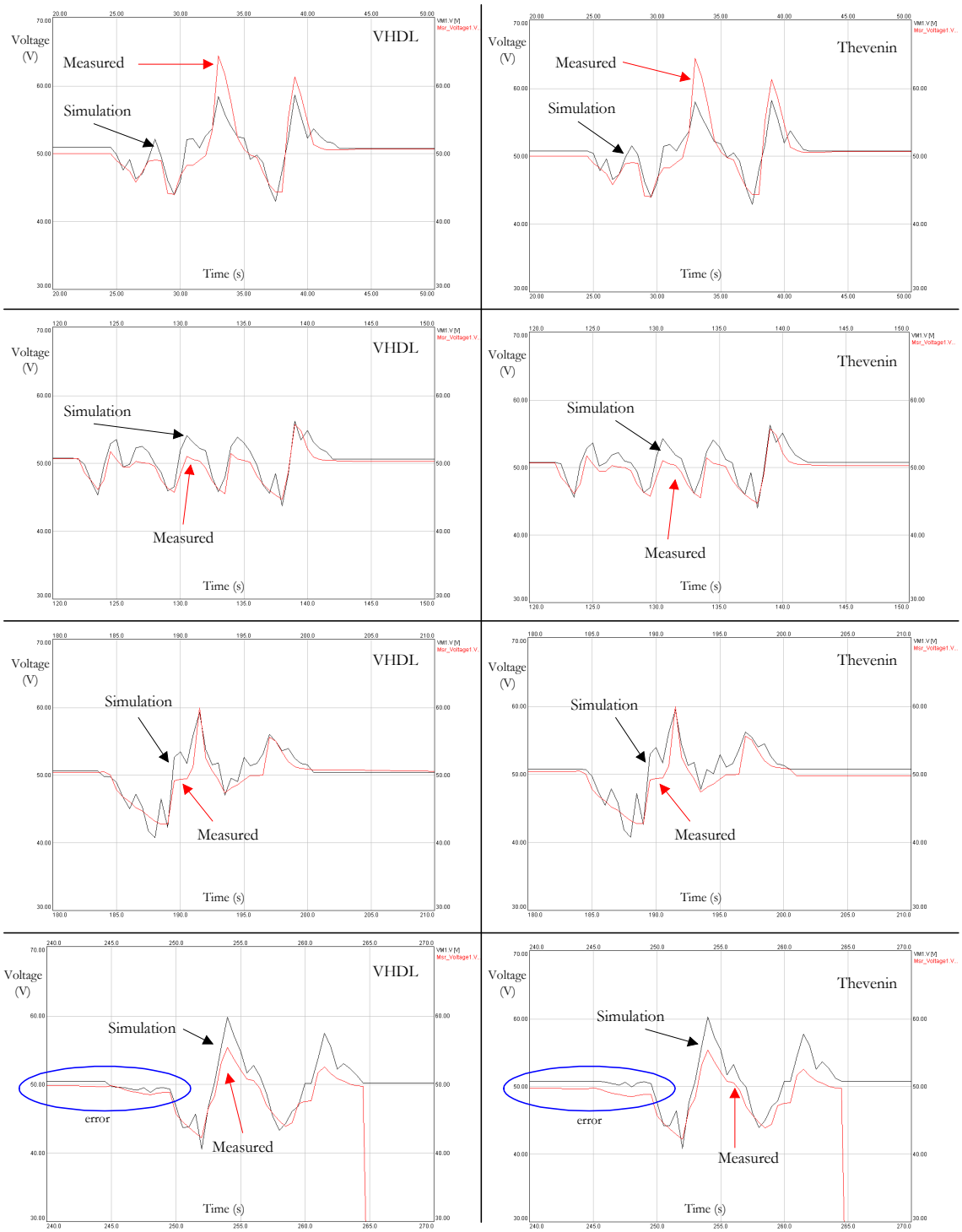

Figure 3.14 Comparison of terminal voltages between VHDL-AMS and Thevinin models against measured values

3.17 Ultracapacitors

Ultracapacitors function as per secondary batteries in terms of storing and delivering energy. However, the charge storage mechanisms itself is very different compared to batteries. As opposed to batteries, which produce electric charge through chemical processes, ultracapacitors store energy in the form of static charge. Since the energy is stored in the same from that it is used, ultracapacitors offer faster charging and discharging rates compared to batteries of similar volume. The energy densities of ultracapacitors are however comparatively less than that of batteries by a factor of 10 to 20 [40]. As such, ultracapacitors are not substitutes as secondary batteries but rather regarded as complementary power delivery device. Having a high power density enables ultracapacitors to be employed in a complementary manner with high energy density secondary batteries to form hybrid energy storage systems.

An ultracapacitor cell construction consists of two electrodes, a separator, and an electrolyte as illustrated in Figure 3.15. The electrodes consist of two parts, a metallic current collector and a high surface area active material. A membrane called the 'separator' separate the two electrodes. The separator permits the mobility of charged ions but prohibits electronic conduction. This composite is subsequently rolled or folded into a cylindrical or rectangular form and stacked in a container. Then the system is impregnated with an electrolyte, which is either a solid state, organic or aqueous type. The decomposition voltage of the electrolyte determines the maximum operating voltage of an ultracapacitor. Owing to the very small separation distance between the electrolytes, as well as the large effective surface of the active material, large capacitance magnitudes in terms of Farads are obtainable. The magnified insert in Figure 3.15 illustrates the large surface area of the active material.

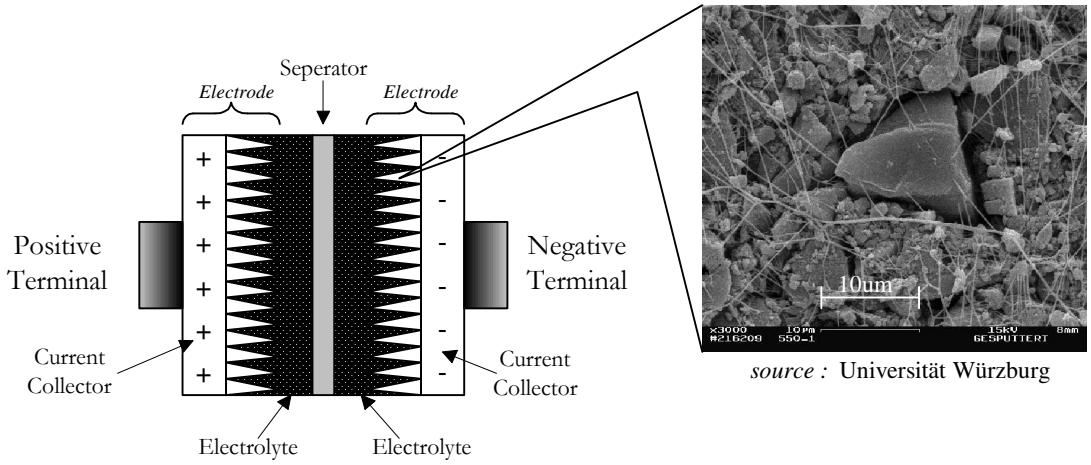

source : Universität Würzburg

Figure 3.15 Basic cell construction of an ultracapacitor

Ultracapacitors are not constrained to the same physical limitations as dielectric capacitors. The discharge characteristics and equivalent circuits of ultracapacitors are similar to conventional low farad capacitors but there are some fundamentally different properties between the two types. The large capacitance ultracapacitors arise from the very large specific area obtainable from the use of porous nano-carbon materials. Based on charging and discharging the interfaces of high specific-area materials such as porous carbon materials or porous oxides of some metals, these devices are able to store and releases immense amounts of electric charge and corresponding energy at high densities (expressed in Wh/kg). Hence, they can be operated at specific power densities (expressed in W/kg) higher than batteries [103]. In addition, their capacitance for a given physical size of the device is much higher to electrolytic capacitors. Comparing a 350F - 2.5V ultracapacitor (Maxwell BCAP 0350F, length = 62mm, diameter = 33mm, weight = 60g) with a 2200μF –100V electrolytic capacitor (Evox-Rifa PEH200, length = 60mm, diameter = 35, weight = 85g) shows that the energy density of the ultracapacitor is approximately 140 times greater than the electrolytic capacitor. For this reason proprietary terms such as *Ultracapacitors* and *Supercapacitors* have been used to describe the high-energy storage capability of these devices.

A significant difference between charging and discharging an ultracapacitor compared to charging and discharging a battery system is that there is always an intrinsic increase in

voltage on charge and a decrease in voltage on discharge of ultracapacitors [43]. In contrast, an ideal battery system exhibits a fairly constant voltage during discharge and recharge except when the state of charge approaches its extremes. The high degree of reversibility of charge acceptance and delivery, and hence its capability for excellent operating power levels compared with batteries of comparable size arises because there is no slow chemical processes between charge and discharge. Ultracapacitors also demonstrate cycle lives up to one million under suitable conditions [5]. This is because only storage and delivery of electrostatic charge takes place at the extended two-dimensional interface of high-area materials. No slow chemical phase changes take places within the ultracapacitors as does in the three-dimensional chemical materials within secondary batteries.

3.18 Ultracapacitor Modelling

At present, there are several propositions of ultracapacitor model representation [99]. The simplest of all is the classical equivalent circuit with the lumped capacitance, equivalent parallel resistance (EPR) and equivalent series resistance (ESR). Figure 3.16 shows the classical equivalent circuit with the three parameters. Determination of these parameters provides a first approximation of an ultracapacitor cell.

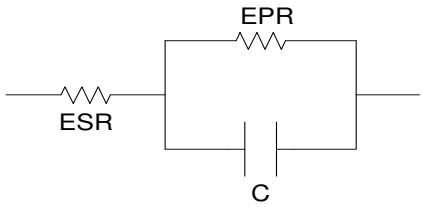

Figure 3.16 Classical equivalent circuit of an ultracapacitor

The EPR represents the current leakage and influences the long-term energy storage. In multiple series connections of ultracapacitors, the EPR influences the cell voltage distribution due to the resistor divider effect. Using empirical methods, Sypker and Nelms [104] showed that the EPR is related to the voltage decay ratio by,

$$EPR = \frac{-t}{\ln\left(\frac{V_2}{V_1}\right)C} \qquad (3\text{-}32)$$

where V_1 is the initial voltage, V_2 is the final voltage and C is taken as the rated capacitance. Through experimental measurements of voltage decays of several ultracapacitors having various capacitance values, it was shown that the EPR effects could be neglected for transient discharge calculations. However, the EPR value is important when cell balancing of series connected ultracapacitors is considered. Section 3.8 describes cell balancing in more detail. Examining the ESR effects, further empirical verifications by Sypker and Nelms [105] showed that this parameter has not significantly dependent on the terminal voltage nor the charge rates. Hence the ESR can be considered as a non time dependent parameter.

Describing a more detailed terminal representation model, Zubieta and Bonert [106] proposed and investigated a three RC branch network with one branch having a voltage dependent capacitance. Each branch of the circuit shown in Figure 3.17 has a different associated time constant. The authors [106] assigned the first branch, containing R_i as the "immediate branch". This branch dominates the ultracapacitor behaviour in the order of a few seconds. The "delayed effect branch", with R_d has influential behaviour in the range of minutes. The third branch is the "long-term" branch. This branch governs the long-term response of the circuit after periods exceeding ten minutes. Finally, the branch with resistance R_{Leak} represents the ultracapacitor leakage current. The "immediate branch" contains a voltage dependent capacitor C_{i1} that reflects the voltage dependency of the cells double-layers capacitance

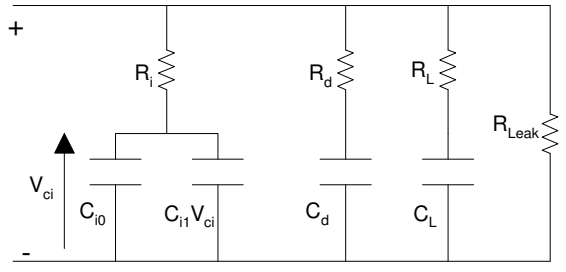

Figure 3.17 Brach representation ultracapacitor model
(Reproduced from Zubieta and Bonert's [106])

As with the battery model, Surewaard et al.[99] and Buller et al.[100] investigated a ultracapacitor equivalent circuit though impedance spectroscopy measurements. The mathematical expression for $Z_{pore}(j\omega)$ has only two independent parameters (C, t). Including L and R_i, only four parameters have to be extracted from the measured spectra. The graph of Figure 3.18 shows a comparison between the measured impedance data and the simulated data obtained using the circuit model. In the depicted frequency range the best approximation shows nearly perfect agreement with the measured data.

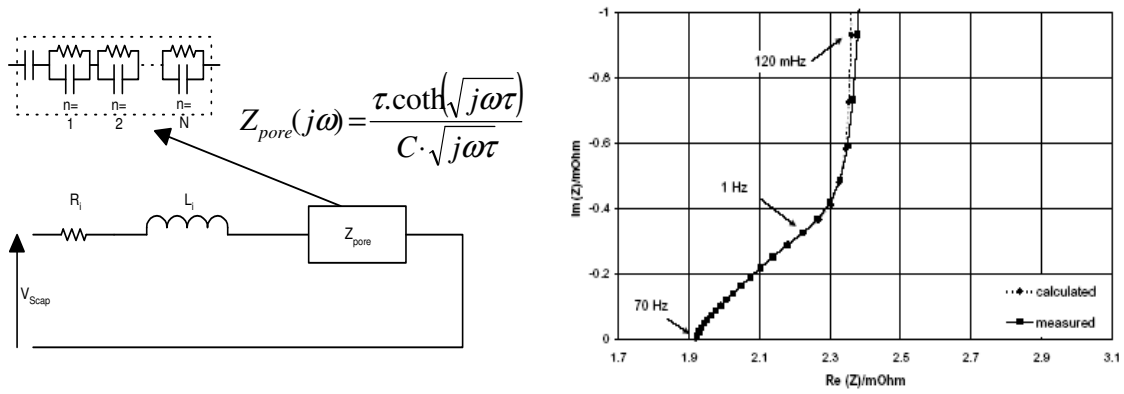

Figure 3.18 Ultracapacitor model through impedance spectroscopy

(Graph reproduced from Buller et al.[100])

The nonlinearity of high 'C' capacitors must be considered in the ultracapacitor model as it has significant influence in the estimation of the exploitable energy. Vermillion [107] investigated the non-linearity of the ultracapacitor RC time constant and found that the 'time constant' of ultracapacitors is in fact 'not constant'. A complete derivation can be found in [107], however the final solution is reproduced here to show comparison of the time constant difference between a dielectric capacitor and a ultracapacitor.

$$t = \frac{2}{c}\left[\sqrt{b^2 - cq_0} - b - \sqrt{b^2 - cq} + b\ln\frac{b - \sqrt{b^2 - cq_0}}{b - \sqrt{b^2 - cq}}\right] \qquad (3\text{-}33)$$

where,

$$b \equiv \frac{C_0}{2\alpha R}\ , \qquad c \equiv \frac{1}{\alpha R^2}\ , \qquad C = C_0 - \alpha V = \frac{q}{V}$$

V is the voltage across the ultracapacitor, C_o is the static capacitance at zero voltage, α is an empirically determined constant and q is the stored charge

Currently, more complex models are being investigated to capture other long-term effects such as charge leakage and temperature parameters. However, if the required observation of the model and the actual practical usage of the ultracapacitor is only for relatively of short cyclic periods, a more simplified equivalent circuit is sufficient as leakage resistance and other long-term steady state losses may be negligible.

3.19 Ultracapacitor Power and Energy

Sizing of an ultracapacitor system requires the specification of the power and energy requirements. For a fixed ultracapacitor bank, these quantities dictate the number of ultracapacitors needed but do not represent the same constraints [108]. The minimum number of ultracapacitors needed is determined by the energy profile that the supercapacitive bank has to assume. However, due to the voltage decay property of ultracapacitors, not all the stored energy can be utilised. Therefore the sizing is based on the usable energy that the ultracapacitor bank can transfer. Following this, the usable energy can either be consumed very fast or throughout a long period. How fast the energy can be extracted determines the power constraint.

The fundamental electrical equations defining an ultracapacitor are:

$$i = C\frac{dv}{dt} \qquad (3\text{-}34)$$

$$E = \frac{1}{2}Cv^2 \qquad (3\text{-}35)$$

The energy capacity, E of an ultracapacitors is directly proportional to the square of its voltage magnitude, which decays over time. Therefore the available energy of an ultracapacitor bank during discharge follows;

$$E\Big|_{k}^{k+1} = \frac{1}{2}C(V_{(k)}^2 - V_{(k+1)}^2) \tag{3-36}$$

As shown in 3.36, the usable energy of an ultracapacitor bank depends on the minimum to maximum allowable voltage ratios. Defining V_{max} as the maximum terminal voltage and V_{min} as the minimum voltage, a voltage discharge ratio, *vdr* in percentage is defined as,

$$vdr = \frac{V_{\min}}{V_{\max}}100 \tag{3-37}$$

and the usable energy follows;

$$E_u = \frac{1}{2}CV_{\max}^2 - \frac{1}{2}CV_{\min}^2 = \underbrace{\frac{1}{2}CV_{\max}^2}_{E_{\max}}\left(1-\left(\frac{vdr}{100}\right)^2\right) \tag{3-38}$$

where E_{max} is the maximum stored energy and E_u is the usable energy

For a ultracapacitor bank having *n* identical ultracapacitors, the total usable energy E_{Tu} is

$$E_{Tu} = nE_u \tag{3-39}$$

Therefore for a given energy specification, the number of ultracapacitors required can be found by using (3.38) and (3.39) to obtain,

$$n = \frac{2E_{Tu}}{CV_{\max}^2\left(1-\left(\frac{vdr}{100}\right)^2\right)} \tag{3-40}$$

Using (3.40), the following was computed for various *vdr* values to obtain the corresponding number of 2600 F ultracapacitor required for a usable energy level of 50 kJ. The graph in Figure 3.19 shows the plot of ultracapacitor cell numbers versus the voltage discharge ratio, *vdr*. The graph and table shows that a large number of ultracapacitors in parallel is required to maintain a high voltage discharge ratio. Although the storable energy increases with the number of ultracapacitors in parallel, the usable energy is constrained by the allowable voltage deviation during discharge.

vdr(%)	*n* (rounded up)	Actual Stored Energy (kJ)
50	9	73.125
60	10	81.250
70	13	105.625
80	18	146.250
90	33	268.125

Parameters

C = 2600 Farad

V_{max} = 2.5V

E_{Tu} = 50kJ

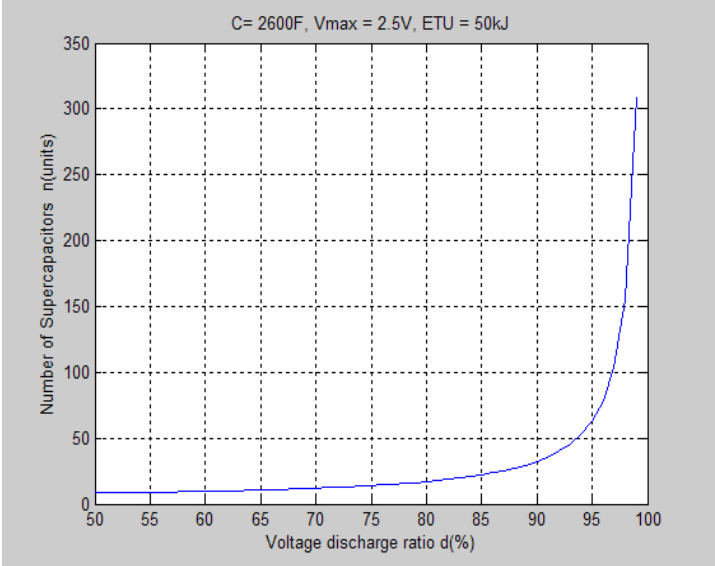

Figure 3.19 Ultracapacitor cell number dimensioning for usable energy

The determination of required number of ultracapacitors from the above derivation was obtained based on energy requirements only. From simulations, it is seen that for a voltage discharge ratio of 90%, the number of ultracapacitors required is 33 units. Although the actual stored energy of the 33, 2600F ultracapacitors is 286.12 kJ, the usable energy at (*vdr*=90%) is only 50 kJ(13.9Wh). The usable energy criterion has also been expressed in terms of energy quality [47]. Depending on the physical reaction properties (faradic depositions) within the ultracapacitors' double layer construction, the energy quality can differ. Huggins [47] showed that this energy quality value could range form 37.5% to 90%.

3.20 Ultracapacitors in series

Developments in ultracapacitor design and fabrication have led to the achievement of high specific energy density and high power density devices with capacitance values in the magnitude of several hundred Farads having equivalent series resistance (ESR) of less than 1 milliohm (DC measurements). Although high in capacitance value, the achievable single unit ultracapacitor voltage is at present limited to 2.5V. This cell voltage depends on the breakdown voltage of the electrolyte used in the ultracapacitor construction. Organic electrolytes have a higher dissociation voltage (typically 2V to 2.5V) and are most commonly used in commercially available ultracapacitors. Aqueous electrolytes exhibits lower resistance but have a lower cell voltage, typically 0.9V.

To obtain a higher working voltage as required in an electric vehicle application, ultracapacitors are commonly connected in series to form a fixed capacitor bank with a lower total capacitance but higher terminal voltage. Several publications [60, 82, 83, 109] have shown the implications and design methods of a series ultracapacitor energy storage bank in electric vehicles.

There is a fundamental problems associated with multiple series connections of ultracapacitors. Voltage balancing between series connections is crucial in order to prevent cell destruction and also to utilise maximum energy storage capability. With reference to the series connection of *n* number of ultracapacitors as shown in Figure 3.20, the following equation expresses the unequal voltage distribution effect.

$$Vc_x = V_{bus}\left(\frac{k \cdot Rc_x}{Rc_1 + ... + Rc_n} + \frac{(1-k)\cdot 1/C_x}{1/C_1 + ... + 1/C_n}\right) \tag{3-41}$$

where $0 \le k \le 1$

From the state of completely discharged (*t=0*), the capacitors (C_1 to C_n) are charged from 0 volts. During the charge cycle, *k* has a value of 0 and the voltage distribution between the ultracapacitors is dependent on the variation of capacitance. After settling time when

$t \to \infty$, k= 1 and the voltage distribution then is predominately influenced by the parallel resistances.

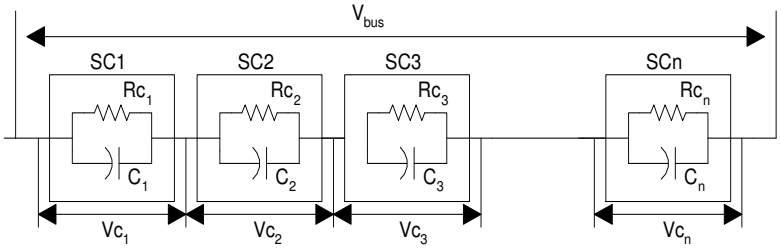

Figure 3.20 Ultracapacitor cells in series

Using exaggerated equivalent parallel resistance values to demonstrate the cell voltage equalisation phenomena, the following circuit comprising of four ultracapacitors was simulated. In Figure 3.21, four Maxwell PC1000 Ultracapacitors with capacitance values of 1000 Farads were pre charged to a maximum terminal voltage of 2.5V and then disconnected from the voltage source.

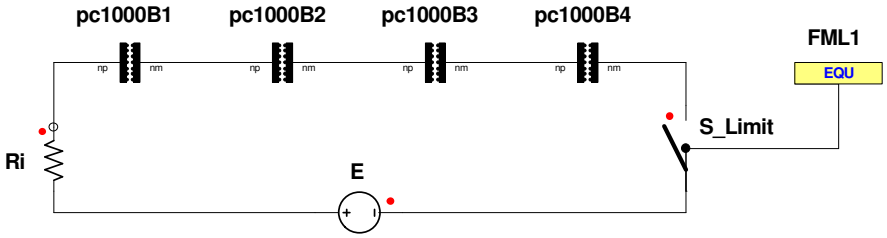

Figure 3.21 Ultracapacitor in series simulation model

The simulated voltage discharge curves shown in Figure 3.22 exemplify the voltage variation problem. Because of the uneven voltage effect each ultracapacitor in the fixed series network must withstand the highest terminal voltage expressed by equation (3.40).

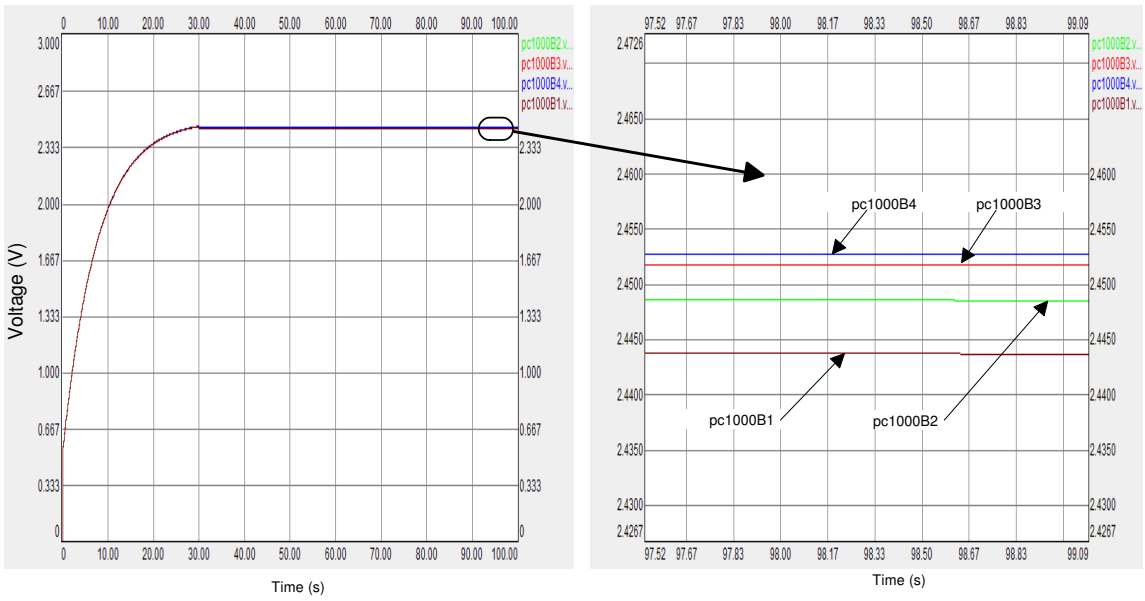

Figure 3.22 Simulation results showing voltage deviation of four Ultracapacitor in series

In order to prevent voltage imbalance, various passive and active voltage balancing techniques have been suggested. Passive voltage balancing uses voltage dividing resistors in parallel with each ultracapacitor to allow current to flow around higher voltage ultracapacitors into lower voltage devices, thus balancing the voltage. Linzen et al. [82] considered four equalisation methods and examined the performance benefits and reliability of the different configurations shown in Figure 3.23.

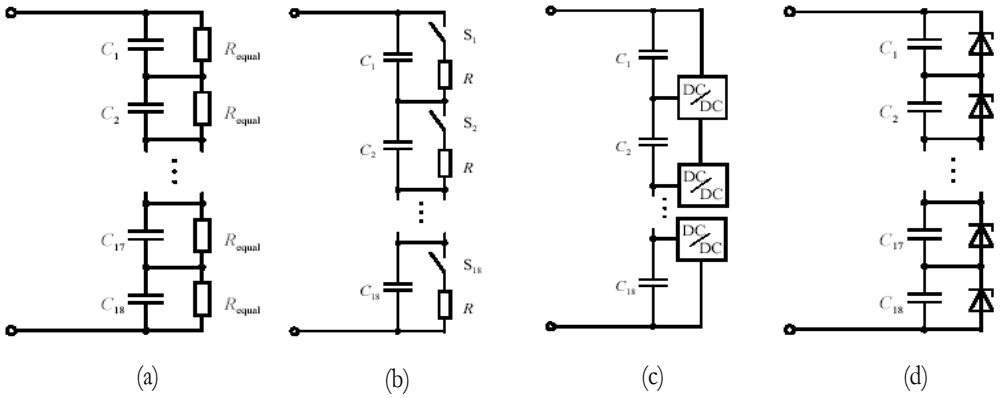

Figure 3.23 Series cell equalisation methods

(Reproduced from Linzen [82])

In the circuit configurations of Figure 3.23 (a) and (d) are passive cell balancing methods. The main disadvantage of circuit (a) is the high power losses of the external resistors. In circuit (d), the Zener diodes also exhibits power losses but the dominant disadvantage in this set-up is the strong temperature dependency of the Zener voltage, an effect that is not tolerable in vehicular applications. The switched resistor method in (b) is an active balancing method that places a bypass resistor across the cells when the cell voltage exceeds a pre-defined value. This method however requires the individual measurement of each cell in the series network. A more complex active balancing method is the use of DC/DC converters connected across neighbouring cells, Figure 3.23(c). The authors of [82] claimed that although the efficiency of this method is high, the hardware and the control systems would be too complicated and costly to implement. Miller and Everett [58] introduced a non-dissipative cell equaliser circuit. Their patent pending design shown in Figure 3.24 is able to transfer 300mA between adjacent pairs of cells in a 14V module containing a string of six ultracapacitors.

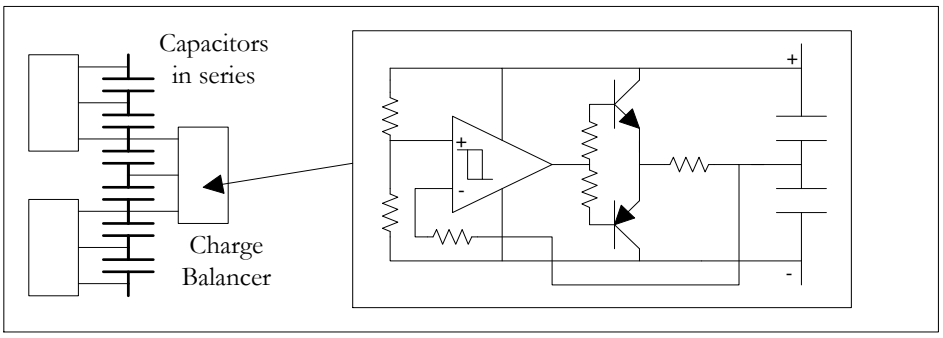

Figure 3.24 Cell balancing technique-Maxwell Technology

(Reproduced from Miller and Everett [58])

3.21 Hybridisation of Batteries and Ultracapacitors

The following simulation demonstrates that the mitigation of peak power required for vehicle launch assist to an appropriately sized ultracapacitor bank permits the usage of a lower capacity battery pack in the design. This related to an overall weight reduction in the power delivery unit.

System parameters:
Terminal Voltage: 60V
Peak Current: 83A
Battery Pack : Sealed Lead Acid Type, 10Ah & 17Ah
Ultracapacitor : 2600F, 2.5V, 0.47kg

Considering the simple load profile (load current) shown in Figure 3.25, the first simulation subjects the battery to the entire profile. This was done using a 10Ah 1hour battery pack with a total battery pack weight of 19.8 kg. Figure 3.26 shows the battery current tracing the load demand. The variation in the load demand and the battery supply is due to the fixed voltage reference used in the simulator and the ESR effect of the battery model. Note that the end State of charge is approximately 40%.

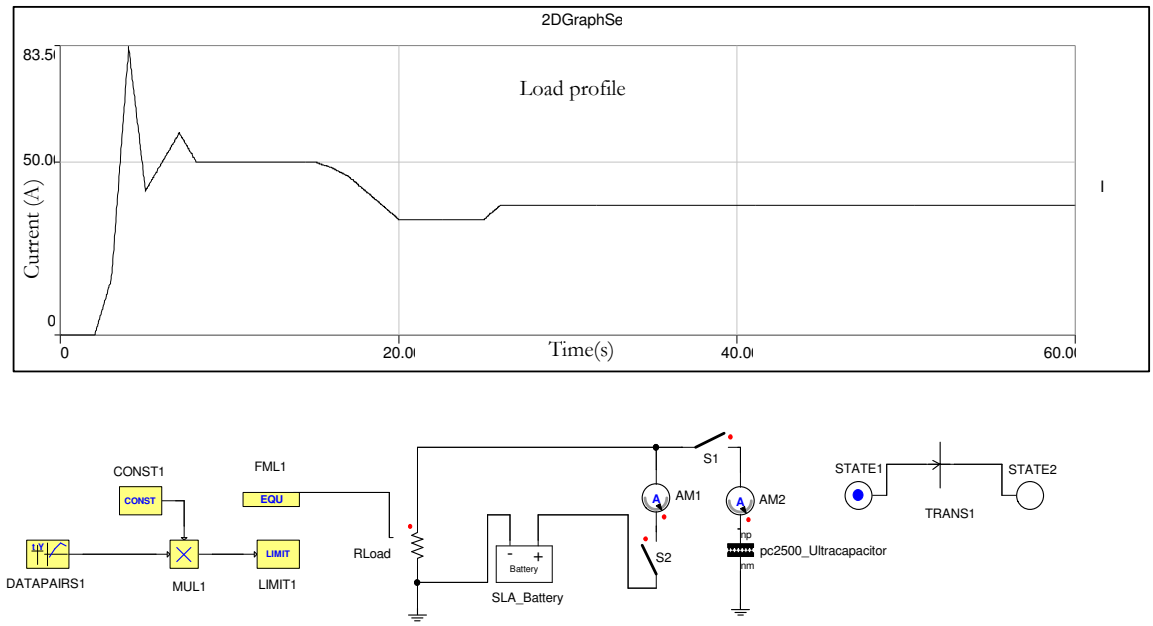

Figure 3.25 Battery and ultracapacitor VHDL-AMS simulation model and test load profile

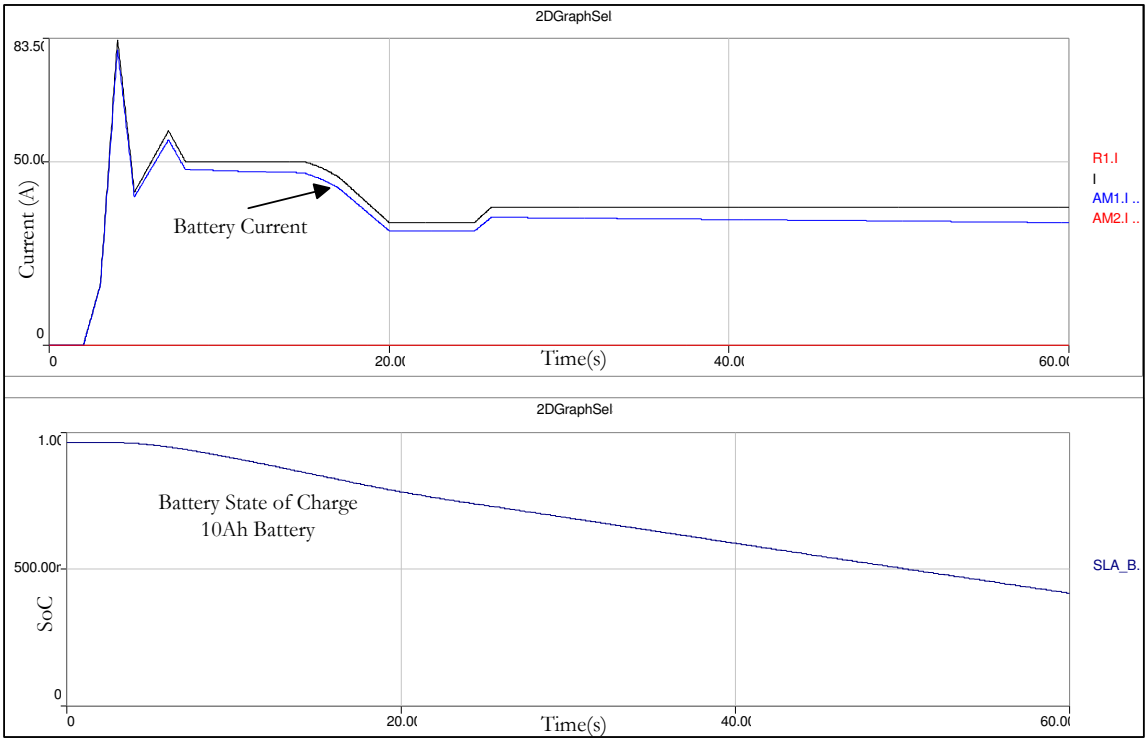

Figure 3.26 Battery current and SoC plot for a specific load demand profile

Following this, the 10Ah Battery is augmented with an ultracapacitor pack to service the peak demand load demand. The ultracapacitor bank consists of 24 units in series to achieve the required terminal voltage. The total weight of the hybrid energy system resulted in an increase to 31.2 kg of energy storage system mass. The current delivery segmentation between the battery and ultracapacitor is shown in Figure 3.27. The battery pack 'end state of charge' is approximately 75% in this case.

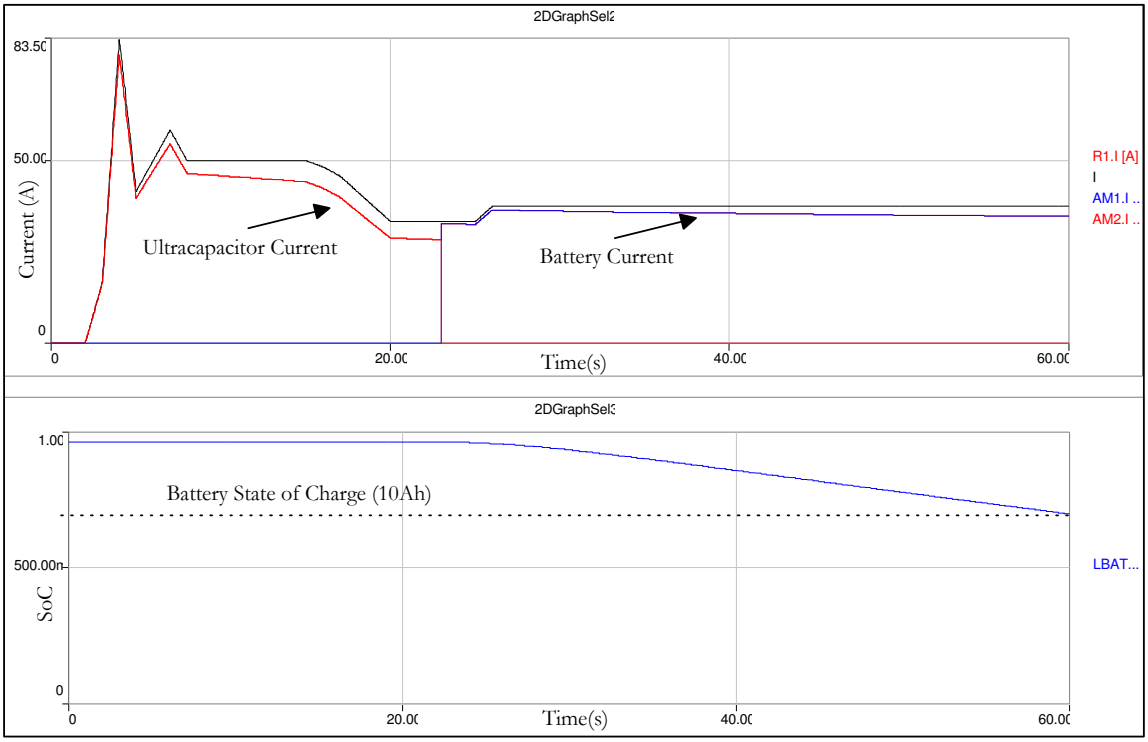

Figure 3.27 Peak power mitigation to an ultracapacitor system.

To obtain the same 'end state of charge' as the above hybrid energy system using only a battery pack, a larger capacity battery pack is therefore required. Simulations indicate that a 15Ah 1-hour battery pack with a total mass of 34.2 kg is required to match the end remaining capacity of the battery-ultracapacitor hybrid system (31.2 kg). Figure 3.28 shows the current and state of charge of the larger capacity battery system. The similarity in required capacity is made by assuming that since the 10Ah battery discharges to 75% SoC in the hybrid configuration, a 15Ah battery is allowed to discharge to 50% SoC at the end of the test cycle to justify the comparison. With this simple load profile alone, the effective of a battery-ultracapacitor hybrid energy system is justifiable. As discussed earlier, the consequence of operating the battery system at high power levels results in a decrease in sustainable energy. For this reason, the mitigation of peak powers to a supplementary energy system such as the ultracapacitor does prove constructive.

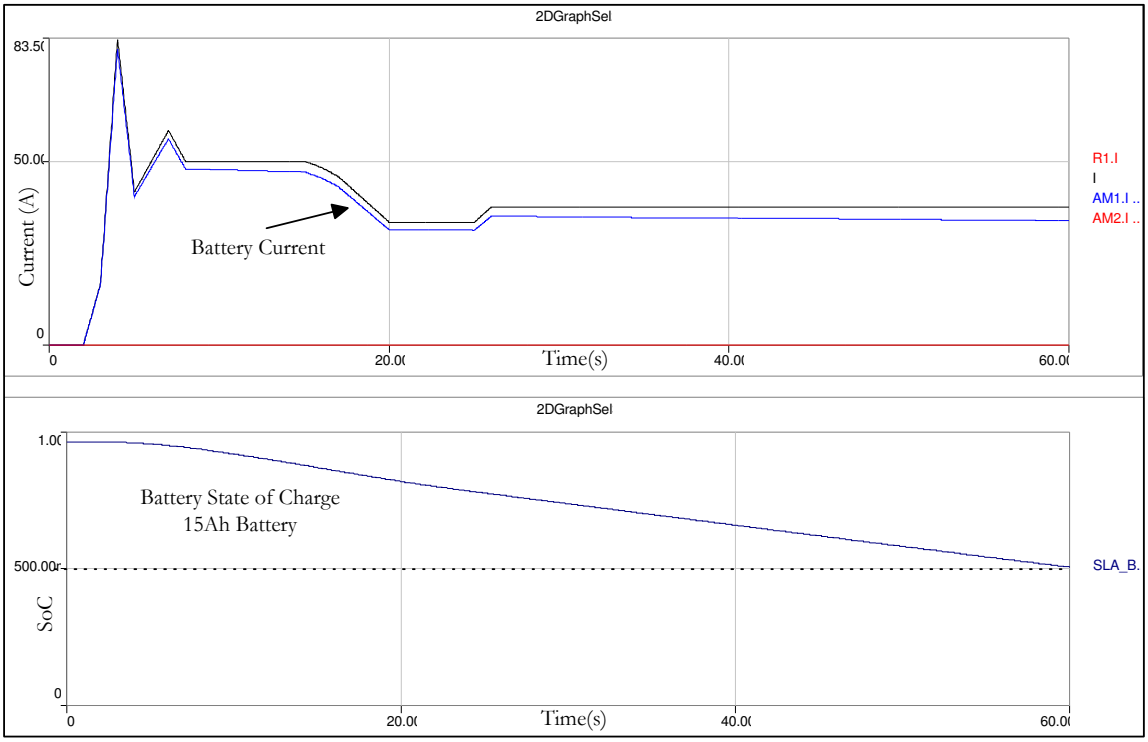

Figure 3.28 Battery current and SoC plot for a higher capacity battery pack

3.22 Summary

In order to manage the energy expenditure of both batteries and ultracapacitors as energy systems, it is essential to be able to measure the energy content of both systems. The methods discussed in this chapter showed how the estimation of the battery and ultracapacitor state of charge is performed. As far as electric vehicle energy management is concerned, the accuracy of these estimations influences the autonomy of the vehicle. Comparatively, determining the SoC of ultracapacitors is less demanding as oppose to batteries. Although long-term SoC deviations do occur in ultracapacitors due to the effect of the long-term impedance branches, these effects are minor since the ultracapacitors are used for successive peak power delivery rather than long-term energy storage. As such, monitoring the voltage of the ultracapacitors provides a good estimate of the ultracapacitor SoC.

In section 3.11, it was shown that the estimation of the batteries using Peukert's equation is acceptable as long as the batteries are not operated at high power rates. In fact, Peukert's equation was developed to estimate battery capacity under constant current discharge [110]. However, for a strategic power and energy management system that limits the power delivery of the batteries, the use of this estimation technique is justifiable but by no means ideal.

From the understanding on battery behaviour and operating limitations stems the knowledge that an increase in both the energy efficiency and battery life can be expected if the battery ideal operating constraints are followed. This translates to operating the battery system within some operating boundaries and mitigating peak powers and high power discharges to the ultracapacitors. For the battery system, parameters that need to be considered are the battery discharging power limit, the charging power limit, the rate of discharge and the rate of charging.

The simulation of hybridising batteries and ultracapacitors showed that the mitigation of peak powers to the ultracapacitors results in a weight reduction in comparison to a battery – only system. Although the simulation only divides the power demand into two segments with no active power blending performed, it does demonstrate and support the grounds of a battery-ultracapacitor system for loads having large peak to average power ratios. The next chapter discusses the power and energy demands of a typical electric vehicle and follows to presents a further case study of hybridising batteries and ultracapacitors.

CHAPTER 4

ELECTRIC VEHICLE POWER AND ENERGY REQUIREMENTS

" Truth is ever to be found in the simplicity, and not in the multiplicity and confusion of things"
Isaac Newton, 1642-1727

This chapter describes the power and energy requirements of land based electric vehicles. The various operating modes that the vehicle is subjected to throughout a mission profile are presented in order to analyse the instantaneous tractive power requirements and net energy expenditure. To approximate the power and energy requirement parameters, the longitudinal dynamics of the vehicle is examined. The derivations of parameters that influence the vehicle tractive efforts are based on Newton's second law of motion. After describing the vehicle kinetics, an empirically validated vehicle model developed using SIMPLORER® is presented. Using this vehicle model, two industry standard drive profiles followed by a modified drive profile are examined to illustrate the effect of arbitrating power flow for a battery and ultracapacitor energy storage system. Using a VHDL-AMS model for the battery system and a simplified first order model for the ultracapacitor system, simulations are presented to show the segmentation of a vehicle power demand spectrum.

4.1 Vehicle Longitudinal Dynamics

For any mission profile, an electric road vehicle is subjected to forces that the onboard propulsion system has to overcome in order to propel or retard the vehicle. These forces are composed of several components as illustrated in Figure 4.1 .The effort to overcome these forces by transmitting power via the vehicle drive wheels and tyres to the ground is known as the total tractive effort or total tractive force (F_{TR}).

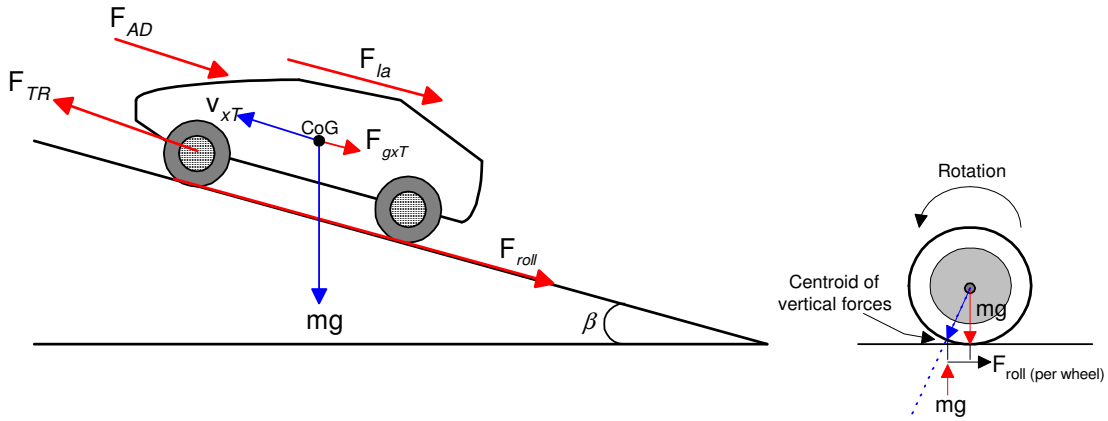

Figure 4.1 Vehicle longitudinal forces representation

The total tractive force expressed as a composition of forces is,

$$F_{TR} = F_{la} + F_{gxT} + F_{roll} + F_{AD} \tag{4.1}$$

where F_{la} is the linear acceleration force, F_{gxT} is the gravitational force acting on the vehicle on non-horizontal roads, F_{roll} is the rolling resistance force, and F_{AD} is the aerodynamic drag force.

Linear acceleration force , F_{la}

The linear acceleration force is derived from Newton's second law of point mass motion and is expressed as,

$$F_{la} = m \frac{d}{dt} v_{xT} (dt) = ma \tag{4.2}$$

where a is the linear acceleration of the point mass m travelling at a varying tangential velocity v_{xT}.

Gravitational force , FgxT

The gravitational force depends on the slope angle of the road in respect to the horizon. This forced is induced by gravity when the vehicle travels on a non-horizontal plane. A climbing mission of the vehicle results in a positive force while a descending mission results in a negative force. This force is expressed as,

$$F_{gxT} = mg \sin \beta \tag{4.3}$$

where the vehicle inclination angle β is expressed in radians, m is the total vehicle mass and g is the acceleration due to gravity (9.81m/s^2).

Rolling resistance force, F_{roll}

With reference to the diagram on the right side of Figure 5.1, F_{roll} is produced by the hysteresis of the tyre at the contact surface with the roadway. When the tyre rolls, the centroid of vertical forces on the wheels move forward from beneath the axle towards the direction of motion of the vehicle. The weight acting on the wheel and the road normal forces are misaligned and thus exert a retarding torque. This force opposes the rotation of the wheel and is expressed as,

$$F_{Roll} = \text{sgn}[\, v_{xT} \,] mg \, (C_0 + C_1 v_{xT}{}^2) \tag{4.4}$$

where sgn[V_{xT}] is a the signum function of the vehicle tangential velocity, V_{xT} and is given as,

$$\text{sgn}[\ v_{xT}\ ] = \begin{cases} 1 & if\ v_{xT} \geq 0 \\ -1 & if\ v_{xT} \leq 0 \end{cases} \quad (4.5)$$

C_0 and C_1 are rolling resistance coefficients. Typical values of C_0 ranges between 0.004 and 0.002 [1], while typical C_1 values are several magnitudes less than C_0.

Aerodynamic Drag Force, F_{AD}

The aerodynamic drag force, F_{AD} acting on a vehicle is due to the viscous friction of the surrounding air acting on the vehicle surface and the pressure distribution induced by the downwash of trailing vortices behind the vehicle. The force opposes the motion of the vehicle and is influenced by the frontal area, shape and protrusions of the vehicle shell design. As there are multiple factors that contribute to this resistive force, it is commonly approximated using a prismatic vehicle body with a frontal area. The stagnation pressure caused by the product of the frontal area and ambient air density is multiplied by a constant drag coefficient. The total aerodynamic drag force is then expressed to include the vehicle and headwind velocity as,

$$F_{AD} = \text{sgn}[v_{xT}]\left\{0.5\rho C_D A_F (v_{xT} + v_0)^2\right\} \quad (4.6)$$

where ρ is the air density in kg/m^3, C_D is the aerodynamic drag coefficient, A_F is the vehicle equivalent frontal area in m^2 , V_{xT} and v_0 are the vehicle tangential velocity and head wind velocity respectively and are in m/s. The air density parameter ρ is temperature, altitude and humidity dependent. However, a value of 1.25kg/ m^3 for ρ is typical. For accurate values of the aerodynamic drag C_D , the use of wind tunnels or CFD simulations are required. Typical figures of C_D for passenger vehicles ranges from 0.19 to 0.3 [95] and 0.8 to 1.5 for larger vehicles such as busses and trucks [2].

4.2 Vehicle Propulsion Power Demand

With the tractive force $F_{TR,}$ the instantaneous tractive power can be expressed as,

$$P_{TR}(t) = F_{TR}(t) \cdot v_{xT}(t) \tag{4.7}$$

where F_{TR} can be expressed as the sum of the forces described in the previous sections as,

$$F_{TR} = ma + mg\sin\beta + \text{sgn}[v_{xT}]mg(C_0 + C_1 v_{xT}^{\ 2}) + \text{sgn}[v_{xT}]\{0.5\rho C_D A_F (v_{xT} + v_0)^2\} \tag{4.8}$$

Depending on the value of P_{TR} , it is possible to classify the various operating modes of the vehicle

- For $P_{TR} > 0$, the vehicle is in traction mode with a positive tractive effort.
- For $P_{TR} < 0$, the vehicle is in braking mode (regenerative or service braking) with a negative tractive effort
- For $P_{TR} = 0$, two possibilities occur in this condition. The first is when the vehicle is costing with the resistive force losses exactly equal to the decrease in kinetic energy (coast mode). The second indicating the vehicle is at rest (dwell mode).

In the interests of managing power and energy of multiple energy systems, classification of the vehicle operation modes is as important as identifying the rate of change of power demands during the various modes. Figure 4.2 illustrates the vehicle tractive power demand represented as the propulsion load power (P_{Load}) for the different operating modes.

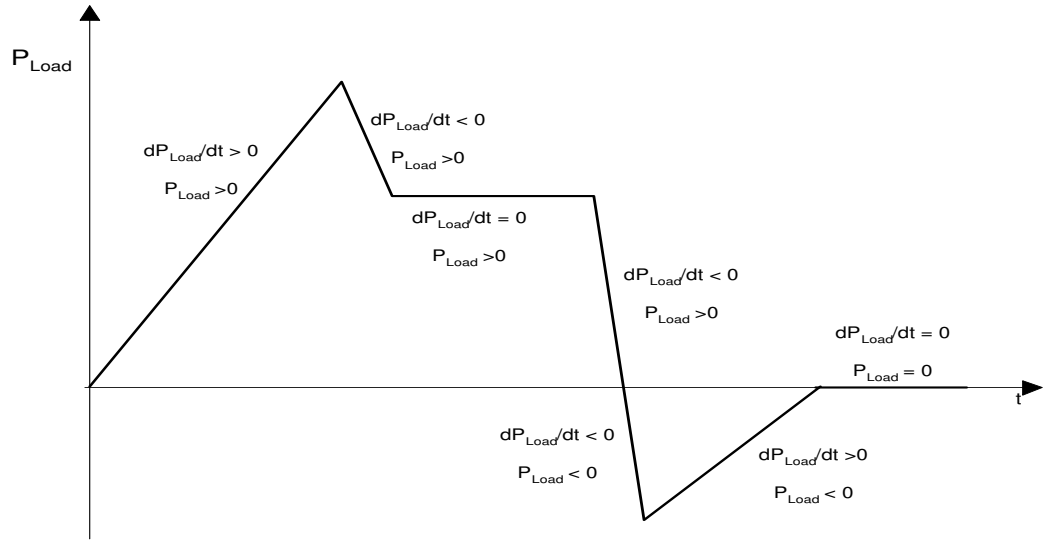

Figure 4.2 Propulsion power on a generic drive section

Adapted from Di Napoli et al.[111]

The electric vehicle propulsion load represents the bulk of the power demand from the energy storage systems. Comprising of traction motor, traction drive and traction controller, the propulsion system defines the capability of the vehicle to trace a given velocity and terrain profile.

4.3 Vehicle Propulsion Energy Demand

Dimensioning of the onboard energy storage systems in an electric vehicle are based on both the instantaneous power demand as well as the energy demand. Following the acceleration interval as shown in Figure 4.3, the mean tractive power over the interval Δt is

$$\overline{P_{TR}} = \frac{1}{t_f}\int_0^{t_f} P_{TR}(t)dt \tag{4.9}$$

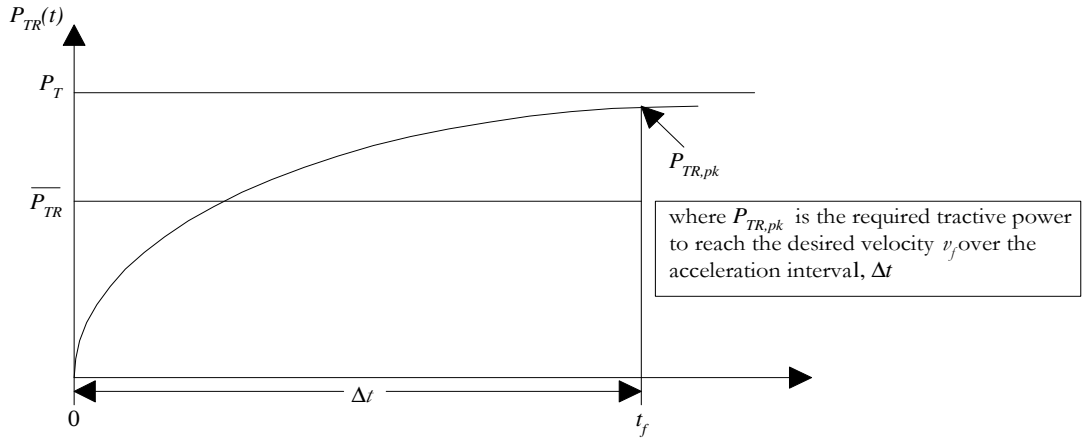

Figure 4.3 EV acceleration interval

Design and sizing of an energy storage system to meet the propulsion demands for a given acceleration and steady state velocity profile is obtained from the energy requirement of the propulsion system. The rate of change of energy is defined by the tractive power and is given by,

$$\frac{de_{TR}}{dt} = P_{TR}(t) \tag{4.10}$$

where e_{TR} is the instantaneous tractive energy. Following this, the energy required by the propulsion load over an interval is obtained by integration of the instantaneous power equation as,

$$\int_{e_{TR}}^{e_{TR(t_f)}} de_{TR} = \int_{t=0}^{t_f} P_{TR}\,dt \tag{4.11}$$

$$\Rightarrow \Delta e_{TR} = t_f \overline{P_{TR}}$$

The propulsion system has the capability of harnessing energy through regenerative braking. Therefore, the propulsion power is fundamentally different form the non-propulsion power in that the power flow is bi-directional. Figure 4.4 illustrates the total available regenerative energy that is dissipated at the friction brakes in a fuel cell vehicle without any regeneration capability. The results of Markel et al. [112] can be used to determine the minimal battery and ultracapacitor size that would be able to recapture all of the available regenerative

braking energy. Regenerative braking occurs in discrete events, each with a unique duration and power profile. The US06 cycle has some significantly large regenerative braking events that have peak powers of over 50 kW for durations of up to 30 seconds for the SUV test vehicle. Apart from being sized accordingly, the energy storage system has to be receptive to the regenerative energy. In some cases, the surplus power can be diverted to the non-propulsion loads if the power system infrastructure permits this.

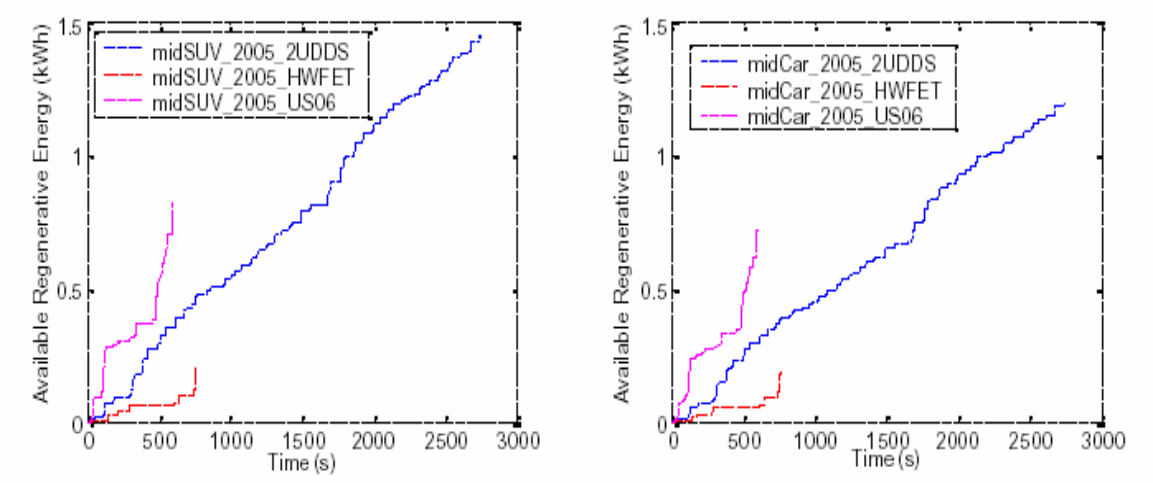

Figure 4.4 Available regenerative energy for an SUV and midsize Car

(Reproduced from Markel et. al [112])

4.4 Regenerative Braking

An important attribute of electric propulsion systems is the ability to recapture some of the electrical energy via regenerative braking. During regenerative braking, the kinetic energy of the vehicle should be ideally fully converted and recuperated by the energy storage systems via the DC distribution Bus. Practically, only 30% to 50% [5] of this energy is recoverable due to conversion losses. The principle behind regenerative braking is that the traction motor produces negative electromagnetic torque and hence assumes the operation of a generator. In order for regeneration to take place, the propulsion powertrain infrastructure from the energy source to the traction wheels must be bidirectional and the energy source itself must be receptive to reserve power flow. Figure 4.5 illustrates the quarter-model (single wheel) regenerative power conversion stages from wheel to energy storage system.

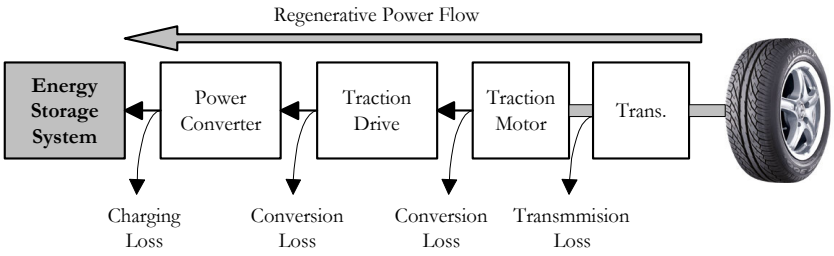

Figure 4.5 Illustration of Regenerative power flow

The amount of regenerative energy that can be recuperated depends on several factors, primarily the motor, deceleration rate and the receptiveness of the energy storage system. In rapid decelerations events, especially from high velocities, the magnitude of power that the traction motor is required to convert would be very large. To process this high power in a short period would require a traction motor with a significantly large power rating. The kinetic energy that the motor can convert within the required deceleration time then has to be transferred to the energy storage system. Therefore, the maximum electrical power that the motor and the power transfer infrastructure can handle dictates the absolute regenerative power limit (Regen. power limit) of the system. The regenerative braking power can be expressed as,

$$P_{brake} = \frac{J_T\left[(\omega 2(\omega 2 - \omega 1\right]}{t2 - t1} \tag{4.12}$$

where,

J_T is the total inertia reflected at the traction motor shaft (kgm^2)

$\omega 2$ is the initial traction motor angular velocity (rad/s)

$\omega 1$ is the final traction motor angular velocity (rad/s)

t2-t1 is the deceleration time from $\omega 2$ to $\omega 1$ (s)

Figure 4.6 shows a generic deceleration profile

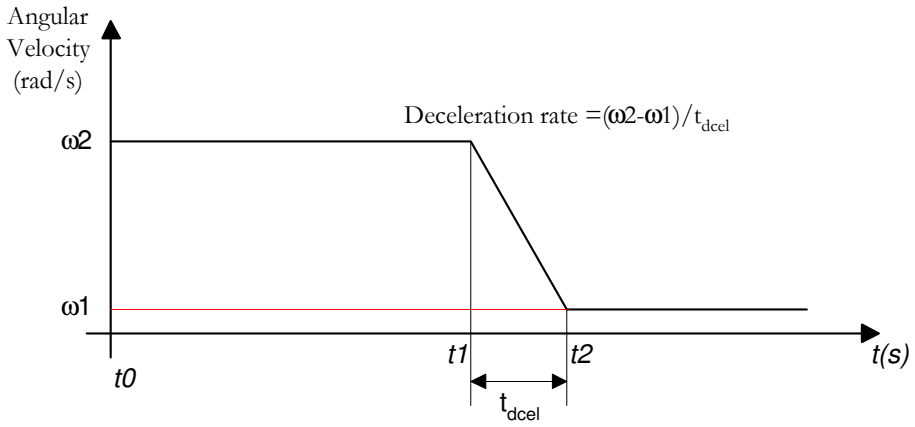

Figure 4.6 Generic deceleration profile

As for the energy storage system, the ability to restore the recoverable energy depends on a parameter that can be defined as the 'source receptivity', ϖ, where

$$\varpi = \left(\frac{E_{regen} - E_{loss}}{E_{res}} \right) \tag{4.13}$$

and,

E_{regen} is the regenerative energy caused by vehicle deceleration, E_{loss} is the energy loss during conversion and E_{res} is the energy recaptured by the energy storage system. In an ideal system with full recuperation, $\varpi = 1$.

For maximum recuperation to occur, change in kinetic energy will equal the charge in stored energy such that,

$$\Delta E_{kin} = \Delta E_{sto} \tag{4.14}$$

As such, for an EV that utilises ultracapacitors as the energy storage system for recuperation of regenerative braking power, the capacity of the ultracapacitor bank is dimensioned based on the following,

$$\underbrace{\frac{1}{2}m(vs^2{}_{\max} - vs^2{}_{\min})}_{\max change\ in\ vehicle\ kinetic\ energy} \approx \underbrace{\frac{1}{2}C(v^2{}_{UC\max} - v^2{}_{UC\min})}_{\max change\ in\ UC\ storable\ energy} \tag{4.15}$$

and so the magnitude of the maximum regenerative braking power can be expressed as

$$P_{regen}\max = \frac{\Delta E_{kin}}{t_{dcel}\min} \tag{4.16}$$

where t_{dcel} min is the minimum deceleration time from maximum to minimum velocity.

Referring to Figure 4.5, the overall regenerative energy harnessing efficiency can be expressed as,

$$\begin{aligned}\eta_{regen} &= \frac{energy\ \ avaialble\ \ at\ \ the\ \ wheels}{energy\ \ recuperated\ \ from\ \ the\ \ wheels} \\ &= \eta_{Trans} \cdot \eta_{TRMotor} \cdot \eta_{TRDrive} \cdot \eta_{PEConverter} \cdot \eta_{chg}\end{aligned} \tag{4.17}$$

4.5 Vehicle Model - SIMPLORER

With the longitudinal dynamics equations described in Section 4.1, a simulation model of an electric vehicle can be constructed. Developed in SIMPLORER[102], the simulation model serves several purposes. First, it provides a platform to obtain power and energy requirements of the energy storage systems for a given propulsion profile. With the resultant power and energy requirements, appropriate dimensioning of the energy system can then be performed. The model also serves as a platform to analyse power and energy management strategies and the effect it has on the energy storage systems. Figure 4.7 shows the vehicle simulation model. The input parameter to the model is a drive profile signal (vehicle velocity in km/h). The model calculates the vehicle tractive power demand and converts this value to

electrical terminal power seen at the energy source. Positive traction power is converted by means of varying the DC-Bus load resistance while negative traction (regenerative braking) power is translated to a current injection on the DC bus. The end result is the conversion of tractive effort for a given velocity trajectory to electric load power at the DC bus. The energy expenditure of the vehicle is simply calculated as the time integral of the terminal power. Validation and tuning of the model was achieved by subjecting the actual test vehicle developed for this work to an arbitrary drive profile and then comparing empirical versus simulated terminal current and voltage measured at the energy sources.

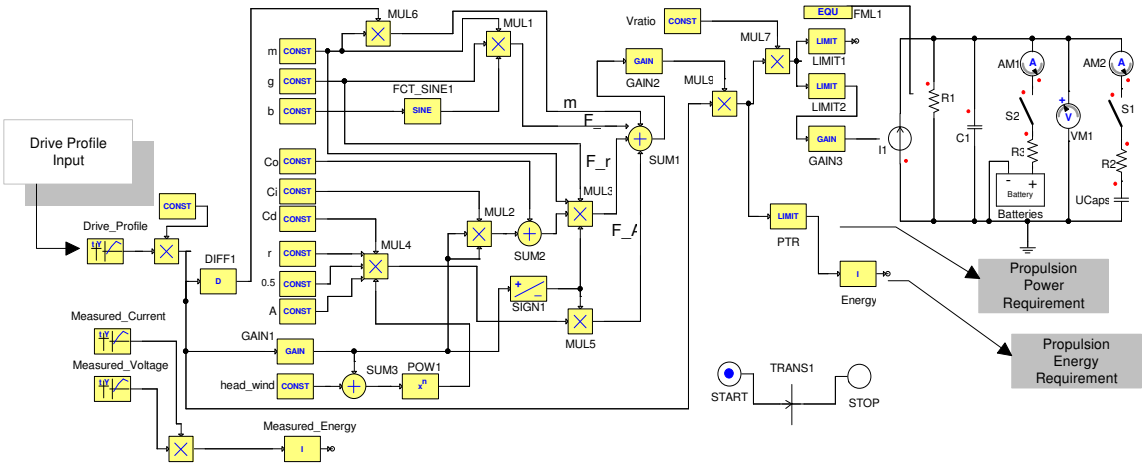

Figure 4.7 SIMPLORER vehicle simulation model

4.6 Case study of the effectiveness of combining batteries and ultracapacitors to service a vehicle power and energy demands

With standard drive cycles obtained from ADVISOR and using the vehicle and energy storage model developed in SIMPLORER, the effectiveness of combining batteries with ultracapacitor for a high mobility multipurpose wheeled vehicle (HMMWV) is demonstrated as follows. Table 4.1 provides the data of the modelled vehicle.

Vehicle Mass	6000 kg (including payload and maximum allowable mass for electric propulsion system)
Frontal area	3.2 m^2
Rolling resistance coefficients	$C_0 = 0.02$ $C_1 = 0.01$
Aerodynamic drag coefficient	0.3
Gradient	0 degrees

Table 4. 1 Vehicle data used for the three case studies

The vehicle model is subjected to three drive cycles and is specified to have a maximum velocity of 100km/h. In the three scenarios considered, the energy expenditure with and without energy recuperation via regenerative braking are compared. Power management between the batteries and ultracapacitors is employed on the basis that the peak battery discharge power is limited to 50kW with a rate of change (dP/dt) fixed at 10kW/s. The same charging power limit is assumed but with a charge acceptance rate assimilated by imposing a fixed 5kW/s restriction on the charging power. The task of the ultracapacitor is to then service the remaining power requirements. The ultracapacitor peak power limit and rate of charge limit is limitless and thus simply compensate for the difference between the required power and what batteries are limited to deliver. In all thee cases, the ultracapacitor model is charged and is always capable of serving any power request by automatically compensating for capacity and state of charge. The block diagram in Figure 4.8 illustrates the power equilibrium between load power, battery power and ultracapacitor power throughout the drive profile.

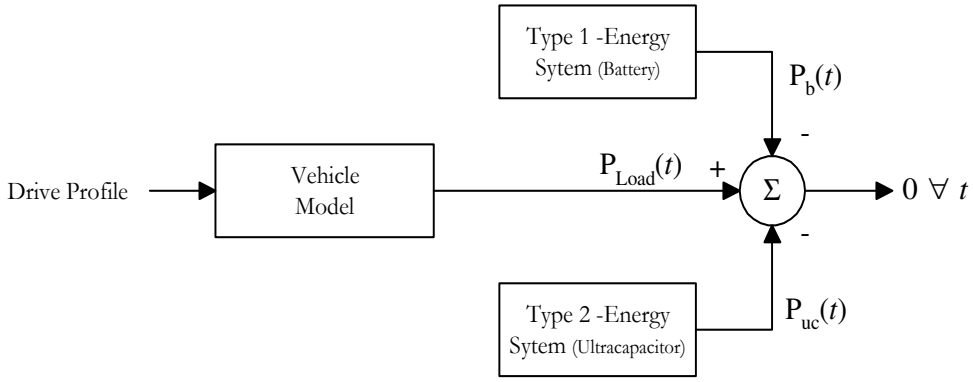

Figure 4.8 Representation of load, battery and ultracapacitor power equilibrium to satisfy a drive profile

CASE 1

Case 1 considers the vehicle model subjected to the first 600 seconds of an Urban Dynamometer Driving Schedule (UDDS). The cycle was initially developed to describe an urban route. It basically comprises of several transient phases with many speed peaks, which start from rest. Figure 4.9 depicts this drive profile. Salient points of the profile are as follows.

- Dive profile consisting of 7 segments of start-stop sequences
- Near maximum velocity is reached
- Rapid acceleration and decelerations
- Minimum vehicle coasting requirement
- Maximum Velocity of 91 km/h
- Maximum Acceleration of 1.38ms^{-2}
- Maximum Deceleration of 1.4ms^{-2}

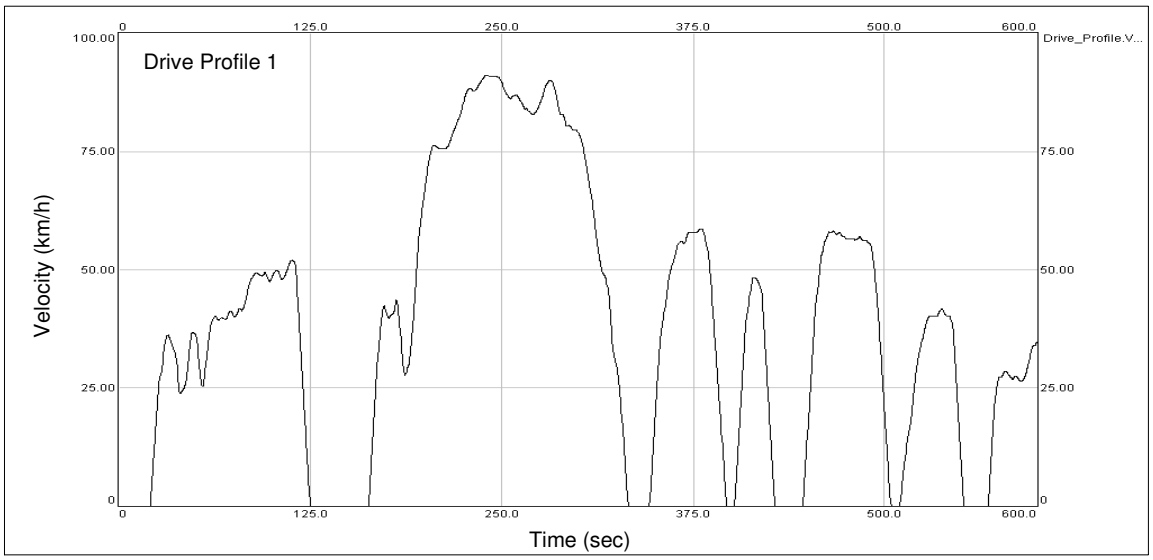

Figure 4.9 Case 1 - Drive profile

For the drive profile, the power demand generated by the model is shown in Figure 4.10. The drive profile demanded a peak positive power (motoring) of 122kW, peak negative power (regenerative) of 117kW and an average power of 50kW. With the battery operating constraints specified earlier, the proportion of battery power to service the load demands is as shown in Figure 4.11

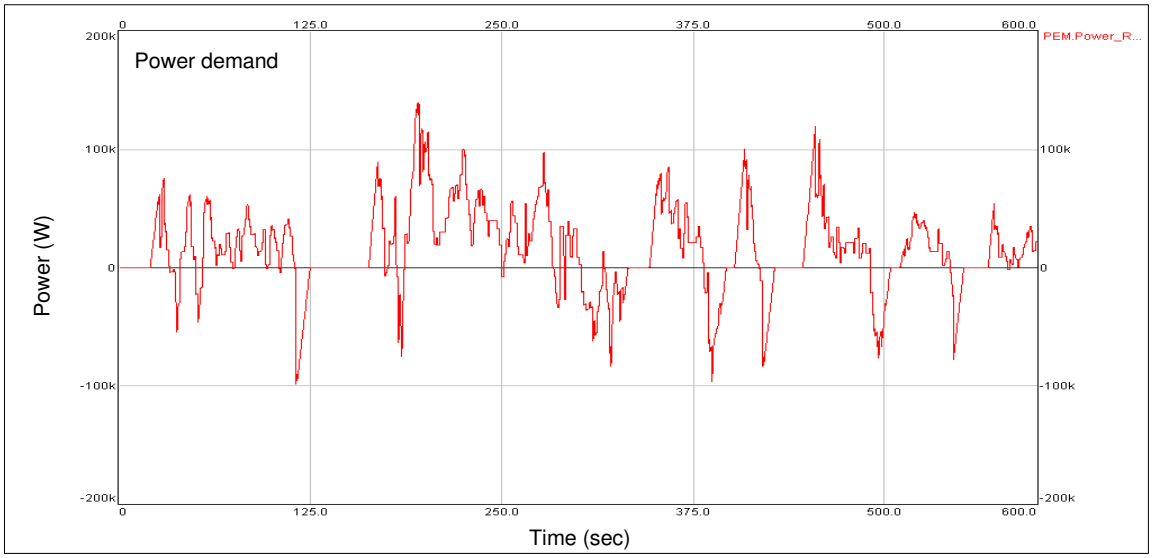

Figure 4.10 Case 1 - Power demand profile (P_{Load})

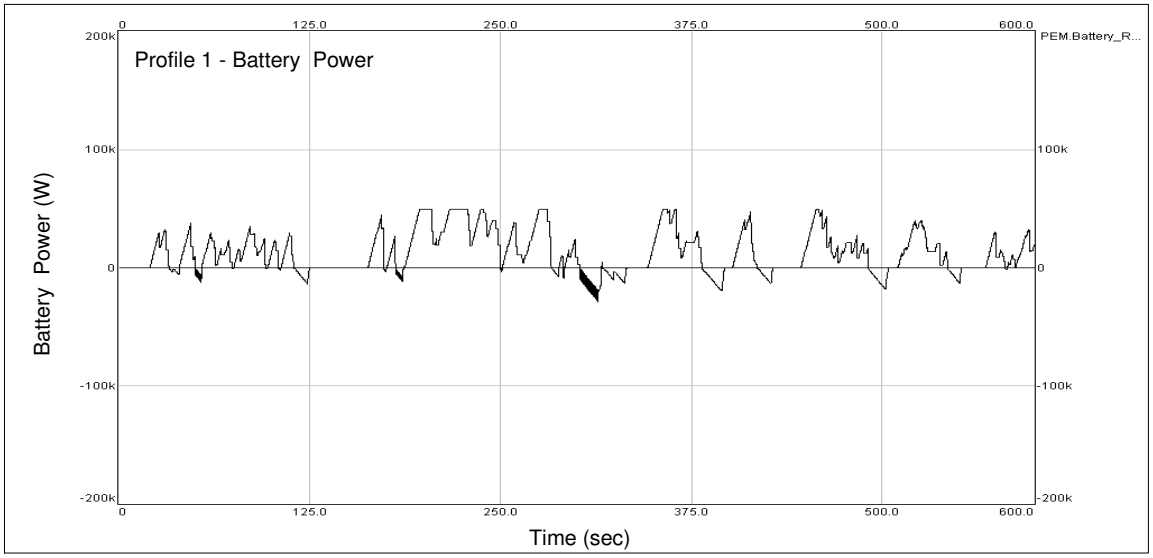

Figure 4.11 Case 1 - Battery power (P_b)

The task of the ultracapacitor system is then to exude and absorb the power that the battery system is unable to handle so as to meet the power equilibrium requirement outlined in Figure 4.8. The proportion of power serviced by the ultracapacitors is shown in Figure 4.12 while the power split between the battery and ultracapacitor compared to the demanded load power is shown in Figure 4.13. As can be seen, both positive and negative peak powers are mitigated to the ultracapacitor system.

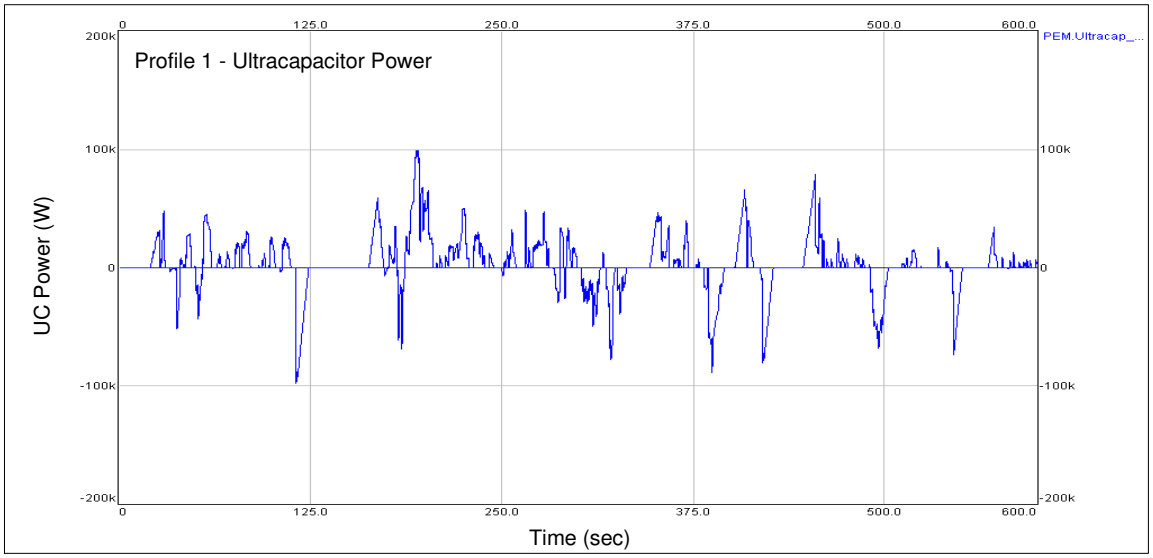

Figure 4.12 Case 1 - Ultracapacitor power (P_{uc})

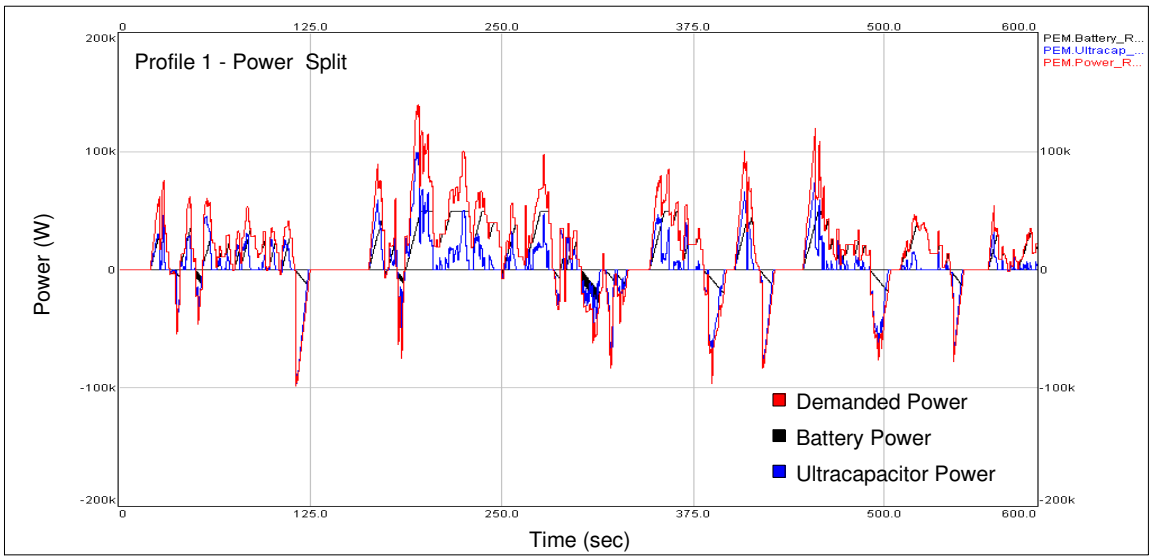

Figure 4.13 Case 1 - Power split profile

A comparison of the energy expenditure over the drive profile with and without the ability to manage the power splits and to recuperate regenerative energy is presented in Figure 4.14. The corresponding energy profile of the battery and ultracapacitors are show in Figure 4.15. As highlighted in Figure 4.15, the reduction of energy expenditure (indicated by the downward arrow), is a result of the ultracapacitors recharging via regenerative energy.

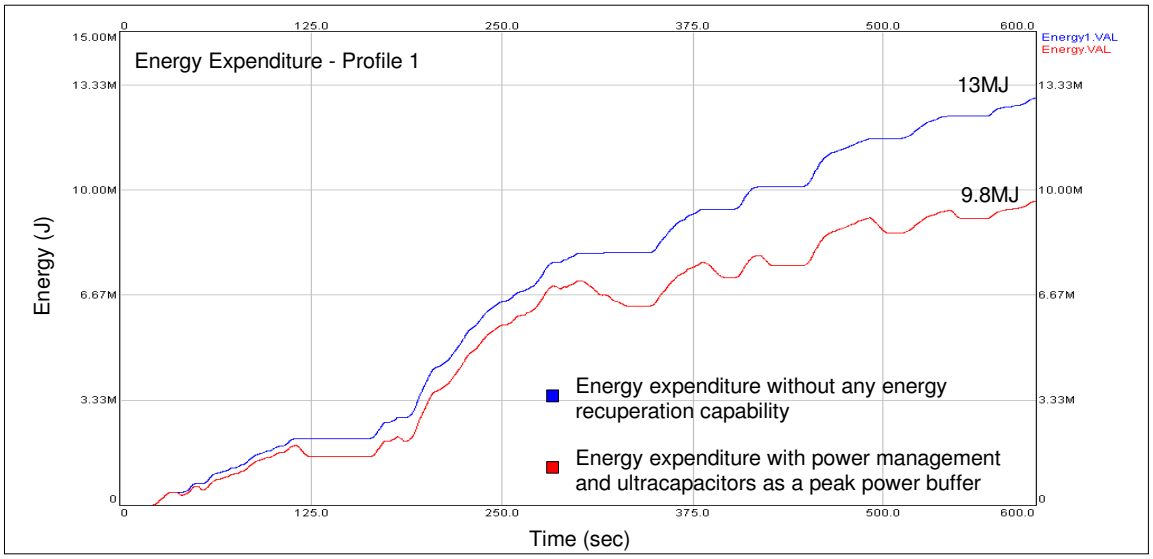

Figure 4.14 Case 1 - Total energy expenditure

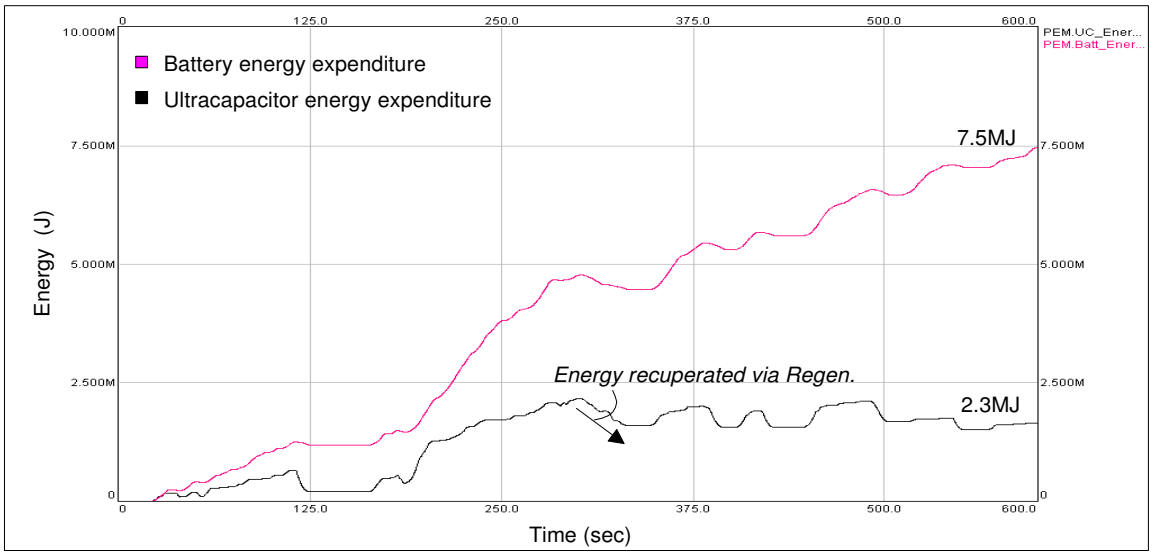

Figure 4.15 Case 1 – Battery and ultracapacitor energy expenditure

CASE 2

Case 2 considers the vehicle model subjected to the first 600 seconds of a derated US06 drive profile. The standard US06 cycle was developed to describe a driving pattern with high loads on an urban route and has a maximum speed of 128km/h. The version of the cycle used in this case is scaled down by 50% but still maintains the nature of the cycle. In comparison to the maximum specified vehicle velocity of 100km/h, this profile subjects the vehicle to more of a medium velocity range. Figure 4.16 depicts this drive profile. Salient points of the profile are as follows.

- Drive profile consisting of 6 segments of start-stop sequences
- Long travel time at medium velocity
- Short acceleration & deceleration cycles
- Maximum Velocity : 64 km/h
- Maximum Acceleration :1.78ms^{-2}
- Maximum Deceleration : 1.6ms^{-2}

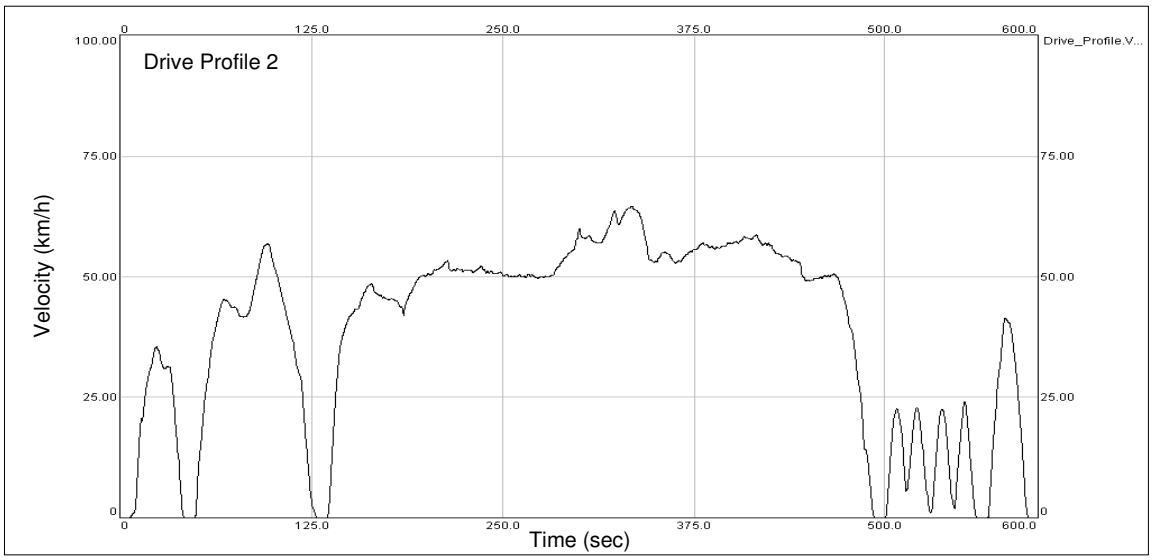

Figure 4.16 Case 2 - Drive profile

For this drive profile, the power demand generated by the model is shown in Figure 4.17. The drive profile demands a peak positive power (motoring) of 87kW, peak negative power (regenerative) of 46kW and an average power of also 50kW. With the same battery operating constraints as Case 1, the proportion of battery power is shown in Figure 4.18

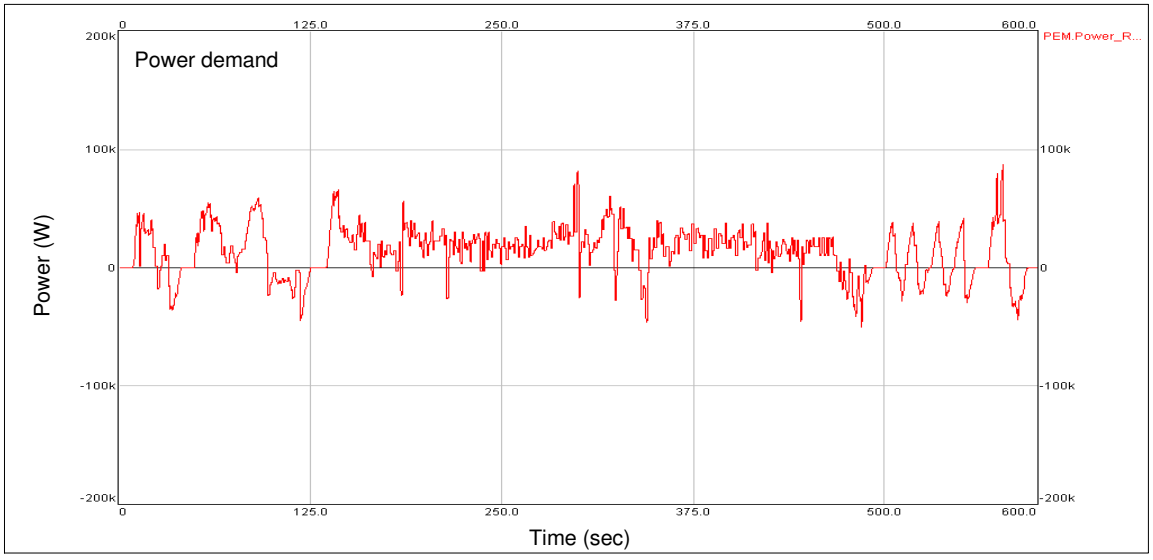

Figure 4.17 Case 2 - Power demand profile (P_{Load})

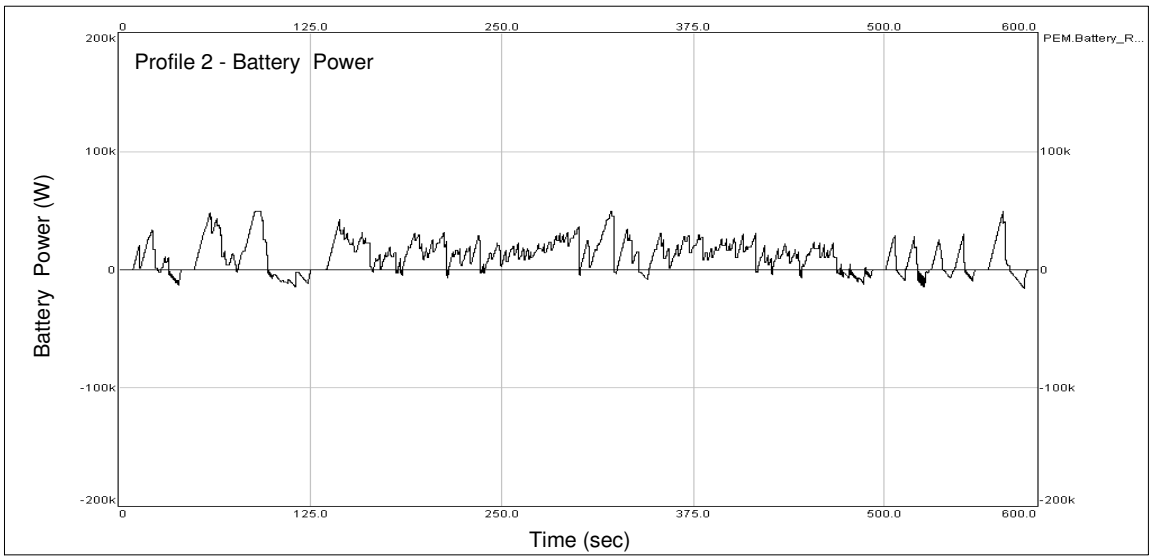

Figure 4.18 Case 2 - Battery power (P_b)

As with Case 1, the ultracapacitor services the remaining power demand to maintain power equilibrium. The proportion of power serviced by the ultracapacitors for this scenario is shown in Figure 4.19. Similarly, the power split between the battery and ultracapacitor compared to the demanded load power is shown in Figure 4.20

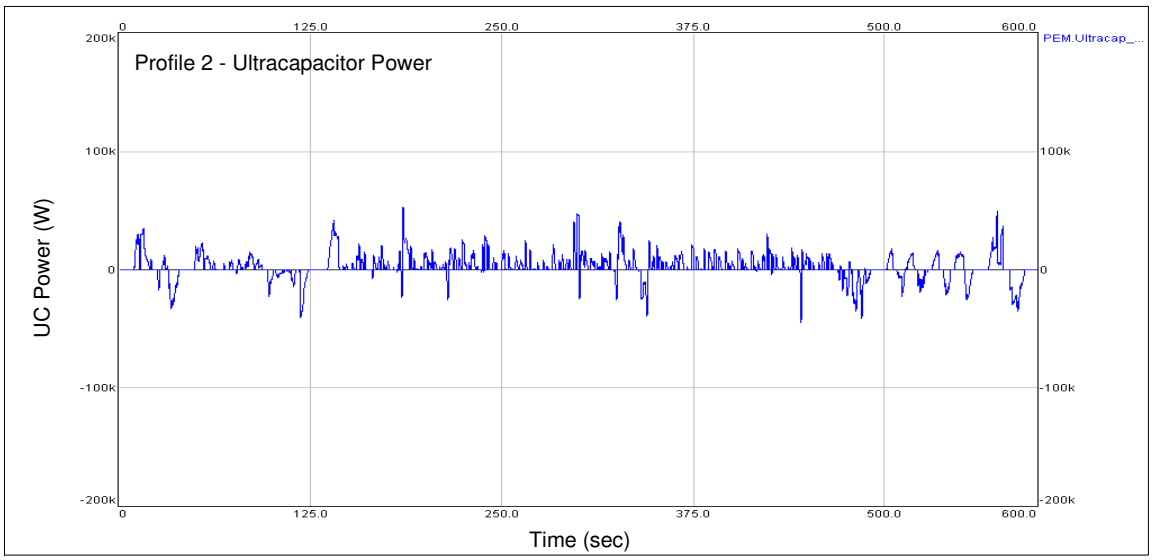

Figure 4.19 Case 2 - Ultracapacitor power (P_{uc})

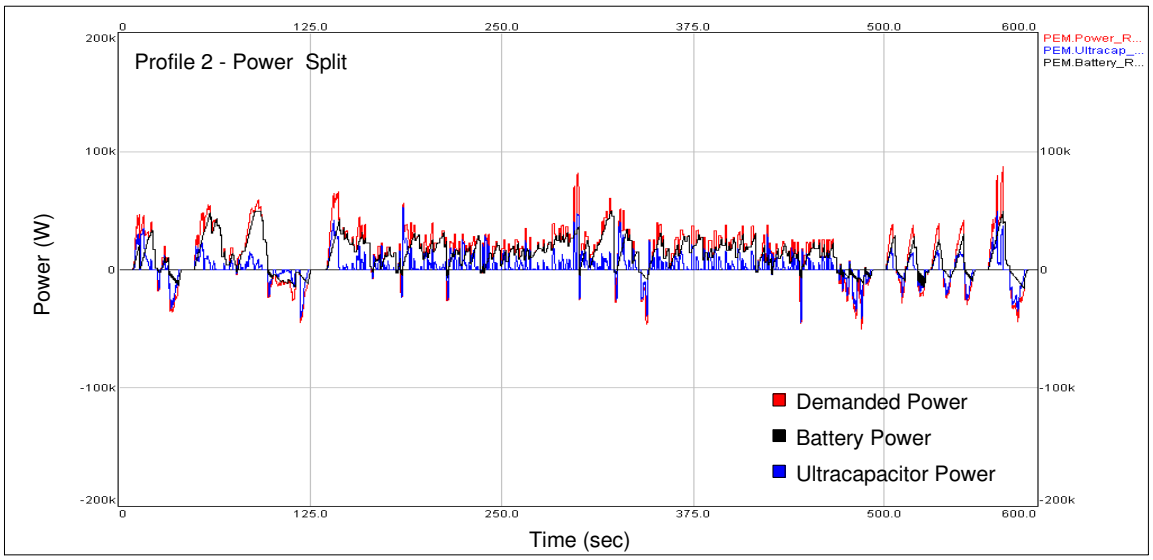

Figure 4.20 Case 2 - Power split profile

The comparison of the energy expenditure over the drive profile with and without the ability to manage the power splits and to recuperate regenerative energy is presented in Figure 4.21. The associated energy profile of the battery and ultracapacitors show in Figure 4.22.

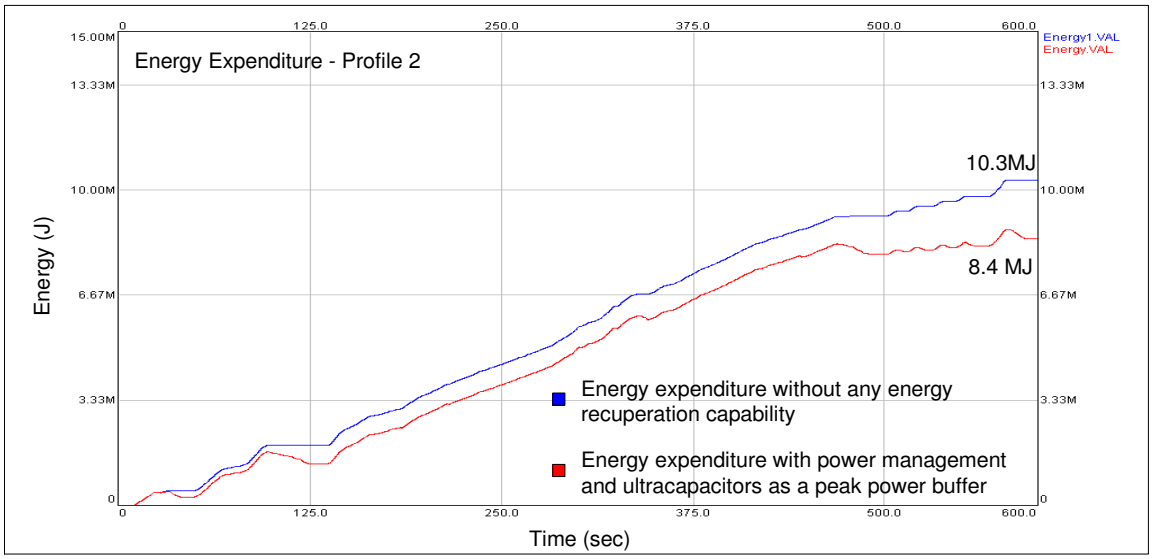

Figure 4.21 Case 2 - Total energy expenditure

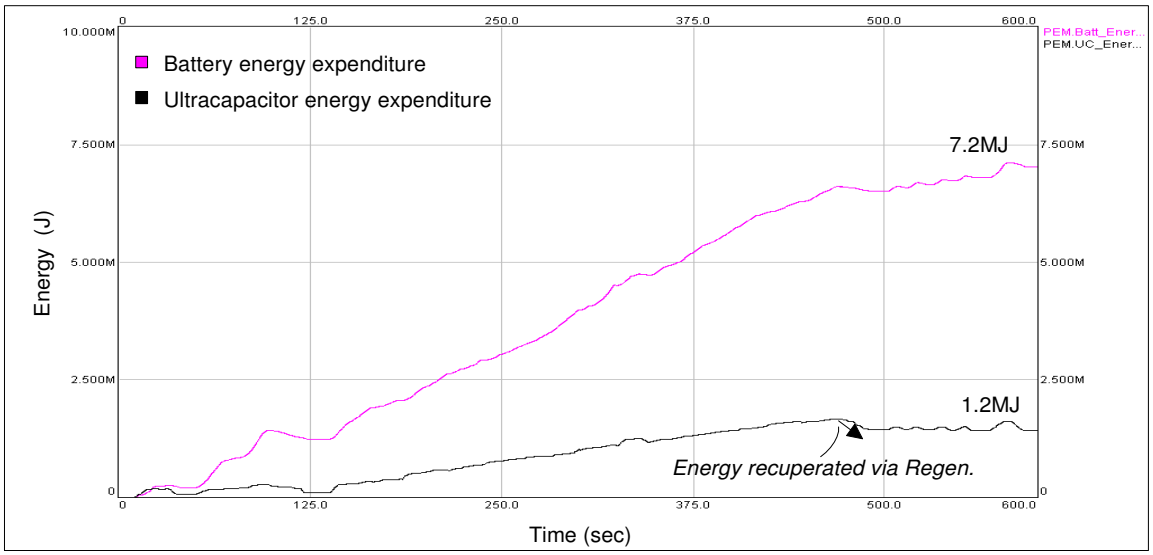

Figure 4.22 Case 2 – Battery and ultracapacitor energy expenditure

CASE 3

Case 3 considers the vehicle model subjected to a derived profile. The first 125 seconds and the last 50 seconds are extracted from the derated US06 cycle described in Case 2. The rest of the profile assumes a constant velocity. Although a perfectly constant velocity is artificial and not commonly realisable, the purpose of the simulation is to examine the effect of loads having comparatively long periods of constant power. Figure 4.23 depicts this drive profile. Salient points of the profile are as follows.

- Drive profile consisting of 4 segments
- Long travel time at constant velocity (constant power)
- Low peak to average power ratio
- Maximum Velocity : 51 km/h
- Maximum Acceleration :1.78ms^{-2}
- Maximum Deceleration : 1.6ms^{-2}

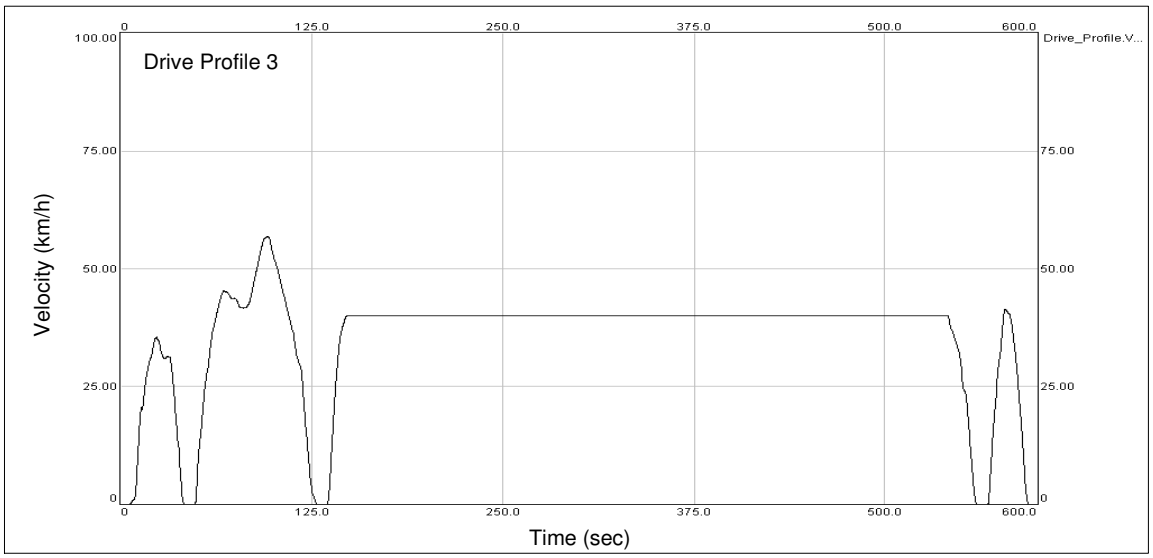

Figure 4.23 Case 3 - Drive profile

With this third profile, the power demand throughout the majority of the mission is constant and well below the maximum battery power limit. This can be seen in Figure 4.24. The low peak to average power ratio results in the battery providing almost all the energy required throughout the profile. The corresponding energy expenditure profiles are shown in Figure 4.25 and Figure 4.26.

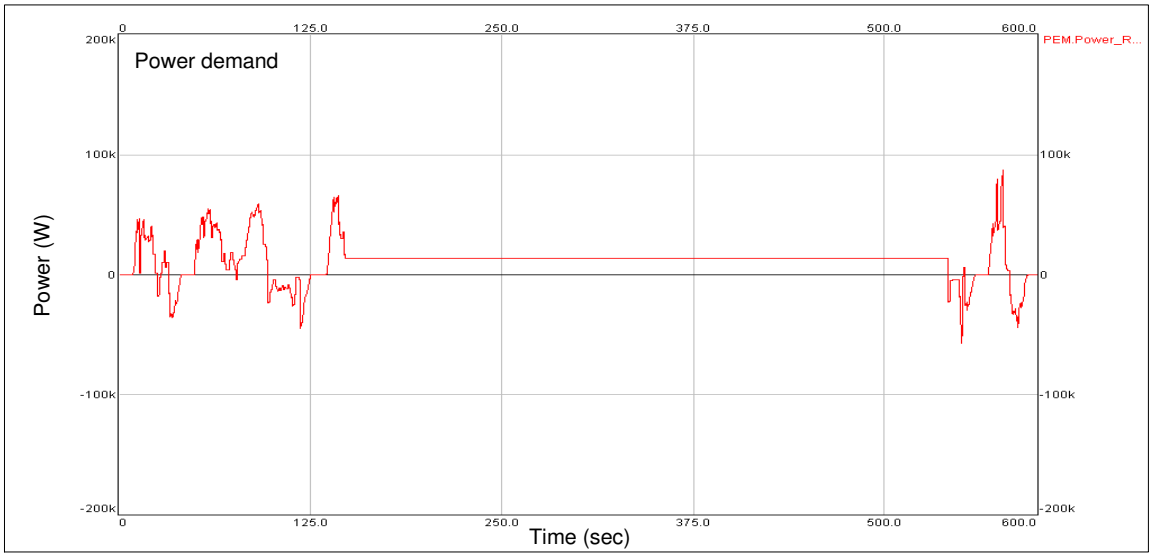

Figure 4.24 Case 3 - Power demand profile (P_{Load})

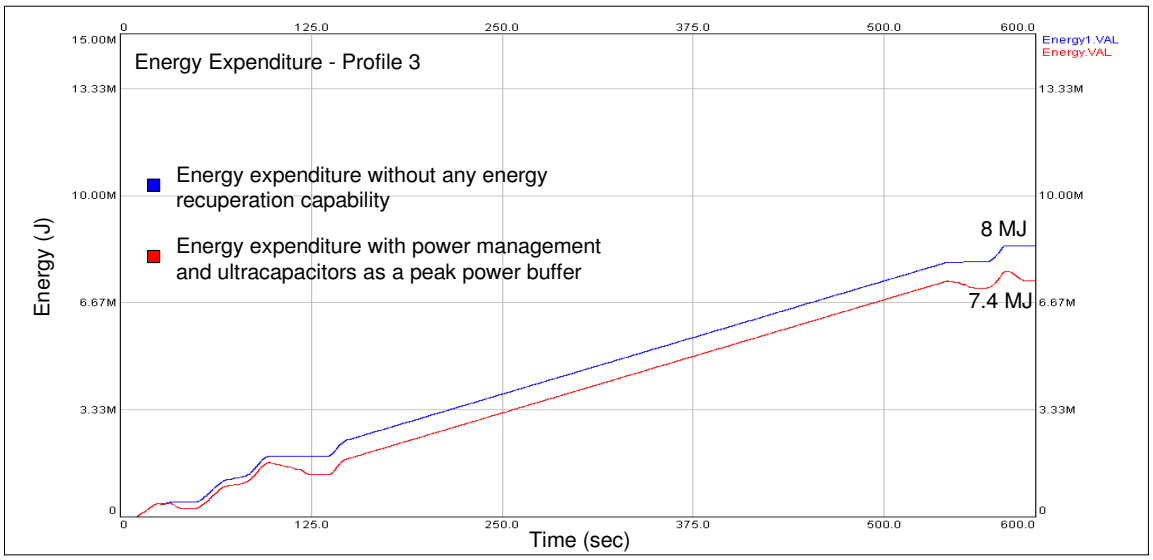

Figure 4.25 Case 3 - Total energy expenditure

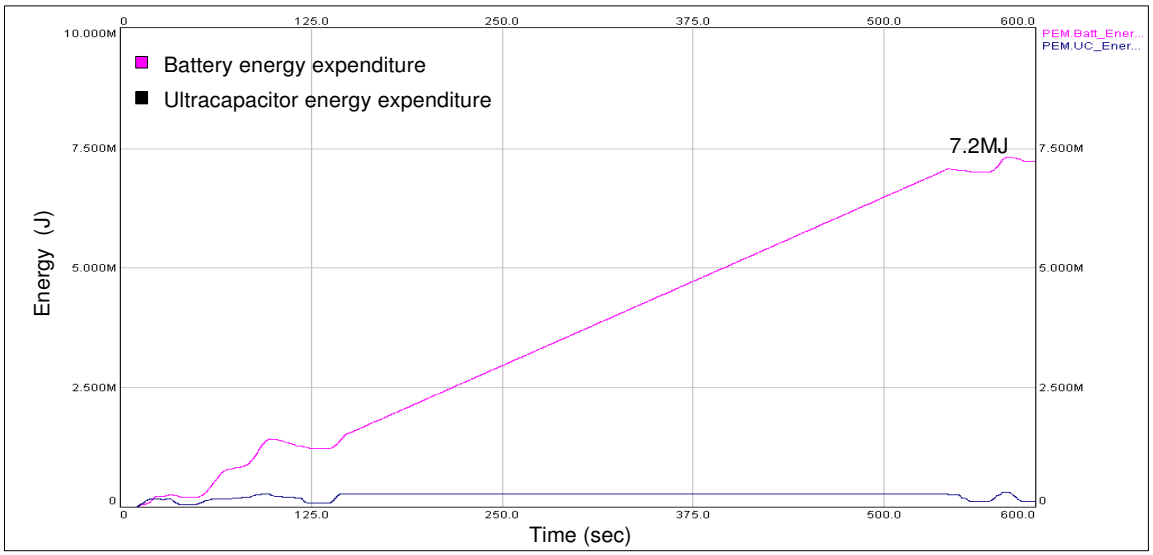

Figure 4.26 Case 3 – Battery and ultracapacitor energy expenditure

DISCUSSION

From this case study, the suitability of the battery-ultracapacitor hybrid energy source options and the need for power and energy management is objectively evaluated. In all three cases, the arrangement of power splits (power management) is to assume that the battery is the main energy source and hence provides the average or steady state power while transient

power is provided by the ultracapacitors. The charging and discharging rate limiter imposed on the battery provides a means to differentiate between steady state and transients.

The net energy expenditure of the system and assuming perfect energy recuperation with N representing the end of the drive cycle is,

$$E_{NET} = \left[\int_{t=0}^{t=N} (P_{Batt_{discharge}} dt + P_{Ucap_{discharge}} dt) + \int_{t=0}^{t=N} (P_{Batt_{charge}} dt + P_{Ucap_{charge}} dt) \right] \quad (4.18)$$

The mitigation of peak powers to the ultracapacitors results in the reduced peak power demand overhead on the batteries. It was explicated in Chapter 3 that if the batteries were to service these momentary peaks, the resultant capacity and hence battery mass would increase as well. In case 1 and case 2, the relatively high peak to average power demand ratios favour the addition of ultracapacitors along with the associated power distribution. The more cyclic nature of case 1 with a higher number of regenerative events, also justifies the augmentation of ultracapacitors. In case 3 however, the augmentation serves minimum benefit since the battery alone services most of the power demand profile. This is seen in Figure 4.25 as a small difference between the energy expenditure profiles. In comparison, case 1 and 2 shows a larger difference in terms of energy expenditure with and without power management. This translates to the ability to achieve higher vehicle autonomy with a hybrid energy system in place.

With reference to the ultracapacitor power profiles of case 1 and case 2 (Figure 4.12 and Figure 4.19) and the corresponding ultracapacitor energy profiles (Figure 4.15 and Figure 4.22), it is seen that both power and energy profiles in case 1 has more oscillatory segments that are close to each other. This indicates that the ultracapacitors in case 1 are subjected to more frequent discharge-charge cycles. What this implies is that the ultracapacitors in this case can be sized smaller in capacity due to the fact that a charge depletion during a positive peak is consecutively replenished by negative peak events. This is not so in the case 2. Although the magnitude of the positive peaks in case 2 are smaller compared to case 1, they

occur more frequently before regenerative events. This can be seen in the comparison of the ultracapacitor power profile shown in Figure 4.27.

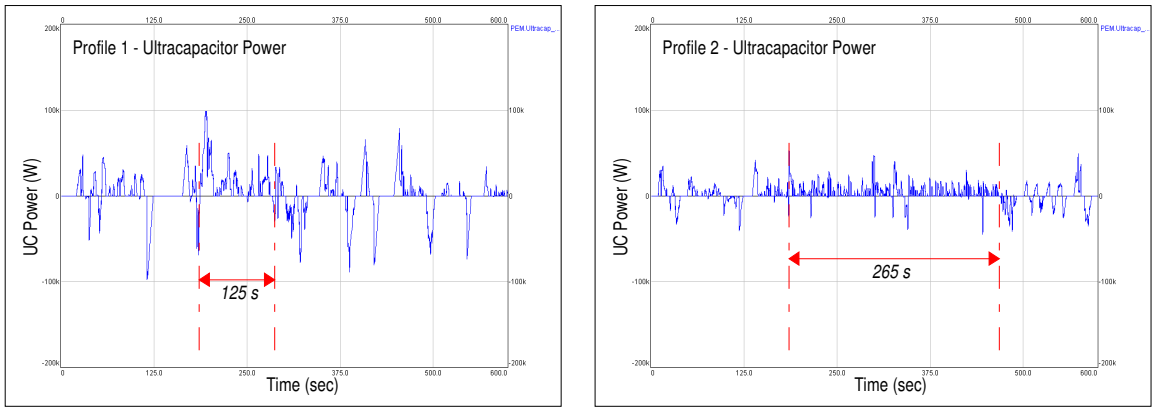

Figure 4.27 Comparison of ultracapacitor power

Accordingly, in all cases, the ultracapacitor system maximum energy storage requirement can be stated as,

$$E_{UC}\ \max = \max\left(\int_{t1}^{t2} P_{UC} dis\ dt\ \ , \int_{t3}^{t4} P_{UC} chg\ dt\right) \tag{4.19}$$

where the interval [t1,t2] is the maximum period that that the ultracapacitor has to supplement the battery power by supplying power ($P_{uc}dis$) before an opportunity to charge the ultracapacitor occurs. The interval [t3,t4] is the maximum period where continuous charging power via regenerative braking at power level $P_{uc}chg$ occurs.

In all three cases, it is therefore possible to dimension the ultracapacitors based on the cyclic power demands if the power profiles are known in advance. However, it is also necessary to have the ultracapacitors at the right state of charge so as to be able to deliver the power during the positive peaks and receptive to power during negative peaks. A case where the ultracapacitors are suitably dimensioned but are at an undesirable state of charge can occur under certain circumstances. For example, when the ultracapacitors are fully or almost fully charged and the vehicle is subjected to a rapid deceleration, the charging power generated as a result of regenerative braking cannot be directed to the ultracapacitors. The third segment of the drive profile in case 1 shows such a likely event.

A situation such as this occurs when the vehicle accelerates gradually up to speed at power levels within the battery peak power and power rate limits. By definition of power management, the ultracapacitors are not required to service this slow load transition. If the vehicle were then subjected to a rapid deceleration, the ultracapacitors would be unreceptive to the regenerative power because of its state of charge (or energy level). It is for this reason the problem now becomes more of an energy management issue rather than a power management one. To cater for such a situation, a method to actively control the ultracapacitor energy content becomes necessary. If the power profiles are known *a priori*, then optimised methods to programme the ultracapacitor state of charge may be used. However, standard drive cycles could be used to benchmark power splits and energy management strategies. Although these drive cycles were developed for emission tests of ICE vehicles, they do provide realistic velocity profiles ranging from aggressive urban driving to high-speed highway modes.

4.7 Summary

This chapter explicated the underlying principle behind vehicle power and energy management. Beginning with the fundamentals of vehicle propulsion power and energy demands, an Analog Mixed Signal (AMS) vehicle model developed with SIMPLORER was presented. Using the model, three case studies were presented to demonstrate power and energy demands under variations in drive cycles. The discussion objectively described the advantages of a strategic power and energy management system to arbitrate the power delivery and energy content of hybrid energy systems. To summarise, vehicle power demands that have high peak to average power ratios as well as the opportunity for regenerative energy recuperation justifies the cause to have a hybrid energy system. What has not been considered thus far is the technique to electrically combine the power from the energy systems. As such, the next chapter will further refine the problem of managing power and energy and introduce a structured method to address the problem. It then follows through with a structured implementable solution.

CHAPTER 5

THE MANAGEMENT OF POWER AND ENERGY

" The whole of science is nothing more than a refinement of everyday thinking "
*- **Albert Einstein, 1879-1955***

As describe in the literature review section, the power and energy management of multiple energy systems within electric vehicle architectures have been addressed through various approaches. Identifiably, the basic problem involves the instantaneous power blending of several power sources as well as a controlled intervention of the energy expenditure and the state of charge progression. The reason why the term 'management' is used rather than 'control' when describing the problem is not apparent but some conjectures can be made. The fundamental question that has not been clearly answered is, " How does the concept of 'management' fit into the problem description? ". The pursuit of identifying why the term 'management' has been adopted in this particular application domain has led to new insights and rationales in adapting a management methodology. Although several management models such as administrative management, information management, management by objectives and scientific management do provide structured management frameworks, it was found that the hierarchical structure of classical management methodology best fits the problem description investigated in this work. In this chapter, classical management concepts and the applicability of these concepts to the topic of power and energy are

presented. Following this, a novel concept of power and energy management that encompasses the essence of management methodology is introduced. A refinement of the concept leads to the inception of a modular power and energy management structure. The novel modular structure contributes to a more unified description of power and energy management and also aids as a systematic design framework during practical implementation. This chapter decomposes the power and energy management problem into modular blocks and then proceeds to demonstrate a reconstruction of the problem in the form of an implementation framework.

5.1 Adopting the general concept of management

Management is a practice of utilising all available resources to obtain a desired result. It entails the effective utilisation and coordination of resources to achieve defined objectives with maximum efficiency. Management focuses on the entire organisation from both a short and a long-term perspective. As a complete process, management involves forming a strategic vision, setting objectives, identifying a strategy and then implementing and executing that strategy. From this basic definition alone, the relevance of extending the methodology to managing power and energy becomes more apparent.

In most organisations, the management structure consists of several levels or tiers as a demarcation of hierarchy or chain of command. Members or processes at each level in the hierarchy exist to address and execute very different tasks at different timescales but collaborate in reaching a common objective. The highest level of the hierarchy is essentially responsible for making top-level decisions that influence the long-term goals of the organisation. Directives from the top-level are then issued to the middle-level process. The long-term objective of these directives need not be apparent or explicitly defined to the middle-level process. What is imperative is that the middle-level has sufficient information communicated down from the top-level to enable it to successfully carry out its own decision making process. Similarly, the top-level also does not necessarily require detailed information about how the middle-level executes its operational decisions.

Under the directives and constraints imposed by the top-level management, the middle-level would handle the continuous operational decisions based on some predetermined management policy. Since middle-level management often handles the more operational related tasks, periodic decisions within these processes takes place more frequently compared to the top-level management. Periodically, the top-level may evaluate its current strategy and long-term targets and consequently alter its directives, which are communicated to the middle-level.

The next classification in the hierarchy is the lower-level management, which generally handles the detail execution stage of a large process. With operational instructions dictated by middle-level management, the lower-level management carries out rapid decisions that influence the actual process implementation. Similar to the timescale relationship between top-level and middle-level, the decision making rate that takes place within the lower-level process is of a higher frequency compared to the middle-level. As a descriptive example, in a production process, the mid-level management would handle the day-to-day operations while the lower level manages the hour-by-hour production process.

The framework of hierarchical management permits the decision levels, decision objectives, decision-making rates and the interactions between the levels to be clearly definable for a given process. The scalability and flexibility of such a framework allows independent changes to be made at any level without having to restructure the entire management process. As long as each level adheres to predefined level-to-level interaction protocols, a change to the internal operations in one level does not affect other levels. As such, the framework exhibits a form of modularity. Figure 5.1 illustrates a typical hierarchical management model.

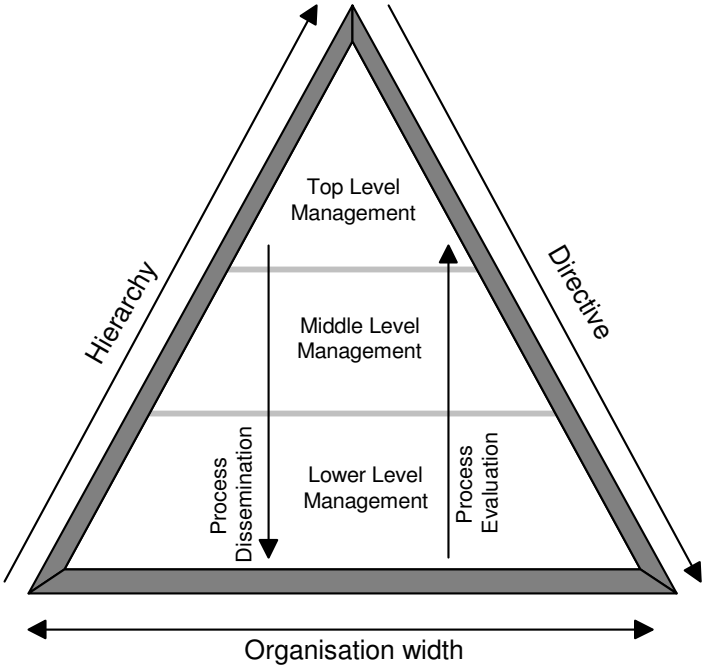

Figure 5.1 Hierarchical management model

The concept of a hierarchical management structure provides a systematic dissemination and evaluation of processes. Decisions making at each of the levels is carried out at different iteration rates since the disseminated processes takes place at different timescales. Top-level decisions that dictate the strategy of the organisation require several middle and even more low-level decisions to take place before measuring the overall progress and executing new directives. All three levels are essentially decision making processes but with different decision iteration rates. As Figure 5.2 illustrates, several lower-level decisions take place before a middle-level decision and several middle-level decisions occur before a top-level decision. In organisational practice, the decision frames need not be constrained by rigid time frames. However, as will be shown, the concept of discrete and deterministic decisions is particularly useful when adopting this methodology to automatic systems such as vehicle power and energy management.

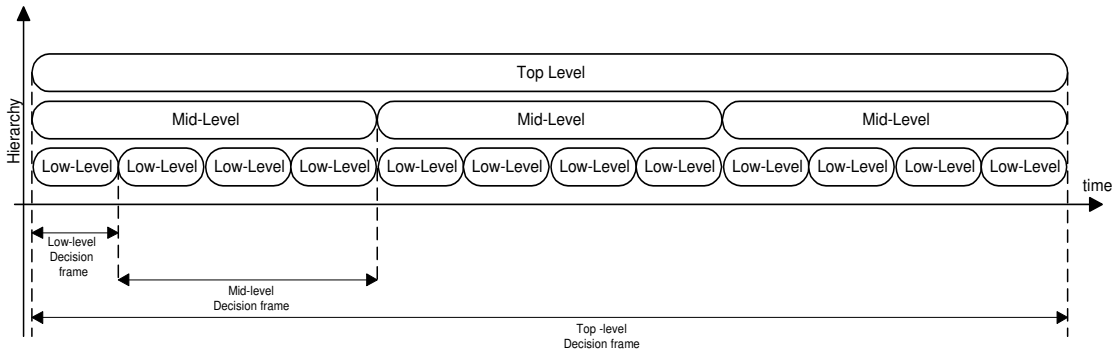

Figure 5.2 Decision time frames of hierarchical management

Examination of the hierarchical management model reveals several concepts that can be adapted to describing and designing a power and energy management system. The modularity of the model demonstrates that a large management process can be distributed into several processes with each process having a definable task. Although this is useful in any control problem, the fact that the processes are interlinked and take place at different timescales is particularly interesting to the application of power and energy management. The reason for this is because power (P) and energy (E) are parameters that are simply related to each other by 'time' (t).

$$P = \frac{\Delta E}{\Delta t} \quad \text{or} \quad E = \int P \, dt \tag{5-1}$$

Since energy is simply a measure of the accumulated use of power over a period of time, the management of energy can be associated as hierarchically higher than the management of power. The following section describes the adaptation of a hierarchical management model and its application to power and energy management of multiple sources in electric vehicles.

5.2 Adaptation of hierarchical management concepts to Power and Energy Management

With similarities to ideas found in hierarchical management methodology, the concept of a modular Power and Energy Management System (PEMS) structure presents a novel method to approach and describe electric vehicle power and energy management. The framework itself lends this multidisciplinary problem to be approached and in a systematic breadth before depth manner. As there are several processes involved in a power and energy management system, ranging from long-term decisions of energy expenditure to very high-speed control of the power electronics, the modular structure facilitates each major part of the process to be addressed independently and finally consolidated to form a complete system.

Recalling the hierarchical management model of Figure 5.1 some overlap in concepts can be extracted to produce a similar model specifically for the application of power and energy management. Figure 5.3 illustrates the adaptation of the classical hierarchical management model

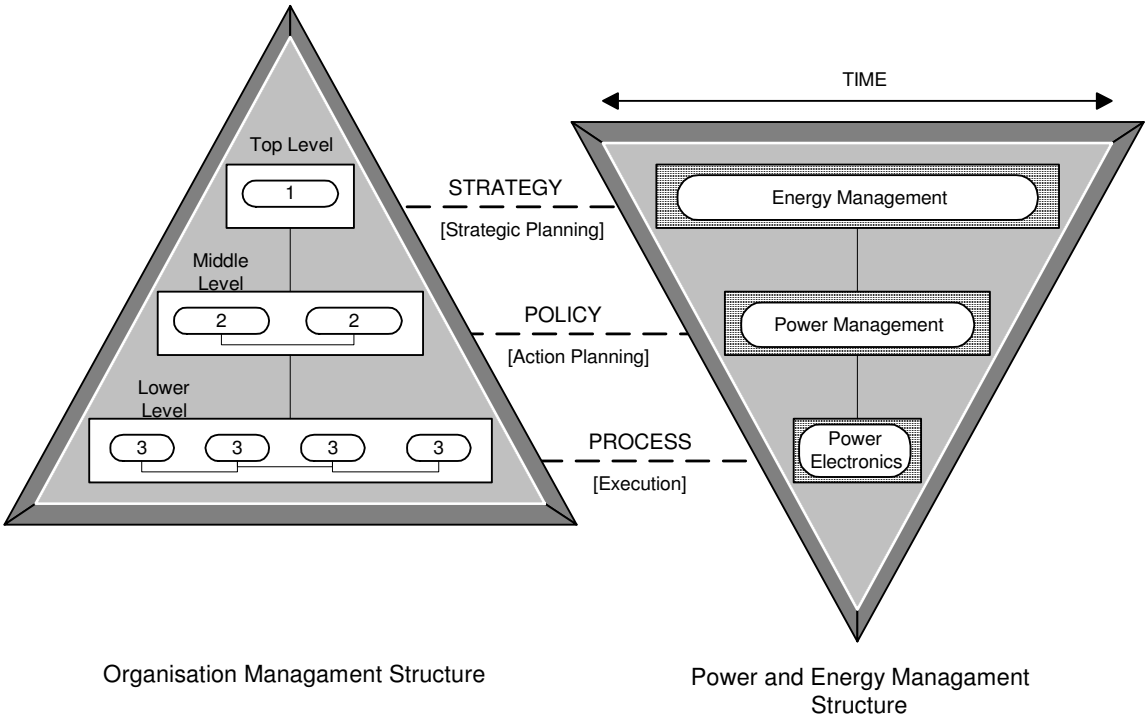

Figure 5.3 Analogy betweena hierarchical management model and a Power and Energy management structure

While the breadth of the organisation management structure increases lower down the management hierarchy to represent an increase in sub-processes (or workforce), the breadth of the power and energy management structure increases in relation to time. This correlation is illustrated in Figure 5.3 with the inversion of the triangle representing the power and energy management structure. With both structures however, the hierarchical tiers correspond to the same level of management mission, with the same downstream propagation of directives. Accordingly, the top tier of both structures handles the strategic planning or long-term strategies while the middle level decides on appropriate actions to take, which is then fed downstream to the lower level for execution.

Forming this analogy of power and energy management with conventional management methodology serves several purposes. Firstly, it permits the multi-objective multi-time horizon problem of managing power and energy to be decomposed and reclassified in a structured format. As a modular structure, it facilitates the development of each tier independently once the links between the tiers are established. As a total system, the methodology adds more completeness to the problem definition by linking the many sub-processes involved in the management of power and energy. In contrast with many approaches that consider sub-problems without addressing how they might fit into a larger picture, the adaptation of the proposed methodology addresses the problem holistically. The next section refines the concepts and heuristic derivation just described to form a completely modular power and energy management structure.

5.3 A Modular power and energy management structure (M-PEMS)

A novel approach that adopts the management methodology previously described provides a new perspective to the problem description of electric vehicle power and energy management. The concept begins by modularising the power and energy management system into hierarchical process shells with definable functionality and interface. The first tier in the hierarchical framework is the energy management. This involves long-term periodic time segment decisions of energy expenditure. Since energy itself is simply the time integral of power, decisions in energy management takes places at an iteration rate slower

than power management. The decisions of energy management are accordingly termed as the '**strategy**' of the system that takes places within an Energy Management Shell (EMS). The energy management strategy processes the slower dynamic parameters such as the battery and ultracapacitor SoC, the vehicle kinetic energy and the operating mode of the vehicle. The EMS then provides periodic manipulation of a set of control parameters to the next stage of the PEMS process in order to implement a given strategy.

The next stage in the hierarchical process is the power management. With the prescription for action stipulated by the EMS strategy, the power management process determines power-split decisions for the multiple energy storage system. These power management decisions are termed as the '**policy**' of the system that is executed within a Power Management Shell (PMS). The PMS is tasked to adhere to a given policy under constraints that are periodically altered by the EMS strategy. Since the PMS handles the continuous power split between the multiple energy systems, its iteration rate is several magnitudes higher than the EMS. Both the EMS and PMS structure forms a method to loosely separate the control of 'energy' and 'power'.

For a dual energy storage system comprising of batteries and ultracapacitors, determining the instantaneous power split ratio between the ultracapacitor and battery whilst regulating the DC bus voltage is the power management problem. Maximising the battery SoC, keeping the ultracapacitors at the optimum SoC as well as maximising the useable energy of both systems is the energy management problem. The two objectives of managing power as well as energy cannot be completely decoupled. However, it is valid to classify the power management problem as a fast decision making problem and energy management as a slower decision making problem, both of which share some common control variables.

The final stage in the modular structure is the Power Electronics Shell (PES), which is responsible for the actual power blending of multiple energy sources using power spit ratios determined by the PMS. The PES decomposes the reference power trajectories into appropriate control switching functions, which is then fed to a power electronics interface. Voltage and current regulation as well as system protection takes places within this process shell.

The complete modular structure can be described as hierarchical decision epochs as follows; the EMS provides a prescription for action to the PMS policy, which in turn generates the feed forward reference power trajectories to the PES. Outputs of the PES are duty cycle commands to the power electronic converter. Concisely, the EMS handles the system energy content, the PMS handles the power distribution and the PES processes the system voltages and currents. The three shells complete the PEMS implementation requirement. The illustration in Figure 5.4 and the following description summarises the modular structure.

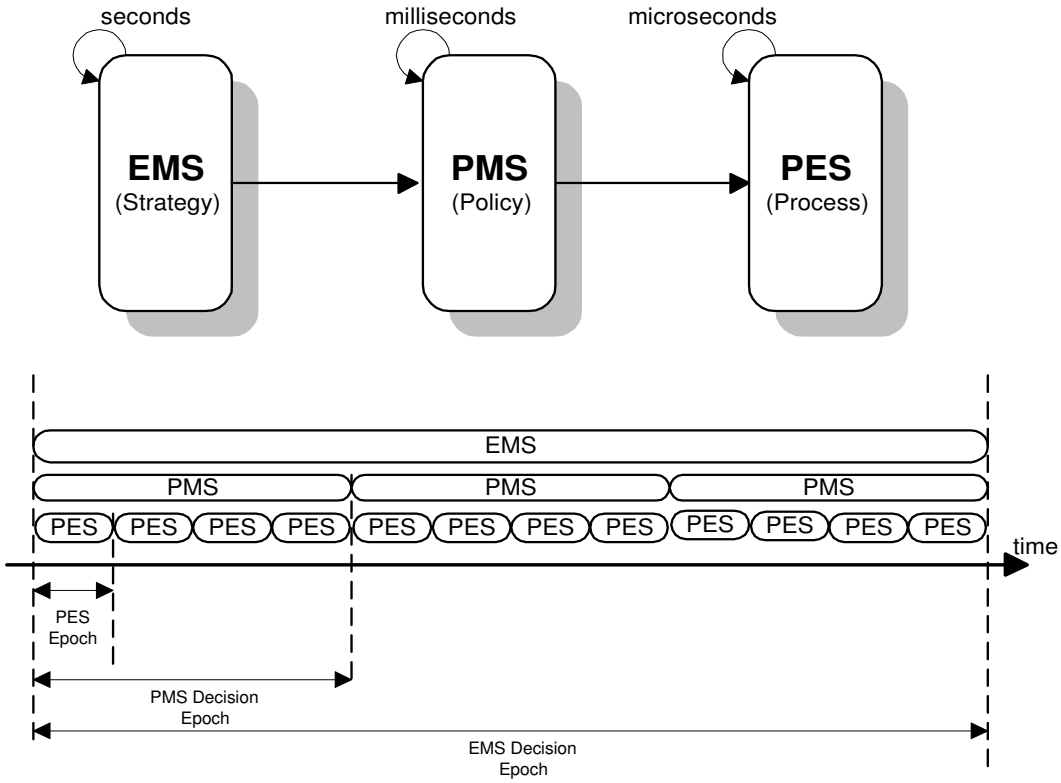

Figure 5.4 Concept of a modular power and energy management structure M-PEMS

Long term objectives- Energy Management Shell – ***Strategy***

- Decision epoch in terms of seconds with the period dictated by the energy storage system and vehicle longitudinal dynamics.

Medium term objective- Power Management Shell - ***Policy***

- Decision epochs in terms of milliseconds with the period dictated by the power demand dynamics

Short/Immediate term objectives - Power Electronics Shell – ***Process***

- Decision epochs in terms of microseconds with the period dictated by the power electronics converter topology and circuit dynamics

This modularity in the structure permits internal changes to be made within individual shells while still retaining the operational integrity of the rest of the system.

5.4 Energy Management Shell (EMS)

The Energy Management Shell (EMS) is responsible for the long-term decisions of energy expenditure and recuperation. Decisions within the EMS are based on parameters with time constants that are generally expressed in terms of seconds. These parameters are related to the energy storage state of charge, longitudinal dynamics of the vehicle and system temperature variations.

Strategies can be classified according to their dependency on the knowledge of future power demands and situational awareness. As described in Chapter 2, several non-causal control methods that suggest strategies based on future and predicted mission profiles have been extensively investigated. Although theses strategies serve in providing definitive benchmarks in terms of maximum achievable energy utilisation, these non-causal methods are not readily implementable. This is because with practical scenarios, the complete mission profile is not often known *a priori*. Even with a well-planned path, altitude, gradient and velocity profile, the total vehicle electrical power demands are not entirely exact. Due to this sensitive dependency to parameter variations, decisions made by non-causal strategies may not yield the forecasted end result for misclassified or arbitrary mission profiles. The reader is referred to [18] for an outline of non-causal optimal control energy management strategies for vehicles.

Heuristic and expert system approaches are candidates for EMS strategy implementation. Often designed using Boolean rule base or fuzzy inference engines, these methods offer a pragmatic solution. The primary advantage of such strategies is that they are intuitive to

conceive and implement. They offer a qualitative rather than a numerical description of the system. Strategies are formulated based on a set of static rules, which are tuned in an empirical recursive manner or using offline optimisation techniques. Empirical tuning of these strategies however requires expert knowledge of system threshold settings.

In any case, the strategy within the EMS observes and controls system parameters with relatively slow changing dynamics. The classification of 'slow changing' parameters is dependent on their time constants. Primarily, the vehicle longitudinal velocity, the energy system state of charge and the system temperature are parameters with rate of change specified in time magnitudes of seconds.

Unlike the charge sustaining strategies found in HEV systems, the endpoint SoC of the battery pack is not the same as the start point SoC in pure EVs. The SoC of the ultracapacitors however are cyclic and ideally would have a maximum value when the vehicle is at low or zero speed. EMS strategies indirectly serve as a vehicle range and autonomy extension under the assumption that the ultracapacitors are at a receptive state of charge to recuperate the regenerative energy and at a high state of charge to service peak power requests. Figure 5.5 illustrates the difference between a charge depleting and a charge sustaining energy storage system.

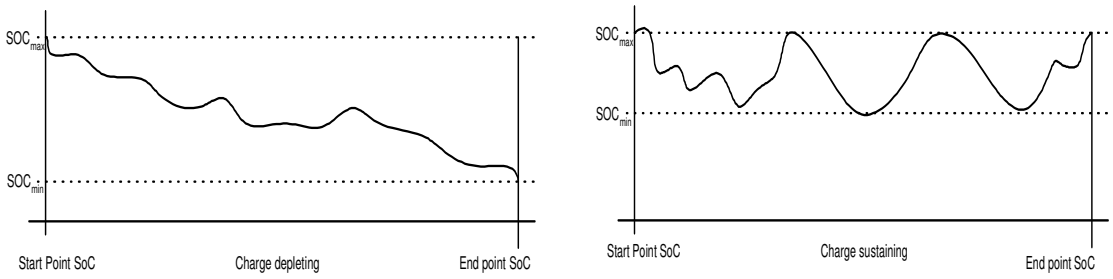

Figure 5.5 Charge depleting versus charge sustaining

5.5 Power Management Shell (PMS)

The objective of the Power Management Shell (PMS) is to determine the power distribution between the multiple energy systems under continuous vehicle power demands. A policy within the PMS specifies the decision rules and constraints for generating these power

distribution commands or actions. The task of the PMS is then to cyclically implement the policy as a deterministic task and choose a set of actions from a set of allowable action states. Some similarities in this concept of defining policies prescribing actions from a set of action states are to be found in stochastic decision making theory [113].

In the case of a system comprising of batteries and ultracapacitors as the energy source, a power management policy that mitigates peak power from the battery to the ultracapacitors results in an increase in the energy efficiency of the batteries and therefore also contributes to extending the autonomy of the vehicle. A policy may also include the prevention of over discharging and over charging beyond the rated power limits and to prevent high frequency power fluctuations of battery system. In any case, the primary goal of a power management policy is to continuously satisfy the load requirements. For *m* number of energy storage systems denoted by *Pe* with index *i*, the power equilibrium between the required load power and the delivered power can be generically expressed as,

$$P_{Load}(t) = \sum_{i=1}^{i=m} Pe_i(t) \quad \forall t, \quad i, m \in \aleph^+ \tag{5-2}$$

with the maximum (discharging) power and minimum(charging) power constraints as,

$$Pe_{i,\min} \le Pe_i(t) \le Pe_{i,\max}, \quad i = 1,..m, \tag{5-3}$$

where, $Pe_{i,\min} \le 0 < Pe_{i,\max}$

A policy for power splits between a battery pack and an ultracapacitor pack can be formulated and solved formally using several methods. As discussed in Chapter 2, there are various approaches to this. A common method, as also investigated at an early stage of this work, [*see Paper 2 in Publication list*] is to express a power management policy as a minimisation of a cost function. In a system sourced by batteries and ultracapacitors and for a load power (P_{req}) demand profile, a correlation between battery power and ultracapacitor power can be expressed by the following objective function,

$$J = \min_x \sum_{k=1}^{k=N} \{P_{req}(k) - (\underbrace{w_1(k).P_{uc}(k)}_{\substack{effective \\ Ultracapacitor \\ Power}} + \underbrace{w_2(k).P_b(k)}_{\substack{effective \\ Battery \\ Power}})\} \tag{5-4}$$

where,
P_{req} is the requested load power
P_{uc} is the fitting value corresponding to ultracapacitor power
P_b is the maximum defined battery power
w_1 is the weighting factor of ultracapacitor power
w_2 is the weighting factor of battery power
N is the time segment over the drive cycle

With a fixed maximum battery power (Pb), the objective is to determine optimal sharing of battery and ultracapacitor power for a given load power request within the following constraints

$$w_1, w_2 \in [0,1] \quad (5\text{-}5)$$
$$w_1 + w_2 = 1 \quad (5\text{-}6)$$
$$0 \le P_{uc} \le P_{\max} \quad (5\text{-}7)$$

where P_{max} is the maximum load power

It is desirable that for the objective function, load power requirements of less than the maximum defined battery power be predominately contributed by the battery itself. Using nonlinear least squared optimization methods, the optimization routine generates a proportioning ratio of ultracapacitor and battery power that satisfies the required load power demand. This method is not without its caveats. Although, by including more constraints to the objective function, the biasing of the power splits can be further tuned, this method requires the power demand of entire demand cycle to be known in advance and requires a substantial amount of time to compute. Hence it only serves as a tool for offline analysis of a power management policy. A more practical technique to implement a power management policy will be presented in Section 5.8.

5.6 Power Electronics Shell (PES)

As presented in Chapter 2, the active hybridisation of multiple electrical energy systems requires some form of power electronics interfacing method. The facility and operation to do this can be encapsulated within the PES. The PES is then seen as the downstream process in the hierarchy that performs the actual summation of power from multiple energy sources. Power split decisions generated by the upstream PMS process is decomposed into

the required controlled switching functions. With reference to Figure 5.6, these switching functions are PWM signals with varying duty-cycles represented by D1 and D2. Generically, for *m* number of reference power signals (Pe_i), $D1_i$ represents the duty cycle derived from the charging power reference while $D2_i$ is derived from the discharging power reference.

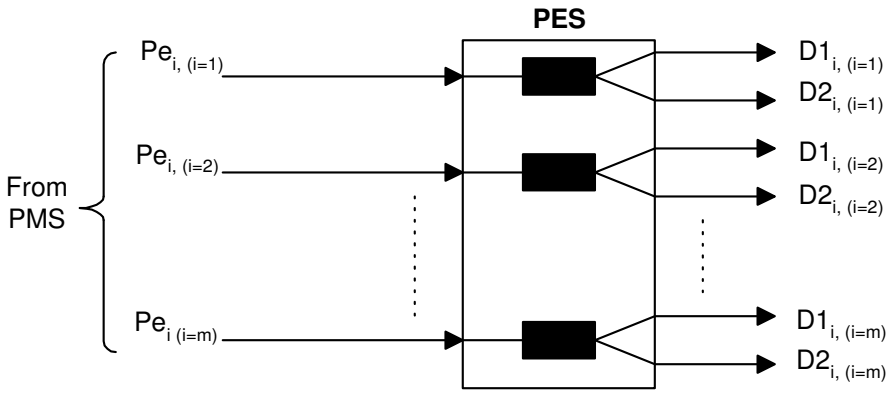

Figure 5.6 Generic PES structure

5.7 M-PEMS implementation for a battery - ultracapacitor powered Electric Vehicle

The concept described in the previous sections can be readily implemented in power and energy management of electric vehicle sourced by batteries and ultracapacitors. The first stage in the design is to identify the input-output or connection matrices between the process shells. With reference to Figure 5.7, the EMS input parameters are slow charging variables such as the vehicle velocity, operation mode, energy source state of charge and temperature. Output variables of the EMS are battery and ultracapacitor parameters that influence power management. These variables are, the maximum battery discharging power, the battery recharging power, the battery positive and negative rate of power change, the maximum ultracapacitor discharging power, the maximum ultracapacitor charging power and the magnitude of the ultracapacitor charging power.

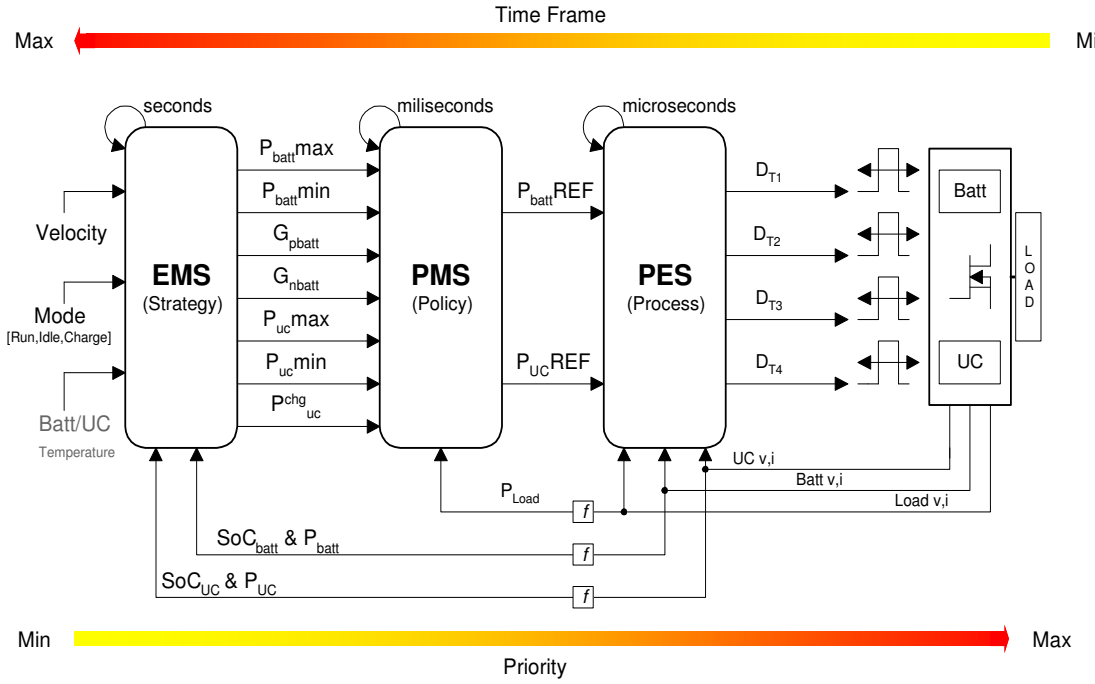

Figure 5.7 M-PEMS implementation for a battery-ultracapacitor sourced EV

Based on the values of the input parameters as well as the measured load power, the PMS produces two output parameters corresponding to the battery and ultracapacitor reference power trajectory derived by the PMS policy. The PES generates the duty cycle commands required by the selected converter topology. For a half bridge topology, the number of duty cycle signals required for n number of electrically rechargeable energy storage systems and m number of non-electrically rechargeable systems is $2n+m$. Since both the batteries and ultracapacitors are electrically rechargeable, the required duty cycles are equal to four. The following three sections demonstrate the implementation of the M-PEMS by addressing each shell individually. For clarity of explanation, the operation of the PMS is presented first followed by the EMS and PES.

5.8 Implementation of a PMS Policy

As describe in section 5.3, the PMS executes a policy under constraints dictated by the EMS strategy. A policy requires a formal definition. Here a policy is formulated to mitigate both positive and negative peak power demands from the batteries to the ultracapacitors while adhering to the battery power limitation and trajectory gradient constraints.

The policy of the PMS is intended to satisfy the following discretised power balance equation,

$$P_{Load}(k) = P_{batt}(k) + P_{uc}(k) \quad \forall k \tag{5-8}$$

subject to the following constraints,

$$P_{batt,uc}(\min) \leq P_{batt,uc}(k) \leq P_{batt,uc}(\max) \tag{5-9}$$

$$P_{batt}(k) \leq P_{batt}(k-1) Gp_{batt} \qquad if \; P_{batt}(k) > 0 \tag{5-10}$$

$$P_{batt}(k) \leq P_{batt}(k-1) Gn_{batt} \qquad if \; P_{batt}(k) < 0 \tag{5-11}$$

where,

P_{Load} is the load power at the DC bus, P_{batt} is the battery pack power, Gp_{batt} is the battery positive slew coefficient, Gn_{batt} is the battery negative slew coefficient, $P_{batt,uc}$ max is the maximum battery discharging (sourcing) power, P_{batt} min is the maximum battery charging (sinking) power.

As presented in Chapter 3, limiting both the maximum battery power and the step change in power has a positive attribute of extending the run time and the long-term life cycle of the battery [5] [94] [95]. These factors are incorporated into the policy as constraints (5-10) and (5-11). The battery power limits ($P_b max_i$, $P_b min_i$) and the power rate limits (dP_b/dt) as a function of the battery state of charge is illustrated in Figure 5.8. In the diagram, Gp_{batt} (affix 'p' to indicate positive power) and Gn_{batt} (affix 'n' to indicate negative power) respectively represent the discharging and charging power rate constraints within a specified PMS

decision epoch window (ΔPMS). The inclusion of these constraints in the PMS policy definition hence permits control of the step change of both discharging and charging power levels.

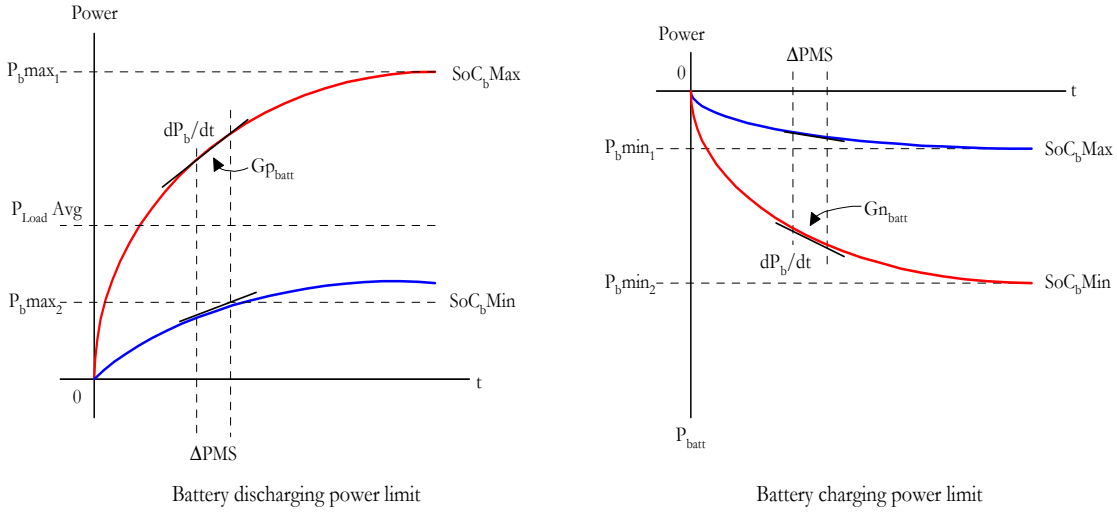

Figure 5.8 Battery discharge and charge power limitation

The power management policy operates to correct load disturbances in the DC bus in a receding time horizon. The horizon time window is in fact the PMS decision epoch, which is time-constrained to generate the reference power trajectories. The operation of such a method is with the assumption that an intermediate energy storage device between the battery – ultracapacitor systems and the load has sufficient energy to service all load demands within the PMS epoch. This intermediate link is the DC bus capacitance, which is sized to meet the load regulation requirements. Under theses assumptions, the power proportioning ratio between the battery and ultracapacitors are derived within the power management shell as follows:

For the battery system, the PMS policy determines a reference power trajectory as,

$$P_{batt}(t+DT) = \begin{cases} \min[P_{b1}, P_{b2}, P_{b3}] & if\ P_{Load}(t) > P_{avg} \\ \max[P_{b1}, P_{b4}, P_{b5}] & if\ P_{Load}(t) < 0 \\ P_{b6} & if\ 0 \le P_{Load}(t) < P_{avg} \end{cases} \quad (5\text{-}12)$$

where

$$P_{b1} = P_{Load}(t + DT) \quad (5\text{-}13)$$

$$P_{b2} = P_{batt}(t) + G_{pbatt} \cdot DT \quad (5\text{-}14)$$

$$P_{b3} = P_{batt}\max \quad (5\text{-}15)$$

$$P_{b4} = P_{batt}(t) + G_{nbatt} \cdot DT \quad (5\text{-}16)$$

$$P_{b5} = P_{batt}\min \quad (5\text{-}17)$$

$$P_{b6} = P_{Load}(t + DT) + P_{uc}^{chg}(t + DT) \quad (5\text{-}18)$$

where, P_{avg} is the power level at or below which opportunity charging of the ultracapacitor is permissible, P_{uc}^{chg} is the battery to ultracapacitor charging power and *DT* is defined as the time step of the PMS epoch where *DT* =ΔPMS.

Formulation of the PMS policy decision criteria to determine the ultracapacitor reference power is accomplished using a similar technique. Unlike the battery systems, the ultracapacitors can be subjected to rapid and high power demand cycles. If the ultracapacitor system is dimensioned with the capability to meet the maximum instantaneous load power demands, the rate at which the power can be transferred will meet the rate at which the power is demanded. Because of this power delivery quality, a step change limiter on the ultracapacitor reference power is not required. This is illustrated in Figure 5.9 as a constant discharging and constant charging power limit within the PMS decision epoch.

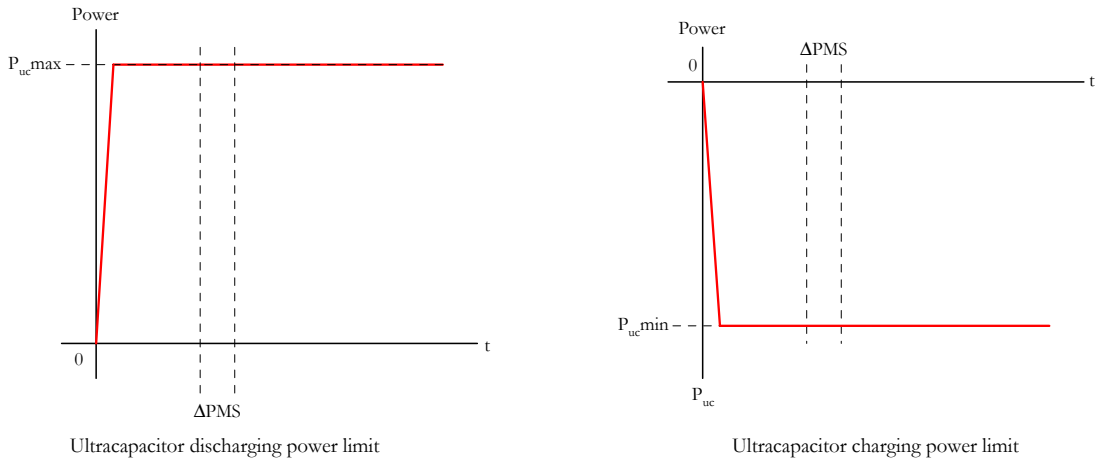

Figure 5.9 Ultracapacitor discharge and charge power limitation

Following this, the ultracapacitor pack reference power trajectory is determined as,

$$P_{uc}(t+DT) = \begin{cases} \min[\ P_{u1}, P_{u2}\ ] & if\ \ P_{Load}(t) > 0 \\ \max[\ P_{u1}\ , P_{u3}\ ] & if\ \ P_{Load}(t) < 0 \\ P_{u4} & if\ \ 0 \le P_{Load}(t) < P_{avg} \end{cases} \tag{5-19}$$

where

$$P_{u1} = P_{Load}(t+DT) - P_{batt}(t+DT) \tag{5-20}$$

$$P_{u2} = P_{uc}\ \max \tag{5-21}$$

$$P_{u3} = P_{uc}\ \min \tag{5-22}$$

$$P_{u4} = -\,|\,P_{uc}^{chg}(t+DT)\,| \tag{5-23}$$

and P_{uc} is the ultracapacitor power, P_{uc}max is the maximum ultracapacitor discharging power and P_{uc}min is the maximum ultracapacitor charging power.

The power splits between the battery and the ultracapacitor are not determined simultaneously but rather sequentially. Referring to the policy that was just described, equation (5-19) is evaluated after equation (5-12). The policy is said to be Markovian [113] since it depends only on the previous state. It is also considered a stationary-deterministic

policy, since the policy is fixed and the action is chosen with certainty and within the decision epoch.

Figure 5.10 provides an illustration of the PMS policy. Essentially, the policy evaluates the load demand, which comprises of peak power, continuous power and ultracapacitor charging power (opportunity charging) demands. The power balance equation (5-8) still holds valid during opportunity charging since the sinking power operation of ultracapacitor is seen as an increase in the load and hence the battery power services both the actual load demand as well as the ultracapacitor charging demand.

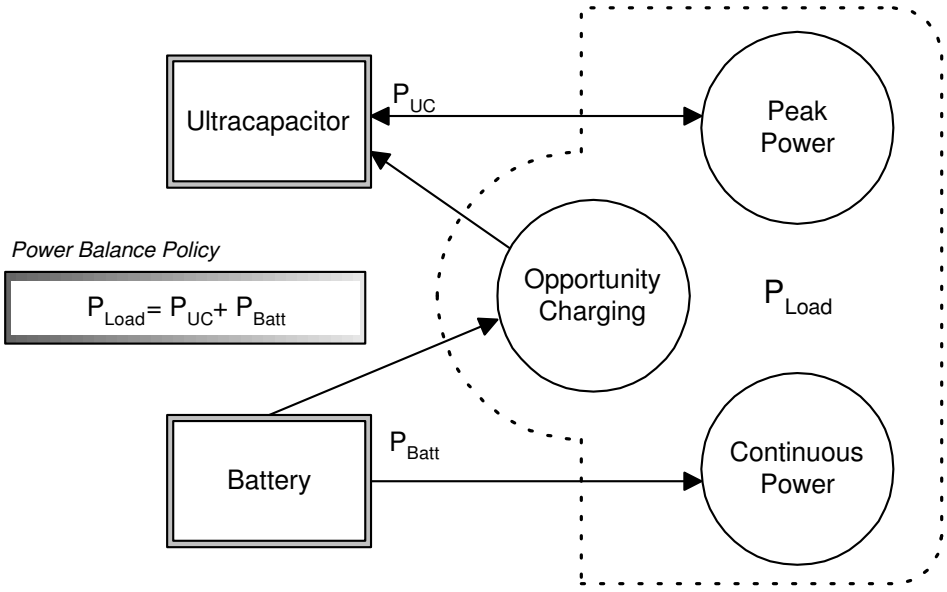

Figure 5.10 Illustration of the PMS policy

Figure 5.11 shows the PMS policy acting on an arbitrary load demand profile. As dictated by setting the policy variables, the battery services all power requests within the specified operating constraints while both positive and negative peak power requests are mitigated to the ultracapacitor bank. In the simulation, $P_{batt,}$ max is set to 30kW with a Gp_{batt} of 5kW/s and no regenerative capability on the battery pack, (P_{batt} min = 0). The forced restriction of the battery positive step change is illustrated in Figure 5.12.

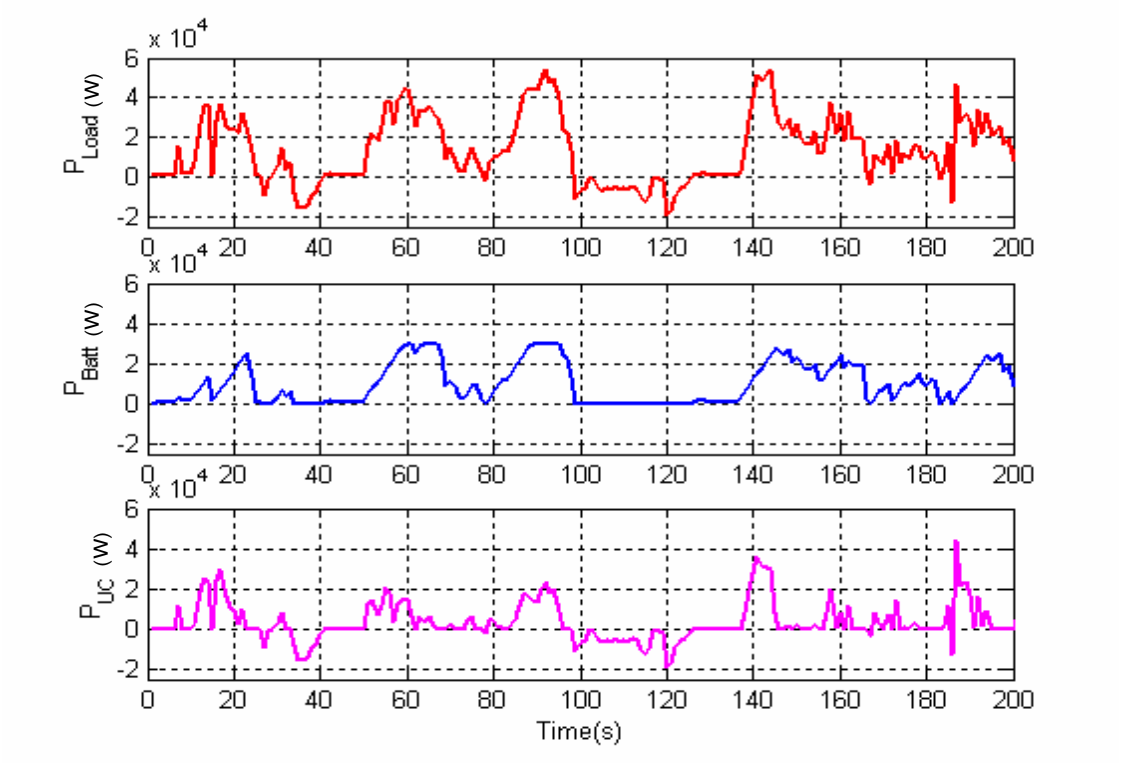

Figure 5.11 Load power and battery vs. ultracapacitor power split.

(Peaks and all regenerative powers are handled by the ultracapacitors)

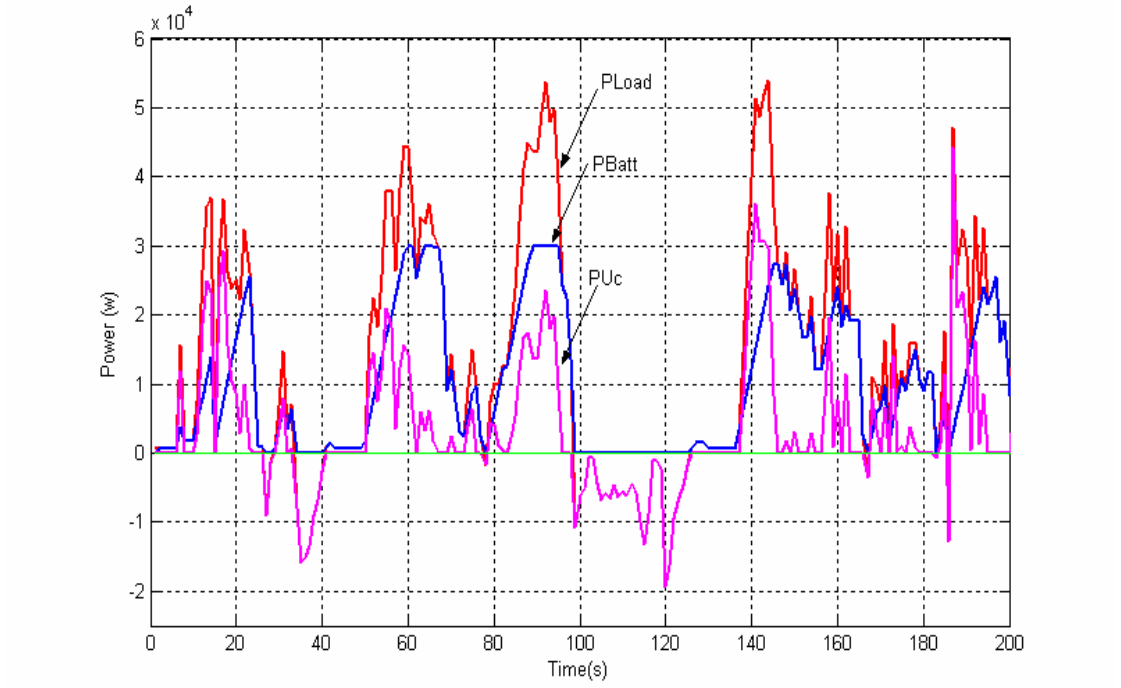

Figure 5.12 Superimposed load power demand and battety –ultracapacitor power split.

(The effect of G_{pbatt}, which limits the response of the battery is noticeable during positive peak)

To enforce and guarantee that the power balance policy (equation 5-8) is always met, an addition to the policy definition is required. Since the reference power of the ultracapacitors is determined after the battery reference power, there is a possibility that insufficient ultracapacitor power levels may causes the power balance equation not to be satisfied. This occurs at a condition when,

$$P_{uc}\max\ (k) < P_{Load}\ (k) - P_{batt}\ (k) \tag{5-24}$$

Under this condition, the battery power is increased to compensate for the unavailable ultracapacitor power by altering the predetermined reference battery power such that,

$$P'_{batt}\ (k) = P_{Load}\ (k) - P_{uc}\max\ (k) \tag{5-25}$$

From a power management point of view, this condition results in a non-ideal situation, which causes the maximum battery power limit to be exceeded in order to satisfy the power balance policy. For the purpose of policy evaluation over a period of time, it is possible to capture this condition and encode it as a penalty tracking function as follows,

$$Pf_{PMS} = i\{k, P'_{batt}, P_{uc}, P_{Load}\} \tag{5-26}$$

where i is an incremental index with initial value zero and advances by a unit step each time (5-25) is invoked such that,

$$i(k) = \begin{cases} i(k-1)+1 & if\ \ P_{uc}\max\ (k) < P_{Load}\ (k) - P_{batt}\ (k) \\ i(k-1) & otherwise \end{cases} \tag{5-27}$$

Therefore a high value of i results in a high PMS policy penalty count. The invocation of each penalty point as well as the respective power values is then traceable with reference to time step k.

An important difference with the power management policy is that power split decisions are made using only power fluctuations at the DC Bus rather than the conventional methods of monitoring the throttle input (driver input). This leads to the ability of including propulsion as well as non-propulsion loads in the implementation framework without changing the formulation of the policy.

5.9 Implementation of an EMS Strategy

Consider a strategy to maintain the kinetic to electrical energy balance correlation (5-28) by regulating the SoC of the ultracapacitor bank as a function of the vehicle velocity

$$E_{uc} + E_{kin} = K \tag{5-28}$$

with constraints that battery and ultracapacitor SoC ranges between

$$SoC_{batt,uc}(\min) \leq SoC_{batt,uc}(k) \leq SoC_{batt,uc}(\max) \tag{5-29}$$

where E_{uc} is the instantaneous energy of the ultracapacitor bank and E_{kin} is the instantaneous kinetic energy of the vehicle, with both the energy levels balanced by constant K.

The strategy is to ensure that the ultracapacitors are held at an acceptable state of charge such that the ultracapacitors are both capable of delivering peak power requests and are receptive to regenerative power conditions. Since no prior information regarding the mission profile is known, the energy balance strategy can be assumed as a speculation of energy usage under uncertainty. As the strategy implemenation tool, fuzzy logic control is employed. The fuzzy logic controller operating within the EMS follows a repetitive cycle that can be described as follows. Measured variables and derived parameters are mapped into fuzzy sets through a fuzzification process, which also capture the uncertainties of the measured values. Following this, a fuzzy inference engine evaluates the fuzzy sets according to control rules defined in a fuzzy logic rule-base. Based upon rule-base evaluation, an

output fuzzy set is produced. The final output of the controller is single scalar value representing the control action performed on the input variables.

As fuzzy logic permits systems to be controlled by heuristic representation of how the system should behaves [114], this feature is employed to generate the battery maximum power ($P_{batt}max$) reference output of the EMS. In this application, the rule base is designed using heuristic reasoning of the energy management strategy. Base on the following postulates, dictated by the energy balance equation of vehicle kinetic energy to ultracapacitor potential energy (5-28), a fuzzy inference system (FIS) is implemented.

Heuristic reasoning- 1

" If the vehicle is travelling fast and close to its maximum velocity, and the ultracapacitor state of charge is high, then reduce the maximum battery power limit so that the power management shell will be forced to use the energy stored in the ultracapacitor and accordingly bias the feed forward reference power trajectories towards the ultracapacitors, thus reducing its state of charge "

Heuristic reasoning- 2

" If the vehicle is at medium velocity, whereby a rapid power demand to accelerate the vehicle could occur, but the ultracapacitors are at a low state of charge, then increase the battery power limit so that opportunity charging of the ultracapacitors by the battery system can take place ".

The vehicle speed input is defined by three membership functions, {Slow, Medium, Fast}. Similarly, the ultracapacitor SoC membership function is defined by {Low, Medium, High}. With x_1 and x_2 as the state variables and y representing the output variable, the FIS is represented as a two input one output system in a generic form of conjunctive rules as follows:

$$\underbrace{IF\ x_1\ is\ A_{i1}\ AND\ x_2\ is\ A_{i2}}_{Fuzzy\ Rule\ Antecedent}\ THEN\ \underbrace{y_i = \Psi_i(x_1, x_2)}_{Fuzzy\ Rule\ Consequent} \tag{5-30}$$

With $P_{batt}max$ as the output function of the fuzzy inference system, an instance of a rule statement to construct the fuzzy rule base is as follows:

FIS $\rightarrow$ ***IF*** Speed is FAST ***AND*** Ultracapacitor SoC is HIGH ***THEN*** $P_{batt}max = P_{batt}max_i$

For the 2 antecedent fuzzy rule, the firing strength for the i-*th* rule is given as [96],

$$\beta_i = \prod_{j=1}^{j=2} Aij \tag{5-31}$$

Through recursive computation for each rule, the crisp fuzzy logic output variable $P_{batt}max$ output is evaluated as,

$$P_{batt}\max = \frac{\sum_{i=1}^{i_{\max}} \prod_{j=1}^{j=2} A_{ij}(x_j)\Psi_i}{\sum_{i=1}^{i_{\max}} \prod_{j=1}^{j=2} A_{ij}(x_j)} \tag{5-32}$$

Figure 5.13 provides a graphical illustration of the Fuzzy Inference System.

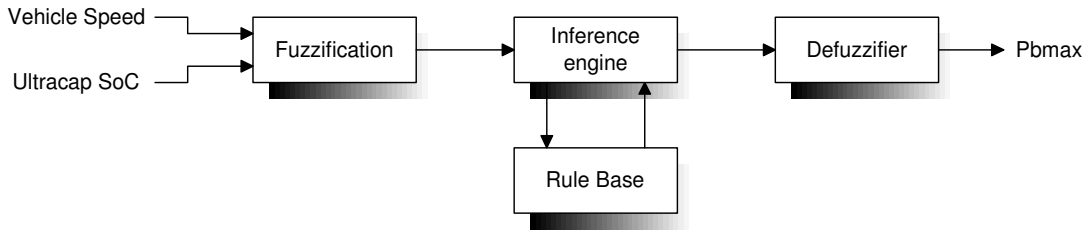

Figure 5.13 EMS Fuzzy Inference System block diagram

By regulating the parameter $P_{batt}max$, which is fed to the PMS, the proportioning ratio of powers can be biased towards the ultracapacitors. In effect, this forces ultracapacitor energy to be drawn even though the load power demand trajectory does not explicitly require it. Figure 5.14 graphically depicts the mapping of the FIS antecedents (velocity and Ultracapacitor SoC) while Figure 5.15 shows the FIS decision surface composed of 9 rules (i=9).

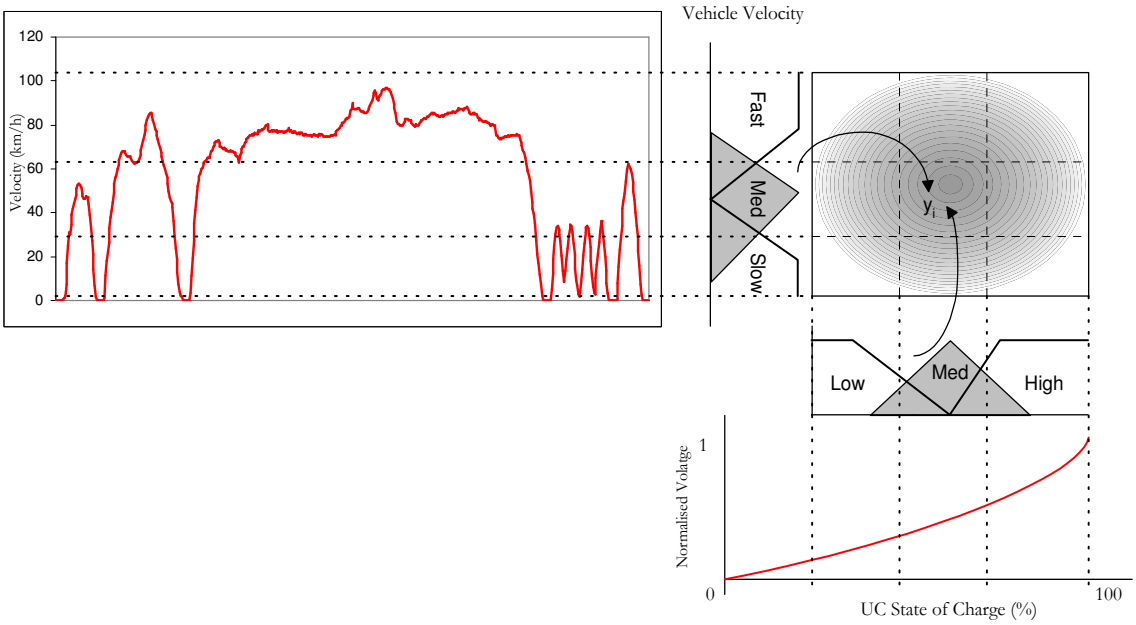

Figure 5.14 Illustration of the FIS mapping from antecedent space to consequent space

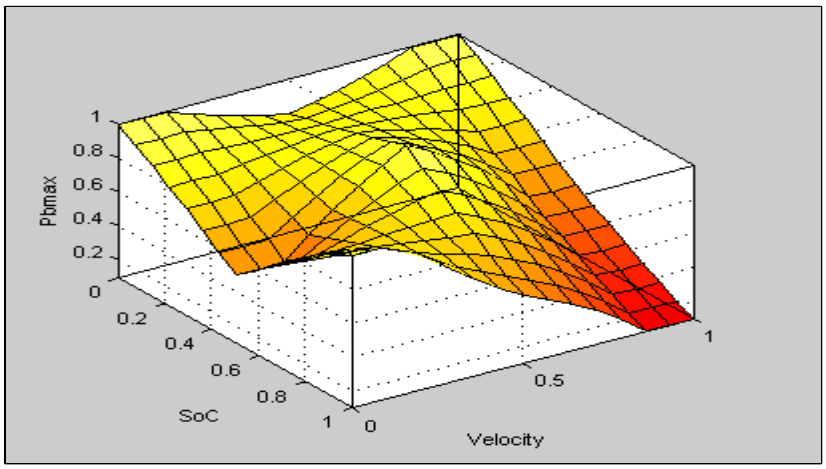

Figure 5.15 FIS decision surface for the EMS.

(Velocity and ultracapacitor are the antecedents and $P_{batt}max$ is the consequent)

In this strategy, only P_{batt}max is varied throughout the decision epochs with all other outputs held at constant values determined by design. The influence of the EMS over a standard US06 schedule is illustrated in Figure 5.16 and Figure 5.17. With both simulations, the starting SoC of the ultracapacitors are equal and set just below the maximum value. In Figure 5.16, the EMS is not activated and so the power split between the battery and ultracapacitor is determined by the fixed policy constraints of the PMS. Ultracapacitor power is only required when the load demand exceeds the defined battery capability and no intervention of its target SoC is performed. As shown in the second graph of Figure 5.16, during the second deceleration to zero speed event the ultracapacitor is charged via regenerative braking but only to its maximum SoC. For illustration purpose, the SoC graph of Figure 5.16 shows the rise of SoC above the maximum value as the extra capacity required to harness the regenerative energy. In this scenario, the activation of dissipative (dynamic) brakes is required. This is shown in the bottom graph of Figure 5.16.

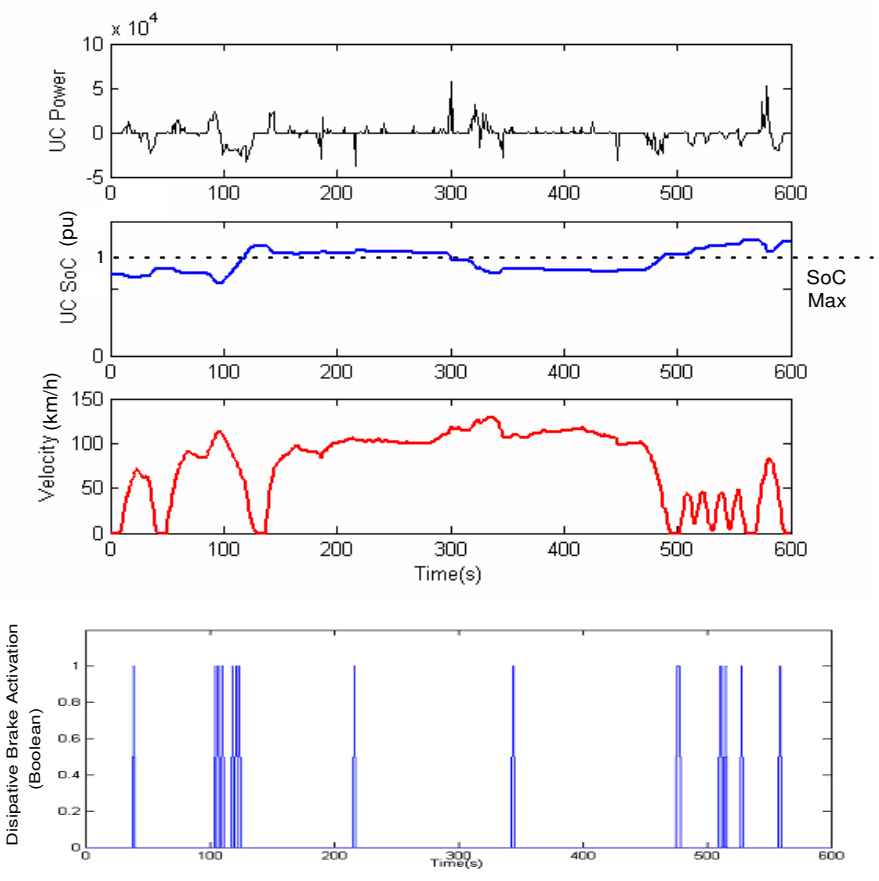

Figure 5.16 Simulation of ultracapacitor SoC without the EMS.

(Activation of dissipative brakes is necessary to absorb access regenerative power)

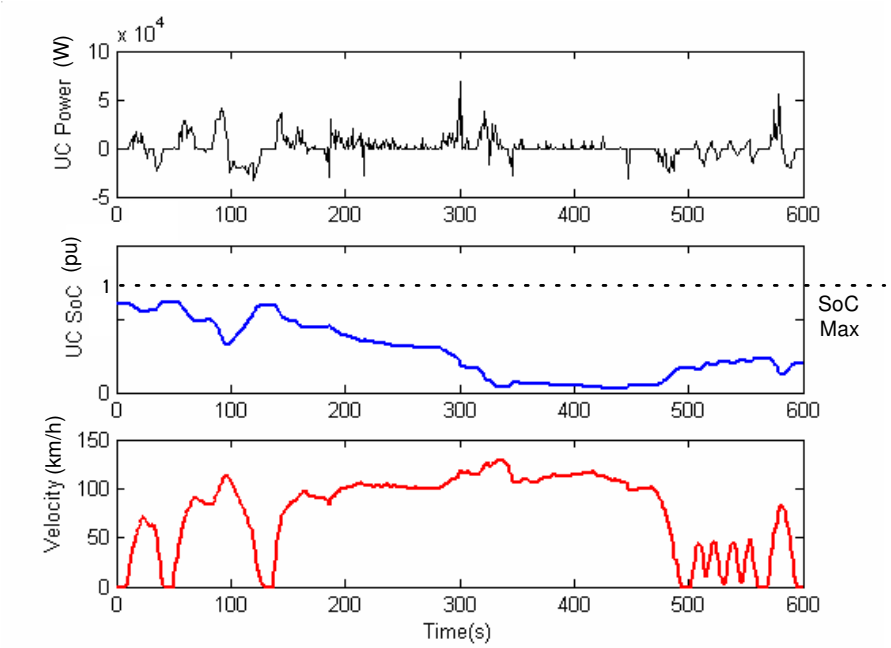

Figure 5.17 Simulation of ultracapacitor SoC wit the EMS active.

(The EMS drives the ultracapacitor SoC down during high velocity)

The activation of the EMS with the fuzzy inference engine to regulate the ultracapacitor SoC in relation to the vehicle speed is shown in Figure 5.17. As shown in the second graph of Figure 5.17, the EMS drives the ultracapacitor SoC down as the vehicle cruises at high velocity. The EMS senses that both the vehicle and the ultracapacitor SoC falls in a HIGH membership function and thus reduces the maximum battery power reference value ($P_{batt}max$) fed to the PMS. Since the policy of the PMS mandates the power balance equation (5-28) be satisfied, the ultracapacitor power is increased to compensate for the battery power limit. This effectively reduces the ultracapacitor SoC in anticipation of a regenerative event. Comparing the ultracapacitor power graphs of Figure 5.16 and Figure 5.17, shows that with the EMS activated, more ultracapacitor power is used at high velocity to regulate the target SoC. The use of dissipative brakes is not required in the second scenario as the ultracapacitors are receptive to regenerative energy.

The results satisfactory demonstrate the concept of the hierarchical execution of an energy management strategy. It exemplifies the downstream propagation of EMS strategy directives

to a fixed PMS policy. As described, the formulation of the strategy and the selection of control thresholds are based on heuristic knowledge and thus by no means represent an optimal strategy. It does however represent a strategy that attempts to maintain the ultracapacitor energy system within operating boundaries that favour energy recuperation for an unknown mission profile.

5.10 Extending the EMS strategy

With the strategy just described, only one of nine parameters linking the EMS to PMS of the M-PEMS implementation structure (Figure 5.7) is controlled. In the demonstration, the assumptions were that all other PMS input parameters were held constant. Even with this, the effect of the EMS as an ' energy manager ' is plainly demonstrated. Figure 5.18 shows how the EMS strategy can be extended to control other PMS input variables. In the diagram, control block f_1 having velocity and ultracapacitor SoC as the input parameter and P_{batt}max as the controller output corresponds to the fuzzy inference system previously described.

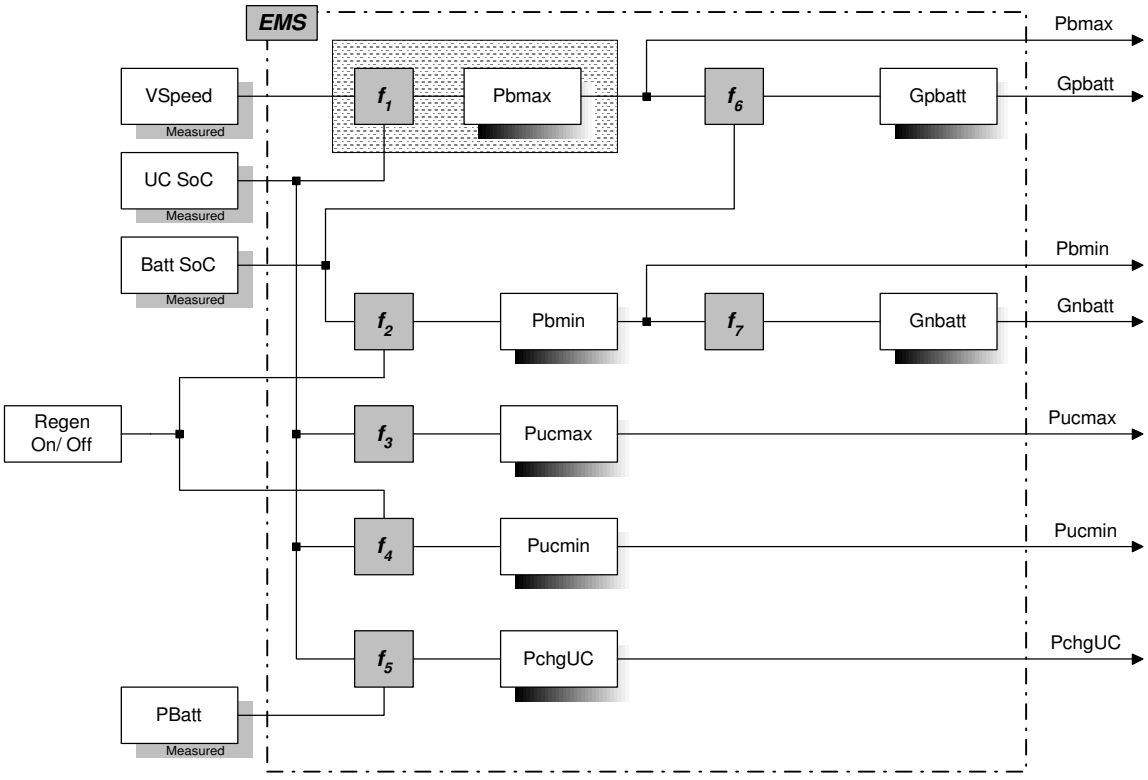

Figure 5.18 Extended EMS strategy framework

5.11 Implementation of a Power Electronics Shell

Operation of the PES can be formally represented as a state machine. The design of the state machine is done in three steps. First, the possible power demand segments that capture the direction of the power demand trajectories is identified. The identification of the power demand segments are shown in Figure 5.20. Following this, the battery and ultracapacitor operating modes are defined based on the classification of the power demand. Table 5.1 lists the eight operating combinations of the batteries and ultracapacitors. The unique operating states of the battery and ultracapacitor are defined using sequential Boolean representation [000] to [110]. The notion behind this representation is that the MSB of the three digits represents the battery state while the LSB represents the ultracapacitor state and the middle bit represents the DC Bus. With the exception of State [011], a '**1**' in the corresponding bit positions indicate an outgoing power flow while a '**0**' indicates an incoming or zero power flow. In State [011] however, the batteries are being charged via the DC bus while the ultracapacitors fully charged but are inactive (zero power). This state also captures the condition when the batteries are being charged by an external source. Figure 5.19 illustrates the representation of the PES states.

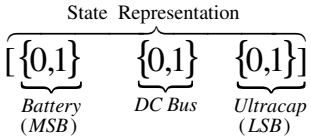

Figure 5.19 Three digit PES State represenation

Finally, the possible transitions between these states are determined based on permissible battery, and ultracapacitor and vehicle operating status change. With the possible operating modes and transitions, the action space of the power electronics shell (PES) is encoded and verified as a finite state machine as shown in Figure 5.21. Along with eight operating modes defined in Table 5.1, a Start, Stop and State BR are added to complete the state machine. The transition to state BR only occurs when the ultracapacitors are fully charged and the batteries are unreceptive to regenerative power. In such an event, the DC bus voltage rise is limited by the activation of the dynamic brake resistor to thermally dissipate the access energy. This condition was demonstrated in Section 5.9 (EMS).

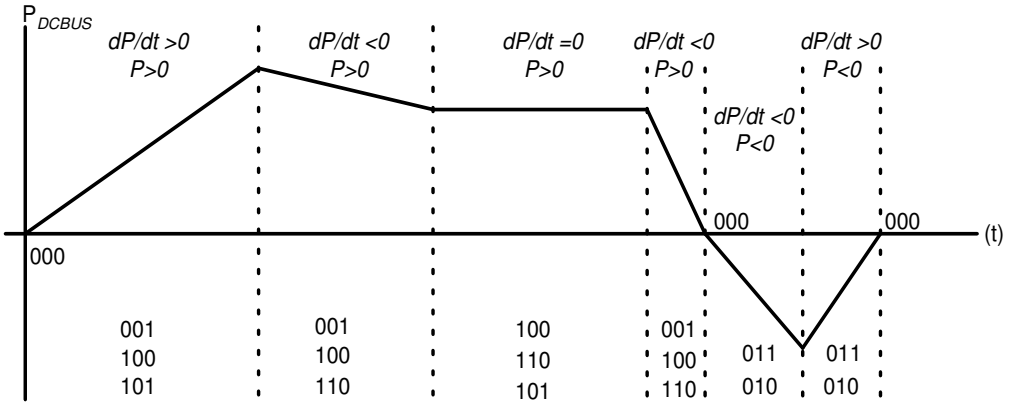

Figure 5.20 Segmentation of a generic power demand profile

State	Battery	Ultracapacitor	Operating condition
000	Quiescent / Transition	Quiescent / Transition	Zero load condition or zero battery/ ultracapacitor current crossing to next state
001	Quiescent	Discharging	Conditions require only the ultracapacitors to service the requested load demand.
010	Quiescent	Charging	Ultracapacitors are charging via regenerative DC Bus power.
011	Charging	Quiescent	Ultracapacitors are fully charged and surplus regenerative power diverted to batteries at limited charging rate
100	Discharging	Quiescent	Batteries are discharging within operating constraints and the ultracapacitor are at target SoC
101	Discharging	Discharging	Both batteries and ultracapacitors are discharging within specified maximum discharge rate and power level
110	Discharging	Charging	Batteries are servicing all load demands and charging the ultracapacitors
BR	*Quiescent*	*Quiescent*	*Atypical condition requiring activation of dissipative brake resistor for failsafe operation*

Table 5.1 PES stipulated operating modes

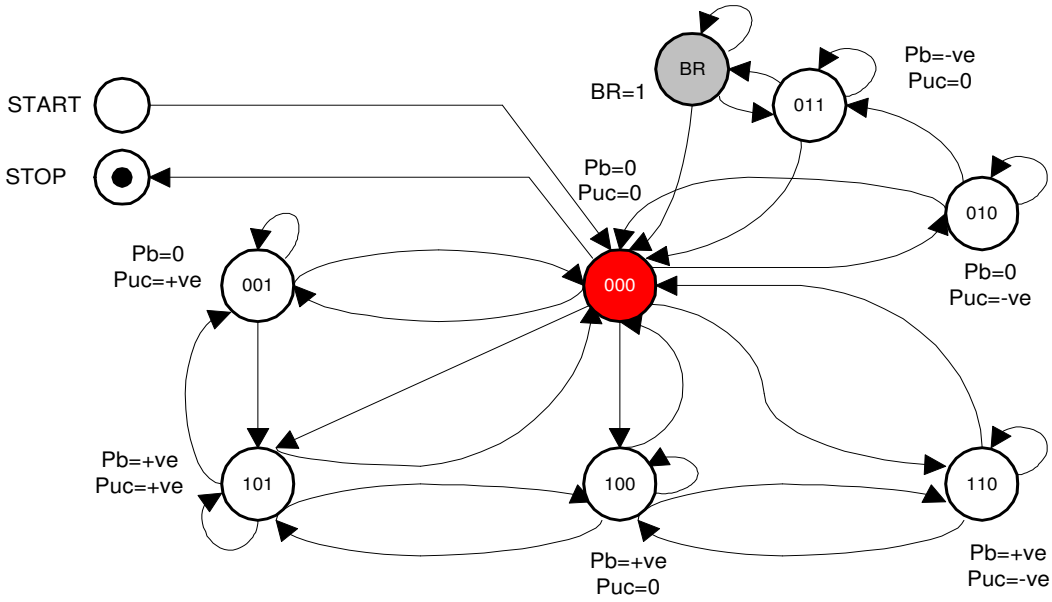

Figure 5.21 PES State machine representation

The transitions between states are associated with the load power demands, which is normally a desired command by the vehicle driver or mission sequencer. In other situations, transitions are a result of the energy system state and rather than a direct load demand. For example, the transition from the state where only the battery services the load demand while the ultracapacitor is inactive (STATE 100) to a state that the battery services the load and charges the ultracapacitor (STATE 110).

Recalling the generic PES structure illustrated in Figure 5.6, the outputs of the PES are duty cycle commands. The task of the PES involves the mapping of the input feed forward reference power variables to the output duty cycle control variables. Along with the reference power to be converted, there will also be the associated thermal power losses and cross-coupling power losses involved during the power conversion process. Thus, the mapping of duty cycle D_{Ti} to reference power P_{ref} through connection matrix A and power loss matrix P_{loss} can be generically expressed as,

$$[D_{Ti}] = [A].[P_{ref}] + [P_{loss}] \tag{5-33}$$

For a PES with two reference powers (Pb, Puc) and four duty cycle outputs ($D_{T1,}$ $D_{T2,}$ $D_{T3,}$ D_{T4}*),* the generic expression of (5-33) can be rewritten as,

$$\begin{bmatrix} D_{T1} \\ D_{T2} \\ D_{T3} \\ D_{T4} \end{bmatrix} = \begin{bmatrix} A_{mn} & \cdots \\ \vdots & \end{bmatrix} . \begin{bmatrix} Pb \\ Puc \end{bmatrix} + \begin{bmatrix} P1 \\ P2 \\ P3 \\ P4 \end{bmatrix} \tag{5-34}$$

where,

P1, P2, P3 and P4 are the associated converter losses and the connection matrix A having m row and n columns is to be determined. D_{T1} and D_{T2} are the respective duty cycles for battery charge and discharge while $D_{T\,3}$ and D_{T4} respectively represent the ultracapacitor charge and discharge duty cycles.

In addition to constructing connection matrix A, there is a need to construct a state transition matrix for the PES state machine. To accomplish both these tasks, some expansion to the reference power signals is required. The reference power for both batteries and ultracapacitors are split into discharging (positive) and charging (negative) power values and represented as {Pb^+, Pb^- , Puc^+, Puc^-}. In addition, Boolean flags {#Pb^+, #Pb^- , #Puc^+, #Puc^-} indicating the direction of power flow are derived as shown in Figure 5.22.

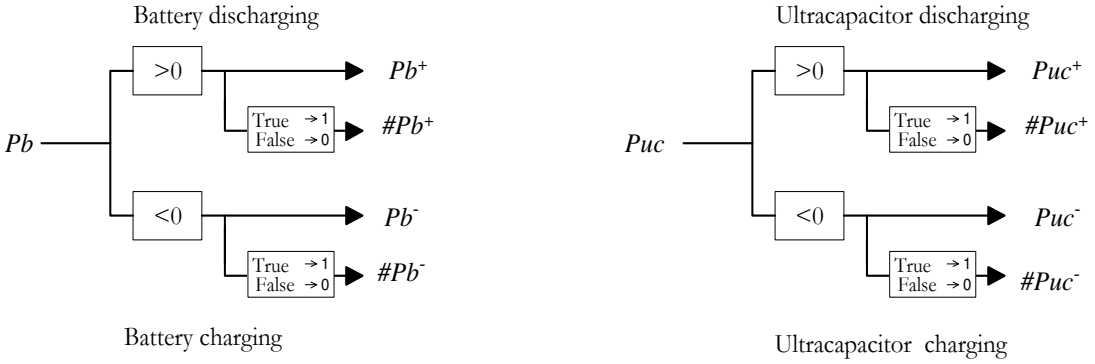

Figure 5.22 Expansion of the PES power reference signals

With the reference power input matrix expanded to 4 x 1, the connection matrix *A* takes a 4 x 4 dimension to from an agreeable matrix equation as follows,

$$\begin{bmatrix} D_{T1} \\ D_{T2} \\ D_{T3} \\ D_{T4} \end{bmatrix} = \begin{bmatrix} A_{11} & A_{12} & A_{13} & A_{14} \\ A_{21} & A_{22} & A_{23} & A_{24} \\ A_{31} & A_{32} & A_{33} & A_{34} \\ A_{41} & A_{42} & A_{43} & A_{44} \end{bmatrix} . \begin{bmatrix} Pb^{+} \\ Pb^{-} \\ Puc^{+} \\ Puc^{-} \end{bmatrix} + \begin{bmatrix} P1 \\ P2 \\ P3 \\ P4 \end{bmatrix} \tag{5-35}$$

By nature that the batteries and ultracapacitors cannot charge and discharge simultaneously, four diagonal elements in the connection matrix can be set to zero. This results in the following,

$$\begin{bmatrix} D_{T1} \\ D_{T2} \\ D_{T3} \\ D_{T4} \end{bmatrix} = \begin{bmatrix} 0 & A_{12} & A_{13} & A_{14} \\ A_{21} & 0 & A_{23} & A_{24} \\ A_{31} & A_{32} & 0 & A_{34} \\ A_{41} & A_{42} & A_{43} & 0 \end{bmatrix} . \begin{bmatrix} Pb^{+} \\ Pb^{-} \\ Puc^{+} \\ Puc^{-} \end{bmatrix} + \begin{bmatrix} P1 \\ P2 \\ P3 \\ P4 \end{bmatrix} \tag{5-36}$$

Further reduction of elements in the connection matrix can be attained by considering the operating modes of the PES state machine and by eliminating non-applicable conditions. The four duty cycles are then expressed as,

$$D_{T1} = Pb^{+}A_{12} + P1 \qquad \text{in state [011]} \tag{5-37}$$

$$D_{T2} = Pb^{+}A_{12} + Puc^{+}A_{23} + Puc^{-}A_{24} + P2 \qquad \text{in states [101 , 100 , 110]} \tag{5-38}$$

$$D_{T3} = Pb^{+}A_{31} + Puc^{+}A_{34} + P3 \qquad \text{in states [110 , 010]} \tag{5-39}$$

$$D_{T4} = Pb^{+}A_{41} + Puc^{+}A_{43} + P4 \qquad \text{in states [001 , 101]} \tag{5-40}$$

Thus the connection matrix reduces to,

$$A=\begin{bmatrix} 0 & A_{12} & 0 & 0 \\ A_{21} & 0 & A_{23} & A_{24} \\ A_{31} & 0 & 0 & A_{34} \\ A_{41} & 0 & A_{43} & 0 \end{bmatrix} \tag{5-41}$$

The elements of the connection matrix A depend on the actual power electronics architecture. Elements of the matrix are in fact the power stage transfer functions that transform the reference power into voltage and current parameters. It is within this matrix that loop regulations requiring measurement of system currents and voltages is performed. Representing the PES as a state machine provides the flexibility of varying the control elements of the connection matrix as the PES shifts from one state to another. Together with a state transition matrix, the connection matrix allows different regulation modes to be incorporated at each state.

The following procedure is to determine the state transition matrix. The State transition matrix is required to switch between the sates described in PES state machine (Figure 5.21). As defined, the PES states are represented using a 3 digit Boolean identifier. With the Boolean flags to discriminate between charging and discharging, the state transition matrix is constructed as 4 x 3 state transition matrix as follows,

$$\begin{bmatrix} \#Pb^{+} & \#Pb^{-} & \#Puc^{+} & \#Puc^{-} \end{bmatrix} \cdot \begin{bmatrix} S_{11} & S_{12} & S_{13} \\ S_{21} & S_{22} & S_{23} \\ S_{31} & S_{32} & S_{33} \\ S_{41} & S_{42} & S_{43} \end{bmatrix} = \underbrace{\begin{bmatrix} S1 & S2 & S3 \end{bmatrix}}_{PES\ \ STATE} \tag{5-42}$$

To conform to the stipulated PES finite operating modes, the transition matrix valid for all PES states excluding State BR can be shown to be equal to,

$$S=\begin{bmatrix} S_{11} & S_{12} & S_{13} \\ S_{21} & S_{22} & S_{23} \\ S_{31} & S_{32} & S_{33} \\ S_{41} & S_{42} & S_{43} \end{bmatrix}=\begin{bmatrix} 1 & 0 & 0 \\ 0 & 1 & 1 \\ 0 & 0 & 1 \\ 0 & 1 & 0 \end{bmatrix} \tag{5-43}$$

For example, when both the batteries and ultracapacitors are discharging, $\#Pb^{+}=1$, $\#Pb^{-}=0$, $\#Puc^{+}=1$ and $\#Puc^{-}=0$, thus creating matrix [1 0 1 0]. Multiplying this matrix with the state transition matrix *S* results in,

$$\underset{\substack{\uparrow \\ \#Pb^{+}}}{1} \quad \underset{\substack{\uparrow \\ \#Pb^{-}}}{0} \quad \underset{\substack{\uparrow \\ \#Puc^{+}}}{1} \quad \underset{\substack{\uparrow \\ \#Puc^{-}}}{0} \cdot \begin{bmatrix} 1 & 0 & 0 \\ 0 & 1 & 1 \\ 0 & 0 & 1 \\ 0 & 1 & 0 \end{bmatrix}=\underbrace{\begin{bmatrix} 1 & 0 & 1 \end{bmatrix}}_{PES\ STATE} \tag{5-44}$$

As required, the resulting PES state [1 0 1] corresponds to the operating condition stipulated in Table 5.1. Sequential analysis for all the allowable conditions validates the State transition matrix.

5.12 Summary

The foundation of the proposed methodology and system architecture is modular and hence permit the problem to be divided into manageable processes. Each process is addressed independently of others. Protocols and interconnecting variables among the processes are drawn such that the system can work as a whole, thus addressing the general hypothesis of forming an analogy between classical management methodology and the underlying principles of managing power and energy to create a more unified description of the EV power and energy management problem.

Perhaps the biggest advantages of the modular structure are that of its scalability and usability. Changes can be made in a methodical manner without a complete redesign or overhaul of other processes. It offers a systematic means of developing EV power systems from building blocks, enabling similarities in one design requirement to be used in others. This attribute bares similarity to frameworks found in object-oriented programming (OOP), whereby a system is decomposed according to key abstraction of the applications. This advantage aids design and more importantly, the explication of the entire power and energy management system much clearer. Figure 5.23 summarises the M-PEMS framework.

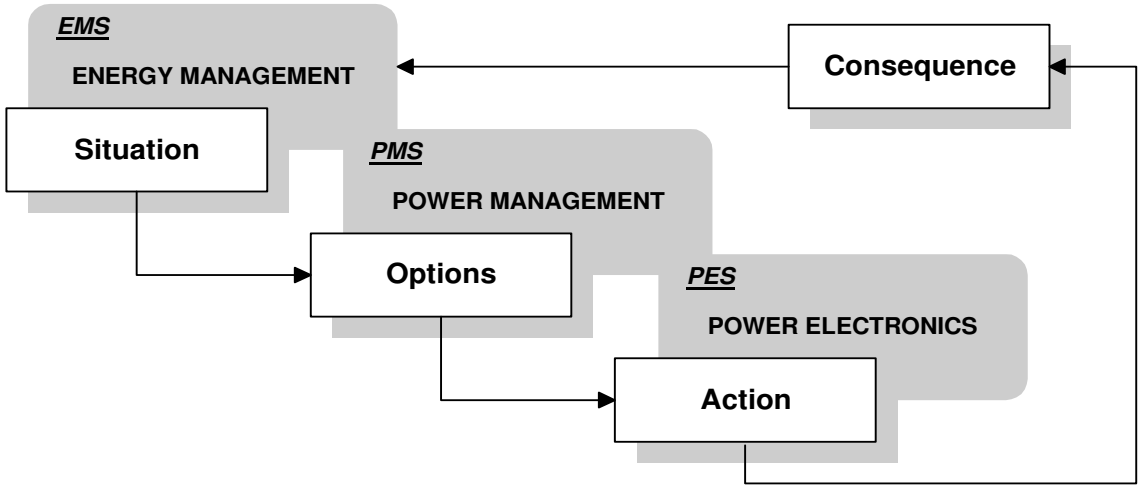

Figure 5.23 Overview of the M-PEMS concept

CHAPTER 6

HARDWARE DESCRIPTION

Hofstadter's Law states that," It always takes longer than you expect, even when you take into account Hofstadter's Law." - ***Douglas R. Hofstadter***

A considerable effort of this research programme has been dedicated towards the development of a test vehicle to serve as an experimental setup for power and energy management research. This chapter describes the experimental vehicle and the corresponding energy storage systems. Starting form a pure battery driven vehicle, the energy system was then augmented with the addition of an ultracapacitor bank. Apart from manufacturer's information, there is very limited experimental data on ultracapacitor field-testing. As such, the vehicle provided a means to obtain unbiased empirical data to substantiate research claims and also to serve as a test platform for further work.

6.1 The experimental vehicle

The experimental vehicle developed for this work consists of a modified go-kart chassis propelled by a 12kW Lynch motor, driven by a 4-quadrant DC Motor controller. Figure 6.1 along with data in Table 6.1 describes the test vehicle specification. The propulsion power source units comprises of deep discharge SLA batteries and self-balancing ultracapacitor modules. Instrumentation and control is designed around the National Instruments Compact Field Point (CFP) architecture.

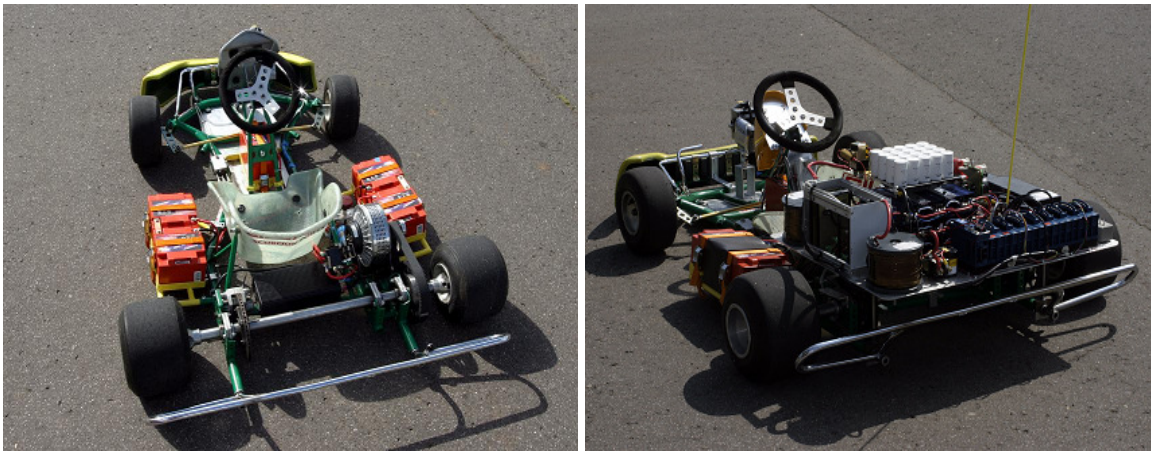

Figure 6.1 Baseline vehicle (Left) and the vehicle augmented with dual energy systems (Right)

Vehicle mass (Including Driver)		254.3 kg
Frontal area		1.04 m^2
Motor peak power		12 kW
Maximum velocity		42 km/h
Energy Storage System	Battery	Ultracapacitor
Module capacity / Max. Voltage	27 Ah / 13.8V	58 F / 15V
Module ESR @ 1kHz	5m ohm	10m ohm
Module max. stored energy	320 Wh	1.8 Wh
Module mass	11.2 kg	0.68 kg
Quantity /Configuration	4 / series	9 / 3x3 matrix
System nominal voltage	48V	45V
Power Electronics Interface		
Peak power		15 kW
DC link voltage		55V to 65V
Semiconductor technology		MOSFET
Switching frequency		20 kHz
Thermal dissipation mode		Air cooled heat sink
Inductors		392μH (Air core)

Table 6.1 Vehicle Data

Figure 6.2 shows the subsystem layout and the weight distribution of the vehicle

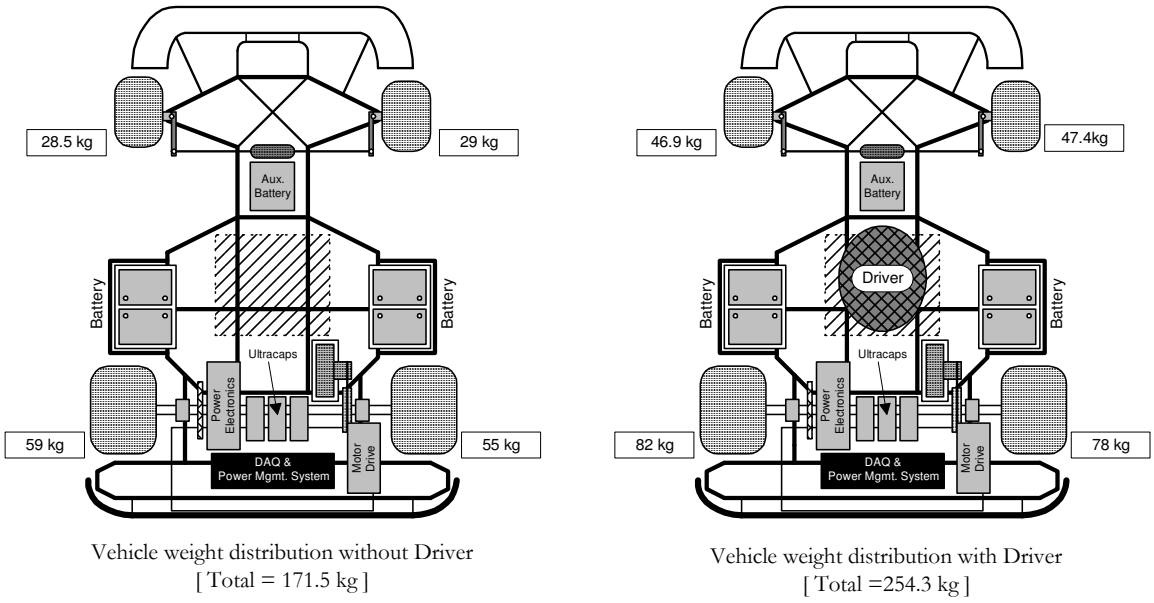

Figure 6.2 Weight distibution of the vehicle

6.2 Battery System

The traction system battery pack is of a sealed lead acid type. The lead acid battery pack consists of four 27Ah (1 hour) Odyssey® SLI Drycell™ battery modules connected in a series string to obtain a nominal battery system terminal voltage for 48V. The batteries are specified for deep discharge to a minimum terminal voltage of 10.2V per module. An addition battery module with the same capacity as the traction system battery modules served as the power supply for the instrumentation and control system. Figure 6.3 presents a graph produced by experimental tests of the battery system. Representing both power and energy in a single plot is adapted from standard Ragone plots [115]. Presenting the power and energy curves in this form clearly segments the energy efficient operating region of the battery. From the plot, it is seen that operating the battery at power limits to the left of the crossover point results in a reduction in the net usable battery energy. Form this plot alone; the guide for a maximum battery power is obtainable.

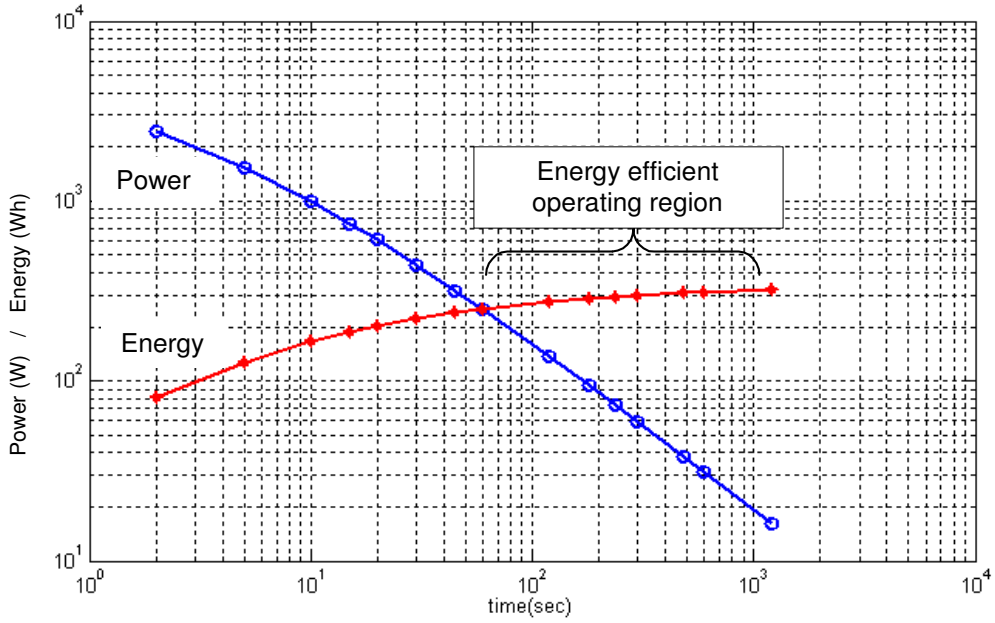

Figure 6.3 Power delivery and Energy capacity plot

6.3 Ultracapacitor System

The ultracapacitor pack consists of nine Maxwell® BMOD0350-15 modules with non-dissipative module-to-module series charge balancing circuitry. The ultracapacitor modules are configured as a 3x3 matrix, effectively creating a 58F / 45V pack with a maximum energy storage capacity of 16.3Wh (58.7kJ). Since the available energy bandwidth of the ultracapacitor bank is bounded by the maximum (V_{max}) to minimum (V_{min}) terminal voltage swing, the usable ultracapacitor energy E_{UC} reduces according to

$$E_{UC} = \left(1 - \frac{V^2_{\min}}{V^2_{\max}}\right) E_{\max} \qquad (6\text{-}1)$$

where E_{max} is the maximum storable energy of the ultracapacitor pack. Using (6-1), with a minimum ultracapacitor terminal voltage of 20V, the usable ultracapacitor energy of the system results to 13.1Wh (47.1kJ). This would normally translate to the capability of delivering traction power of 10kW for approximately 4.7seconds. In practice, this would only be valid if the DC-DC converter has the corresponding current handling capacity, in

this case 400A.. Using maximum power transfer theorem, the maximum ultracapacitor power under matched impedance discharge is

$$P_{UC}\ \max = \left(\frac{Vuc^2}{4ESR_{DC}} \right) \tag{6-2}$$

The ESR_{DC} of each ultracapacitor module is 19mΩ. With the 3x3 configuration and the inclusion of cable and termination resistance, the ultracapacitor pack maximum discharge power using (6-2) with a total pack ESR_{DC} of 25mΩ and voltage of 45V computes to 20.25kW. The power transfer efficiency under this condition is only 50%. For higher transfer efficiencies [5], the discharge power reduces to

$$P_{UC}\ \max' = \eta(1-\eta)\left(\frac{Vuc^2}{ESR_{DC}} \right) \tag{6-3}$$

A maximum power of 12kW is sufficient in this design since this is the peak traction motor power. Solving for power transfer efficiency using (6-3) yields, η = 82%.

6.4 Instrumentation and Control System

System Current Measurements

Battery and ultracapacitor currents are measured using two LEM- LC 300 Hall effect current transducers while the DC bus current is measured using a lower capacity LEM – LT 200 current transducer. All three LEM modules are powered by +/- 15V bias voltage with 47ohm burden resistors for current measurement. The voltage measured across the burden resistors is scaled in the data acquisition software to represent the actual currents. A 500Hz low pass filter is selected for all the current measurement channels.

System Voltage Measurements

Voltage measurement points are the battery, ultracapacitor and DC bus terminal voltage. All the measurements are obtained through scaling of the actual terminal voltages. Using resistive voltage dividers and single-pole low pass filters (1kHz), these terminal voltages are scaled down by a factor of 11 and measured via 3 separate channels of a designated voltage measurement module. Rescaling is performed in the data acquisition software. Both current and voltage measurement modules provide galvanic isolation between the input and signal paths. The instrumentation method is shown in Figure 6.4.

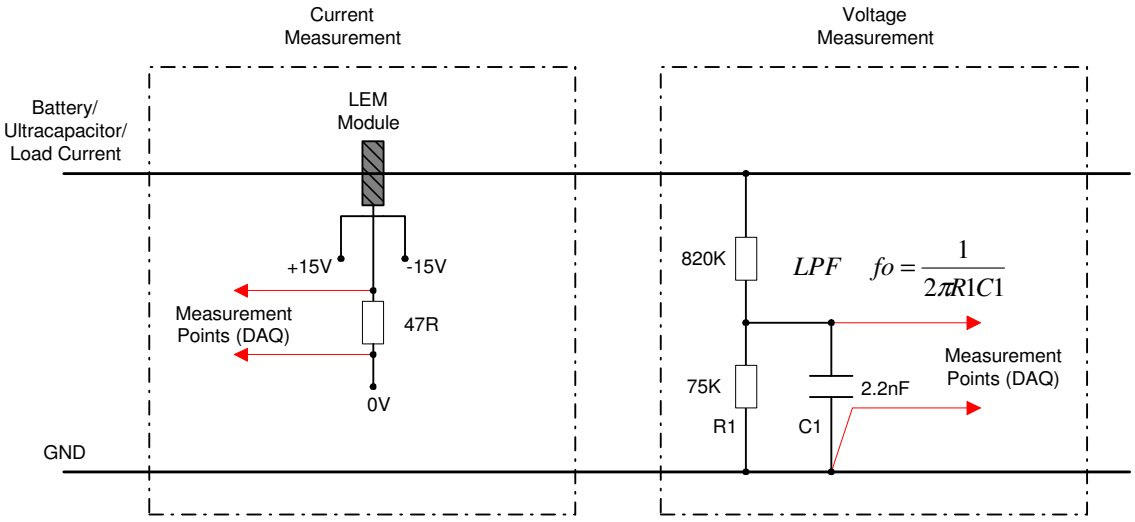

Figure 6.4 Voltage and current measuring method

Protection, disconnects and power distribution

Two 300A Fuse links provides protection against uncontrollable fault currents. The fuses are placed on the incoming battery supply and on the outgoing DC distribution bus. Two DC (400A) contactors provide controlled disconnection of the DC bus and also the Ultracapacitors. Every attempt was made to minimize Joule heating by using low electrical resistance cables and interconnects in the vehicle power distribution system.

Drive Cycle Profiler

In order to achieve experimental repeatability, a drive cycle profiler was designed and developed. The profiler functions as an automatic throttle controller that is independent of central control module. By sequentially altering the speed reference signal to the traction drive, the drive cycle profiler alters the vehicle target velocity. For the same vehicle and driver mass with the same tyre pressure and similar ambient conditions, the profiler is able to reproduce four pre-programmed drive cycles in any order.

The drive cycles were designed based on the SAE J227 [1] drive segments with specific refinement to include a rapid acceleration and rapid deceleration segment. Given the limits of the test track, the vehicle was subjected to a driver-controlled random test cycles to enable data acquisition on the acceleration, deceleration, maximum speed and distance traverse that the vehicle can demonstrate. Having established the operating limits of the vehicle, the data was then used to design the four test cycles. Figure 6.5 depicts the developed test cycles. Segment 1 mimics a moderate drive cycle with gradual acceleration followed by a gradual deceleration without bringing the vehicle to zero speed during the test. Segment 2 represents a more aggressive start-stop scenario. With maximum acceleration and deceleration segments, this segment was designed to mainly examine regenerative braking events and the receptivity of the ultracapacitors and batteries to regenerative power. Segment 3 subjects the vehicle to maximum velocity at maximum acceleration followed by sequential step mode decelerations. Segment 4 initially subjects the vehicle to a lower acceleration rate followed by short run at constant speed and then to a high acceleration. The vehicle is then decelerated rapidly till zero speed where a 2 second dwell time is introduced before rapidly accelerating the vehicle again.

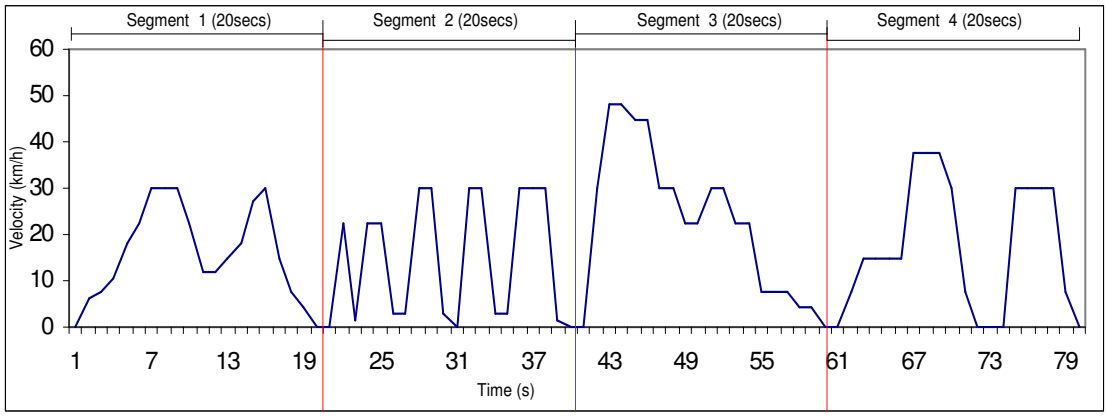

Figure 6.5 Developed test profiles

Control System Architecture

The control system is designed around the National Instruments Compact Field Point (CFP) architecture. This system was chosen due to its robust operating condition tolerance and flexibility of developing real-time control process treads. To facilitate online monitoring of the vehicle during test runs, a wireless link was added to transmit system parameters to a Lab View visualisation environment running on a remote PC. The power and energy management framework described in Chapter 5 was implemented with LabView® -7 and hosted in the CFP real time controller.

Acquisition of data and process input variables was accomplished via the CFP voltage, current and counter/timer input modules. The analog and digital output modules fascinated controller commands. The four PWM signals required for the operation of the Power Electronics Shell was derived external to the CFP. Four independent programmable controllers (PIC) were designed to convert the duty cycle values generated via the CFP analog (0-5V) output module to four 20kHz fixed frequency – variable duty ratio PWM signals. Four enable signals were also made available as outputs of the CFP for each PWM channel. This provided a method to synchronize the PWMs as well as to feed an interlock circuit that prevents cross conduction of the power electronic switches. Optical isolation between the PWM signals and the power electronics drive circuitry was designed into the system. Details of this are to be found in the Appendix section.

With reference to the PES structure described in Chapter 5, the start-up and shutdown procedure mandatory for the safe operation of the vehicle power system was also implemented within the control system. Before entering State 000, the controller executes essential preconditioning of the power system. Most importantly, the precharging of both the DC bus and the ultracapacitors require supervisory control to limit large inrush currents. Similarly, a shutdown sequence returns the power system to a safe mode before exiting state 000. Figure 6.6 illustrates these sequences. In the diagram <Master> refers to the main controller enable signal (Master switch).

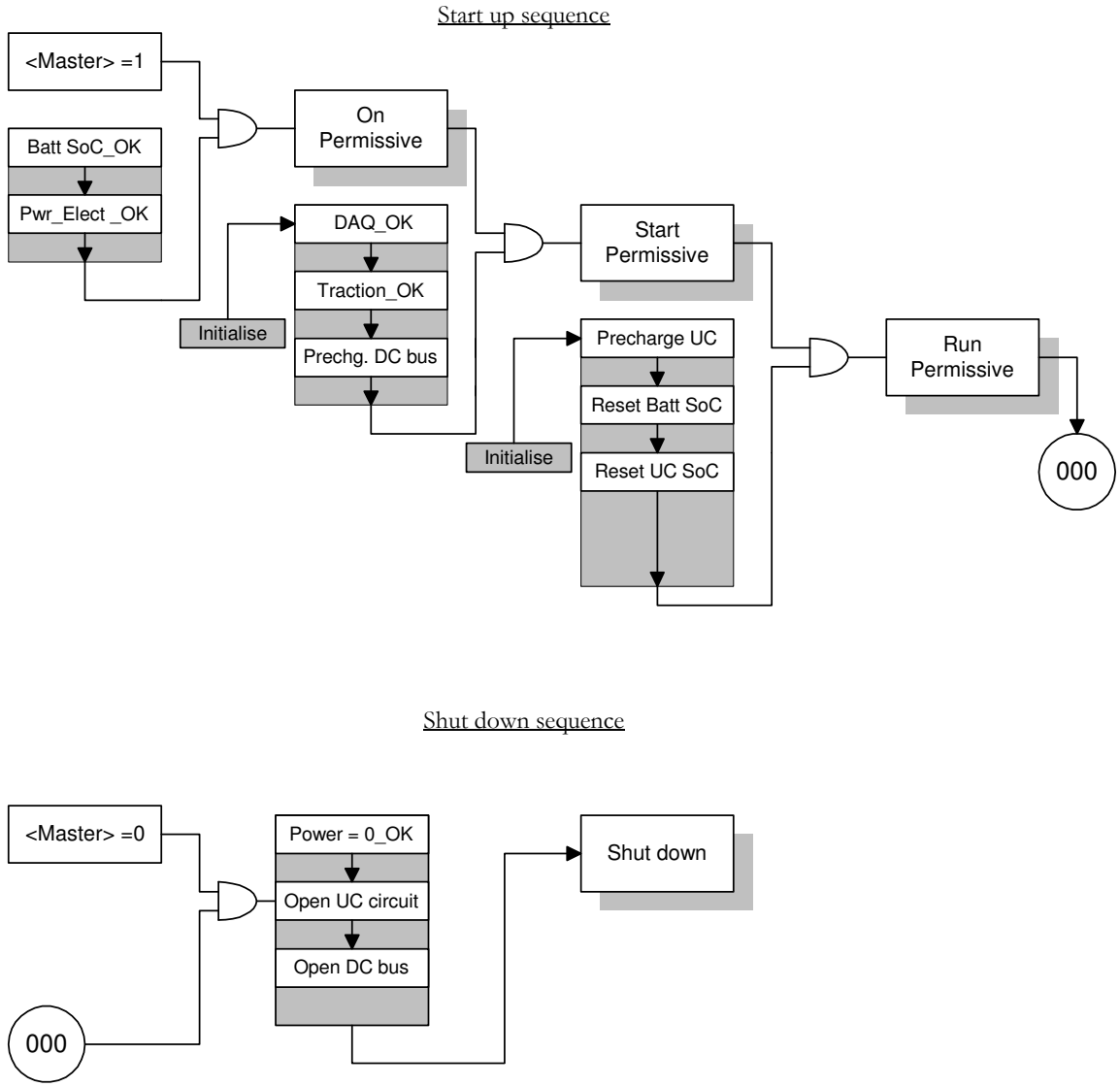

Figure 6.6 Start-up and Shutdown sequence

CHAPTER 7

IMPLEMENTATION FRAMEWORK

Today's scientists have substituted mathematics for experiments, and they wander off through equation after equation, and eventually build a structure which has no relation to reality." — ***Nikola Tesla, 1856 – 1943***

To facilitate active power sharing of multiple energy sources and hence implement a power and energy management system, the need of an appropriate power electronics interface is imperative. Specification of power flow to and from the energy storage systems mandates a power electronics topology capable of bidirectional power transfer. This chapter provides a quantitative design procedure of the required power electronics shell (PES) hardware, which forms the implementation framework for the M-PEMS. Based on the vehicle, battery and ultracapacitor system specification, a sizing methodology of the passive and active components necessary to implement the battery-ultracapacitor interface is presented. Due to the high stresses associated with wide-input voltage range converters, these passive components place an added overhead in terms of mass and volume. Detail design procedures as well as the factoring of this overhead in the implementation of a power and energy management scheme have received limited attention in the past. As this chapter will discuss, the analysis of the implementation requirements further contributes towards a more detailed problem description of integrating multiple energy storage systems. Methods to interface several electrical power sources involve power-electronics intensive solutions and are not trivial and there is a lack of literature describing experimental procedures and protocol to aid researchers. With this in mind, the procedure described in this chapter provides sufficient design details for replication of the PES implementation framework.

7.1 Design Rationale

A power electronics interface is required to facilitate the active power sharing between the battery system, the ultracapacitor system and the load system. In Chapter 3, it was shown that the battery discharge voltage characteristic is fairly constant while the ultracapacitor voltage decays linearly with the state of charge. In order to utilise most of the ultracapacitor energy, the interface between the ultracapacitor and the DC bus is required to have a wide input voltage range. In addition, the interface is required to facilitate bi-directional power flow for the two sources. As described in Chapter 2, various topologies have been explored for this purpose. As the implementation framework, a two input bidirectional DC-DC converter was adopted for this work. A recent study by Lukic et al. [92] also showed that a bidirectional DC-DC converter for both batteries and ultracapacitors is the more efficient and flexible of all present interfacing topologies. From the point of efficiency, stability and failure modes tolerance, the dual bidirectional interface topology offers a higher figure of merit. An additional justification for the use of DC-DC converter structures on both inputs is to maintain a general premise that either energy source may have wide input voltage swings.

7.2 Converter Topology

Figure 7.1 shows the basic schematic of the converter topology. Depending of the active switching states of power electronic switches T1 to T4, both the direction and magnitudes of battery and ultracapacitor power flow can be controlled.

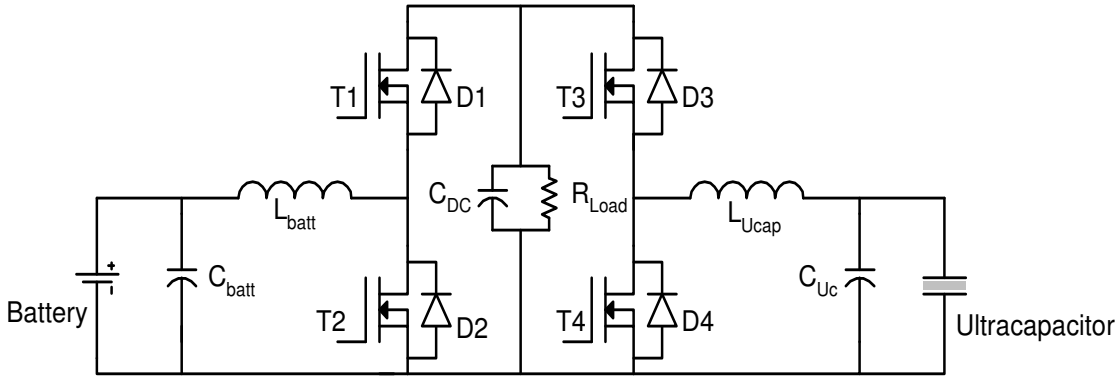

Figure 7.1 Bidirectional DC-DC converter topology

7.3 Theory of operation

For the converter to operate as controllable step-up (boost)/step-down (buck) converter, the nominal terminal voltage across the DC bus capacitor C_{DC} is required to be higher than both the battery and ultracapacitor maximum terminal voltage. In battery boost operation mode, switch T2 and freewheeling diode D1 provide the active circuit path while the switch and diode pair T4 and D3 performs a similar operation for the ultracapacitor voltage boost. During buck operation, switch T1 and diode D2 are active on the battery side and T3 and D4 are active on the ultracapacitor side. The power electronics switches T1 to T4 are controlled by variation of duty cycles at a fixed PWM switching frequency, $f_{sw.}$

From a zero DC bus voltage condition, the battery precharges the DC bus capacitance via a precharge resistor up to the battery terminal voltage (see Appendix for schematic details). Subsequently, the battery boost circuit is initialised and begins to increase the charge of the DC bus capacitance through modulation of switch T2 with freewheeling current flowing to the DC bus via diode D1. The DC bus capacitance then sustains this terminal voltage, which is higher than the battery system voltage. Precharging of the ultracapacitors from the battery is carried out by modulating T3, which effectively operates the circuit on the ultracapacitor side as a buck converter. The higher DC bus voltage serves as the input source to the ultracapacitor buck converter. Similarly, charging the ultracapacitors during regenerative braking events is also performed by modulating T3. Load power sharing between the

batteries and ultracapacitors is achieved by operating both sides of the converter in boost mode by actively controlling T2 and T4.

Connecting an external DC supply across the DC bus and modulating switch T1 facilitates charging of the battery system. As a short circuit prevention mechanism, protection circuitry is required to ensure that the simultaneous activation of (T1 and T2) or (T3 and T4) is prohibited.

Figure 7.2 illustrates the active switches in relation to the Power Electronics Shell (PES) state transition machine.

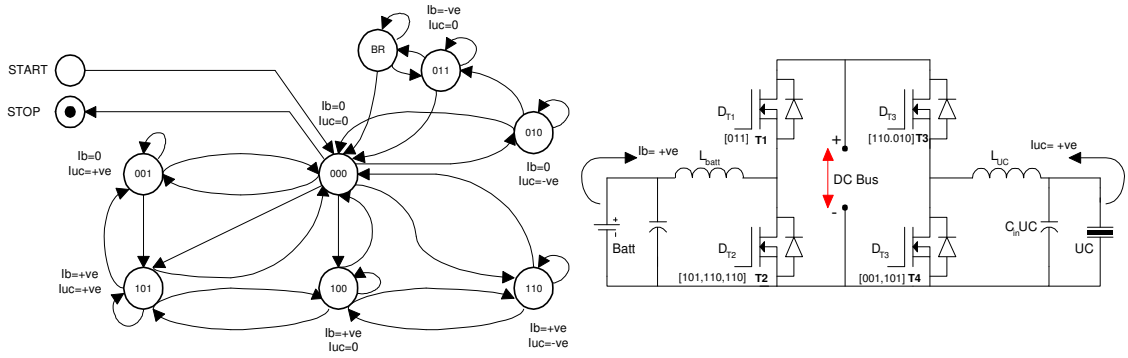

Figure 7.2 Active switches of the converter in relation to the active states of the PES State machine

7.4 Converter operating specification

Specification of the circuit passive and active components is based upon the operational requirement of the converter and the operating constraints of the energy sources. Table 7.1 lists the functional requirements that serve as the converter design parameters.

Parameter	Notation	Values
Maximum converter power	Pmax	15kW
Battery output voltage range (Discharge Mode)	$V batt_{dis}$	52.8V ~ 40.8V
Battery input voltage range (Charging Mode)	$V batt_{chg}$	40.8V ~ 56.8V
Ultracapacitor output voltage range (Discharge Mode)	$V uc_{dis}$	45V ~ 20V
Ultracapacitor input voltage range (Charging Mode)	$V uc_{chg}$	20V ~ 45V
DC Bus voltage	V_{DC}	55V ~ 65V
Switching frequency	f_{sw}	20kHz
Percentage Battery discharge current ripple	-	1%
Percentage Battery charging current ripple	-	1%
Percentage Ultracapacitor discharging current ripple	-	0.5%
Percentage Ultracapacitor charging current ripple	-	0.5%

Table 7.1 Converter requirements

The passive components are sized by considering the different converter operation modes in isolation. First, the duty cycle ranges of the power electronic switches operating at the design frequency are determined using the input/output voltage swing constrains. Using fundamental buck/boost circuit topology derivations, the converter operating in battery boost, battery buck, ultracapacitor boost and ultracapacitor buck modes are treated separately in order to design the magnetic and capacitive components under maximum operating conditions. The circuit analysis neglects component and cable resistance as well as the voltage drops across the diode and switches. Effects of series resistance in the capacitive and inductive filter components will be addressed in the section describing the physical component design. For clarity, only the respective circuit paths of interest are diagrammatically illustrated in the four subsequent sections.

7.5 Battery Boost Mode - Discharge mode (STATE 100)

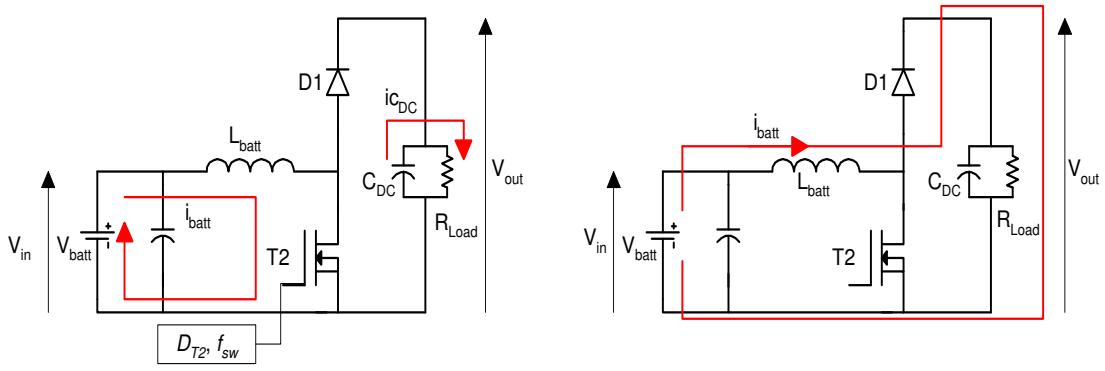

a) Current flow when T2 is ON

b) Current flow when T2 is OFF

Figure 7.3 Active converter section during battery boost mode

The voltage range of the battery is a function of both state of charge and the current drawn from it. Four cells are used in the vehicle model with each having an open circuit voltage swing of 10.2V to 13.2V. A series connection results in the battery pack voltage operating range of between 40.8V and 52.8V assuming minimum interconnection losses between units.

The output to input voltage transfer function of a boost converter in continuous conduction mode (CCM) is found using KVL loops as follows,
During the conduction period of switch T2,

$$V_{in} - L_{batt}\frac{di_{batt}}{dt_{on}} = 0 \tag{7-1}$$

$$\Rightarrow \quad V_{in} - L_{batt}\frac{\Delta i_{batt}}{D_{T2}} f_{sw} = 0 \tag{7-2}$$

rearranging,

$$V_{in}(D_{T2}) = L_{batt} \cdot \Delta i_{batt} \cdot f_{sw} \tag{7-3}$$

where D_{T2} is the duty cycle of the switch T2 and f_{sw} is the fixed switching frequency of the converter.

During the conduction period of Diode D1 and when switch T2 is 'off',

$$V_{out} - L_{batt}\frac{di_{batt}}{dt_{off}} - V_{in} = 0 \tag{7-4}$$

$$\Rightarrow \quad V_{out} - L_{batt}\frac{\Delta i_{batt}}{(1-D_{T2})} f_{sw} - V_{in} = 0 \tag{7-5}$$

rearranging,

$$(V_{out} - V_{in})(1-D_{T2}) = L_{batt} \cdot \Delta i_{batt} \cdot f_{sw} \tag{7-6}$$

Equating terms $L_{batt} \cdot \Delta i_{batt} \cdot f_{sw}$ in (7-5) and (7-6) and factoring gives the voltage transfer function as,

$$\frac{V_{out}}{V_{in}} = \frac{1}{1-D_{T2}} \tag{7-7}$$

The battery terminal voltage is at its maximum open circuit voltage at 100% SoC where the unit terminal voltage is 13.2V (52.8V in series). The duty cycle is minimum at this condition and is calculates as,

$$D_{T2}\min = 1 - \frac{Vbatt_{dis}\max}{V_{out}} \tag{7-8}$$
$$= 0.12$$

The lower boundary of battery operation occurs when the unit battery terminal voltage drops to 10.2V (40.8V in series). The resultant duty cycle is maximum in this condition and is calculated as,

$$D_{T2}\max = 1 - \frac{Vbatt_{dis}\min}{V_{out}} \tag{7-9}$$
$$= 0.32$$

Thus, the boost or discharge mode of operation on the battery side considering only the input to output voltage transfer function results in boost duty cycle range of,

$$0.12 \le D_{T2} \le 0.32$$

This boundary condition is used to calculate the steady state operation of the converter and is not the duty cycle limit imposed in the converter control loop. However, the duty cycle for all four switches in the converter under both steady state and transient condition are limited to $D_{Ti} \in [0,1]$, $_{i=\{1,2,3,4\}}$. In practice, the incremental resolution, upper and lower boundary of the duty cycle value is influenced by the method in which it is generated. Analog comparators are able to produce smoother resolutions whereas purpose built digital PWM generators have incremental step resolutions and a smaller duty cycle operating range.

For the switching frequency of 20kHz (50μs period), switch T2 will be in conduction for a maximum of

$$T2_{\max} = \frac{1}{f_{sw}} \cdot D_{T2}\max \tag{7-10}$$

which equates to 16us per period of 50μs

T2 will have a minimum conduction time when D_{T2} is at D_{T2}min. The corresponding conduction time is calculates as,

$$T2_{\min} = \frac{1}{f_{sw}} \cdot D_{T2}\min \tag{7-11}$$

which equates to 6us per period of 50μs

During the conduction period of T2, the inductor voltage is simply $Vbatt_{dis}$.

$$Vbatt_{dis} = L\frac{di_{batt}}{dt} = L\frac{\Delta I}{\Delta t} \tag{7-12}$$

Design and sizing of the inductors is always a compromise between physical size, and current ripple rating. Since current ripple contributes to iron losses, copper losses and introduces audible noise, its value is ideally kept low. For a current variation of no more than 1% and a mean current, I_{mean} of 100A, the total peak-to-peak variation is 2A

$$\Delta I = 2(0.01 \cdot I_{mean}) \tag{7-13}$$

The inductance required at maximum $Vbatt_{dis}$ is,

$$\begin{aligned} L &= \frac{(Vbatt_{dis}\ \max)(\Delta t_{\min})}{\Delta I} \\ &= \frac{(52.8)(6 \cdot 10^{-6})}{2} \\ &= 158.4 \mu H \end{aligned} \tag{7-14}$$

Similarly, the inductance required for the same ripple current limit at minimum Vbattdis is,

$$\begin{aligned} L &= \frac{(Vbatt_{dis}\ \min)(\Delta t_{mac})}{\Delta I} \\ &= \frac{(40.8)(16 \cdot 10^{-6})}{2} \\ &= 326\ \mu H \end{aligned} \tag{7-15}$$

The inductance value of 326.4 μH is chosen and corresponds to the minimum value required in order to operate the battery boost converter section within the design specifications.

The DC bus capacitor, CDC must be capable of supplying the full load current while adhering to the specified allowable voltage deviation during the interval when T2 is on and diode D1 is reversed biased. T2 and D1 are complementary and such the maximum 'OFF' period of D1 occurs during the maximum 'ON' period of T2, which in this design is 16μs. With the converter maximum power rating P_{max}, and the nominal DC bus voltage V_{DC}nom, the maximum load current is,

$$I_{Load}\ \max = \frac{P_{\max}}{V_{DC}nom} = \frac{15kW}{60V} = 250A \tag{7-16}$$

The DC bus capacitors will have to sustain a current of 250A for a period of 16μs. The capacitor current is expressed as,

$$ic_{DC} = C_{DC}\frac{dv}{dt} = C_{DC}\frac{\Delta V}{\Delta t} \tag{7-17}$$

For a DC bus voltage variation from nominal of 2% (1.2V), the minimum capacitance requirement is,

$$C_{DC}\ \min = \frac{(ic_{DC}\ \max)(\Delta t_{\max})}{\Delta V} = \frac{(250)(16\cdot 10^{-6})}{1.2} = 3333\mu F \tag{7-18}$$

Selection of inductive and capacitive component values under battery boost operating mode.
Minimum inductance requirement : 326 μH
Minimum DC bus capacitance requirement : 3333μF

7.6 Battery Buck Mode - Charging mode (STATE 111)

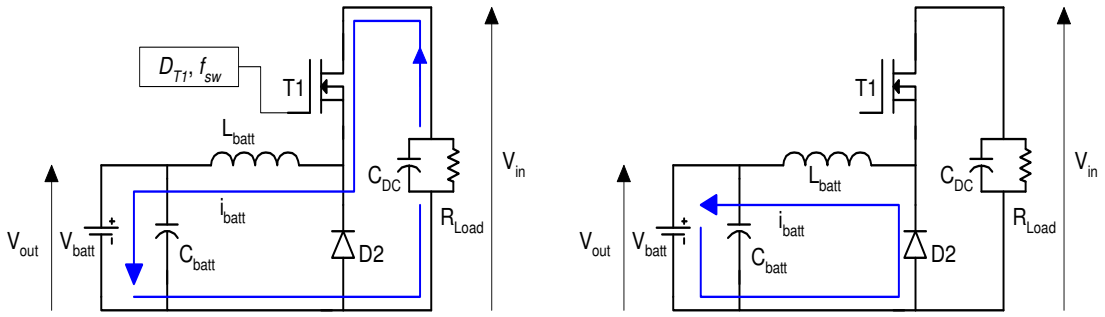

a) Current flow when T1 is ON

b) Current flow when T1 is OFF

Figure 7.4 Active converter section during battery buck mode

In the buck (charging) mode, the DC Bus voltage acts as the input voltage (V_{in}) and the battery voltage is the output voltage (V_{out}) of the converter. Switch T1 operates in a complementary manner with Diode D2. The duty cycle of T1 is represented by D_{T1} with a fixed switching frequency, f_{sw}

During the conduction period of T1, the voltage loop according to KVL is,

$$V_{in} - V_{out} - L_{batt}\frac{di_{batt}}{dt_{on}} = 0 \tag{7-19}$$

$$\Rightarrow \quad V_{in} - V_{out} - L_{batt}\frac{\Delta i_{batt}}{D_{T1}} f_{sw} = 0 \tag{7-20}$$

rearranging,

$$(V_{in} - V_{out})D_{T1} = L_{batt} \cdot \Delta i_{batt} \cdot f_{sw} \tag{7-21}$$

During the conduction period of Diode D2 (when T1 is 'off'), the KVL loop is,

$$V_{out} - L_{batt}\frac{di_{batt}}{dt_{off}} = 0 \tag{7-22}$$

$$\Rightarrow \quad V_{out} - L_{batt}\frac{\Delta i_{batt}}{(1 - D_{T1})} f_{sw} = 0 \tag{7-23}$$

rearranging,

$$V_{out}(1-D_{T1}) = L_{batt} \cdot \Delta i_{batt} \cdot f_{sw} \tag{7-24}$$

Equating terms $L_{batt} \cdot \Delta i_{batt} \cdot f_{sw}$ in (7-23) and (7-24) gives,

$$(V_{in} - V_{out})D_{T1} = V_{out}(1-D_{T1}) \tag{7-25}$$

Therefore, the output voltage is related to the input voltage by,

$$V_{out} = V_{in} D_{T1} \tag{7-26}$$

The input voltage (DC Bus voltage, V_{DC}) to the buck converter section varies from 55V to 65V by design constrain. This voltage is stepped down to adapt to the battery terminal voltage, which swings between 40.8V to 52.8V. Using (7-26) the duty cycle boundaries are determined as follows,

The minimum duty cycle occurs when V_{in} is maximum and V_{out} is minimum, thus for an input voltage of 65V and an output voltage of 40.8V,

$$D_{T1}\min = \frac{40.8}{65} = 0.628 \tag{7-27}$$

Conversely, the maximum duty cycle occurs when V_{in} is minimum and V_{out} is maximum as,

$$D_{T1}\max = \frac{52.8}{55} = 0.96 \tag{7-28}$$

With the duty cycle range, the inductor value required to maintain a mean charging current of 100A with a current ripple of no more than 1% (2A peak to peak) is determined using a rearrangement of (7-24),

$$L_{batt} = \frac{(V_{out})(1 - D_{T1})}{\Delta i_{batt} \cdot f_{sw}} \tag{7-29}$$

A higher inductance is required for a lower output voltage and duty cycle combination. Hence the calculated minimum inductor value is,

$$L_{batt} = \frac{(40.8)(1 - 0.628)}{(2)(20000)} = 379\ \mu H \tag{7-30}$$

The input stage to the battery consists of a series inductor and a parallel capacitor. With the ripple component of the inductor current cycled by the capacitor as shown in Figure 7.5a, the inductor-capacitor combination functions as a low pass filter (LPF) of charging current to the battery system.

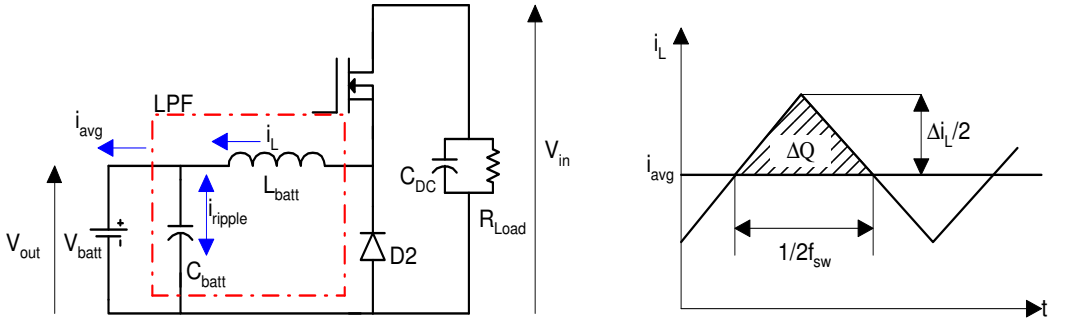

a) Charging current and battery input LPF b) Input capacitor ripple current

Figure 7.5 Low pass filter to smoothen battery charging voltage ripple.

With ΔQ representing the charge of the capacitor, the peak-to-peak voltage ratio, ΔV_{out} can be expressed as,

$$\Delta V_{out} = \frac{\Delta Q}{C_{batt}} = \left(\frac{1}{C_{batt}}\right)\left(\frac{1}{2}\right)\left(\frac{\Delta i_L}{2}\right)\left(\frac{1}{2 f_{sw}}\right) \tag{7-31}$$

from (7-29) and with $i_L = i_{batt}$,

$$\Delta i_L = \frac{(V_{out})(1 - D_{T1})}{L_{batt} \cdot f_{sw}} \tag{7-32}$$

Therefore from (7-31) and (7-32) the capacitance requirement (C_{batt}) for a specified voltage ripple (ΔV_{out}), is expressed as,

$$C_{batt} = \frac{V_{out}(1 - D_{T1})}{8 f_{sw}{}^2 L_{batt} \Delta V_{out}} \tag{7-33}$$

With the previously determined inductance value of 379μH, and specifying a voltage ripple of 250mV, the minimum input capacitance required equates to,

$$C_{batt}\,\min = \frac{40.8(1 - 0.628)}{8(20000^2)(0.000379)(0.25)} \quad = 50\ \mu F \tag{7-34}$$

The inductor-capacitor branch forms a low pass filter with a corner frequency given by,

$$f_c = \frac{1}{2\pi\sqrt{L_{batt} C_{batt}}} \tag{7-35}$$

Selecting a corner frequency sufficiently less than the switching frequency removes the switching harmonic components of the charging current. In this design, a 2200μF/100V capacitor was selected, creating a LPF with a cut off frequency of approximately 170Hz. (with the actual value determined by the final inductor value)

7.7 Ultracapacitor Boost Mode – Discharging mode (STATE 001)

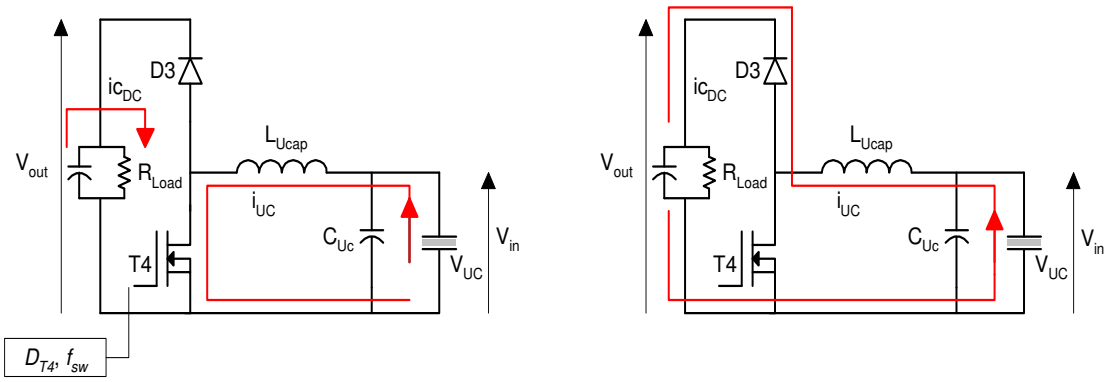

a) Current flow when T4 is ON

b) Current flow when T4 is OFF

Figure 7.6 Active converter section during ultracapacitor boost mode

For the ultracapacitor section in boost operation mode, the derivations of input to output voltage transformation is similar to the battery boost mode. However, with the ultracapacitor system, the input voltage range and upper voltage limit are different. A series-parallel connection of 58F/15V ultracapacitor modules in a 3x3 matrix results in a ultracapacitor system having a maximum terminal voltage of 45V. Since the useable energy content of the ultracapacitors is bounded by the maximum (V_{max}) to minimum (V_{min}) terminal voltage swing as,

$$E_{usable} = \frac{1}{2}C\left(V^2_{\max} - V^2_{\min}\right) \tag{7-36}$$

$$= \left(1 - \frac{V^2_{\min}}{V^2_{\max}}\right)E_{\max} \tag{7-37}$$

where $E_{\max} = \frac{1}{2}CV^2_{\max}$, is the total energy stored in the ultracapacitors

As such, for an active energy utilisation of at least 75%, the ultracapacitor terminal voltage will need to swing down to 50% of its maximum terminal voltage. In this design, with a specified ultracapacitor operating voltage range of $20V \le V_{UC} \le 45V$, the usable energy efficiency equates to 80%. Placing lower input voltage specification would increase the

electrical and thermal stresses of the power electronic components without any significant energy efficiency gain [72].

As with T2 in battery boost circuit, switch T4 is modulated to control the ultracapacitor power flow in discharge mode. The output to input voltage transfer function is,

$$\frac{V_{out}}{V_{in}} = \frac{1}{1 - D_{T4}} \tag{7-38}$$

The ultracapacitor terminal voltage is at its maximum open circuit voltage at 100% SoC where the unit terminal voltage is 45V. The duty cycle is minimum at this condition and is calculates as,

$$D_{T4}\min = 1 - \frac{Vuc_{dis}\max}{V_{out}} \tag{7-39}$$

$$= 0.25$$

The lower boundary of ultracapacitor operation occurs when the system terminal voltage drops to 20V. The resultant duty cycle is maximum in this condition and is calculated as,

$$D_{T4}\max = 1 - \frac{Vuc_{dis}\min}{V_{out}} \tag{7-40}$$

$$= 0.67$$

Thus, the boost or discharge mode of operation on the ultracapacitor side considering only the input to output voltage transfer function results in boost duty cycle range of,

$$0.25 \le D_{T4} \le 0.67$$

For the switching frequency of 20kHz (50μs period), switch T4 will be in conduction for a maximum of,

$$T4_{\max} = \frac{1}{f_{sw}} \cdot D_{T4}\max \tag{7-41}$$

$$\Rightarrow \frac{1}{20kHz} \cdot 0.67$$

which equates to 33.5μs per period of 50μs

T4 will have a minimum conduction time when D_{T4} is at $D_{T4}min$. The corresponding conduction time is calculates as,

$$T4_{\min} = \frac{1}{f_{sw}} \cdot D_{T4}\min \tag{7-42}$$

$$\Rightarrow \frac{1}{20kHz} \cdot 0.25$$

which equates to 12.5μs per period of 50μs

During the conduction period of T4, the inductor voltage is simply $Vuc_{dis.}$

$$Vuc_{dis} = L_{uc} \frac{di_{uc}}{dt} = L_{uc} \frac{\Delta I_{uc}}{\Delta t} \tag{7-43}$$

Since the main reason for ultracapacitor augmentation in a hybrid power system is to handle the higher power demands, the mean ultracapacitor current value is chosen to be higher than the battery mean current. For a current variation of no more than 0.5% and a mean current, (I_{mean}) of 200A, the total peak-to-peak variation on the ultracapacitor side is,

$$\Delta I = 2(0.005 \cdot I_{mean}) \tag{7-44}$$

$$= 2 \text{ A}$$

The inductance required at maximum Vuc_{dis} is,

$$L = \frac{(Vuc_{dis}\max)(\Delta t_{\min})}{\Delta I} \tag{7-45}$$

$$= \frac{(45)(12.5 \cdot 10^{-6})}{2}$$
$$= 281.2\ \mu H$$

Similarly, the inductance required for the same ripple current limit at minimum Vuc_{dis} is,

$$L = \frac{(Vuc_{dis}\ \min)(\Delta t_{mac})}{\Delta I} \tag{7-46}$$
$$= \frac{(20)(33.5 \cdot 10^{-6})}{2}$$
$$= 335\ \mu H$$

The sizing methodology yields a minimum required inductance value of 335 μH. However, unlike the battery system, the duty cycle range of the ultracapacitor boost converter ($0.25 \le D_{T4} \le 0.67$) has a possible duty cycle condition of 0.5. In this event, the previously assumed inductance value is not the minimum required value.

Rewriting (7-5) and (7-7) for the ultracapacitor parameters,

$$L_{uc} \frac{\Delta i_{uc}}{(1 - D_{T4})} f_{sw} = V_{out} - V_{in} \tag{7-47}$$

$$V_{in} = V_{out}(1 - D_{T4}) \tag{7-48}$$

Solving for current ripple gives,

$$\Delta i_{uc} = \frac{V_{out} D_{T4}(1 - D_{T4})}{L_{uc} f_{sw}} \tag{7-49}$$

From (7-49), the maximum current ripple will occur when the duty cycle assumes a value of 0.5. The value of the inductance required to achieve the same ripple current limit of 2A is then calculated by setting D_{T4} = 0.5 in (7-49) and solving for L_{uc},

$$L_{uc} = \frac{V_{out} D_{T4}(1 - D_{T4})}{\Delta i_{uc} f_{sw}} = \frac{60(0.5)(1-0.5)}{2(20000)} = 375\ \mu H \tag{7-50}$$

The final design inductance value of 375 μH is chosen which corresponds to the minimum value required in order to operate the ultracapacitor boost converter section within the design specifications.

The subsequent component to be sized is the DC bus capacitance. As with the battery boost mode, the DC bus capacitor, C_{DC} must be capable of supplying the full load current while adhering to the specified allowable voltage deviation during the interval when T4 is on and diode D3 is reversed biased. As with the battery boost section, with the converter maximum power rating $P_{max,}$ and the nominal DC bus voltage V_{DC}nom, the maximum load current is 250A.

As T4 and D3 are complementary, the maximum 'OFF' period of D3 occurs during the maximum 'ON' period of T4. From the previous T4 'ON' time calculation, the DC bus capacitors will have to sustain a current of 250A for a period of 33μs.

With the DC bus capacitor current expressed as,

$$ic_{DC} = C_{DC} \frac{dv}{dt} = C_{DC} \frac{\Delta V}{\Delta t} \tag{7-51}$$

For a DC bus voltage variation from nominal of 2% (1.2V), the required minimum capacitance is calculated as,

$$C_{DC}\ \min = \frac{(ic_{DC}\ \max)(\Delta t_{\max})}{\Delta V} \tag{7-52}$$

$$= \frac{(250)(33 \cdot 10^{-6})}{1.2}$$

$$= 6875\ \mu F$$

Selection of inductive and capacitive component values under battery ultracapacitor operating mode.

Minimum inductance requirement : 375 μH

Minimum DC bus capacitance requirement : 6875 μF

7.8 Ultracapacitor Buck Mode – Charging mode (STATE 010)

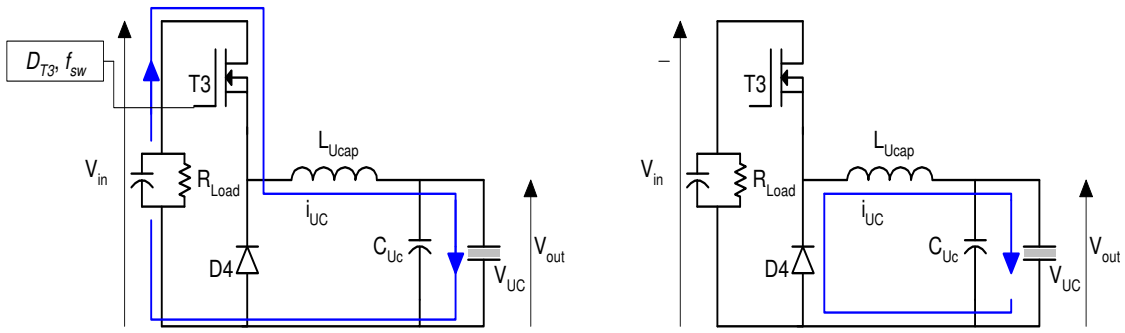

a) Current flow when T3 is ON b) Current flow when T3 is OFF

Figure 7.7 Active converter section during ultracapacitor buck mode

Derivations of the output to input voltage relationship under state CCM in this mode is similar to the battery buck mode. Switch T3 and diode D4 are the active components of interest in this mode. The output voltage is related to the input voltage by,

$$V_{out} = V_{in} D_{T3} \tag{7-53}$$

With the ultracapacitor system, the input voltage (DC Bus voltage, V_{DC}) to the buck converter section varies from 55V to 65V by design constrain. The converter steps down this voltage to adapt to the ultracapacitor terminal voltage, which varies between 20V and 45V. Using (7-26), the duty cycle boundaries are determined as follows,

The minimum duty cycle occurs when V_{in} is maximum and V_{out} is minimum, thus for an input voltage of 65V and an output voltage of 20V,

$$D_{T3}\min = \frac{20}{65} = 0.31 \tag{7-54}$$

Conversely, the maximum duty cycle occurs when V_{in} is minimum and V_{out} is maximum as,

$$D_{T3}\max = \frac{45}{55} = 0.82 \tag{7-55}$$

Since the ultracapacitors are capable of charging at a much higher power rate than the battery system, the mean current taken as the design parameter is higher. With the duty cycle range, the inductor value required to maintain a mean charging current of 200A with a current ripple of no more than 0.5% (2A peak to peak) using the same method as with the battery buck mode is determined as,

$$L_{uc} = \frac{(V_{out})(1-D_{T3})}{\Delta i_{uc} \cdot f_{sw}} = \frac{(20)(1-0.31)}{2(20000)} = 345\ \mu H \tag{7-56}$$

As in the operation of the ultracapacitor in boost mode, the duty cycle range in buck mode $(0.31 \le D_{T3} \le 0.82)$, has the possibility of a 0.5 duty cycle condition.

From (7-23) and (7-26),

$$L_{uc}\frac{\Delta i_{uc}}{D_{T3}} f_{sw} = V_{in} - V_{out} \tag{7-57}$$

$$V_{out} = V_{in} D_{T3} \tag{7-58}$$

Solving for the ripple current gives,

$$\Delta i_{uc} = \frac{V_{in} D_{T3}(1-D_{T3})}{L_{uc} f_{sw}} \tag{7-59}$$

Similarly, from (7-29), the maximum current ripple will occur when the duty cycle assumes a value of 0.5. The value of the inductance required to achieve the same ripple current limit of 2A is then calculated by setting D_{T3} = 0.5 in (7-29) and solving for L_{uc},

$$L_{uc} = \frac{V_{in} D_{T3}(1 - D_{T3})}{\Delta i_{uc} f_{sw}} = \frac{65(0.5)(1-0.5)}{2(20000)} = 406\ \mu H \tag{7-60}$$

If the input voltage rail in the buck converter is always at the same voltage as in the boost converter, which is also the DC bus voltage, the minimum inductance value for the worst case ripple (DTi =0.5) for both operating modes can be expressed in a general form as,

$$L_{uc}\ \min = \frac{V_{DC}}{4\Delta i_{uc} f_{sw}} \tag{7-61}$$

This is however only valid at nominal DC bus voltage. However in an EV application, the DC bus voltage tends to rise during regenerative braking which is when the converter switches to charge (buck) mode. For this reason, the higher input voltage is considered rather than the nominal voltage when determining the buck converter inductance value.

Following the derivation of the LPF input capacitance in the battery buck converter circuit (7-33), the required minimum capacitance for the ultracapacitor buck converter is,

$$C_{uc} = \frac{V_{out}(1 - D_{T3})}{8 f_{sw}{}^2 L_{uc} \Delta V_{out}} \tag{7-62}$$

With the previously determined inductance value of 375μH, and specifying a voltage ripple of 250mV, the minimum input capacitance required equates to,

$$C_{uc}\ \min = \frac{20(1-0.31)}{8(20000^2)(0.000375)(0.25)} = 46\ \mu F \tag{7-63}$$

A similar value for the input capacitance as used in for the battery side of 2200μF/100V is used on the ultracapacitor side to ensure that the switching harmonics are filtered from the charging current.

Summary of component sizing by ideal circuit analysis

Table 7.2 lists the passive component requirements to meet the functional requirements of the battery and ultracapacitor power interface. For the inductors, a design value of 410μH for both L_{batt} and L_{uc} with an allowance of +/- 5% given for construction tolerance.

	Inductor (L_{batt}, L_{uc})	Input capacitor (C_{batt}, C_{uc})	DC bus capacitor , C_{DC}
Battery Boost mode	326 μH	NA	3333 μF
Battery Buck mode	379 μH	50 μF	NA
Ultracapacitor Boost mode	375 μH	NA	6875 μF
Ultracapacitor Buck mode	406 μH	46 μF	NA

Table 7.2 Summary of converter passive component design parameters

7.9 Reactive component design

Inductors

In general, a high inductance value is favourable for low ripple current, low switching losses and continuous conduction at light loads. However the high unit mass and slower transient response $(di/dt = V_L/L)$ as the inductance increases is not desirable especially in vehicular applications. As such, the choice of inductance is an engineering and economic compromise. In terms of power and energy management, the inductor must be able to transfer energy to and from the source as fast as required with minimum power losses over the entire power bandwidth. The problem is further accentuated by the fact that the source, particularly at the ultracapacitor side, has a wide operating voltage range. For these reasons, the sizing of the inductor is often design specific and often results in a compromise between current ripple and physical size.

The practical approach used in this work is to size the inductance as small as possible for continuous conduction while conforming to a specified ripple current rating. The physical size of the inductor is dimensioned to handle the DC current component and cope with high frequency skin-effect. The following describes the design procedure and justification of the inductor developed for the experimental vehicle.

Inductor requirement

Inductance	410 μH
Voltage	60 V
Average current	100 A
Peak current	300 A
Switching Frequency	20kHz

Table 7.3 Inductor target design parameters

The high current requirement of the inductor requires a core that does not saturate. Since the inductors for the intended converter will also have to handle a large DC current component, the inductor design is significant in the overall power and energy management scheme. The inductor contributes a significant mass to power electronics interface between battery, ultracapacitor and the load. Design approaches are often iterative and results in a compromise between divergent factors such as cost, size, weight and power loss.

The need to handle a large DC current component limits the number of possible core material types that can be used in the design. Ideally, to reduce copper losses, the use of high permeability core materials benefits from less number of turns hence a lower series resistance. However, the limited saturation flux densities in most magnetic materials do not favour large DC currents.

An air core selection results in a much lower inductance-per-turn compared to ferromagnetic materials but permits the required high current conduction without going into core saturation. However, more turns are required to obtain a particular inductance value. The high current handling capability as well as the longer windings necessitates a larger conductor size in order to minimize resistive losses. In addition, the high frequency characteristics of

the inductor current (20kHz) suggest the use of conductors with a higher surface area rather than cross sectional area in order to cope with skin-effects.

Considering the above constraints, the developed inductor was designed and fabricated using an air-core bobbin with flat enamelled cooper conductors. Wheeler's method [116] for multi-layered inductors provides dimensioning guides for the physical coil construction. The following design equations require arbitration of design parameters to achieve the required electrical and physical objectives.

The coil inductance using Wheeler's [116] method is given as,

$$L = \frac{0.8(u_e)(rN)^2}{6r + 9l + 10b} \tag{7-64}$$

To obtain number of turns,

$$N = \frac{1}{r}\sqrt{\left[\frac{L(6r + 9l + 10b}{(0.8)(u_e)}\right]} \tag{7-65}$$

where,

L is the inductance in microhenries
u_e is the effective permeability of the core in henry per metre
N is the number of turns
r is the mean radius in inches
d is the core diameter in inches
l is the core length in inches
b is the coil build in inches

Considering skin effect in the conductor at high frequency switching,

$$\Delta_c = \frac{K_m}{\sqrt{f_{sw}}} \tag{7-66}$$

where

Δ_c is the penetration depth

K_m is the material constant (For copper, K_m ranges from 65 at 20°C to 75 at 100°C)

f_{sw} is the switching frequency

Based on the previous design equations, the generalized structural model of the proposed multi-layered inductor is as shown in Figure 7.8 with the final assembled unit shown in Figure 7.9.

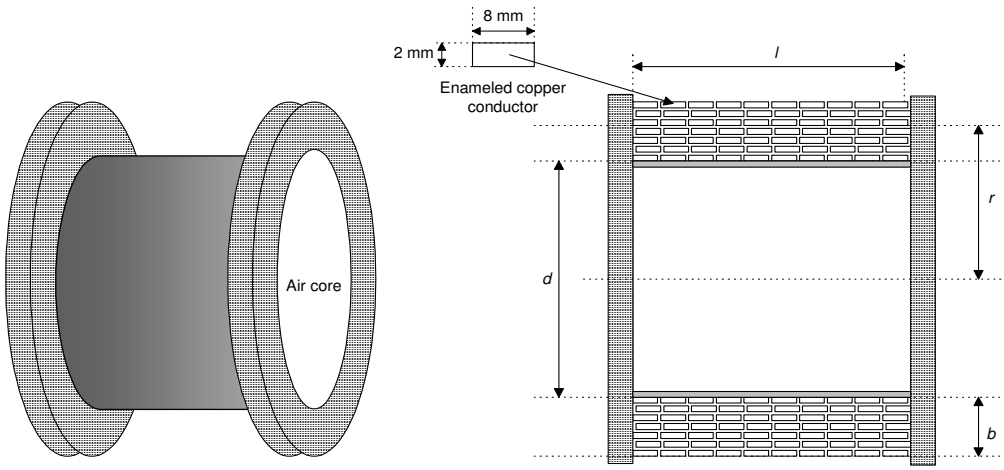

Figure 7.8 Inductor design using flanged air core former and enameled copper conductors

Parameter	Design Value	Final Value
N	70 turns (10 turns ,7 layers)	70 turns (10 turns ,7 layers)
r	63.5 mm	63 mm
l	89 mm	90 mm
b	30.5 mm	30 mm
u_e	1 H/m	1 H/m
Total height	Not considered	108 mm
Total diameter	Not considered	153 mm
DC resistance	Not considered	0.03 ohms (measured)
Inductance	410 μH	392 μH (measured)
Mass	Not considered	4.8 kg

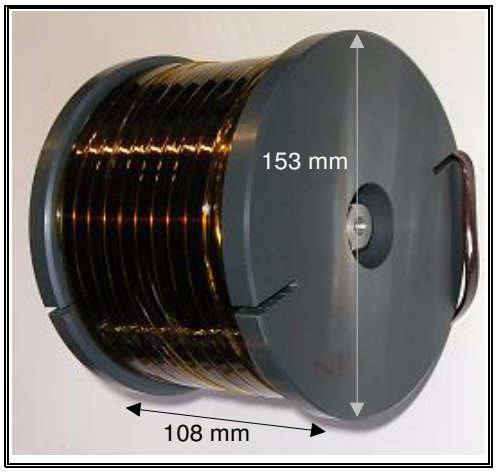

Figure 7.9 Inductor specification and physical 'as-built' configuration

The series resistance of the inductor $R_{L(DC)}$ introduces a power loss during operation as,

$$P_{Loss}L = I_L^{\,2} \cdot R_{L(DC)} \tag{7-67}$$

where I_L is the DC component or mean value of the inductor current

The maximum current that the inductor will experience occurs when the load demand is at maximum and the source voltage is at minimum. As the lowest voltage in the system occurs when the ultracapacitor is at its lowest SoC, the highest current stresses in the converter occur in the ultracapacitor section. Hence the maximum ultracapacitor side inductor current can be expressed as,

$$IL_{UC} = \frac{P_{\max}}{V_{uc(SoC\min)}} \tag{7-68}$$

From (7-68), the implied current handling requirement of the inductor when the ultracapacitor is at its lower voltage threshold of 20V equates 750A in order to transfer a maximum power of 15kW to the load. The occurrence of this highly inefficient situation is mitigated by the following postulates;

1) High power demands of magnitudes close to the maximum power level only occur when the vehicle requires high tractive effort to accelerate from zero or low velocity. Under these circumstances, energy management theory stipulates that the ultracapacitors are at a high SoC ($V_{uc} \sim V_{uc}max$), hence maximum power transfer requires low inductor current.

2) Conversely, when the ultracapacitors are at low SoC ($V_{uc} \sim V_{uc}min$), the vehicle velocity is high. Regenerative braking events from high velocity generates rapid but short power bursts that result in rapidly decaying current flow from the load to the ultracapacitors via the buck converter circuit. Furthermore, the charging action increases the ultracapacitor terminal voltage hence reducing the current required to transfer power. Hence, the inductor does not have to sustain high reverse (charging) current for extended durations.

The effect of the inductor series resistance as well as the ultracapacitor and battery ESR influences the time constant of the inductor in response to a change in current control command. A further design constraint in the inductance value depends on the sampling

period of the digital controller. The time constant for the change in inductor current for the ultracapacitor power converter section is defined as,

$$\tau_{L_{UC}} = \frac{L_{uc}}{(RL_{uc} + ESR_{uc})} \tag{7-69}$$

According to [70], a stable current regulation requires

$$\tau_{L_{UC}} > \frac{1}{2} T_{samp} \tag{7-70}$$

where T_{samp} is the sampling period of the current controller.

Following (7-69) and the sampling time constraint, with the ultracapacitor bank total ESR considering interconnection resistance and the inductor resistance the sampling time for the designed inductor configuration is,

$$\begin{aligned} T_{samp}(uc) &< 2\left(\frac{L_{uc}}{RL_{uc} + ESR_{uc}}\right) \\ &< 2\left(\frac{0.000392}{0.03 + 0.025}\right) \\ &< 14ms \end{aligned} \tag{7-71}$$

Again using (7-69) but for the battery side and considering the mean battery internal resistance and the interconnection resistance, the sampling time constraint is,

$$\begin{aligned} T_{samp}(batt) &< 2\left(\frac{L_{batt}}{RL_{batt} + ESR_{batt}}\right) \\ &< 2\left(\frac{0.000392}{0.03 + 0.04}\right) \\ &< 11.2ms \end{aligned} \tag{7-72}$$

According to Arnet and Haines [70], the inductance upper limit is determined by the bandwidth needed for current regulation. If a voltage regulation loop is superimposed onto a current loop, the required performance of the voltage regulation defines the minimal bandwidth requirements of the current regulation. Theoretically, the response time of the current is not given by the value of T_{samp}**,** but rather by the sampling frequency and the delays of the PWM generating circuitry. In practice, however, a step function of the current set point value can often drive the output of the current regulator into saturation where the duty cycle is forced to either 0 or 1. Under these circumstances the response of the current is independent of any Proportional-Integral (PI) loop coefficient and is solely dependent on T_{samp}, which in fact depends upon the value of the inductors.

DC Bus Capacitance

From previous sections, the maximum DC bus capacitance calculation was based solely on the output voltage ripple constraint. However, a predominant parameter in the DC bus capacitance dimensioning is the current ripple stresses. The capacitor bank must be capable of handling the high frequency current subjected at the DC bus terminals. In addition, a low DC bus capacitor bank ESR is desirable in order to minimize joule heating hence reducing power losses.

According to [117], a significantly large DC bus capacitor is required to act as a low impedance voltage source and surge protector but over sizing the DC bus for an ultracapacitor buck-boost converter results in slow dynamic response introduced by the LC circuit. The final capacitor value selected in the design in [117] was based on simulated circuit behaviour. Other sizing methodology based on the general operation of DC-DC converters [80, 118] suggests calculating the minimum required capacitance for voltage ripple and then ensuring that the ripple current handling capacity is met. The design methodology described in [119] however, showed that the DC bus capacitor and its ESR create an addition system pole that is usually intentionally positioned at a high frequency.

The methodology used in this work to dimension the DC bus capacitor also takes into consideration the power and energy management structure itself. As described in previous

chapters, the power management shell (PMS) feed forwards the reference power trajectories of the battery and ultracapacitor to the power electronics shell (PES). During the finite time involved in sampling the load power, calculating the next power reference trajectory, determining the PES state transition and duty cycle change, the DC bus capacitor acts as an intermediate power buffer. As such, the DC bus capacitor bank is sized large enough to source and sink the load disturbances during the time window of the PMS decision epoch. This is illustrated in Figure 7.10.

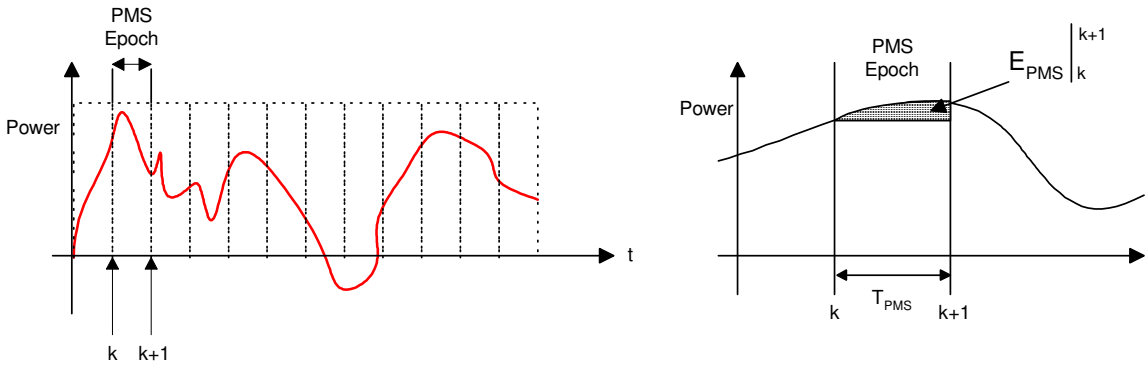

Figure 7.10 Consideration of PMS epoch in dimensioning the DC bus capacitance

On the premise that ultracapacitor reference power and battery reference power levels are fixed during a PMS decision epoch, the DC bus capacitance supplements the occurrence of load power disturbances. The justification of a large DC bus capacitor is also supported by the fact that neither batteries nor ultracapacitors are efficient for high frequency – high power response [120]. This leads to a DC bus bulk capacitance dimensioning scheme that considered the energy capacity requirement per PMS epoch interval, T_{PMS}. The DC bus capacitance dimensioning criteria then follows this sequence;

The minimum capacitance for the converter boost sections to operate within the specified voltage ripple rating is calculated as described in the preceding sections. The first dimensioning constraint then follows,

$$C_{DC}\min \geq C_{DC}\min_{(Batt\_Boost,UC\_Boost)} \tag{7-73}$$

The second dimensioning factor considers the ripple current subjected to the DC bus capacitors, which contribute to Joule heating and ultimately to premature failure. The general expression for the ripple current (RMS) of the capacitors can be stated as,

$$I_{CDC}RMS = \sqrt{\frac{1}{T_{sw}}\left[\int_{0}^{T_{sw}D_{\{T2,T4\}}} i^2_{\{T2,T4\}}(t)dt + \int_{T_{sw}D_{\{T2,T4\}}}^{T_{sw}} i^2_{\{D1,D3\}}(t)dt\right]} \tag{7-74}$$

where T_{sw} is the switching period at switching frequency f_{sw}

Accordingly, the selected DC bus capacitance ripple current rating must be able to handle the calculated RMS current. In practice this would involve configuring the bulk capacitance with multiple capacitor units in parallel in order to fulfil the ripple current requirement.

$$I_{CDC}rms_{(rating)} \geq I_{CDC}rms_{(calculated)} \tag{7-75}$$

To account for the DC bus capacitance required to service load disturbances during a PMS decision epoch, the finite time widow allocation (T_{PMS}) of the epoch must first be defined. The T_{PMS} interval selection criteria depend on the computational time within the PMS algorithm and also the power stage to duty cycle throughput time within the PES. A constraint that is imposed on T_{PMS} is that the interval is smaller than the minimum sampling time,

$$T_{PMS} \leq T_{samp}\min \tag{7-76}$$

As described, T_{samp} is influenced by the converter inductance and circuit series resistance

As for the DC bus capacitor energy capacity requirement during a PMS epoch,

$$E_{DC}\Big|_{k}^{k+1} \geq E_{PMS}\Big|_{k}^{k+1} \tag{7-77}$$

In terms of capacitor voltage deviation and load power disturbance at the DC bus, the above inequality can be expressed in discretised form as,

$$\frac{1}{2}C_{DC}\left[V^{2}{}_{DC}(k)-V^{2}{}_{DC}(k+1)\right] \geq P_{Load}T_{PMS} \tag{7-78}$$

From the above expression, the DC bus capacitance C_{DC} can be found for a predefined T_{PMS} interval, load power and DC bus voltage range.

With the above dimensioning methodology, the final value for the experimental vehicle's DC Bus capacitance follows,

$$I_{CDC}rms_{(ratting)} \geq I_{CDC}rms_{(calculated)} \tag{7-79}$$

Taking a value of 10ms as the T_{PMS} interval, a DC bus voltage swing of 60V to 58V and the load power disturbance during the PMS epoch as 1.0kW, the DC bus capacitance follows,

$$C_{DC} \geq 34782\mu F \tag{7-80}$$

To comply with the RMS current requirement, a final value of 44000μF was used in the design. The added capacitance also provides the headroom for load disturbance to stretch to 1.265kW and to provide additional voltage stiffness. Construction of the capacitor bank consists of 20 units of 2200μF cells connected in parallel via planar bus bars. In addition to fulfilling the RMS requirement, the parallel configuration resulted in low ESR design value of 0.003Ω. The final configuration of the DC bus capacitor bank is as shown in Figure 7.11. Table 7.4 provides a summary of the reactive components used in the implementation framework.

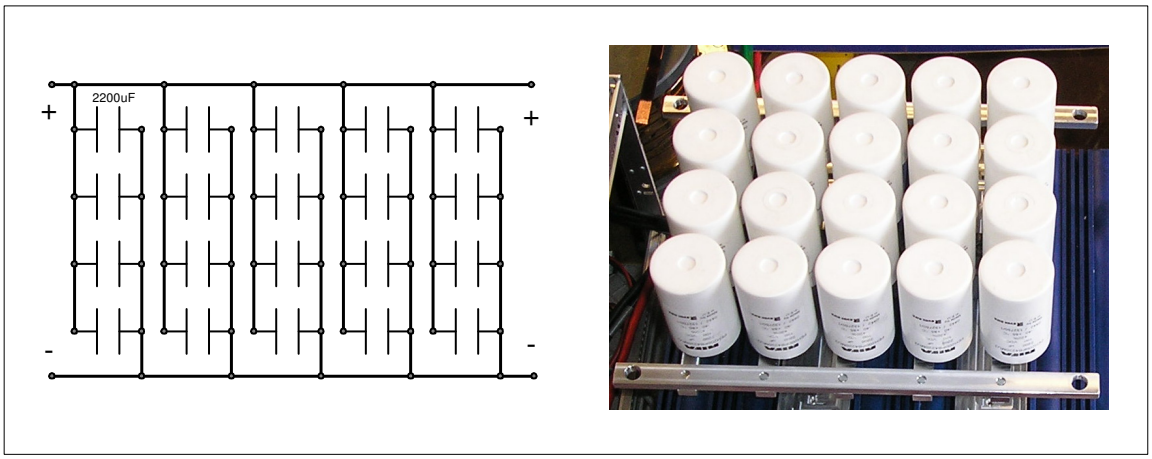

Figure 7.11 Schematic and physical layout of the DC bus capacitor bank.

	Battery side	Ultracapacitor side	ESR
Inductor (L_{batt}, L_{uc})	392μH	392μH	0.03 ohm
Input capacitance (C_{batt}, C_{uc})	2200μF	2200μF	
DC bus capacitor ,C_{DC}	44000μF		0.003 ohm

Table 7.4 Summary of reactive components

7.10 Converter Switching Components

Low on-resistance MOSFETs was selected as the power electronics switches. Each switching branch (T1 to T4) consists of four MOSFETs in parallel to share the load current. The positive temperature coefficient nature of MOSFETs permits parallel operation for forward conduction naturally. Along with the use of the MOSFET body diodes, additional ultra-fast freewheeling diodes (D1 to D4) were added anti-parallel to the power electronic switches. Table 7.5 lists the parameters of the devices.

Device	Voltage rating	Current rating	Physical Device	Configuration
Switches T1, T2, T3, T4	Vpeak = 70V	Ipeak = 250A	MOSFET IRFB 4710 100V, 75A , Rds =0.014ohm	4 units in parallel for each switch set (16 units in total)
Diodes D1, D2, D3, D4	Vpeak = 70V	Ipeak = 250A	Ultra Fast Diode IR- 70EPF02 200V, 600A, Vfd=1.4V	1 unit per switch set.

Table 7.5 Converter power electronic device parameters

Power Losses in the PE switch and diode

The MOSFET conduction loss during forward conduction (ON-State) is a function of the duty cycle *D,* and can be calculated as,

$$P_{con} = \left(\frac{1}{t_{on}} \int_{t_{on}} i_{sw}(t)dt \right)^2 Rds_{(on)} \cdot D$$
$$= I^2{}_{out} \cdot Rds_{(on)} \cdot D \qquad (7\text{-}81)$$

where

$Rds_{(on)}$ is the MOSFET ON- resistance

The switching losses are influenced by the intrinsic MOSFET turn-on time delay $t_{sw(on)}$ and turn-off time delay $t_{sw(off)}$ according to,

$$P_{sw} = \frac{1}{2} I_{ds} \cdot V_{DC(peak)} \cdot f_{sw} \cdot (t_{sw(on)} + t_{sw(off)}) \qquad (7\text{-}82)$$

where

I_{ds} is the MOSFET drain to source current

During the MOSFET diode conduction state, current flowing through the diode develops a forward voltage drop, which dissipates power according to

$$P_{diode} = \Delta V_{diode}\left(\frac{1}{t_{off}}\int_{t_{off}} i_{out}(t)dt\right)\cdot(1-D)$$
$$= \Delta V_{diode}\cdot I_{out}\cdot(1-D) \qquad (7\text{-}83)$$

where t_{off} corresponds to the OFF time of the complementary MOSFET connected in series with the diode. For example, the power loss due to current flowing through diode D1 is calculated based on the OFF time of switch T2.

Therefore the average power loss for a MOSFET-Diode pair during a switching interval is,

$$P_{Loss}sw = P_{con} + P_{sw} + P_{diode} \qquad (7\text{-}84)$$

Power loss as a function of system SoC and power output

The effect of the converter power loss just described can be demonstrated in the context of a power and energy management system as follows. Figure 7.12 shows the converter power loss as a function of the battery and ultracapacitor power flow and corresponding battery and ultracapacitor state of charge. As shown, the power loss when ultracapacitor power is transferred increases as the ultracapacitor SoC decreases. This is due to the voltage decay of the ultracapacitors as the SoC reduces. Comparatively, the battery power loss is less influenced by the decrease in its SoC. As such, discharging the ultracapacitors at high current during a low state of charge results in a high power loss. So, although ultracapacitors are excellent as a peak power buffer, this cost in terms of power transfer efficiency via the converter needs to be considered.

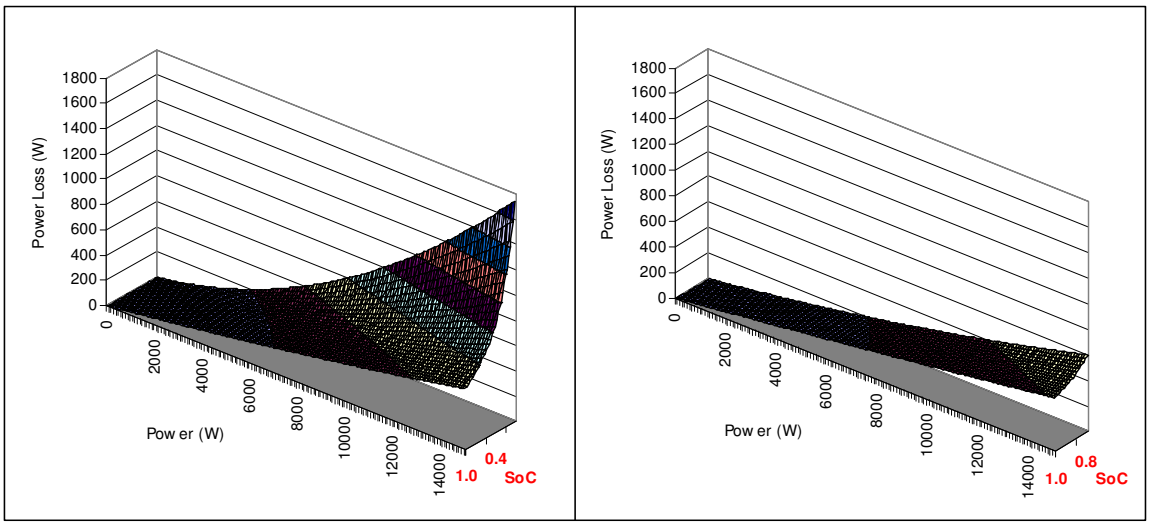

Figure 7.12 Comparison of converter power losses as a function of demanded power transfer and State of Charge (SoC) of the ultracapacitors and batteries.

7.11 Summary

The PES implementation framework presented here provides technical details for researchers seeking information with regards to experimental setup procedures. The derivations of the design values were based upon the selected battery and ultracapacitor specification but the procedure is generic enough to be applied to other sources of electrical power such as fuel cells.

Converters that require a wide input range place additional stresses and losses on both the passive and active components. In this design, the voltage swing of the ultracapacitors was bounded between a maximum value of 45V and a lower value of 20V. This results in the capability to extract 80% of the ultracapacitor energy. To utilise more of the stored energy would require a higher ultracapacitor transfer current and hence higher converter input current, which leads lower energy efficiency. This is where strategies within the energy management shell can address the concern. With information regarding power conversion losses as a function of ultracapacitor SoC, an EMS strategy then has the capability to reduce the allowable ultracapacitor power limits.

CHAPTER 8

EXPERIMENTS AND TYPE TESTS

"It is an experience like no other experience I can describe, the best thing that can happen to a scientist, realising that something that's happened in his or her mind exactly corresponds to something that happens in nature. It's startling every time it occurs. One is surprised that a construct of one's own mind can actually be realised in the honest to goodness world out there. A great shock, and a great joy." – **Leo Kadanoff**

Results of selected experiments and type-tests are presented in this chapter. The first experiment provides empirical verification of the demonstrator vehicle and battery system models. The subsequent experiment presents repeatability testing of the automatic drive-cycle profiler and tests to obtain the operating constraints of the batteries and ultracapacitors. Following this, results of hardware-in-loop tests provide verification of the M-PEMS implementation framework. Both simulations as well as empirical results are presented to support the validity of the M-PEMS framework. Results of a PES type tests are presented to exemplify the operation of the power electronics implementation framework.

8.1. Experiment 1: Model verification

Purpose:

The experiment serves as tests to empirically verify the maximum achievable vehicle acceleration, velocity and stopping distance for the allocated test area. Velocity traces as well the measured battery voltage and battery current acquired from the experiments provides data for the battery model and vehicle model verification.

Procedure:

As per the vehicle hardware specification presented in Chapter 6, the experiment was conducted with the battery system initialised to 100% SoC. The vehicle was then subjected to an arbitrary commanded velocity with the on-board data acquisition set to record data of actual velocity, battery voltage and battery current. The extracted parameters were to facilitate tuning and verification of the battery and vehicle model. At the time of conducting this set of experiments, the capability of the traction drive used on the test vehicle was limited to only positive current

Results:

The measured velocity profile of the vehicle is shown in Figure 8.1. The comparison of measured with simulated battery current and voltage parameters are respectively shown in Figure 8.2 and Figure 8.3.

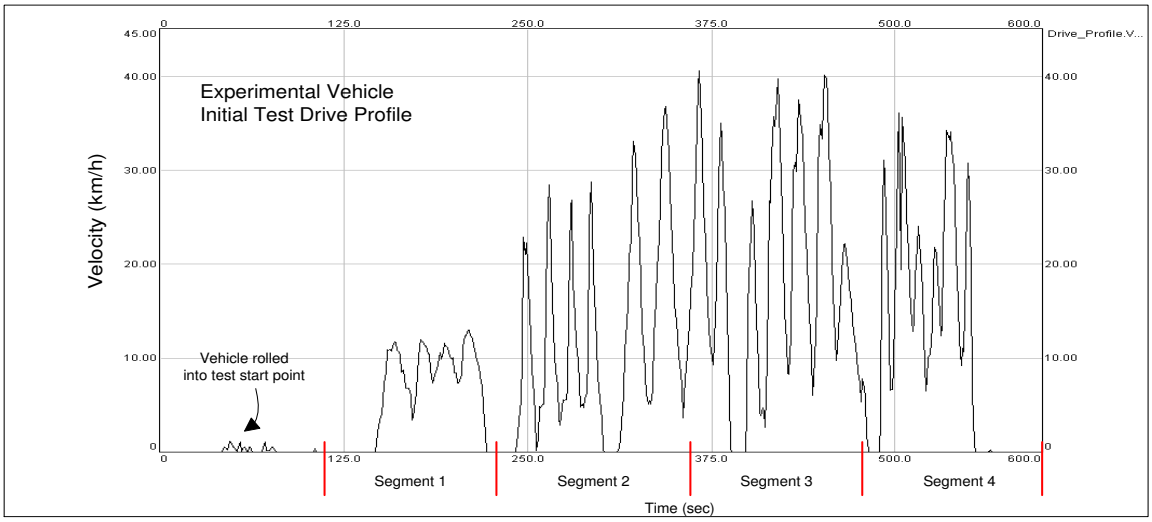

Figure 8.1 Velocity profile of the baseline vehicle obtained for parameter extraction

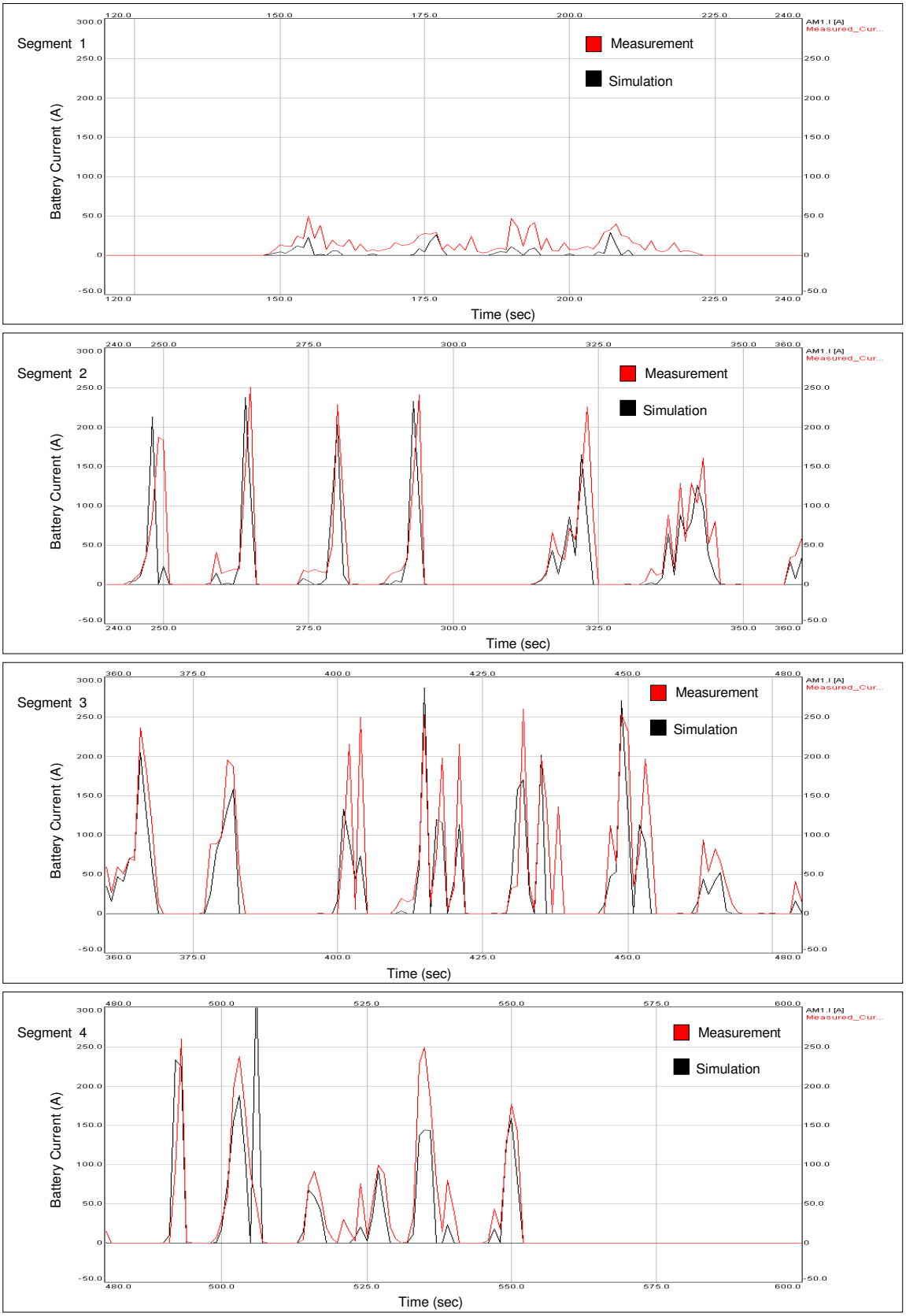

Figure 8.2 Comparison of measured battery current with simulated battery current

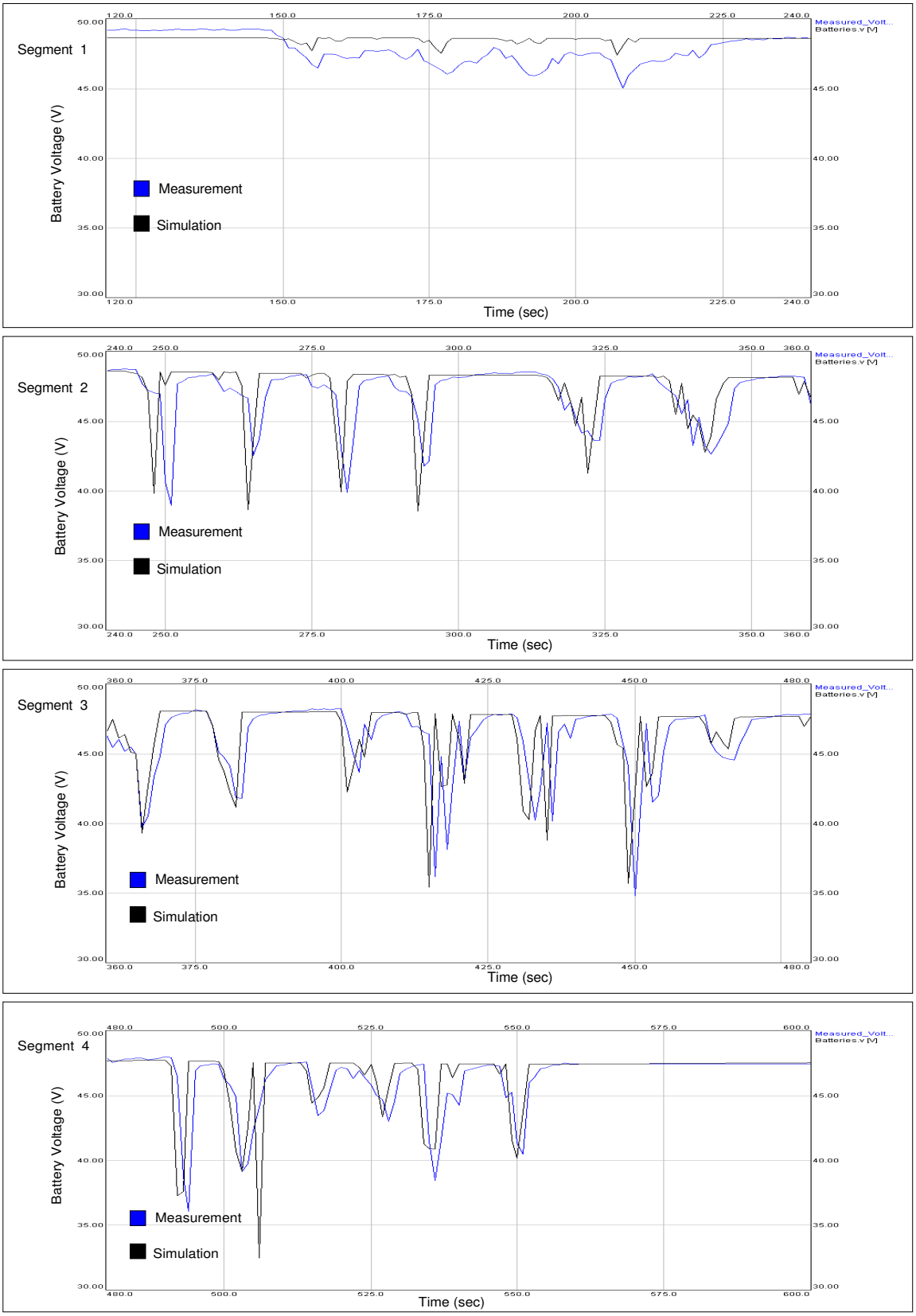

Figure 8.3 Comparison of measured battery voltage with simulated battery voltage

Discussion:

From the 600-second arbitrary test cycle, the maximum velocity that was achieved is 40 km/h. Subsequent (undocumented) tests did demonstrate that the vehicle could reach a velocity of 45km/h. Maximum acceleration was found to be 1.98ms^{-2} and a maximum deceleration of 1.3 ms^{-2}. The deceleration of the vehicle depended on the friction braking. It was also observed (from driver feedback) that a significant amount of mechanical effort via disc brakes was required to bring the vehicle to a complete stop.

From the comparison of simulated and measured battery voltage, the mean error was found to be within 5%. This was derived by calculating the moving average of the error over 1 second sampling periods. Similarly, the battery current mean error was found to be within 9%. It is observed that the battery model is less accurate at lower power demands. This can be seen very clearly in Segment 1 of the tests results. By adding a non-linear scaling factor in the model, it was found that the accuracy at lower power levels could be increased but at the expense of misrepresenting very high power levels instead. The deviation was found to be significant when the batteries were operated above 150A. Since the model proved acceptable for low and mid band power levels with the addition of the scaling factor, it is then valid for simulations within these operating boundaries. This was found to be satisfactory for the scope of this work, which is to introduce a power management system that limits the battery power delivery. In addition, as presented in Chapter 3, limiting the battery power also results in a much more accurate estimation on the battery state of charge.

The experiments validate the battery model used in the developed SIMPLOPER vehicle simulator. This then provided a means to test power and energy management and set the required battery operating boundaries offline.

.

8.2. Experiment 2: Empirical observations and instrumentation tests

Purpose:

Experiment 2 served several objectives, which are described in brief as:

- To verify the design of the test profiles
- To verify that the driver profiler is able to produce experimentally repeatable test profiles.
- To empirically obtain battery-operating constraints under various load demands.
- To empirically test the performance of the ultracapacitors as a vehicle propulsion power source.
- To compare the receptiveness of ultracapacitors and battery pack to regenerative energy during vehicle regenerative braking operation.

Procedure:

With the sizing references described in Chapter 6 and [80], empirical verification of the battery and ultracapacitors constraints were performed to design a M-PEMS for the experimental vehicle. The traction drive used for this experiment and subsequent experimental work was equipped with regenerative power handling capability.

The vehicle was subjected to a predefined 4-segment velocity profile (Figure 8.4) in two sets of experiments. The first tests were conducted with only batteries followed by tests with only ultracapacitors connected to the load. In both cases the total vehicle mass, tyre pressure and ambient conditions were the same.

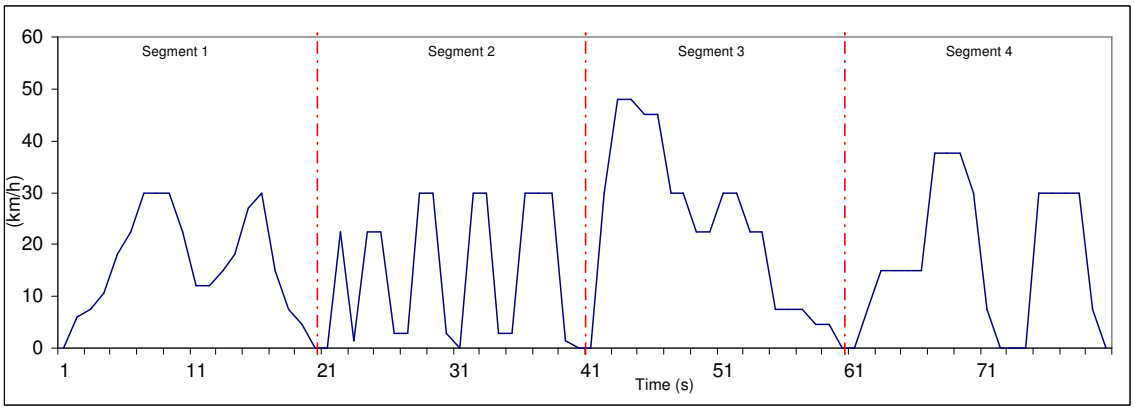

Figure 8.4 Designed test profiles

Results:

Figure 8.5 shows the results of the tests conducted with only batteries and only ultracapacitors servicing the vehicle load demand. The results of the velocity traces are presented on the same graph for ease of comparison. Form the measured velocity data, the profiles are in agreement indicating excellent experimental repeatability. In both experiments, no driver intervention for the vehicle commanded speed was required. The task of the driver was to only initiate the test programme and steady the vehicle on a level travel trajectory. With the regenerative capability of the traction drive, no mechanical braking effort was required to decelerate the vehicle to a complete stop. Maximum deceleration was found to have increased to 1.9ms^{-2}

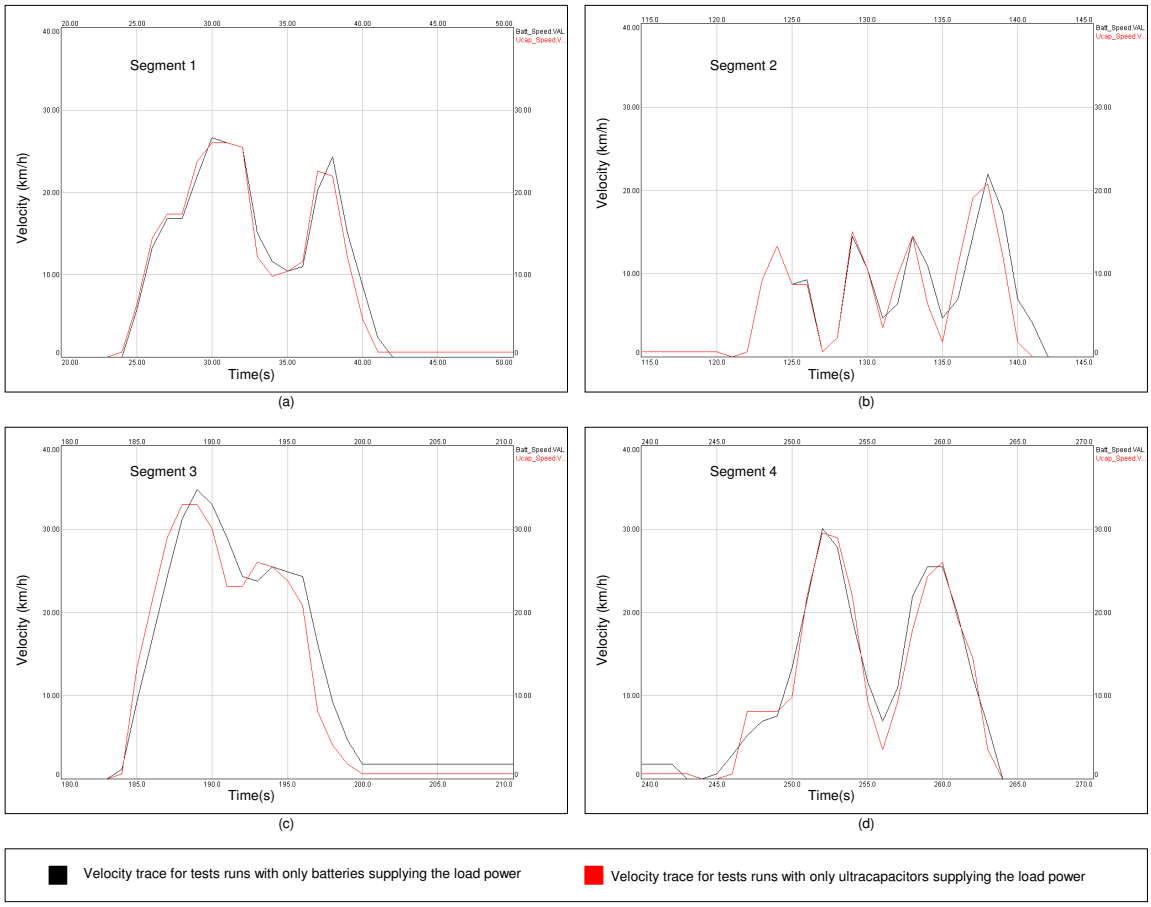

Figure 8.5 Comparison of measured velocity traces

Figure 8.6 shows the battery and ultracapacitor power profiles and the corresponding voltage measurement for the four tests. From the voltage plots, it is seen that the battery voltage experiences an excessive rise. An expansion of this segment is presented as Figure 8.7.

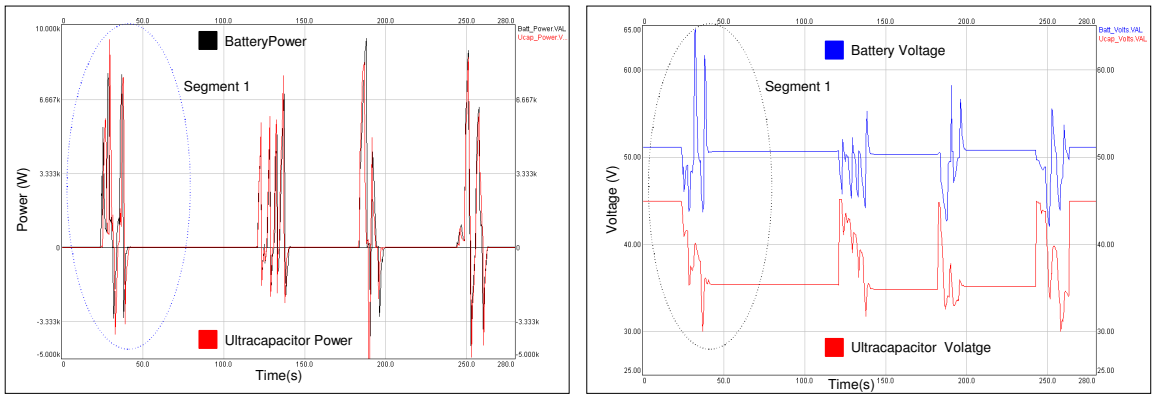

Figure 8.6 Battery and ultracapacitor power and voltage profiles

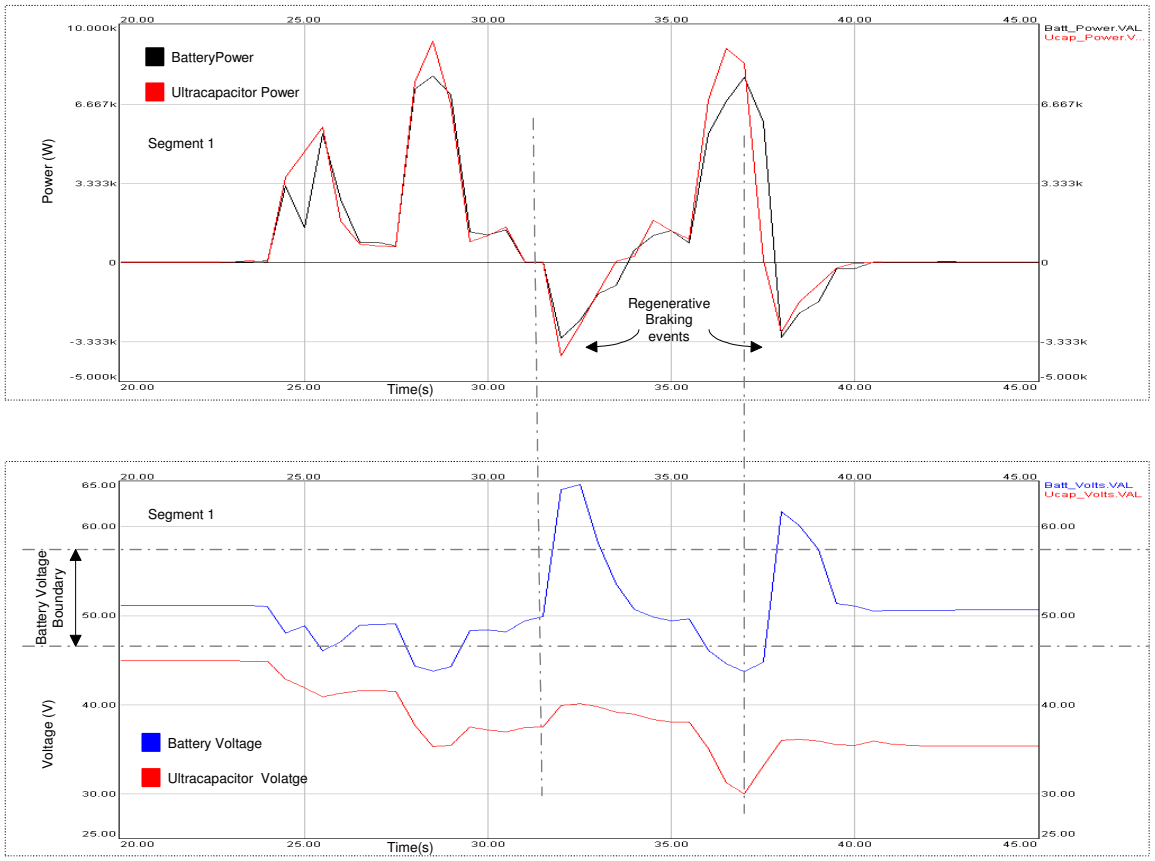

Figure 8.7 Comparison of battery with ultracapacitors in a regenerative braking event

Discussion:

The top graph of Figure 8.7 shows that the power profiles for both tests are similar, indicating that the net energy transfers in both cases are almost equal. A close examination of the voltage measurement (lower graph of Figure 8.7) reveals that during deceleration events, the battery voltage rises significantly above the threshold (gassing) limit. Although the measured power flowing back to the battery indicates that the battery is being charged, the low charge acceptance rate in batteries causes a large portion of the power to be dissipated as losses. The unreceptive nature of high charging current or a rapid change from discharge to charge mode is manifested as a rise in terminal voltage. This immediate rise in the battery pack voltage is attributed to the sudden increase in density of electrolyte in the pores of the active material. In the case of lead acid batteries, repeated operation under these conditions will lead to a reduction in battery life.

Two interesting observation can be made regarding Segment 3. It is seen in Figure 8.6 that a large regenerative power event also takes place in this segment but the battery terminal voltage rise is much less compared to Segment 1. The first reason for this is due to the reduced battery state of charge in Segment 3. Since these tests were carried sequentially with a maximum battery SoC at the beginning of Segment 1, subsequent segments were executed with the SoC depleting. Recalling the discussion in Chapter 3 (Section 3.14) regarding the maximum changing power, it is empirically observed that in this case, the battery charge acceptance rate is higher at lower SoC. This demonstrates the charging power limitation as a function of the battery SoC. The second reason is not very obvious without a closer examination of the drive cycle shown in Figure 8.5. In Segment 1, the change from acceleration mode to deceleration mode is much faster compared to Segment 3. Although the regenerative power event is similar in magnitude, the change from tractive power to regenerative power in Segment 3 is more gradual. As such, the voltage rise phenomenon that occurs due to a rapid change in direction of battery power is less of a factor in this case. It is timely to mention that both these phenomena do not occur in the case of ultracapacitors. With no slow chemical phase changes taking places within the ultracapacitors as does in the batteries, regenerative energy is harnessed more efficiency. Generally, the results empirically confirm that the ultracapacitors are more receptive to regenerative energy.

From the results of the experiment, practical reference parameters can be extracted as the PMS battery operating constraints. Figure 8.8 presents the measured current and voltage waveforms for Segment 1 as projections of the desired voltage boundaries to the corresponding current levels. In the voltage plot, the lower battery voltage is first defined to be approximately 45V. The point x1 marks an instance where the battery voltage crosses beyond this lower limit. The projection of x1 on the time scale to the battery current waveform gives the corresponding current value, which is marked by intersection point x2. From the current plot, the maximum battery current is found to be 150A, thus specifying that the battery power limit (V x I) is to be set at a value of 6.75kW. Similarly, the upper voltage boundary specifies the charging power (or regenerative power) limits. The intersection values and projections using marking points x3 and x4 gives a maximum charging current of 25A . As was discussed previously, charging the battery this way is not efficient and ideally the minimum battery power should be zero with all regenerative braking power handled by the ultracapacitor instead.

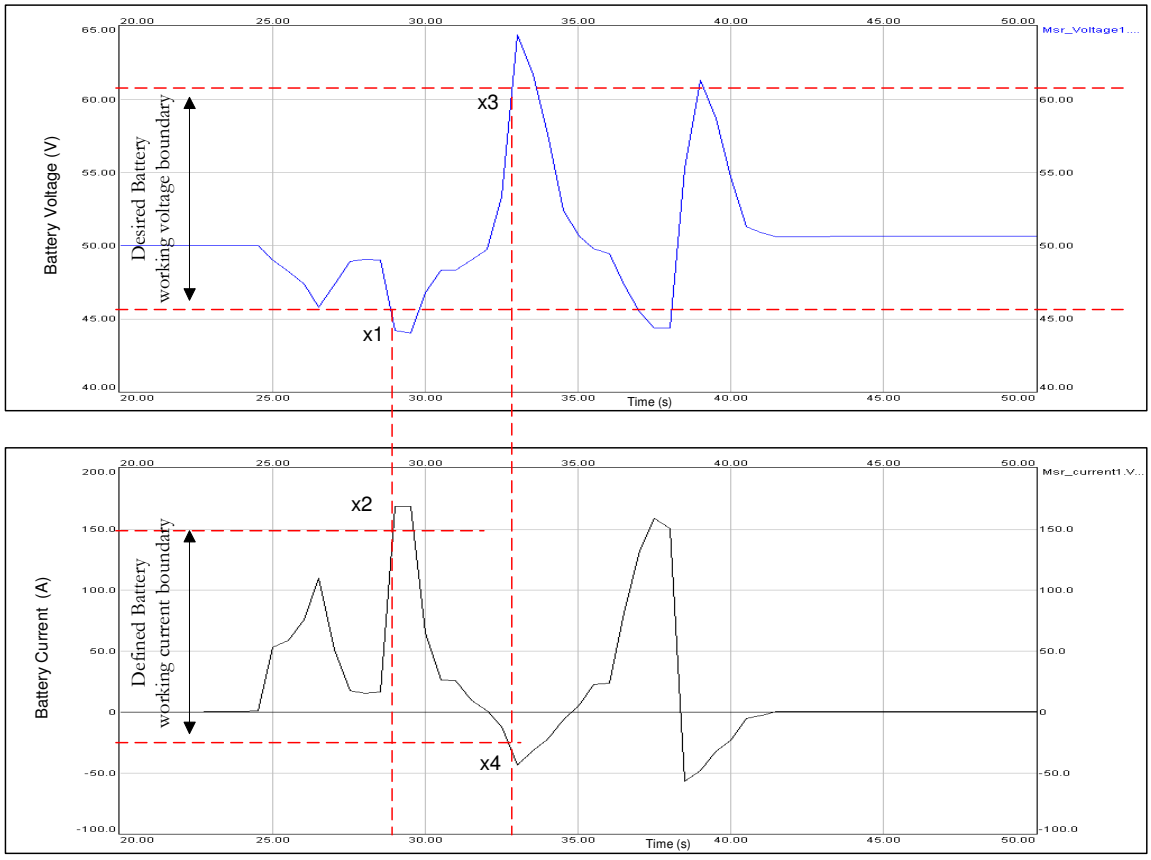

Figure 8.8 Determining battery operating limits empirically

8.3. Experiment 3: Power Management hardware in loop verification

Purpose:

The hardware in-loop experiment is designed to provide verification of the power management shell policy formulation. The experiment aims to verify that the load power can be measured and the corresponding reference power trajectories generated as per the PMS policy and decision epoch constraints.

Procedure:

The experiment was performed using the target hardware specified in Chapters 6. The PMS policy was first simulated using SIMPLORER. Figure 8.9 presents the PMS simulation module. From the previous experiment, the positive battery power limit was found to be 6.75kW. Also from experimental observations, the power delivery bandwidth of the ultracapacitors was set to +/- 10kW. A PMS epoch constraint of 10ms is achieved by setting DT=0.01s and setting the maximum simulation step time to also 0.01s. Both the battery charging power limit and the battery negative slew coefficient (Gn_{batt})are set to zero hence disabling the battery regenerative power capability. The battery positive slew coefficient (Gp_{batt}) is however set to 5kW/second.

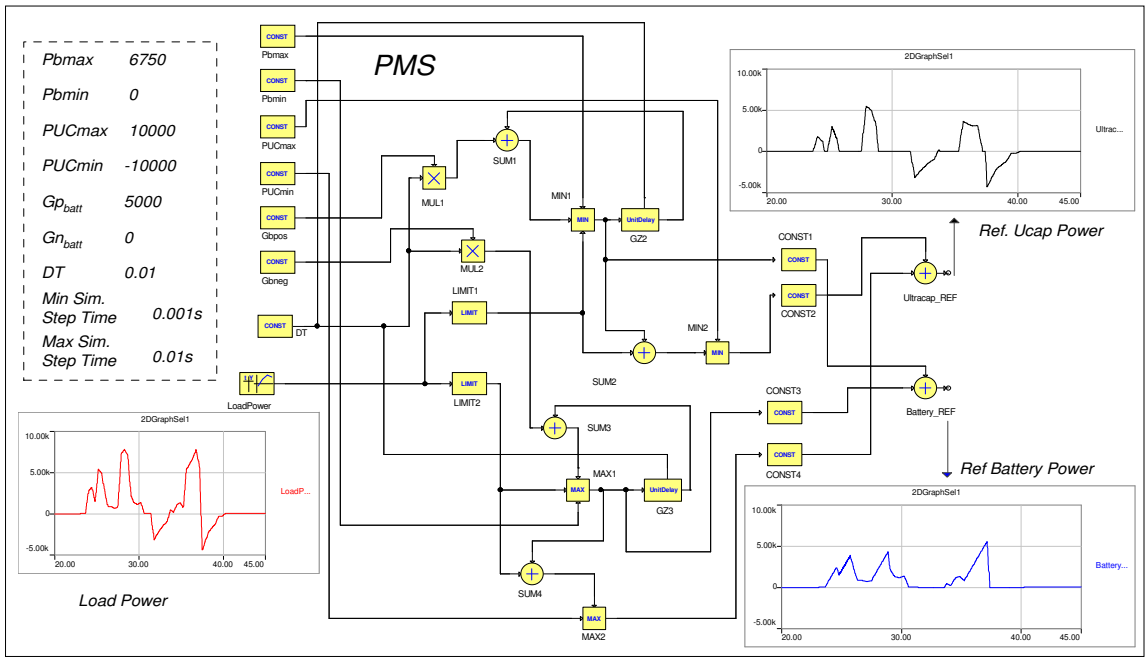

Figure 8.9 PMS simulation module

Implementation of the PMS is as shown in Figure 8.10. Developed in Labview7, the PMS algorithm is executed within the target hardware real-time controller .The PMS deterministic loop is set as 10ms with a Boolean flag to indicate a late finish of the execution. Outputs of the loop are the battery and ultracapacitor feed-forward power references. Acquisition of the measured power is performed using a continuous but interruptible polling subroutine. The measured power is then made available to the PMS via the input variable marked as 'Numeric' in Figure 8.10. Experimental data is stored in memory at a rate of 300 samples per test segment.

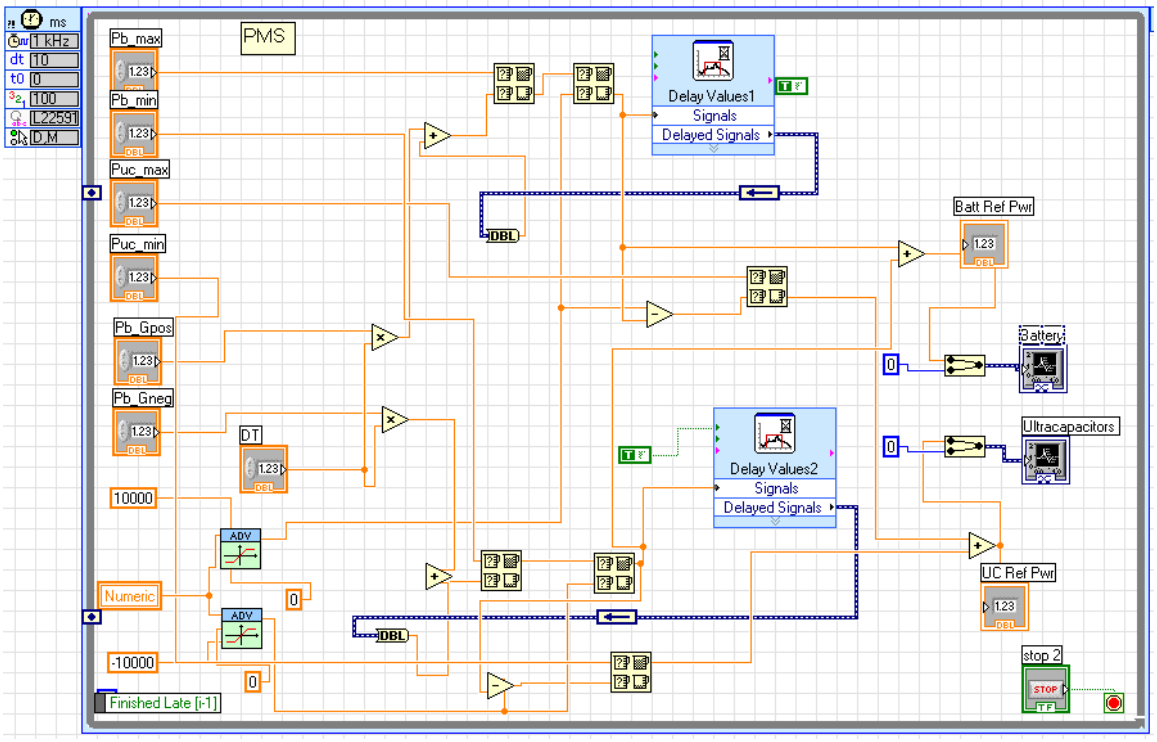

Figure 8.10 PMS Implementation module

Results:

The simulated and implemented power splits generated for the four test segments by the PMS module are presented in Figure 8.11 through Figure 8.18. In the four simulation plots, the battery reference power trajectories conform to the power limit and rate of power constraints. The ultracapacitors handle the transient power demands as well as the load magnitudes above the specified battery power limit.

Test Segment 1

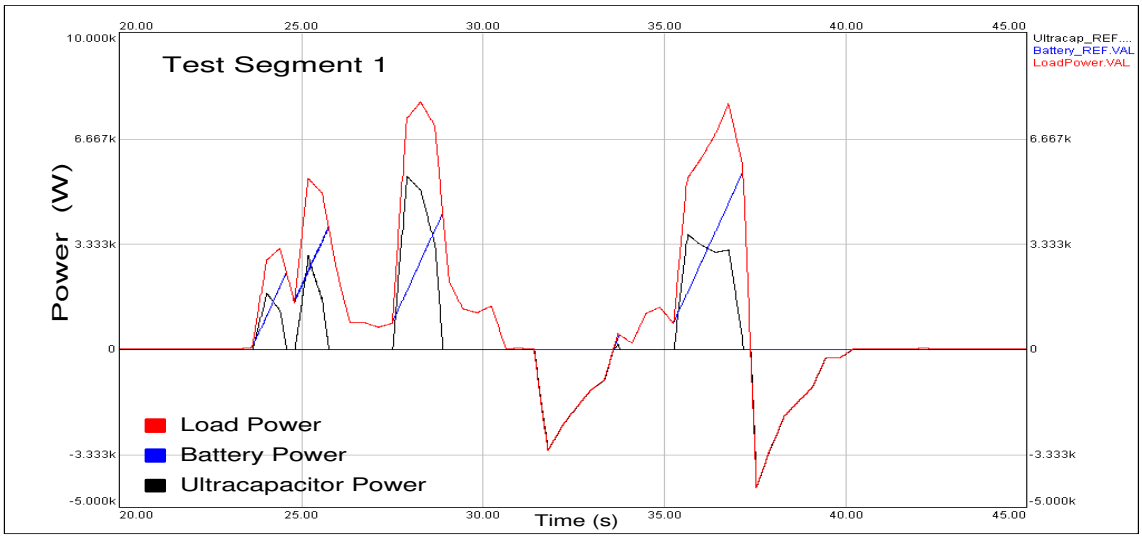

Figure 8.11 Power management in Segment 1- (Simulation)

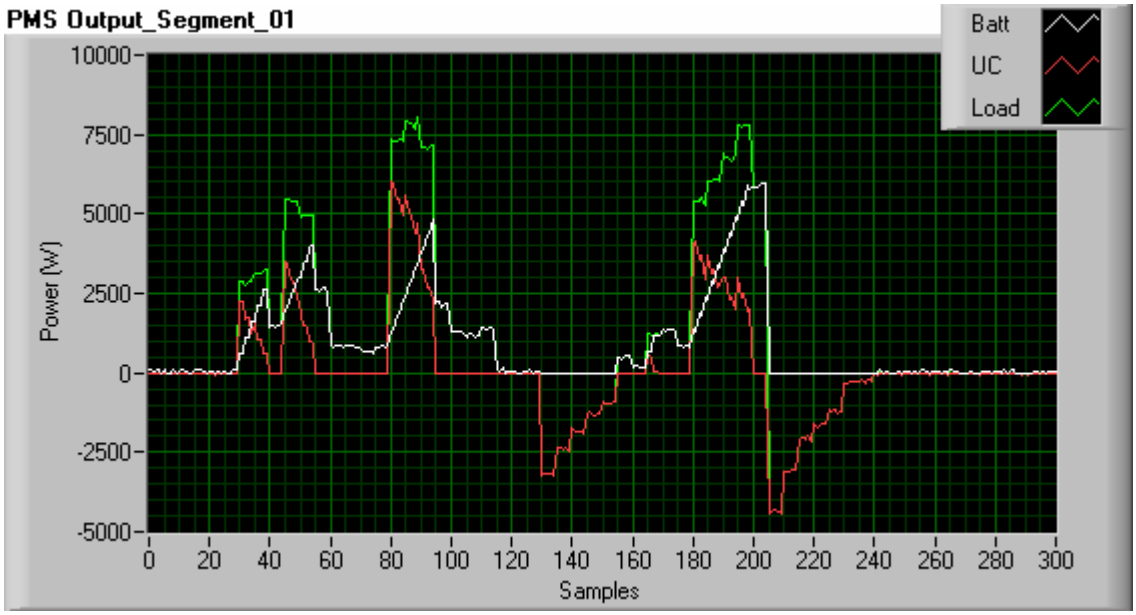

Figure 8.12 Power management in Segment 1-(Implementation)

Test Segment 2

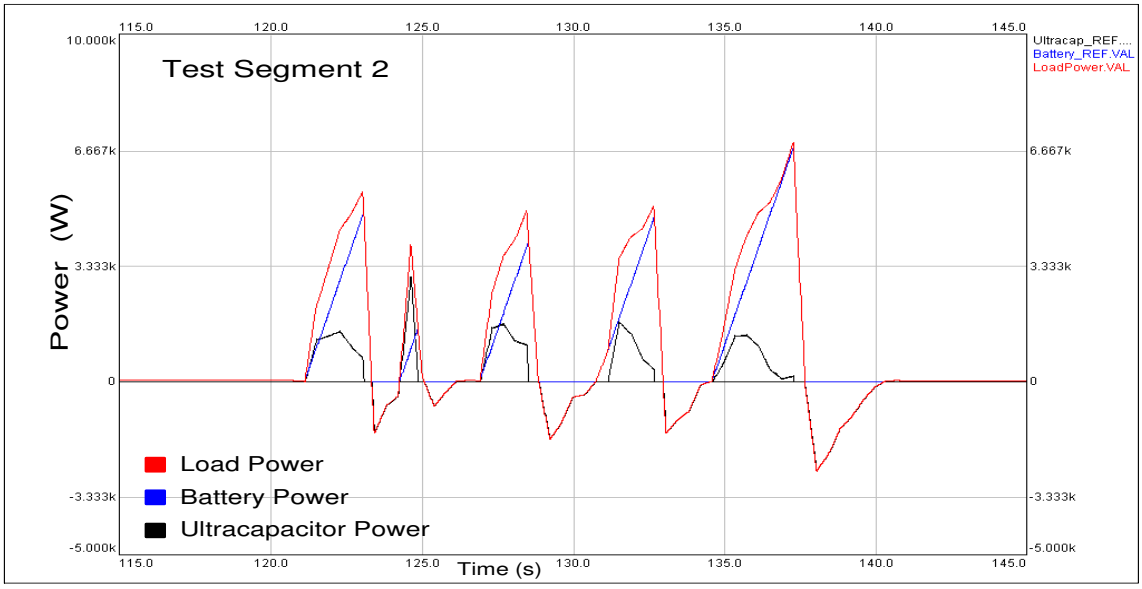

Figure 8.13 Power management in Segment 2 – (Simulation)

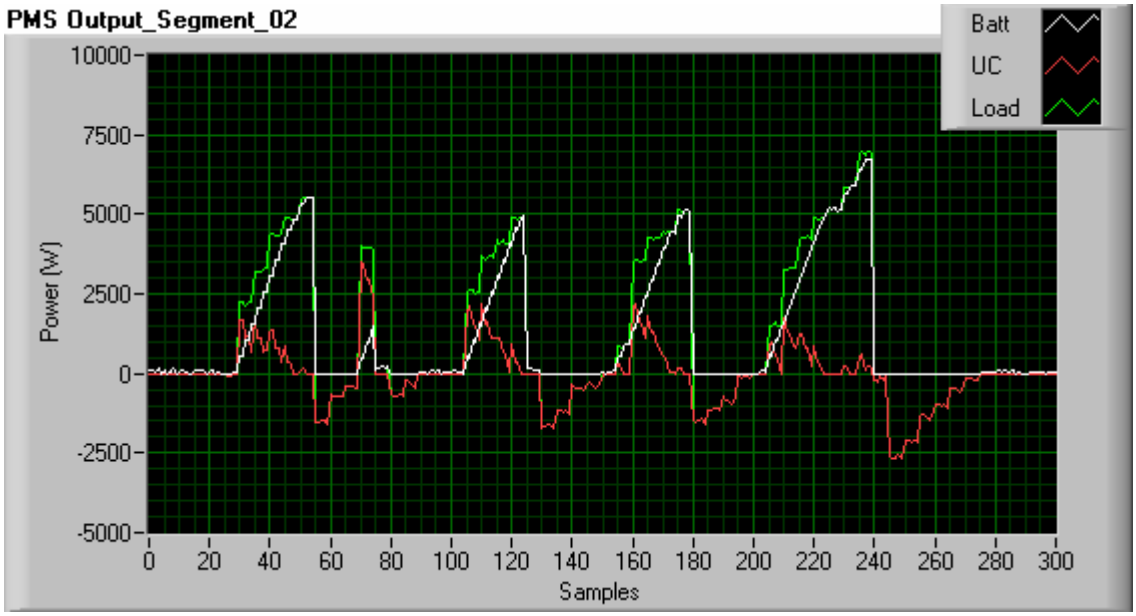

Figure 8.14 Power management in Segment 2- (Implementation)

Test Segment 3

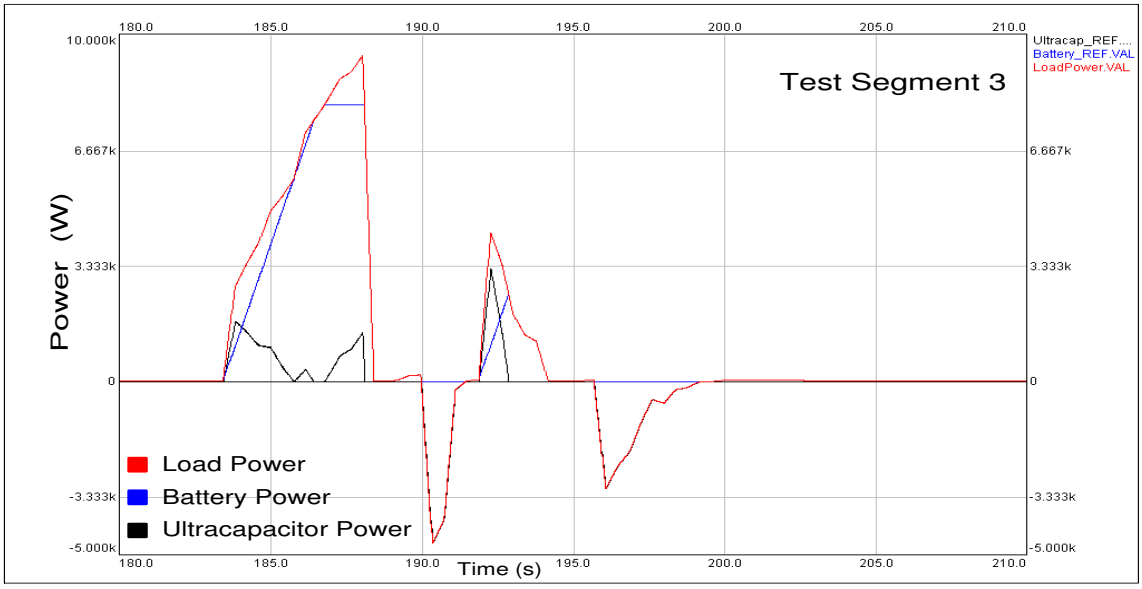

Figure 8.15 Power management in Segment 3- (Simulation)

Figure 8.16 Power management in Segment 3- (Implementation)

Test Segment 4

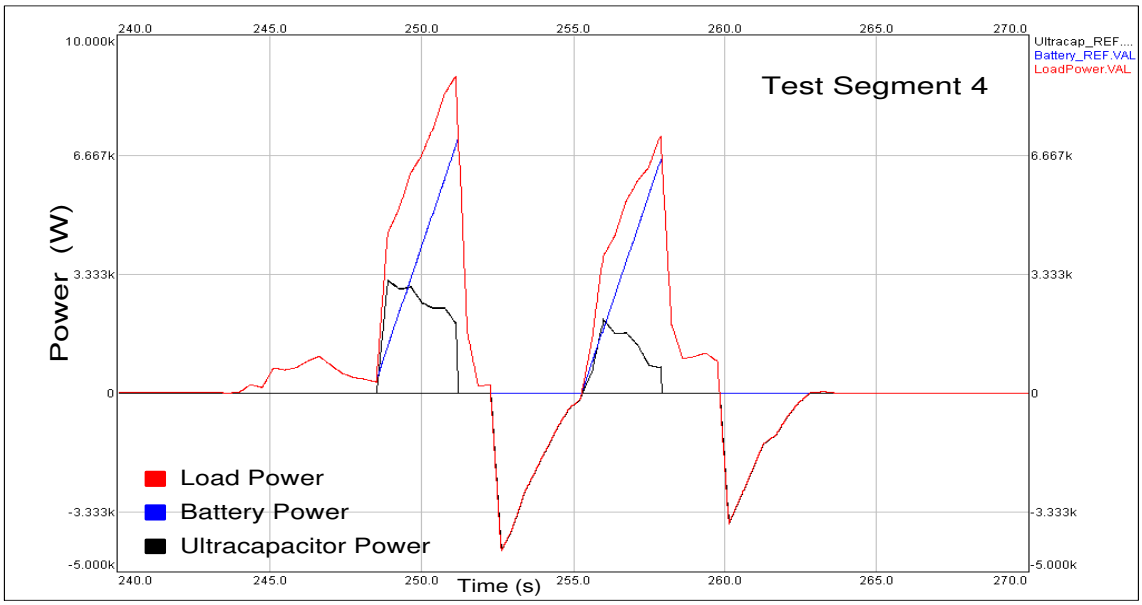

Figure 8.17 Power management in Segment 4- (Simulation)

Figure 8.18 Power management in Segment 4- (Implementation)

Discussion:

Results of the PMS implementation match the simulated ones. For all four-test segments, the PMS loop proved deterministic by generating the reference power splits within the PMS epoch. No 'Finished-Late' flags were reported in the experiment. The experiment verifies that the concept of the PMS generating reference power trajectories by measuring load variation on the DC bus is achievable. At this point, it is timely to reiterate a claim in Chapter 1, which states that, "power split decisions are made using only power fluctuations at the DC Bus rather than the conventional methods of monitoring the throttle input (driver input). This leads to the ability of including propulsion as well as non-propulsion loads in the implementation framework".

Since the previous experiments validate the battery model, an offline method to test the effect of introducing the PMS is accomplished by subjecting the vehicle model to the battery reference power generated by the PMS. With this, a comparison of battery current and voltage with and without the PMS can be made. Figure 8.19 presents simulated comparisons of battery currents while Figure 8.20 compares the voltage profiles. In all four battery current profiles, the introduction of the PMS is manifested as a reduction in current ramp rate. The 5kW/s positive slew rate coefficient (Gp_{batt}) effectively limits the battery current rise to approximately 100A/s. The clamping of the battery current at 150A is most apparent in Segment 3 of Figure 8.19.

The voltage waveforms (Figure 8.20) show that with the PMS activated, the battery voltage operates within the specified bounds. Voltage excursions do not exceed the predetermined 45V lower level. Although not apparent from the experiment, operating the battery system in under such conditions is electrically and thermally preferred [62], and does result in an extension of the battery life cycle.

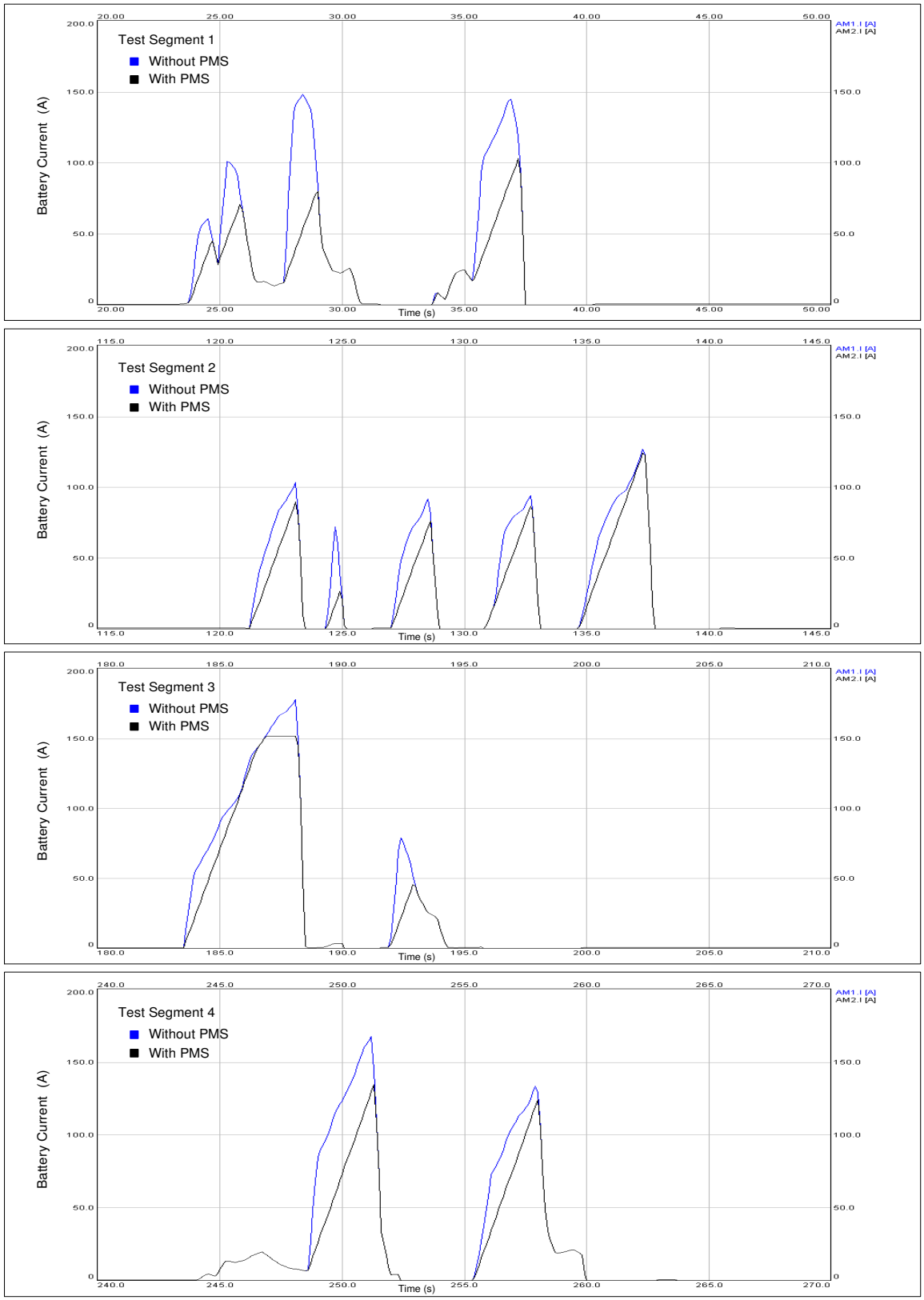

Figure 8.19 Battery Current – with and without PMS

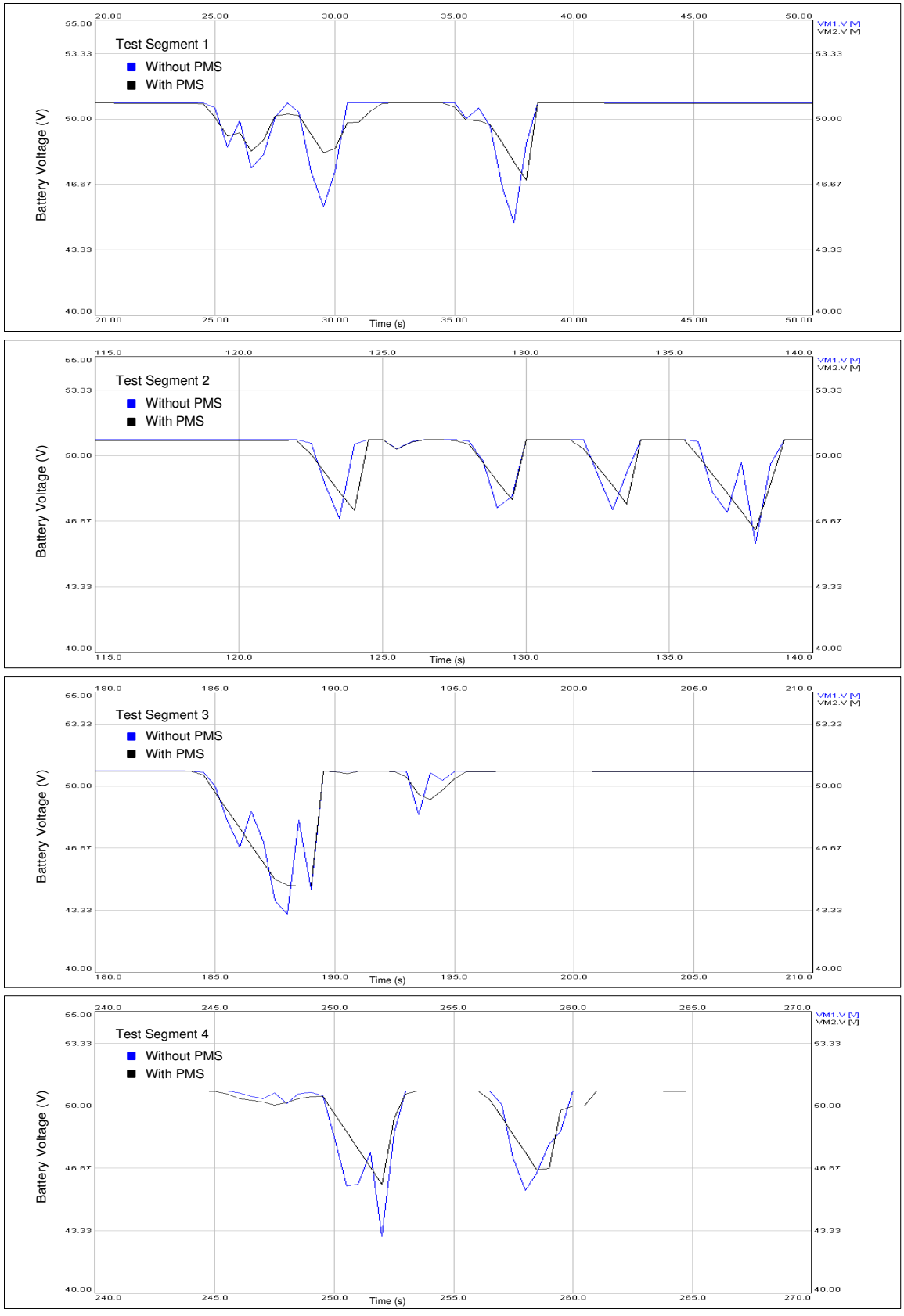

Figure 8.20 Battery Voltage – with and without PMS

Figure 8.21 provides a comparison of the battery energy expenditure with and without power management. The dotted line marks the energy expenditure without a PMS. As seen, the gain in terms of energy savings at the end of the 4 tests is marginal. In this case, only 3.4%. Although the PMS policy limits the peak power delivery of the battery through the use of ultracapacitors, the total energy to propel the vehicle still comes from the battery pack. In addition, to transfer the energy from the battery to the ultracapacitor results in power conversion losses. Therefore, a large energy saving is not to be expected at the end of the short test cycles. As discussed, mitigating high power peaks from the battery system does however result in a long-term gain of extending the battery life as well as the long-term energy storage efficiency.

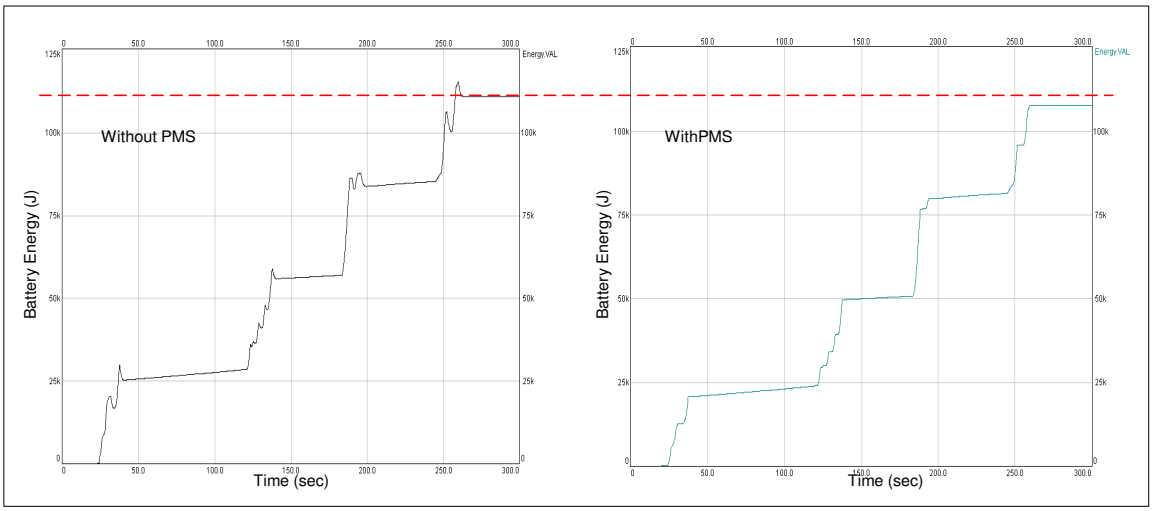

Figure 8.21 Battery energy expenditure after four tests segments

8.4. PES Type Test

Purpose:

This test is to confirm the operation of the Power electronics converter described in Chapter 7. The concept of the M-PEMS specifies the ability of the power split references generated by the PMS be transformed to duty cycle commands by the PES. This test provides both hardware design verification as well as a demonstration of the microsecond PES epochs.

Procedure:

With the circuit analysis presented in Chapter 7, the bidirectional converter developed for this work was first simulated in its complete form using SIMPLORER. This provided a tool to test the design before construction. Figure 8.22 shows the summation model. Values of the components are as per 'As-Built' status of the design (*see Appendix for details*). For the hardware verification, State 101 (battery + ultracapacitor in discharge mode) is selected for type testing. The measured parameters are the battery side inductor current, the battery boost converter PWM signal, the ultracapacitor side inductor current, the ultracapacitor boost converter PWM signal and the load current.

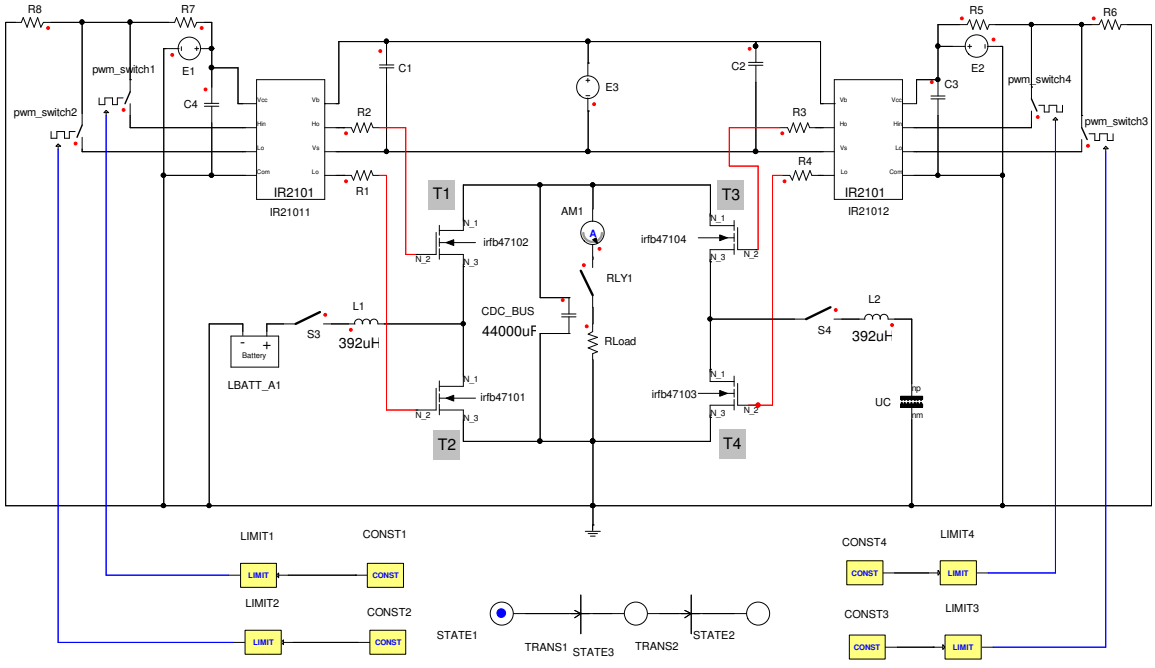

Figure 8.22 Simplorer simulation model

Results:

Figure 8.23 presents the simulated output of the power converter in State 101 within a 500µs time window. In Figure 8.24, the same parameters are shown in oscilloscope screen capture taken during the hardware testing stage. The PMS and PES responding to change in ultracapacitor input voltage is shown in Figure 8.25 as an increase in ultracapacitor side inductor current. Note that the duty cycle of T4 in Figure 8.25 increases to transfer more energy to the inductor in order to compensate for the drop in input voltage.

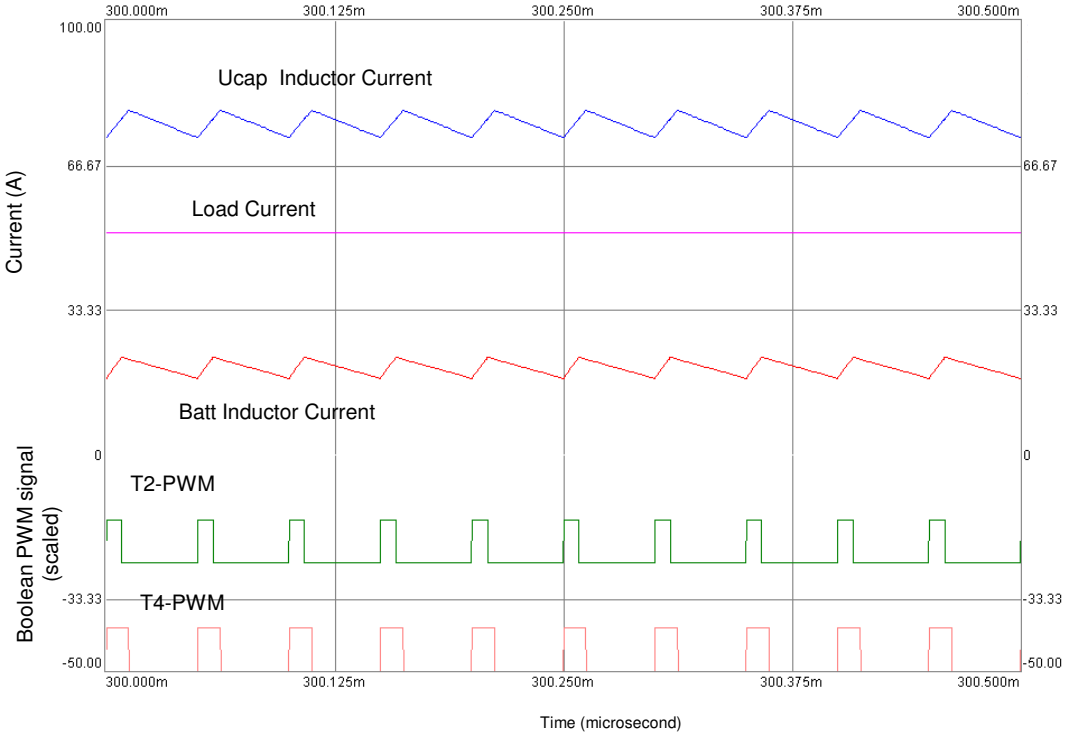

Figure 8.23 Simulated PES parameters

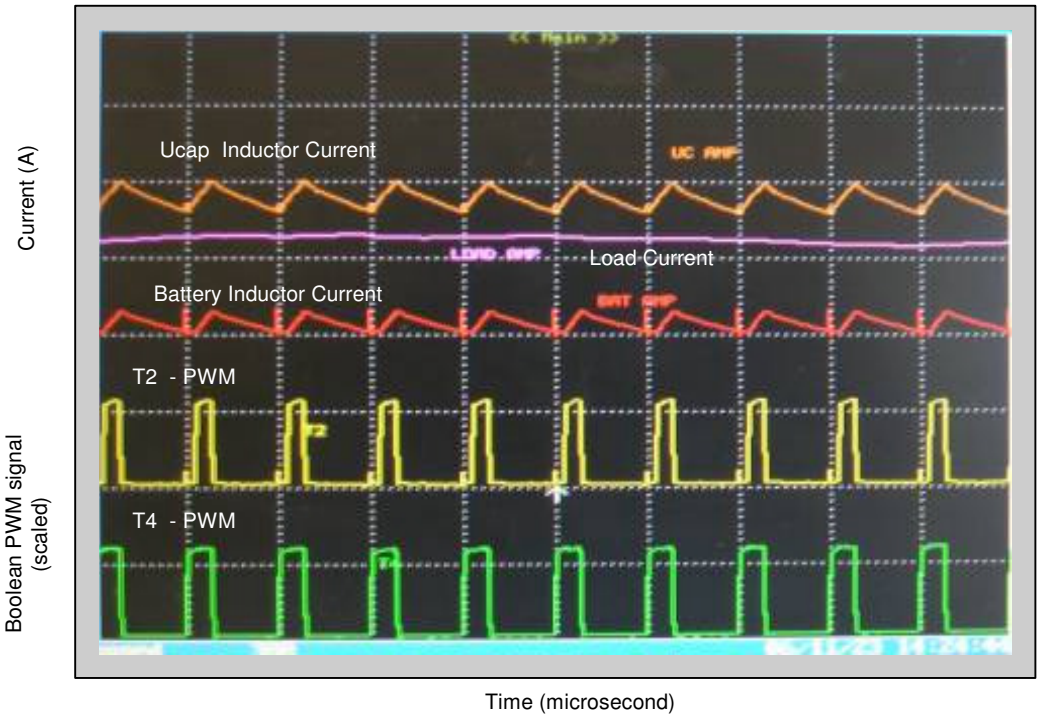

Figure 8.24 Measured PES parameters

Figure 8.25 Measured PES parameters showing an ultracapacitor current increase

Discussion:

Results of the type-test provide design verification of the PES implementation framework. The simulated converter design was validated with measured values of the actual converter. The previous experiment demonstrated the PMS implementation with time scales in terms of milliseconds. Within the PES, the time scales of concern are in microseconds. As the last level in the M-PEMS hierarchical framework, the PES is the process that handles the actual blending of power from the energy sources. The PES functions as the infrastructure that enables the very concept of managing power and energy for a dual energy system to be realised.

This test brings some completeness to the M-PEMS concept put forward in this work. It demonstrates how long-term decisions and strategic planning for energy management is eventually relayed downstream and translated to commanded duty cycle outputs. It also shows that the problem of managing power and energy is a power electronics intensive area of research.

CHAPTER 9

CONCLUSIONS AND FUTURE WORK

"Any piece of knowledge I acquire today has a value at this moment exactly proportional to my skills to deal with it. Tomorrow, when I know more, I recall that piece of knowledge and use it better ". – Mark Von Doren, 1894- 1972

This chapter concludes the dissertation. The chapter summaries the main contributions of this work and presents a forward path to extend the research. In this research, an attempt has been made to provide a new perspective to the problem description of electric vehicle power and energy management. This dissertation has described a comprehensive and systematic framework to address and implement such a power and energy management system. To demonstrate this, the framework was implemented in the development of a test vehicle.

9.1. Conclusions

General

The work presented a holistic approach to the problem of managing power and energy of multiple energy systems within a vehicular architecture. It was demonstrated that the multidisciplinary problem of managing power and energy is decomposable in such a way that three major processes and the links between the processes can be identified. This provides a more structured framework for future research. This dissertation described the formulation of managing power and energy of multiple energy sources for an electric vehicle powertrain. The formulation was derived from adopting a fresh perspective to the power and energy management problem. The analogies presented in this work explicate and demonstrate the problem as a systematic implementation framework. Beginning with an analogy of organisational management philosophy and a heuristic derivation of how the management of power and energy relates to hierarchical management models, the work presented a cogent argument of the hypothesis. At this point, revisiting the first illustration of power split between two energy sources presented in Chapter 2 provides a means to explain how the approach presented in this work addresses the fundamental description of the problem. Figure 9.1 refines the original illustration (Figure 2.2) and explicates the three main processes that add completeness to the power and energy management problem description.

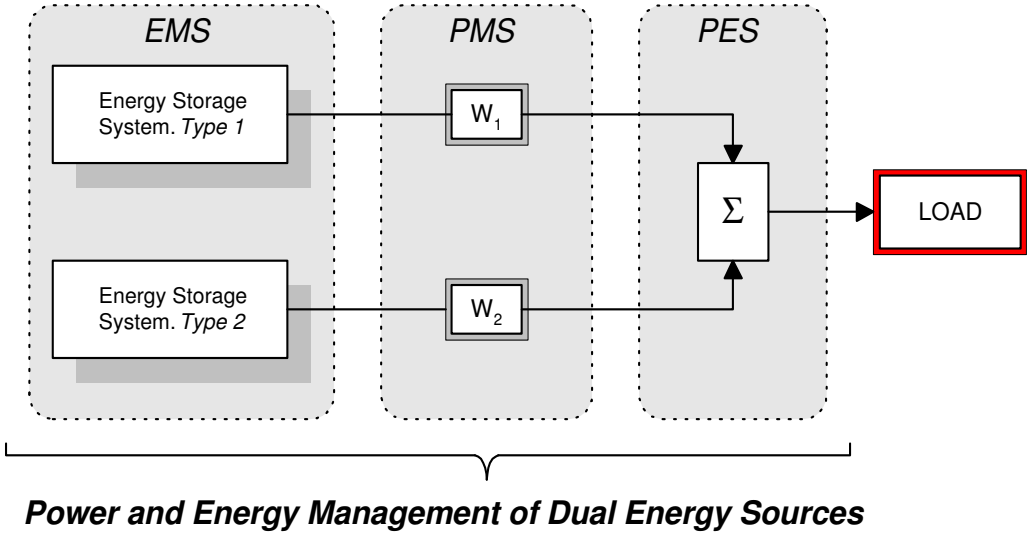

Figure 9.1 Redefining the power split problem and how M-PEMS provides an encapsulated solution

The M-PEMS framework does not only provide a very different perspective to the problem but also an implementation platform that addresses all aspects of managing several electrical energy sources. This approach differs from the approach taken in many publications that divide the research into isolated problems and address sub-problems without demonstrating how they fit into a larger picture.

The review on previous and ongoing work by other researchers in this field provided a comprehensive description and aspects of the research problem. Following this, key issues pertaining to the implementation and systems integration of batteries and ultracapacitors have been discussed in detail. Findings based on the exhaustive literature survey were presented to state the various methods of addressing power and energy management of batteries and ultracapacitors in EV architectures. Through periodic publications, presentations and discussions with other researchers as well as feedback from the industry, this research project has provided timely contributions to this evolving field of study. The active interaction and peer review has also provided a means to assess the concepts put forward in this work.

This work documents detail elements for experimental replication. The requirement of the power electronics interfacing mechanism to facilitate power management has been described in great detail. This was found to be lacking in literature and hence forms a significant contribution and adds depth and perspective to overall problem description. Experimental results obtained from the prototype electric vehicle, successfully demonstrated the capability of arbitrating the power delivery and energy expenditure of multiple energy systems.

The capability and benefit of using ultracapacitors as a battery peak power suppression system was clearly demonstrated. However, it was also shown that although ultracapacitors are able to store and release energy at high rates (high power), extracting the energy for use in a vehicle propulsion system requires a power conversion process in order to fulfil working voltage requirements. The circuit analysis and design in Chapter 7 demonstrated that operating the ultracapacitors at high power levels when at low state of charge results in a high power transfer losses and hence a lower net energy efficiency. So, although these devices offer superior power delivery capabilities, it is not without its limitations. As such, an

energy management strategy is required to keep the ultracapacitors at the right state of charge so that high power transfers are performed with minimum loss.

Although economical evaluation is not within the research scope, it was observed throughout the duration of this work that the cost of the ultracapacitors was frequently a matter of debate when justifying hybrid energy systems. Some conjectures can be made on this argument that the application of ultracapacitors will be limited on the basis of the cost issues. There are many research papers that openly discuss the suitably of ultracapacitors as electric vehicle peak power mitigation devices but stipulate that the technology is unfavourable due to cost constraints. Even if the cost of the ultracapacitors is driven extremely low, there is still a large overhead in terms of the metals and other passive components within the associated power electronics infrastructure. This is rarely discussed in the open literature. To support a cost analysis of ultracapacitor applications, figures should include the power electronics overhead that is fundamentally required to exploit the use of ultracapacitors in EVs. Along with the cost per Kilowatt for the power electronics infrastructure, the weight per kilowatt is also a factor to consider. A recent projection of power electronics metrics (*obtained with permission*) [1], indicate that at present, these figures are circa 5 kW/kg at £12/kW, with figures of 14.1 kW/kg at £1.8/kW expected by the year 2020. This in fact shows where the economic evaluation should be targeted and hence supports grounds for more PES design optimisation.

The following are some general remarks on the three key areas presented in this work.

On energy management

Since with practical scenarios, the exact vehicle power demand profiles are not known in advance and are difficult to accurately predict, and since a battery-ultracapacitor system cannot be dimensioned to capture all possible situations, energy management becomes a trade-off between storage system service life and round trip efficiency. An energy management strategy that tries to regulate the energy system state of charge in anticipation of load demand changes can sometimes lead to energy being transferred back and forth

[1] Personal correspondence with J.M.Miller - Author of 'Propulsion Systems for Hybrid Vehicles' [5]

between sources. Doing so imposes an energy loss penalty and hence a lower round trip efficiency. However, as discussed in chapter 3, it does operate the sources under less stress and hence increases the cycle life.

On power management

The power management policy described in this work is based on the operating constraints of battery and ultracapacitor systems. Chapter 3 presented these constraints and demonstrated the effect of operating these energy systems beyond efficient operating boundaries. Following this, Chapter 4 showed that vehicle power demand profiles typically comprises of large peak to average power ratios. Hence, segmenting the power delivery spectrum of the energy systems with some form of load specialisation technique permits the energy systems to operate within its target efficiency boundaries. Power split decision between the energy sources is then determined based on the policy definition, which is also constrained to generate decisions within a finite time or decision epoch. With both the policy and decision epoch specified, power management can be then encapsulated within an autonomous process called the Power Management Shell.

On power electronics

A high working voltage will result in some reduction in the mass of the power electronics converter and the associated interconnection and disconnection devices. In isolation, this seems favourable. However, doing so then requires an increase in the number of series energy sources to attain the higher terminal voltage. Not only does this shift the mass towards the batteries and ultracapacitors, the longer series string will also require additional series charge balancing circuitry.

The major objectives set out for this project has been accomplished. However, there are several avenues that warrant further investigation. The next section presents a road map of future work as a continuance of this research.

9.2. Future work

In the vehicle power and energy management model, only the propulsion load of the vehicle was considered. Possibilities of incorporating the effect of non-propulsion loads require some investigations. A preliminary study of the ever-increasing non-propulsion loads in vehicles was conducted as part of this research [121, 122]. Following this, further work is required to study the potential of integrating those concepts into the power management (PMS) and energy management (EMS) shells. For instance, a PMS policy may include the prioritised arbitration of non-propulsion when available power is limited while the EMS may include negotiation frameworks to arbitrate the activation of large but non-critical loads in some form of intelligent interaction.

For any type of battery SoC estimation, the application of Peukert's equation should be with the consideration that underestimation can occur. This is because the equation captures the battery discharging capacity at constant current and constant temperature [110]. A more accurate Battery SoC estimation using combined methods may be incorporated in the EMS shell. A method that combines Ah-counting, EMF estimation and a temperature compensation algorithm such as described in [123] would contribute as a more precise lead-acid battery SoC gauge. The EMS strategy demonstrated in Chapter 5 only considers one of the nine controllable parameters that link the EMS to PMS. Further work is warranted to include and analyse the effect and controllability of the other parameters.

Stability analysis of the power management shell (PES) and the sensitive dependence on component variations is another avenue to investigate. Also, since MOSFETS were selected in the final build of the PES implementation framework, some modifications can be made to incorporate synchronous rectification to reduce the power losses of the freewheeling diodes. A description of this technique can be found in [124].

This thesis presented simulation and experiments that demonstrated the possible benefits of multiple energy systems in an EV application. However, further experimentation is needed to test more scenarios and study how the many trade-offs of the implementation hardware is

to be included in measuring the net benefit. Now that the experimentation groundwork is done and the modular but comprehensive research framework defined, the research efforts can now be disseminated in a very structured form.

A series of evaluations via simulations are to be performed to compare the power management policy presented in this work with power split trajectories generated by using the many non-casual methods available in literature. With the developed test vehicle as the model and by using empirically reproducible drive profiles, the comparisons are expected to show interesting differences between the power split decisions generating methods. Using the developed drive profile sequencer, experiments can then follow to produce a comparison between optimal but non-causal power split trajectories and the PMS policy, which can be said to be suboptimal but implemetable.

To quantify the long-term gains that the M-PEMS has to offer, extended and more rigorous road tests are required. The battery system is to be subjected to longer test profiles to quantify any increase in usable energy efficiency. Experimental procedures need to be designed to ensure that the battery charging regimes as well as the charging conditions are controlled and experimentally repeatable in order to trace the battery performance history.

REFERENCES

[1] I. Husain, *Electric and Hybrid Vehicles-Design Fundamentals*: CRC Press, ISBN 0-8493-1466-6, 2003.

[2] C. C. Chan and K. T. Chau, *Modern Electric Vehicle Technology*: Oxford University Press, ISBN 0-19-850416-0, 2001.

[3] M. Ehsani, K. M. Rahman, and H. A. Toliyat, "Propulsion system design of electric and hybrid vehicles," *IEEE Transactions on Industrial Electronics*, vol. 44, pp. 19-27, 1997.

[4] C. C. Chan, "The State of the Art Electric and Hybrid Vehicles," *Invited Paper for the Proceedings of the IEEE*, vol. 90, pp. 247-275, 2002.

[5] J. M. Miller, *Propulsion Systems for Hybrid Vehicles*: IEE, ISBN 0-86341-336-6, 2004.

[6] J. M. Miller, D. Goel, D. Kaminski, H. P. Shoner, and T. Jahns, "Making the case for a next generation automotive electrical system," presented at International Congress on Transportation Electronics, 1998.

[7] J. G. Kassakian, H. C. Wolf, J. M. Miller, and C. J. Hurton, "Automotive Electrical Systems Circa 2005," in *IEEE Spectrum*, vol. 33, 1996, pp. 22-27.

[8] N. Schofield, H. T. Yap, and C. M. Bingham, "A H_2 PEM fuel cell and high energy dense battery hybrid energy source for an urban electric vehicle," presented at IEEE International Conference on Electric Machines and Drives, 2005.

[9] J. M. Miller, A. Emadi, A. V. Rajarathnam, and M. Ehsani, "Current Status and Future Trends in More Electric Car Power Systems," presented at IEEE Vehicular Technology Conference, 1999.

[10] A. Emadi, M. Ehsani, and J. M. Miller, "Advanced Silicon Rich Automotive Electrical Power Systems," presented at Proceedings of the Digital Avionics Systems Conference, 1999.

[11] N. Schofield, H. T. Yap, and C. M. Bingham, "Hybrid energy sources for electric and fuel cell vehicle propulsion," presented at IEEE Vehicle Power and Propulsion Conference,VPPC, 2005.

[12] J. Shen, A. Masrur, V. K. Garg, and J. Monore, "Automotive Electric Power and Energy Management- A Systems Approach," in *Global Automotive Manufacturing, and Technology*, 2003, pp. 53-55.

[13] EU, "EU JOULE III Programme - Energy Research," 1999.

[14] A. Emadi, S. Williamson, and A. Khaligh, "Power electronics intensive solutions for advanced electric, hybrid electric, and fuel cell vehicular power systems," *IEEE Transactions on Power Electronics*, vol. 21, pp. 567 - 577, 2006.

[15] R. H. Staunton, C. W. Ayers, L. D. Marlino, J. N. Chiasson, and T. A. Burress, "U.S. Department of Energy,Year 2006 Report - Evaluation of 2004 Toyota Prius Hybrid Electric Drive System," Oak Ridge National Laboratory, Oak Ridge, Tennessee 37831 May 2006.

[16] J. G. Kassakian, "Automotive electrical systems-the power electronics market of the future," presented at IEEE Applied Power Electronics Conference and Exposition, 2000.

[17] A. Emadi, M. Ehsani, and J. M. Miller, *Vehicle Electric Power Systems- Land,Sea,Air and Space Vehicles*: Marcel Dekker, ISBN 0-8247-4751-8, 2004.

[18] L. Guzzella and A. Sciarretta, *Vehicle Propulsion Systems - Introduction to Modeling and Optimization*: Springer, ISBN 3-540-25195-2, 2005.

[19] N. Jalil, N. A. Kheir, and M. Salman, "A Rule-Based Energy Management Strategy for a Series Hybrid Vehicle," presented at Proceedings of the American Control Conference, 1997.

[20] P. Caratozzolo, M. Serra, and J. Riera, "Energy management strategies for hybrid electric vehicles," presented at IEEE Electric Machines and Drives Conference, IEMDC'03, 2003.

[21] G. Steinmauer and L. d. Re, "Optimal control of dual power sources," presented at Proceedings of the IEEE International Conference on Control Applications, CCA '01, 2001.

[22] R. Langari and J.-S. Won, "Integrated Drive Cycle Analysis for Fuzzy Logic Based Energy Management in Hybrid Vehicles," presented at IEEE International Conference on Fuzzy Systems, 2003.

[23] J. S. Won, "Intelligent Energy Mangament Agent for Parallel Hybrid Electric Vehicles," Texas A&M University, 2003, pp. 104.

[24] J. Hellgren and K. Jonasson, "Comparison of two algorithms for Energy management of hybrid Powertrains," Chalmers University of Technology, Sweden and Lund University, Sweden, 2004.

[25] A. Lohner and W. Evers, "Intelligent power management of a supercapacitor based hybrid power train for light-rail vehicles and city busses," presented at IEEE Power Electronics Specialists Conference,PESC 04, 2004.

[26] M. J. West, C. M. Bingham, and N. Schofield, "Predictive control for energy management in all/more electric vehicles with multiple energy storage units," presented at IEEE International Electric Machines and Drives Conference, IEMDC'03, 2003.

[27] M. Salman, M. F. Chang, and J. Y. Chen, "Predictive Energy Management Strategies for Hybrid Vehicles," presented at IEEE Vehicle Power and Propulsion, VPPC, 2005.

[28] J. S. Chen and M. Salman, "Learning Energy Management Strategy for Hybrid Electric Vehicles," presented at IEEE Vehicle Power and Propulsion, VPPC, 2005.

[29] G. Paganelli, G. Ercole, A. Brahma, Y. Guezennec, and Giorgio Rizzoni, "General supervisory control policy for the energy optimization of charge-sustaining hybrid electric vehicles," *ELSEVIER - JSAE Review*, vol. 22, pp. 511-518, 2001.

[30] J. Moreno, M. E. Ortuzar, and J. W. Dixon, "Energy-management system for a hybrid electric vehicle, using ultracapacitors and neural networks," *IEEE Transactions on Industrial Electronics*, vol. 53, pp. 614-623, 2006.

[31] J. T. Papadimitropoulos, T. G. Chondros, S. D. Panteliou, B. Carlsson, S. Kalogirou, and A. D. Dimarogonas, "Expert system for energy management of electric cars," *SAE Technical Paper Series 1999-01-1154*, 1999.

[32] P. Pisu and G. Rizzoni, "A supervisory control strategy for series hybrid electric vehicles with two energy storage systems," presented at IEEE Vehicle Power and Propulsion Conference,VPPC, 2005.

[33] M. Koot, J. T. B. A. Kessels, B. d. Jager, W. P. M. H. Heemels, P. P. J. v. d. Bosch, and M. Steinbuch, "Energy management strategies for vehicular electric power systems," *IEEE Transactions on Vehicular Technology*, vol. 54, pp. 771-782, 2005.

[34] C.-C. Lin, H. Peng, and J. W. Grizzle, "A Stochastis Control Strategy for Hybrid Electric Vehicles," presented at Proceedings of the 2004 American Control Conference, 2004.

[35] M. J. Kim, H. Peng, C. C. Lin, E. Stamos, and D. Tran, "Testing, Modeling, and Control of a Fuel Cell Hybrid Vehicle," presented at American Control Conference, 2005.

[36] E. Cacciatori, N. D. Vaughan, and J. Marco, "Energy Management Strategies for a parallel hybrid electric powertrain: Fuel ecomomy optimisation with driveability requirements," presented at IET Hybrid Vehicle Conference, Warwick, 2006.

[37] J. M. Miller, P. J. McCleer, M. Everett, and E. G. Strangas, "Ultracapacitor Plus Battery Energy Storage System Sizing Methodology for HEV Power Split Electronic CVT's," presented at Proceedings of the IEEE International Symposium on Industrial Electronics, ISIE 2005., 2005.

[38] M. Uzunoglu and M. S. Salam, "A novel wavelet based load sharing algorithm for fuel cell and ultra-capacitor based hybrid vehicular power system," presented at Proceedings of the 6th IASTED International Conference, European Power and Energy Systems, Rhodes,Greece, 2006.

[39] M. J. Gielniak and J. Z. Shen, "Power management strategy based on game theory for fuel cell hybrid electric vehicles," presented at IEEE Vehicular Technology Conference, VTC Fall, 2004.

[40] M. Endo, T. Takeda, Y. J. Kim, K. Koshiba, and K. Ishii, "High Power Electric Double Layer Capacitor (EDLC□s) from Operating Principle to Pore Size Control in Advanced Activated Carbons," *Carbon Science*, vol. 1, pp. 117-128, 2001.

[41] A. Rufer, P. Barrade, D. Hotellier, and P. Derron, "Supercapacitive energy storage: Power electronic solutions and applications," presented at Associazione Nazionale Azionamenti Elettrici, 13o Seminario Interattivo, Azionamenti elettrici: Evoluzione Tecnologica e Problematiche Emergenti, Bressanone, Italy. source: http://leiwww.epfl.ch, 2002.

[42] R. Kotz and M. Carlen, "Principles and applications of electrochemical capacitors," *Electrochimica Acta - Pergamon -Elsevier Science*, vol. 45, pp. 2483–2498, 2000.

[43] B. E. Conway, *Electrochemical Supercapacitors: Scientific Fundamentals and Technological Applications*: Springer, ISBN 0306457369, 1999.

[44] J. M. Miller and R. Smith, "Ultra-capacitor assisted electric drives for transportation," presented at IEEE International Electric Machines and Drives Conference, 2003.

[45] G. L. Bullard, H. B. Sierra-Alcazar, H. L. Lee, and J. L. Morris, "Operating Principles of the Ultracapacitor," *IEEE Transactions on Magnetics*, vol. 25, pp. 102-106, 1989.

[46] A. F. Burke, "Prospects for Ultracapacitors in Electric and Hybrid Vehicles," presented at 11th Annual Battery Conference on Applications and Advances, 1996.

[47] R. A. Huggins, "Supercapacitors and electrochemical pulse sources," *ELSEVIER journal on Solid Sate Ionics*, vol. 134, pp. 179-195, 2000.

[48] A. Namisnyk, "A survey of Electrochemical Supercapacitor Technology," University of Technology Sydney June 2003 2003.

[49] Kilofarad-International, "KiloFarad International," 2002.

[50] J. R. Anstrom, B. Zile, K. Smith, H. Hofmann, and A. Batra, "Simulation and field-testing of hybrid ultra-capacitor/battery energy storage systems for electric and hybrid-electric transit vehicles," presented at IEEE Applied Power Electronics Conference and Exposition, APEC 2005, 2005.

[51] A. C. Baisden and A. Emadi, "ADVISOR-based model of a battery and an ultra-capacitor energy source for hybrid electric vehicles," *IEEE Transactions on Vehicular Technology*, vol. 53, pp. 199-205, 2004.

[52] P. Barrade and A. Rufer, "The use of supercapacitors for energy storage traction systems," presented at IEEE Vehicle Power and Propulsion Conference, 2004.

[53] R. A. Dougal, S. Liu, and R. E.White, "Power and Life Extention of Battery - Ultracapacitor-Hybrids," *IEEE Transactions on Components and Packaging Technologies, [see also, IEEE Transactions on Components, Packaging and Manufacturing Technology, Part A: Packaging Technologies]"*, vol. 25, pp. 120-131, 2002.

[54] F. Gagliardi and M. Pagano, "Experimental Results of on-board Battery-Ultracapacitor System for Electric Vehicle Applications," presented at Proceedings of the 2002 IEEE International Symposium on Industrial Electronics, 2002.

[55] A. G. Simpson and G. R. Walker, "Lifecycle costs of ultracapacitors in electric vehicle applications," presented at IEEE Power Electronics Specialists Conference, 2002.

[56] A. Burke, "Ultracapacitors: Why, How, and Where is the Technology," *Report of the Institute of Transportation Studies, University of California, Davis. Paper:UCD-ITS-REP-00-17*, 2000.

[57] P. P. Barker, "Ultracapacitors for Use in Power Quality and Distributed Resource Applications," presented at IEEE Power Engineering Society, 2002.

[58] J. M. Miller and M. Everett, "Ultra-capacitor augmentation of the vehicle electrical system to reset its power budget," presented at IEEE Power Electronics in Transportation, 2004.

[59] E. Ozatay, B. Zile, J. Anstrom, and S. Brennan., "Power distribution control coordinating ultracapacitors and batteries for electric vehicles," presented at Proceedings of the American Control Conference, 2004.

[60] M. Okamura, "Energy Capacitor System - Part 1 & Part 2," presented at The 11th international seminar on double layer capacitors and similar energy storage devices, 2001.

[61] R. L. Spyker and R. M. Nelms, "Predicting capacitor run time for a battery-capacitor hybrid source," presented at Proceedings of the International Conference on Power Electronic Drives and Energy Systems for Industrial Growth, 1998.

[62] L. Gao, R. A. Dougal, and S. Liu, "Power enhancement of an actively controlled battery/ultracapacitor hybrid," *IEEE Transactions on Power Electronics*, vol. 20, pp. 236-243, 2005.

[63] L. Gao, R. A. Dougal, and S. Liu, "Active Power Sharing in Hybrid Battery/Capacitor Power Sources," presented at Applied Power Electronics Conference and Exposition, APEC '03, 2003.

[64] X. Yan and D. Patterson, "Improvement of Drive Range, Acceleration and Deceleration Performance In an Electric Vehicle Propulsion System," presented at 30th Annual IEEE Power Electronics Specialists Conference, 1999.

[65] P. H. Mellor, N. Schofield, and D.Howe, "Flywhell and supercapacitor peak power buffer technology," presented at IEE Electric, Hybrid and Fuel Cell Vehicles, 2000.

[66] M. Steiner and J. Scholten, "Energy Storage on board of DC fed railway vehicles," presented at IEEE Power Electronics Specialists Conference, 2004.

[67] J. W. Dixon, M. Ortuzar, and E. Wiechmann, "Regenerative Braking for an Electric Vehicle Using Ultracapacitors and a Buck-Boost Converter," presented at 17th Electric Vehicle Symposium, Montreal, Canada, 13-18 October 2000., 2000.

[68] J. W. Dixon and M. E. Ortuzar, "Ultracapacitors + DC-DC converters in regenerative braking system," *IEEE Aerospace and Electronics Systems*, vol. 17, pp. 16-21, 2002.

[69] T. Markel, A. Brooker, T. Hendricks, V. Johnson, K. Kelly, B. Kramer, M. O'Keefe, S. Sprik, and K. Wipke, "ADVISOR: a systems analysis tool for advanced vehicle modeling," *ELSEVIER Journal of Power Sources*, vol. 110, pp. 1255-1266, 2002.

[70] B. J. Arnet and L. P. Haines, "High Power DC-to-DC Converter For Supercapacitors," presented at IEEE International Electric Machines and Drives Conference, IEMDC 2001, 2001.

[71] S. Pay and Y. Baghzouz, "Effectiveness of Battery-Supercapacitor Combination in electric Vehicles," presented at IEEE Power Tech Conference Proceedings, 2003.

[72] R. M. Schupbach and J. C. Balda, "Comparing DC-DC Converters for Power Management in Hybrid Electric Vehicles," presented at IEEE International Electric Machines and Drives Conference, 2003.

[73] A. Drolia, P. Jose, and N. Mohan, "An Approach to Connect Ultracapacitors to Fuel Cell Powered Electric Vehicle and Emulating Fuel Cell Electrical Characteristics using Switched Mode Converter," presented at The 29th Annual Conference of the IEEE Industrial Electronics Society, 2003.

[74] A. Ohkawa, "Electric Power Control System for a Fuel Cell Vehicle Employing Electric Double-Layer Capacitor," *SAE Technical Paper Series 2004-01-1006*, 2004.

[75] H.-J. Chiu and L.-W. Lin, "A bidirectional DC-DC converter for fuel cell electric vehicle driving system," *IEEE Transactions on Power Electronics*, vol. 21, pp. 950-958, 2006.

[76] M. H. Todorovic, L. Palma, and P. Enjeti, "Design of a wide input range DC-DC converter with a robust power control scheme suitable for fuel cell power conversion," presented at IEEE Applied Power Electronics Conference and Exposition, APEC '04., 2004.

[77] A. H. Weinberg, "A Boost Regulator With A New Energy-Transfer Principle," presented at Proceedings of the Spacecraft Power Conversion Electronics Seminar, 1974.

[78] E. J. Cegnar, H. L. Hess, and B. K.Johnson, "A Purely Ultracapacitor Energy Storage System for Hybrid Electric Vehicles Utilizing a Microcontroller-Based DC-DC Boost Converter," presented at IEEE Applied Power Electronics Conference and Exposition, APEC '04, 2004.

[79] A. Farkas and R. Bonert, "Ultracapacitors as Sole Energy Storage Devices in Hybrid Electric Cars?" presented at Power Electronics in Transportation, 1994.

[80] R. M. Schupbach, J.Balda, M. Zolot, and B. Kramer, "Design Methodology of a Combined Battery-Ultracapacitor Energy Storage Unit for Vehicle Power Management," presented at IEEE 34th Annual Conference on Power Electronics Specialist, 2003.

[81] TOMLAB, "Optimisation Environment. http://tomopt.com/tomlab/. Accessed Nov.2006."

[82] D. Linzen, S. Buller, E. Karden, and R. W. D. Donckner, "Analysis and Evaluation of Charge Balancing Circuits on Performance, Reliability and Lifetime of Supercapacitor Systems," presented at Conference Record of the Industry Applications Conference, 2003. 38th IAS Annual Meeting, 2003.

[83] P. Barrade, S. Pittet, and A. Rufer, "Energy Storage system using a series connection of Supercapacitors, with an active device for equalising the voltages," Laboratoire d'Electronique Inductrielle, Swiss Federal Institute of Technology Lausanne 2000.

[84] P. Barrade, "Series Connection of Supercapacitors: Comparative Study of Solutions for the Active equalization of the Voltages," presented at International Conference on Modeling and Simulation of Electric Machines, Converters and Systems, Ecole de Technologie Supérieure (ETS), Montréal, Canada. source: http://leiwww.epfl.ch, 2002.

[85] J. M. Miller and M. Everett, "Vehicle electrical system power budget optimization using ultra-capacitor distribution modules," presented at IEEE Vehicle Power and Propulsion, 2004.

[86] E. Takahara, H. Sato, and J. Yamada., "Series and parallel connections change over system for electric double layer capacitors (EDLCs) to electric vehicle energy saving," presented at IEEE Power Conversion Conference, PCC, 2002.

[87] E. Takahara, T. Wakasa, and T. Yamada, "A study for electric double layer capacitor (EDLC) application to railway traction energy saving including change over between series and parallel modes," presented at IEEE Power Conversion Conference, PCC, 2002.

[88] L. C. Rosario, J. T. Economou, and P.C.K.Luk, "Short Interval Supercapacitor Switching Networks for Electric Vehicles: A Parametric Approach," presented at IEEE International Vehicular Power and Propulsion Conference -VPP04, Paris, France, 2004.

[89] L. C. Rosario, J. T. Economou, P.C.K.Luk, and T. S. El-Hasan, "Scenario Driven Intelligent Pulsed Power Management," presented at IEE- IMAREST 'Engine as a Weapon' Symposium, Bristol, United Kingdom, 2004.

[90] A. Brahma, Y. Guezennec, and G. Rizzoni, "Optimal Energy Management in Series Hybrid Electric Vehicles," presented at Proceedings of the American Control Conference, 2000.

[91] P. F. Ribeiro, B. K. Johnson, M. L. Crow, A. Arsoy, and Y. Liu, "Energy Storage Systems for Advanced Power Applications," *Proceedings of the IEEE*, vol. 89, pp. 1744-1756, 2001.

[92] S. M. Lukic, S. G. Wirasingha, F. Rodriguez, J. Cao, and A. Emadi, "Power Management of an Ultracapacitor/Battery Hybrid Energy Storage System in an HEV," presented at IEEE Vehicle Power and Propulsion Conference, 2006.

[93] S. M. Naylor, V. Pickert, and D. J. Atkinson, "Fuel Cell Drive Train Topologies-Computer Analysis of Potential Systems," presented at The 3rd IET International Conference on Power Electronics, Machines and Drives, 2005.

[94] T. R. Crompton, *Battery Reference Book*: Butterworth - Heinemann, ISBN 0750625679, 1995.

[95] J. Larminie and J. Lowry, *Electric Vehicle Technology*: Wiley, ISBN 0-470-85163-5, 2003.

[96] J. T. Economou, "Intelligent Energy Source SoC Modelling for a Hybrid Electric Vehicle," presented at IEEE ISIE, Dubrovnik,Croatia, 2005.

[97] J. V. Mierlio, P. V. d. Bossche, and G. Maggetto, "Models of energy sources for EV and HEV: fuel cells, batteries, ultracapacitors, flywheels and engine-generators," *Elsevier Jounal of Power Sources*, vol. 128, pp. 76-89, 2004.

[98] J. B. Olson and E. D. Sexton, "Operation of lead-acid batteries for HEV applications," presented at The Fifteenth Annual Battery Conference on Applications and Advances, 2000.

[99] E. Surewaard, M. Tiller, D. Lizen, and D. Linzen, "A comparison of Different Methods for Battery and Supercapacitor Modeling," presented at SAE Future Transportation Technology Conference- SAE Technical Paper Series 2003-01-2290, 2003.

[100] S. Buller, E. Karden, D. Kok, and R. W. D. Doncker, "Modeling the Dynamic Behaviour of Supercapacitors Using Impedance Spectroscopy," *IEEE Transactions on Industrial Applications*, vol. 38, pp. 1622- 1626, 2002.

[101] E. Surewaard, E. Karden, and M. Titler, "Advanced Electric Storage System Modeling in Modelica," presented at Proceedings of the 3rd International Modelica Conference, 2003.

[102] ANSOFT, "SIMPLORER - High-Performance Electromechanical System Simulation," http://www.ansoft.com/products/em/simplorer/.

[103] B. E. Conway and W. G. Pell, "Power limitations of supercapacitor operation associated with resistance and capacitance distribution in porous electrode devices," *ELSEVIER - Journal of Power Sources*, vol. 015, pp. 169 -181, 2002.

[104] R. L. Spyker and R. M. Nelms, "Double Layer Capacitor/DC-DC Converter System Applied to Constant Power Loads," presented at Proceedings of the 31st Intersociety Energy Conversion Engineering Conference, IECEC 96, 1996.

[105] R. L. Spyker and R. M. Nelms, "Evaluation of double layer capacitor technologies for high power and high energy storage applications," presented at International Conference on Industrial Electronics, Control and Instrumentation, 1997.

[106] L. Zubieta and R. Bonert, "Characterization of double-layer capacitors for power electronics applications," *IEEE Transactions on Industry Applications*, vol. 36, pp. 199 - 205, 2000.

[107] R. E. Vermillion, "Nonlinearity in high-C capacitors," *European Journal of Physics*, vol. 19, pp. 173-178, 1998.

[108] P. Barrade and A. Rufer, "Current Capability and Power Density of Supercapacitors: Considerations on Energy Efficiency," presented at EPE 2003, 10th European Conference on Power Electronics and Applications, 2003.

[109] N. Rizoug, P. Bartholomeus, B. Vulturescu, P. L. Moigne, and X. Pierre, "Voltage Sharing in Supercapacitor Modules: Experimental Study," presented at Proceedings of the 35th IEEE Power Electronics Specialists Conference, 2004.

[110] D. Doerffel and S. A. Sharkh, "A critical review of using the Peukert equation for determining the remaining capacity of lead-acid and lithium-ion batteries," *Elsevier Jounal of Power Sources*, vol. 155, pp. pp 395-400, 2006.

[111] D. Napoli, F. Crescimbini, A. Lidozzi, L. Solero, M. Pasquali, A. Puccetti, and E. Rossi, "Design and testing of a Fuel-Cell powered propulsion system supported by a Hybrid UC-Battery storage," *SAE Technical Paper Series 2004-01-1303*, 2004.

[112] T. Markel, M. Zolot, K. B. Wipke, and A. Pesaran, "Energy Storage System Requirements for Hybrid Fuel Cell Vehicles," in *Advanced Automotive Battery Conference*, 2003.

[113] M. L. Puterman, *Markov Decision Processes - Discrete Stochastic Dynamic Programming*: Wiley-Interscience, ISBN 0-471-61977-9, 1994.

[114] H. B. Verbruggen and R. Babuska, *Fuzzy Logic Control Advances in Application*: World Scientific, ISBN 981-02-3825-8, 1999.

[115] T. Christen and M. W. Carlen, "Theory of Ragone plots," *Elsevier Jounal of Power Sources*, vol. 91, pp. pp: 210-216, 2000.

[116] H. A. Wheeler, "Simple Inductance Formulas for Radio Coils," *Proceedings of the I.R.E*, pp. pp. 1398-1400, 1928.

[117] M. E. Ortúzar, "Design, implementation and evaluation of an auxiliary energy system for electric vehicles, based on ultracapacitors and buck-boost converter," in *Departamento de Ingeniería Eléctrica*. Santiago, Chile: Pontificia Universidad Catolica De Chile Escuela De Ingenieria, 2005, pp. 115.

[118] R. M. Schupbach and J. C. Balda, "35 KW ultracapacitor unit for power management of hybrid electric vehicles: bidirectional DC-DC converter design," presented at IEEE Power Electronics Specialists Conference, 2004.

[119] L. Solero, A. Lidozzi, and J. A. Pomilio, "Design of multiple-input power converter for hybrid vehicles," *IEEE Transactions on Power Electronics*, vol. 20, pp. 1007 - 1016, 2005.

[120] N. Khan, N. Mariun, M. Zaki, and L. Dinesh, "Transient analysis of pulsed charging in supercapacitors," presented at Proceedings of IEEE- TENCON 2000.

[121] L. C. Rosario, J. T. Economou, and P.C.K.Luk, "Multi-Agent Load Power Segregation for Electric Vehicles," presented at IEEE International Vehicular Power and Propulsion Conference - VPPC 2005, Illinois, USA, 2005.

[122] P.C.K.Luk and L.C.Rosario, "Towards a Negotiation-based Multi-Agent Power Management System for Electric Vehicles (Invited Paper)," presented at IEEE International Conference on Machine Learning and Cybernetics, Guangzhou, China, 2005.

[123] M. Coleman, C. B. Zhu, C. K. Lee, and W. G. Hurley, "A combined SOC estimation method under varied ambient temperature for a lead-acid battery," presented at IEEE Applied Power Electronics Conference and Exposition, 2005. APEC 2005, 2005.

[124] B. P. Taylor, A. J. Brown, D. A. Stone, and N. Schofield, "A high power dc-dc converter, employing synchronous rectification of parallel MOSFETs, for use as an electric vehicle battery-to supercapacitor interface," presented at 10th European Conference on Power Electronics and Applications (EPE2003), 2003.

APPENDICES

Appendix A: Schematics

Appendix B: Selected Type Tests

Appendix C: Images

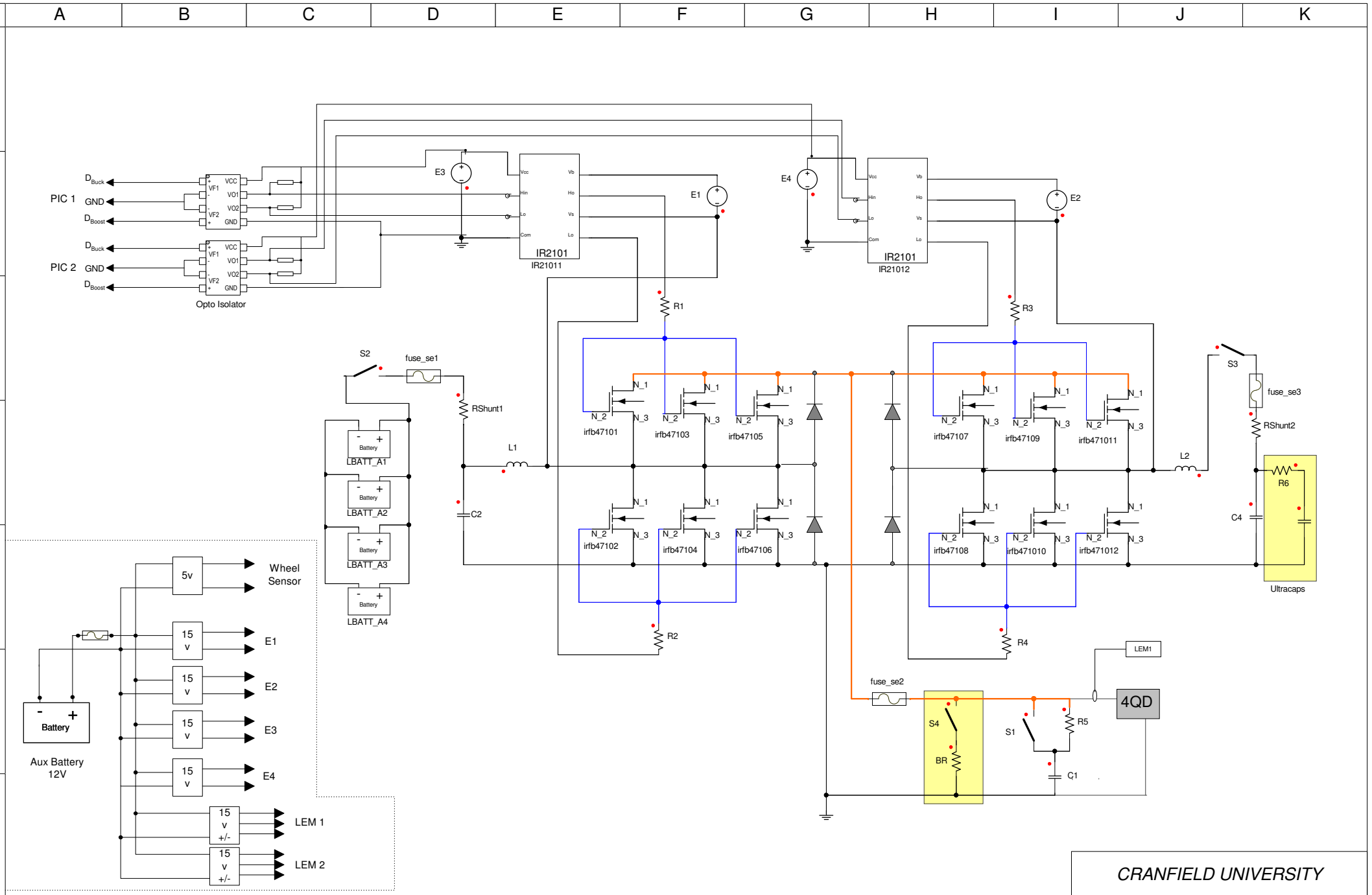

	A	B	C	D	E	F	G	H	I	J	K
1											
2											
3											
4											
5											
6											
7											

ID	PhD Project	Dual Input - Bidirectional Converter - 12kW	Rev. Note: Updated For Go-Kart Design	CRANFIELD UNIVERSITY
	LCR		File C:\PhDProject\Dwg\ELE-001_Rev1	Drawn LCR 10-12-2005 Sheet 1/1
			REV -1	CHK APV Drawing No: ELE-001

TERMINAL BLOCK

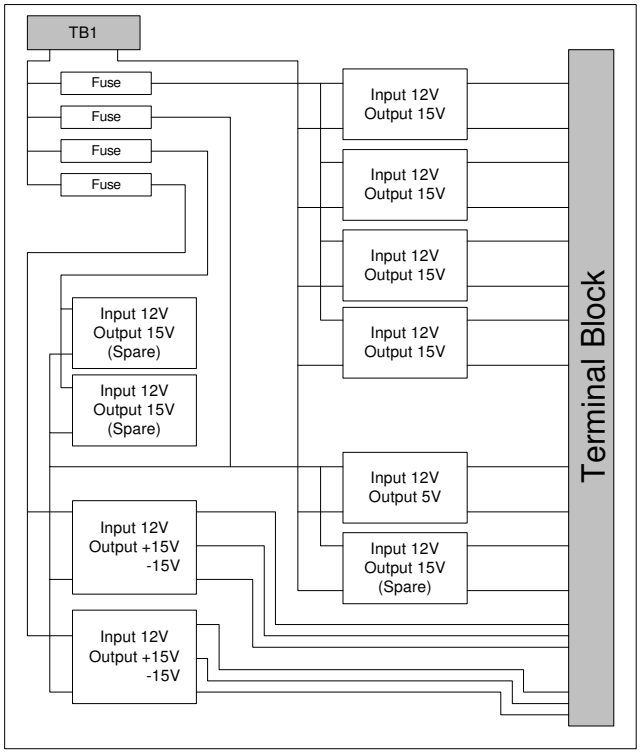

Power Supply Card

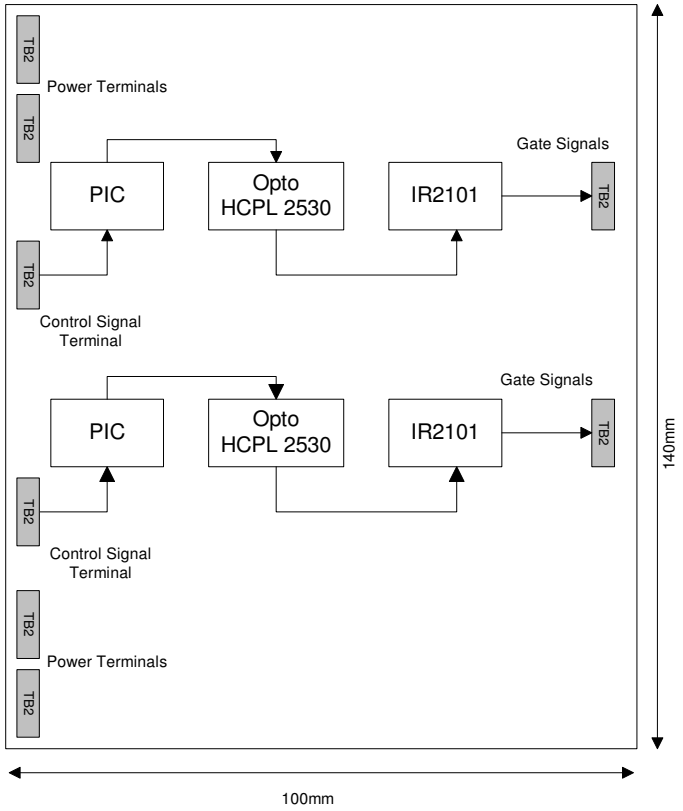

Gate Drive Card

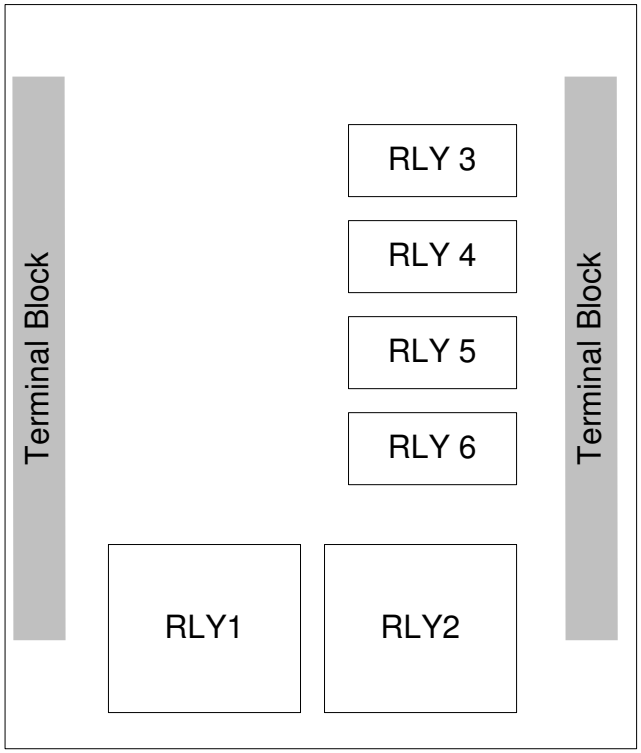

Interposing Relay Card

ID	PhD Project	Module Layout	Rev. Note: Design Draft		CRANFIELD UNIVERSITY
	LCR		File: C:\PhDProject\Dwg\ELE-002_Rev0	REV -0	Drawn: LCR 7-01-2006; CHK; APV; Drawing No: ELE-002; Sheet 1/1

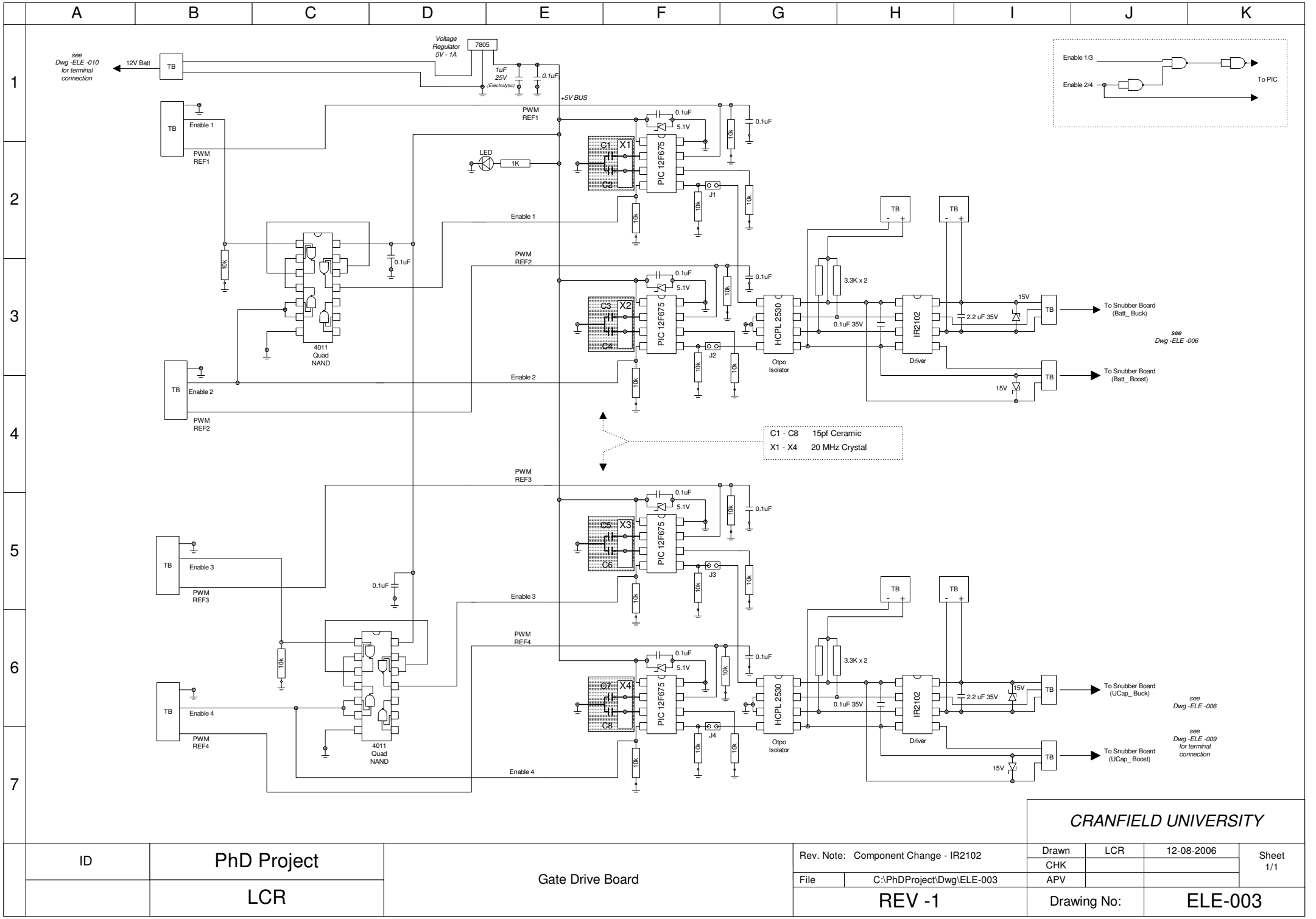

CRANFIELD UNIVERSITY

ID	PhD Project	Gate Drive Board	Rev. Note: Component Change - IR2102	Drawn	LCR	12-08-2006
	LCR		File C:\PhDProject\Dwg\ELE-003	CHK		Sheet 1/1
			REV -1	APV		
				Drawing No:		ELE-003

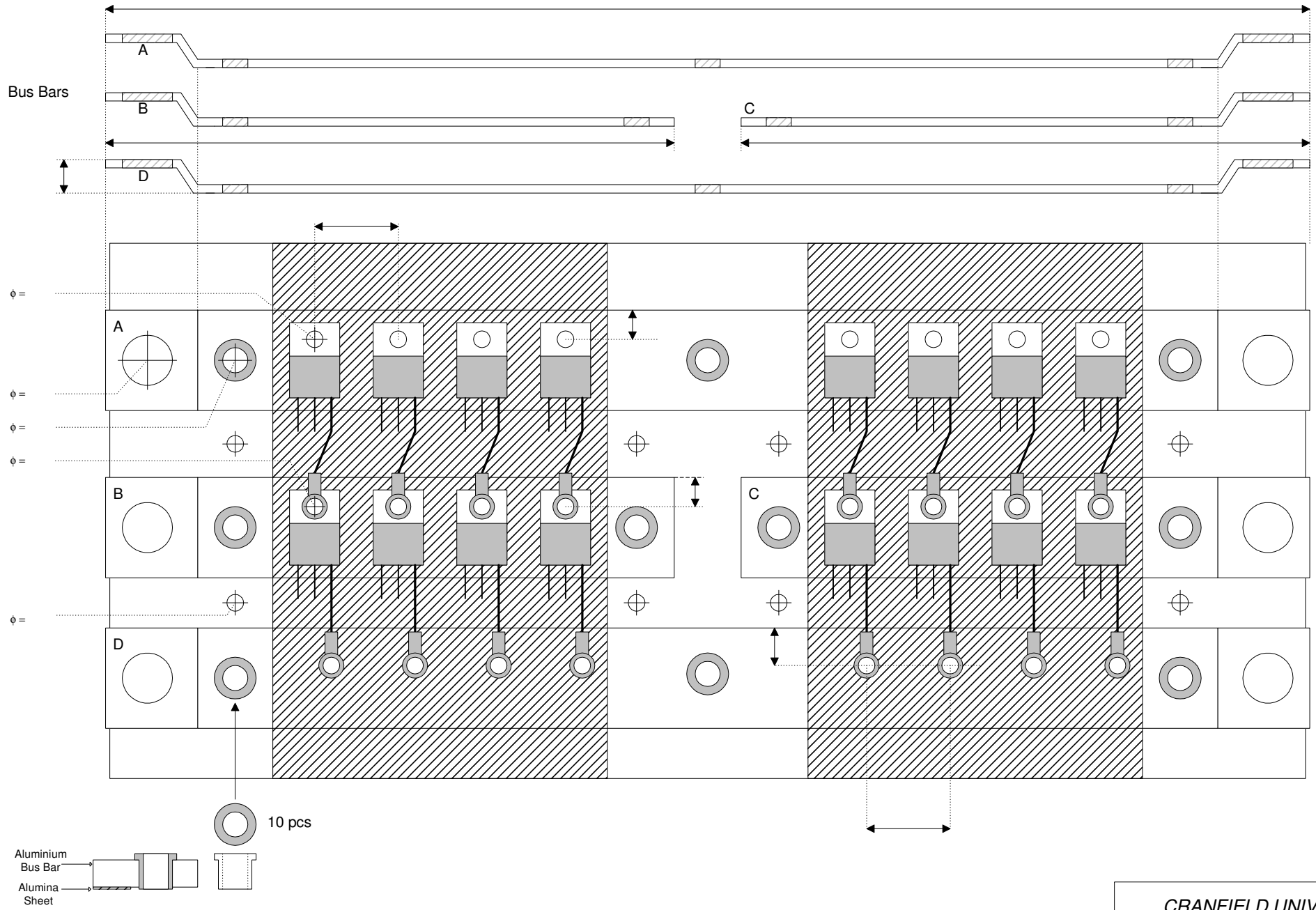

CRANFIELD UNIVERSITY

ID	PhD Project	Main Board Component Layout	Rev. Note: Major change to GA	Drawn: LCR	28-04-2006
	LCR		File: C:\PhDProject\Dwg\ELE-004	CHK	
			REV -1	APV	Sheet 1/1
				Drawing No:	ELE-004

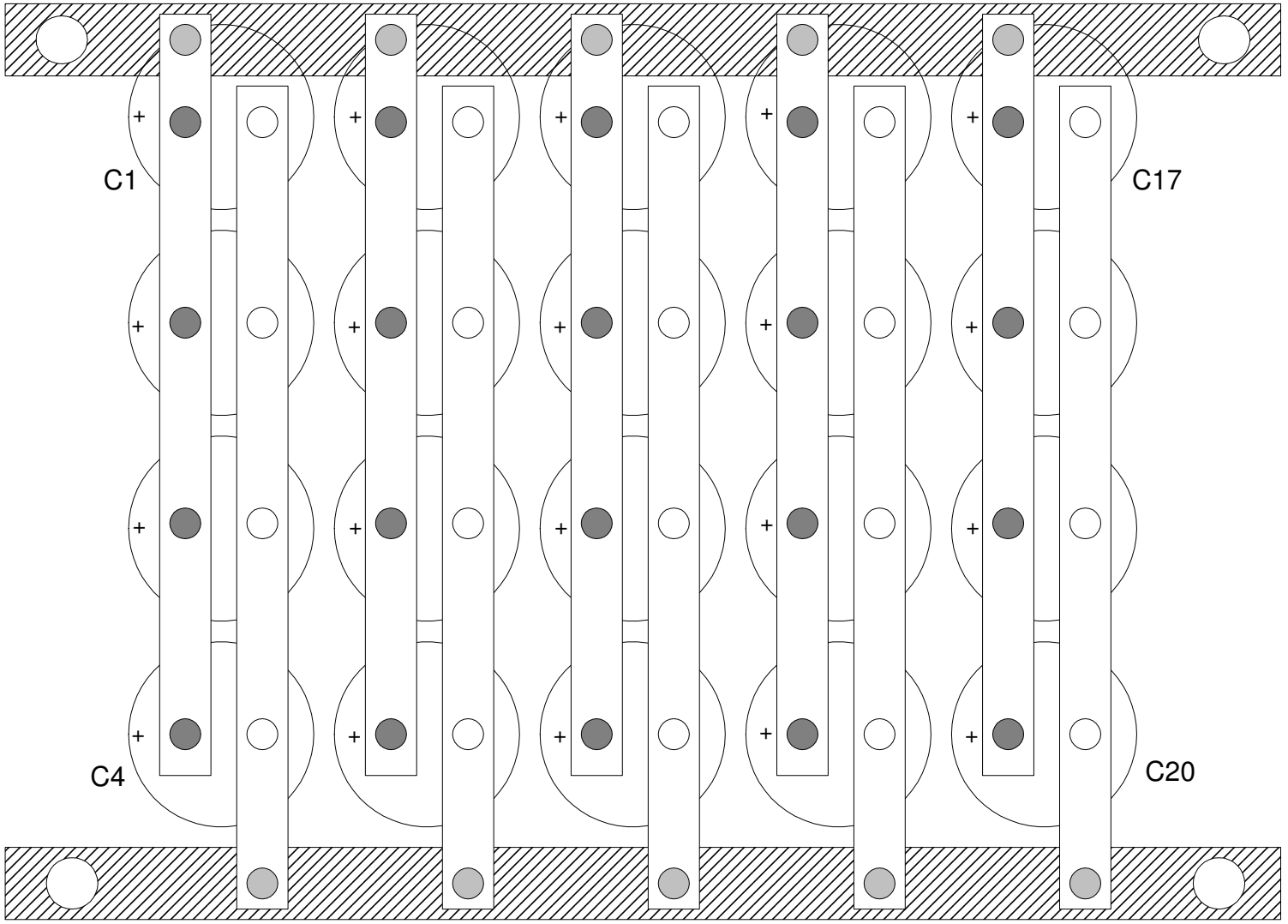

C1- C20 = 2200uF (100V)

CRANFIELD UNIVERSITY

ID	PhD Project	DC Bus Capacitors	Rev. Note: DC Bus capacitors G.A	Drawn	LCR	28-04-2006
				CHK		
	LCR		File C:\PhDProject\Dwg\ELE-005_Rev0	APV		Sheet 1/1
			REV -0	Drawing No:		ELE-005

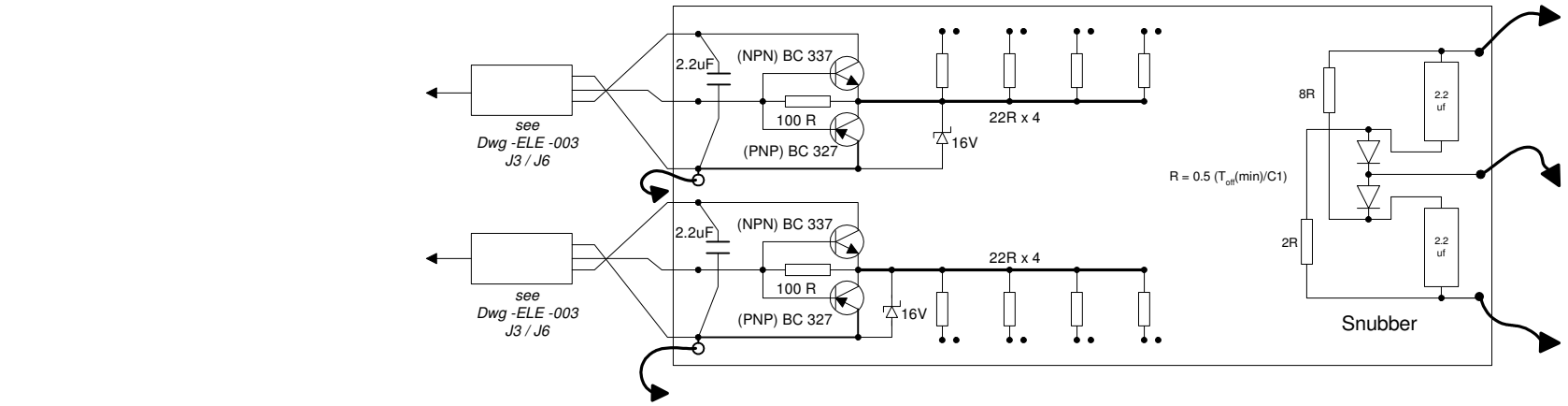

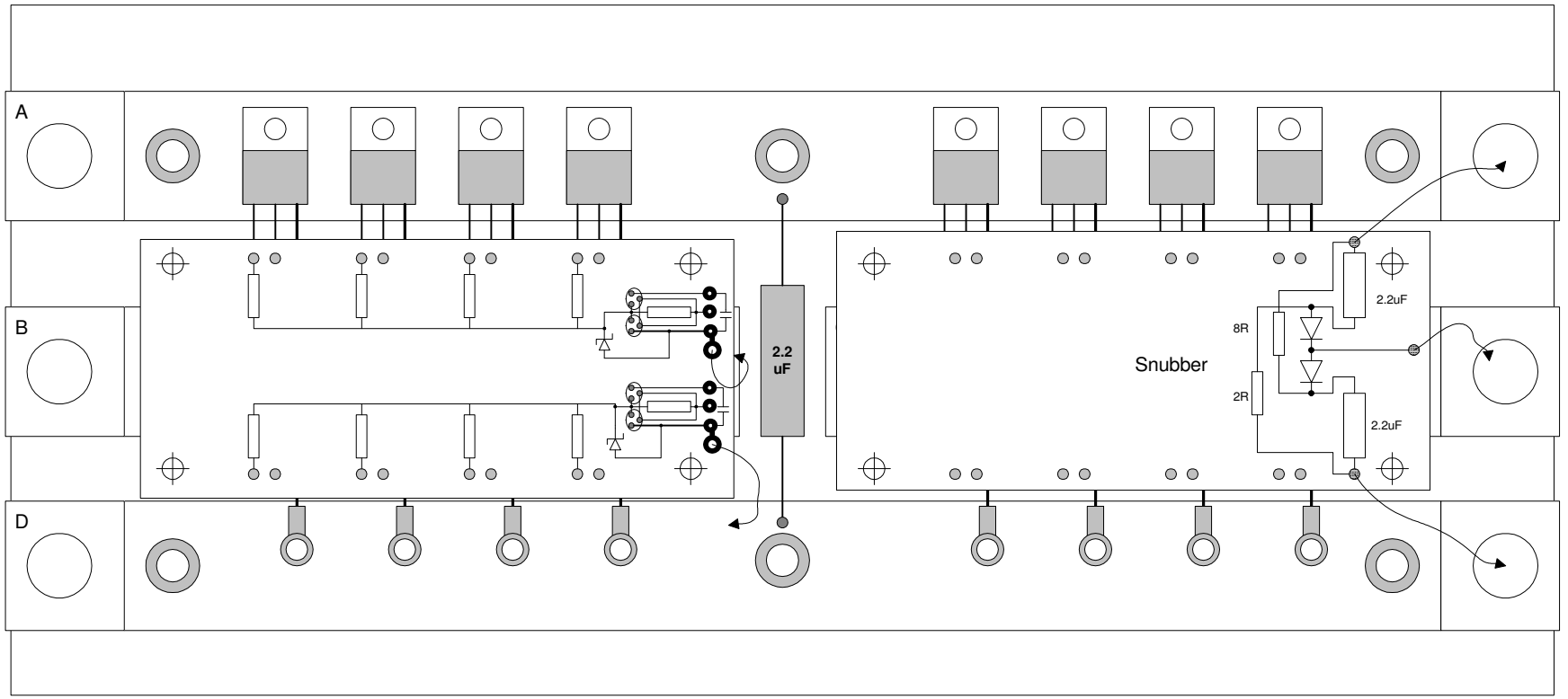

ID	PhD Project	Snubber and Amplifier Boards	Rev. Note: Added 2.2uf Tantalunms(see E2)	Drawn LCR 12-08-2006	Sheet 1/1
	LCR		File C:\PhDProject\Dwg\ELE-006_Rev1	CHK / APV	
			REV -1	Drawing No:	ELE-006

CRANFIELD UNIVERSITY

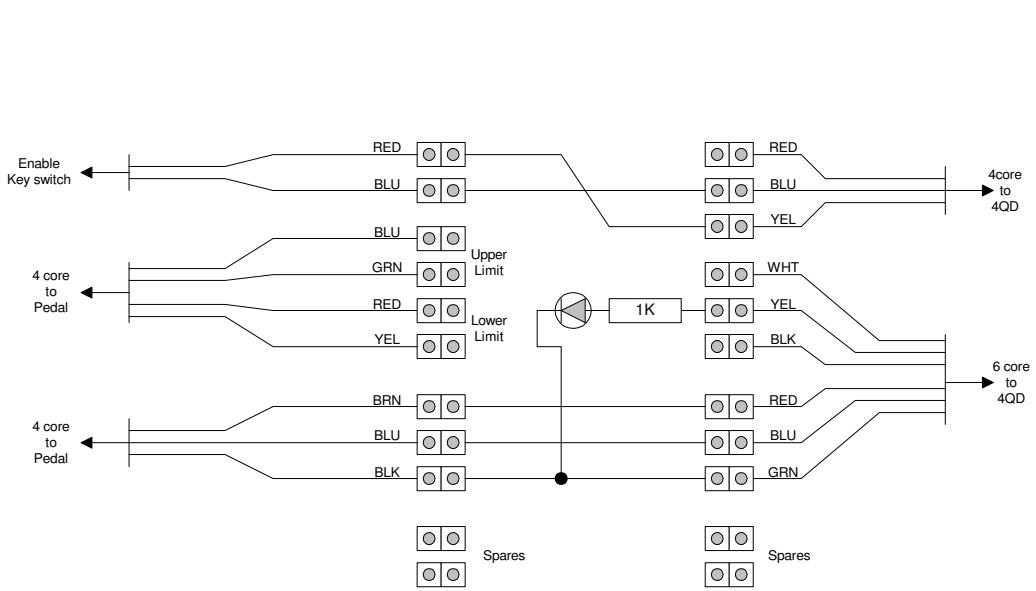

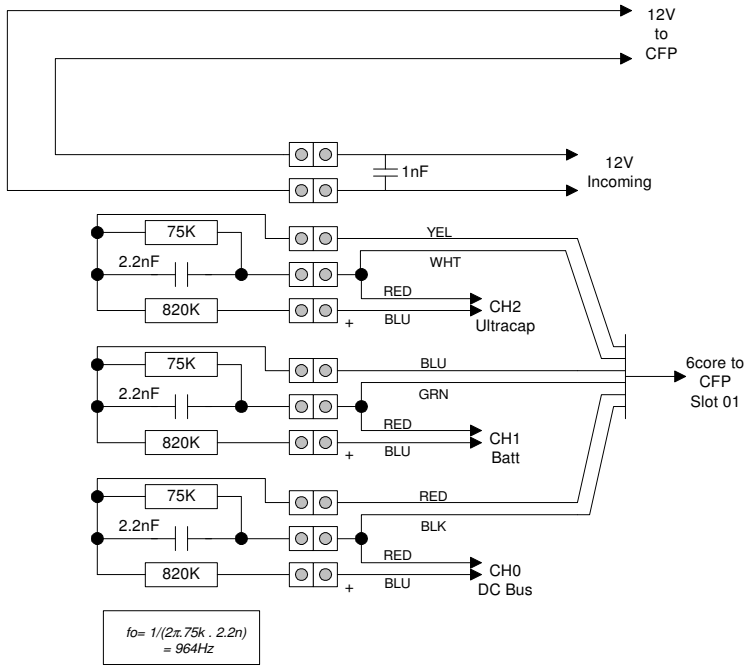

				CRANFIELD UNIVERSITY	
ID	PhD Project	Marshalling board connection diagram	Rev. Note: NIL	Drawn LCR 02-05-2006	Sheet 1/1
	LCR		File C:\PhDProject\Dwg\ELE-007	CHK / APV	
			REV -0	Drawing No:	ELE-007

Schematic Layout

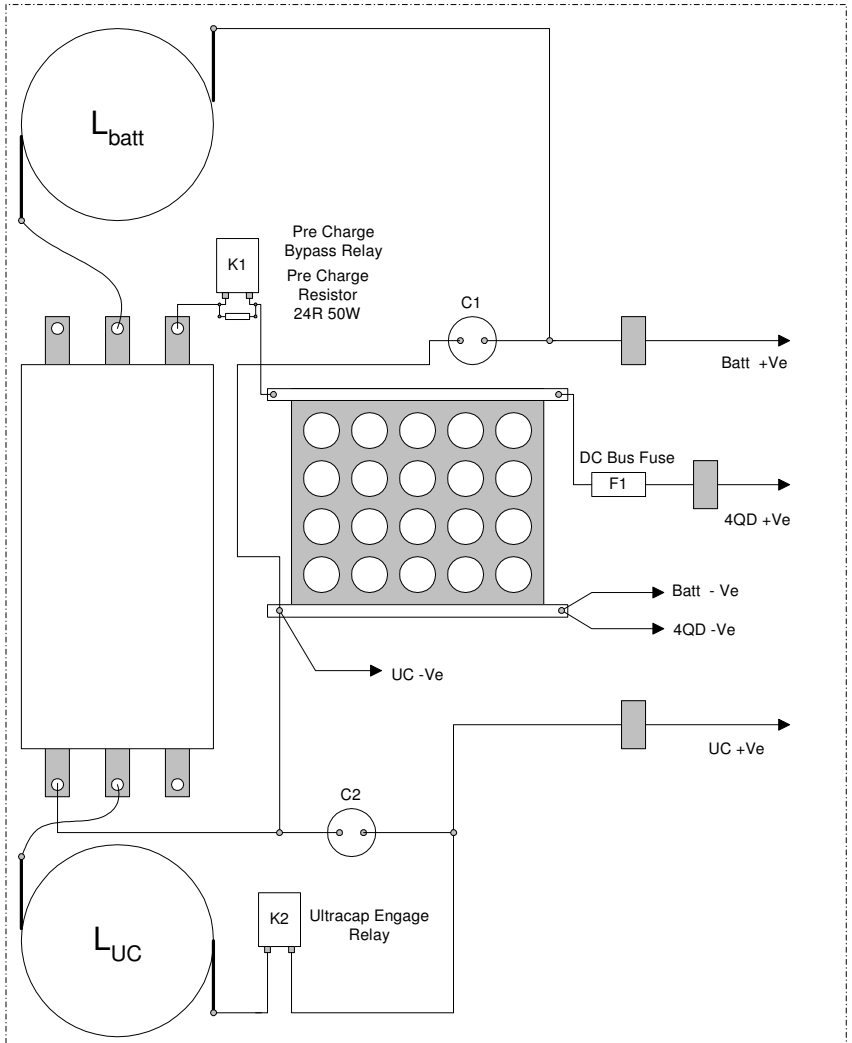

As Built Layout

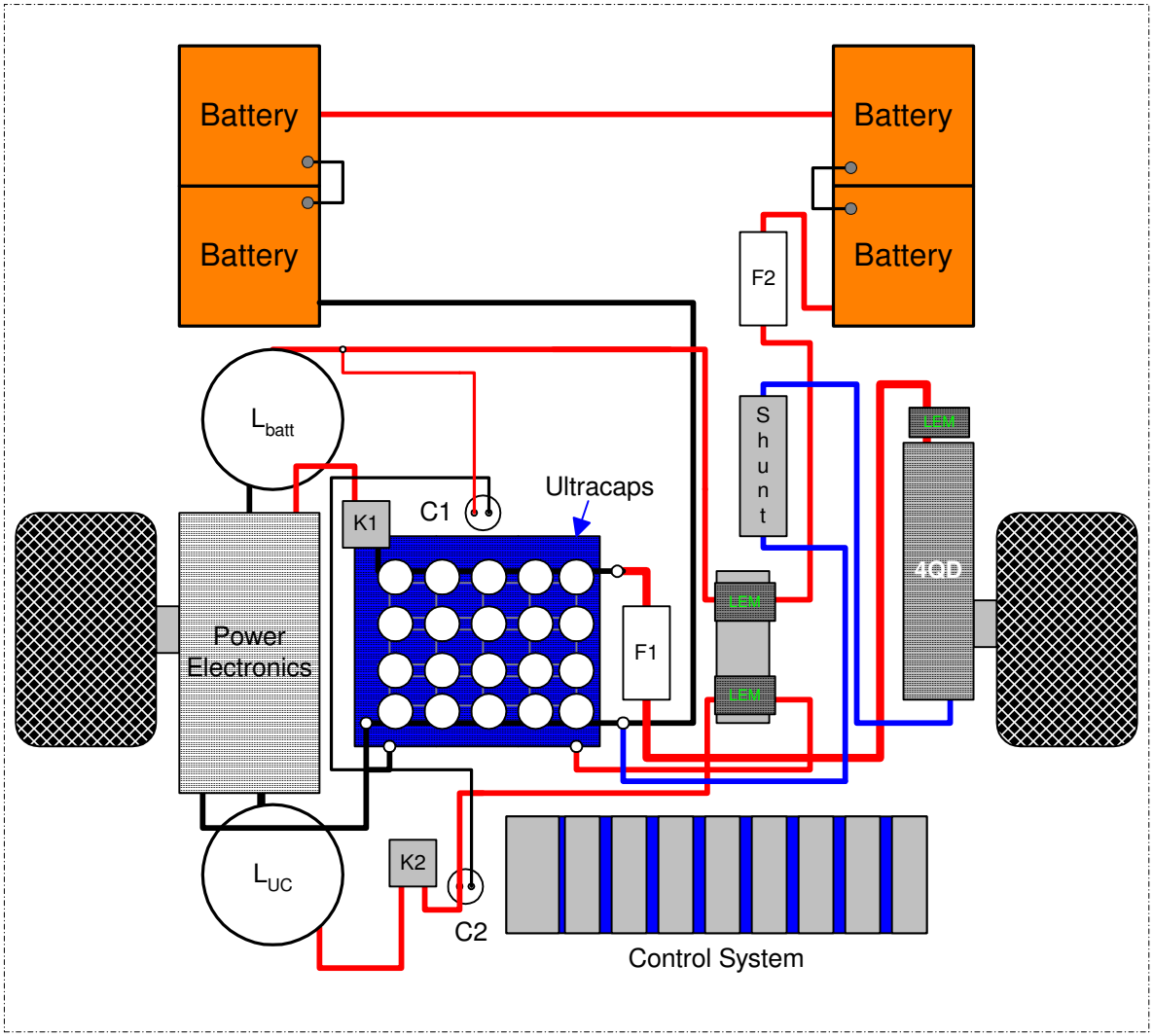

ID	PhD Project	General Layout	Rev. Note: NIL		CRANFIELD UNIVERSITY
	LCR		File C:\PhDProject\Dwg\ELE-008_Rev0	REV -0	Drawn LCR 02-05-2006 / CHK / APV / Drawing No: ELE-008 / Sheet 1/1

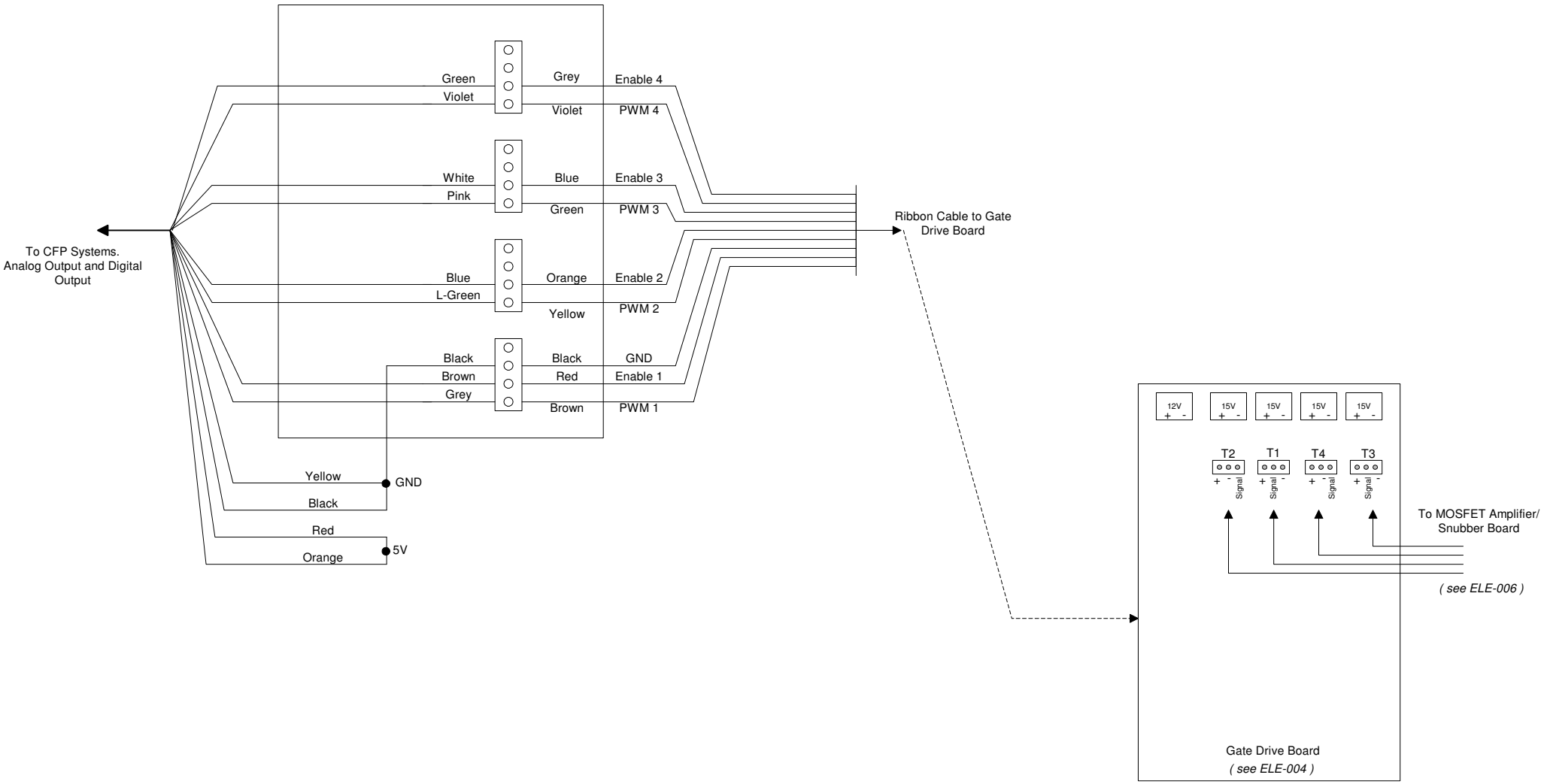

ID	PhD Project	Terminal Board and Interconnections	Rev. Note: NIL		CRANFIELD UNIVERSITY		
	LCR		File	C:\PhDProject\Dwg\ELE-009_Rev0	Drawn	LCR	02-05-2006
					CHK		
					APV		
			REV -0		Drawing No:	ELE-009	Sheet 1/1

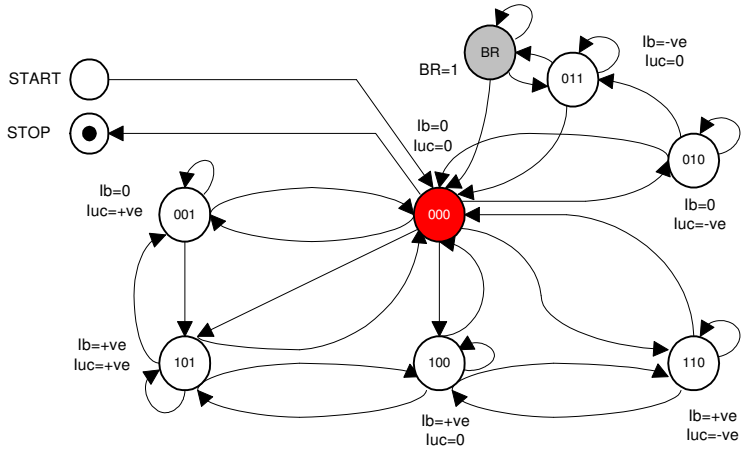

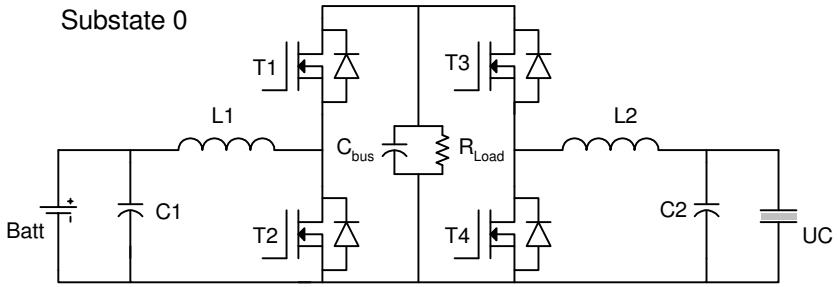

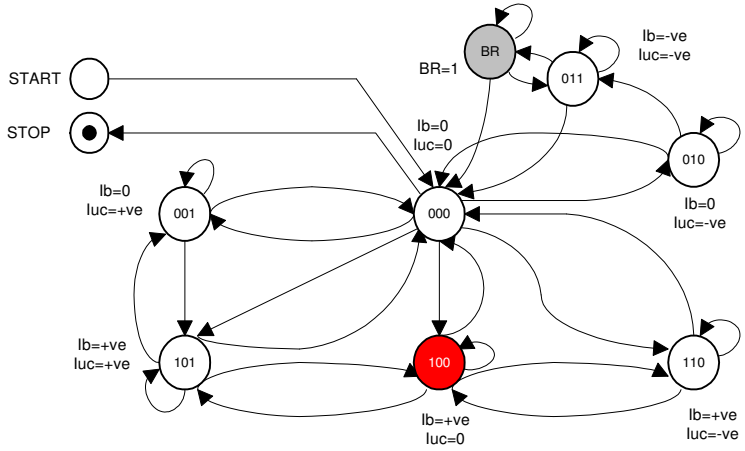

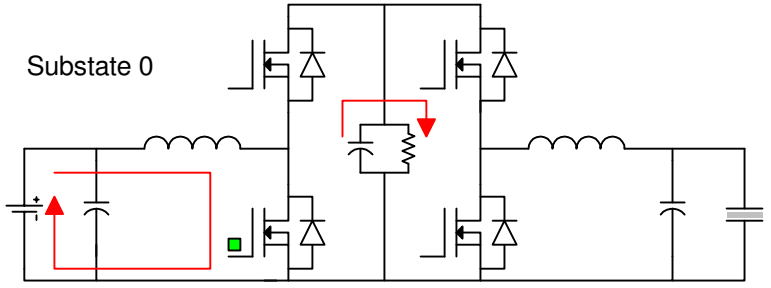

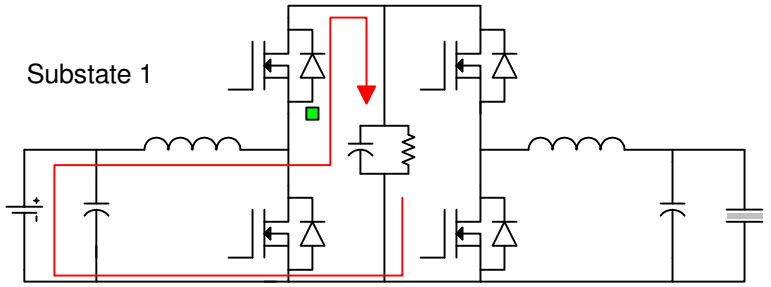

ID	PhD Project	STATE 000 & STATE 100	Rev. Note: NIL		CRANFIELD UNIVERSITY
	LCR		File C:\PhDProject\Dwg\ELE-010_Rev0	REV -0	Drawn LCR 02-05-2006 / CHK / APV / Sheet 1/1 / Drawing No: ELE-010

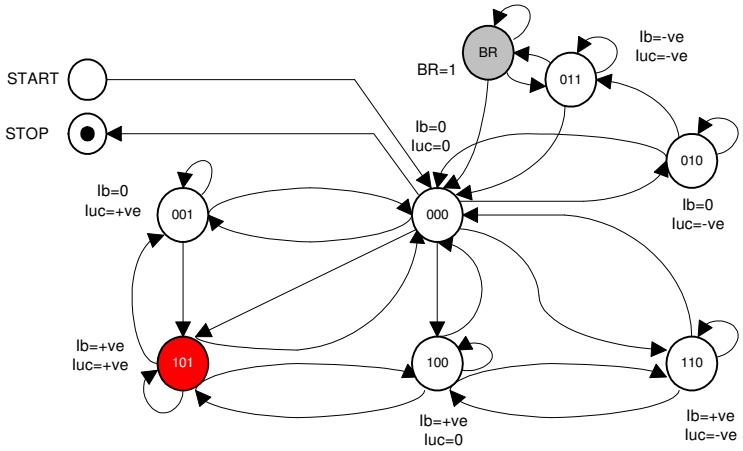

Substate 0

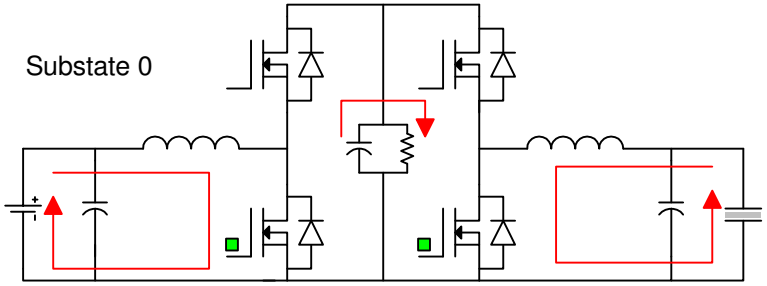

Substate 2

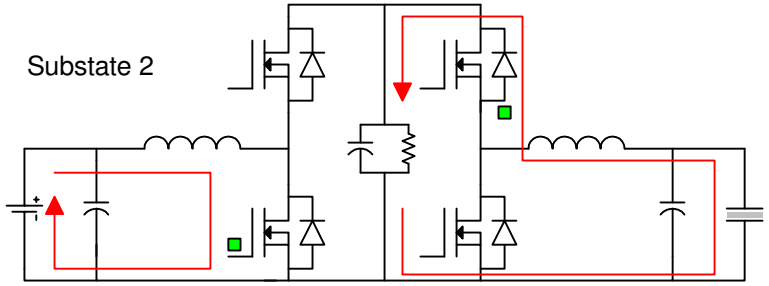

Substate 1

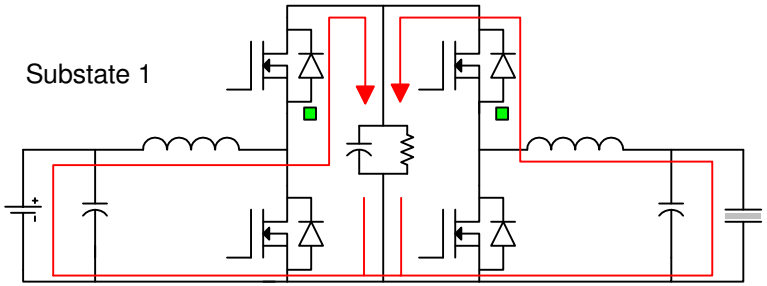

Substate 3

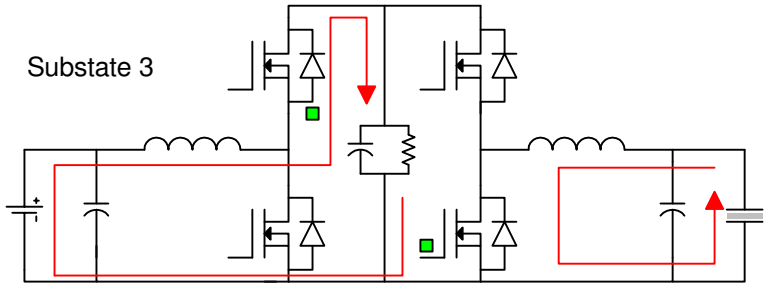

ID	PhD Project	STATE 101	Rev. Note: NIL			
	LCR		File	C:\PhDProject\Dwg\ELE-011_Rev0	REV -0	

CRANFIELD UNIVERSITY

Drawn	LCR	02-05-2006	Sheet 1/1
CHK			
APV			
Drawing No:		ELE-011	

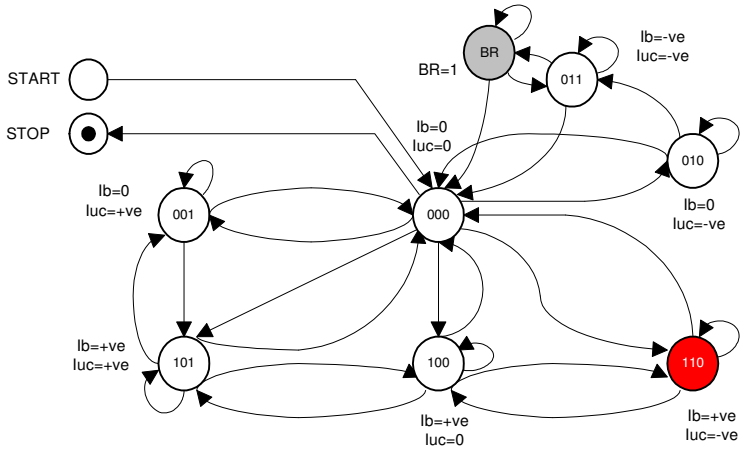

Substate 0

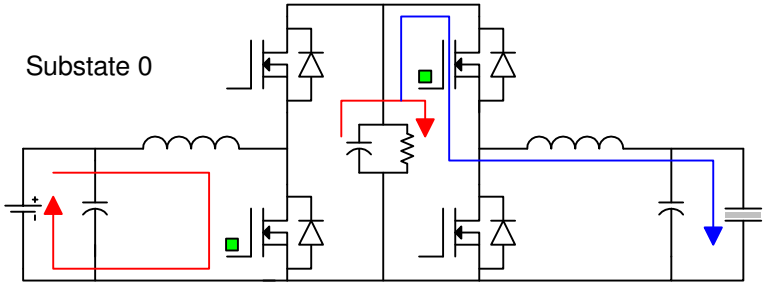

Substate 2

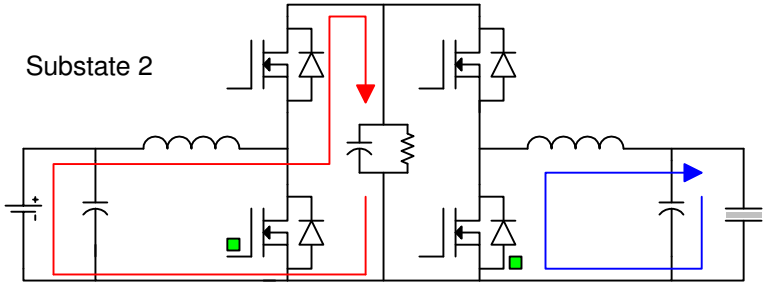

Substate 1

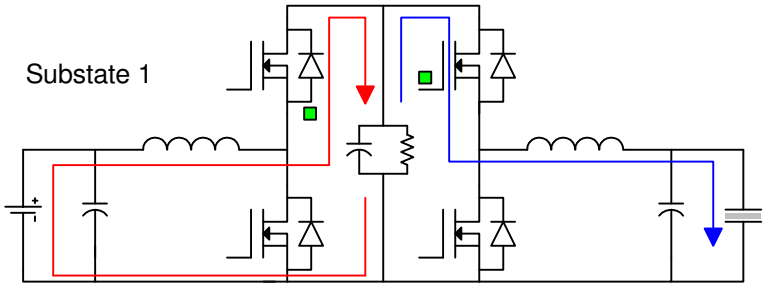

Substate 3

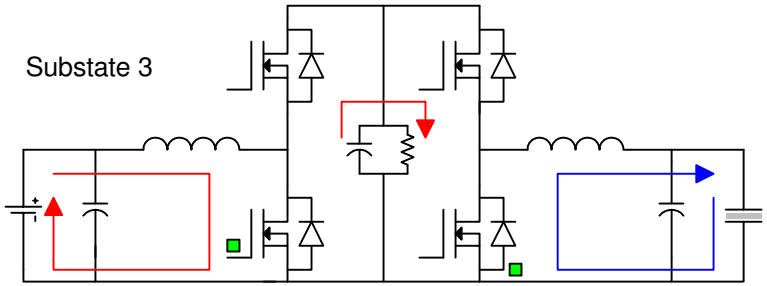

ID	PhD Project	STATE 110	Rev. Note: NIL		*CRANFIELD UNIVERSITY*
	LCR		File C:\PhDProject\Dwg\ELE-012_Rev0	REV -0	Drawn LCR 02-05-2006 / CHK / APV / Drawing No: ELE-012 / Sheet 1/1

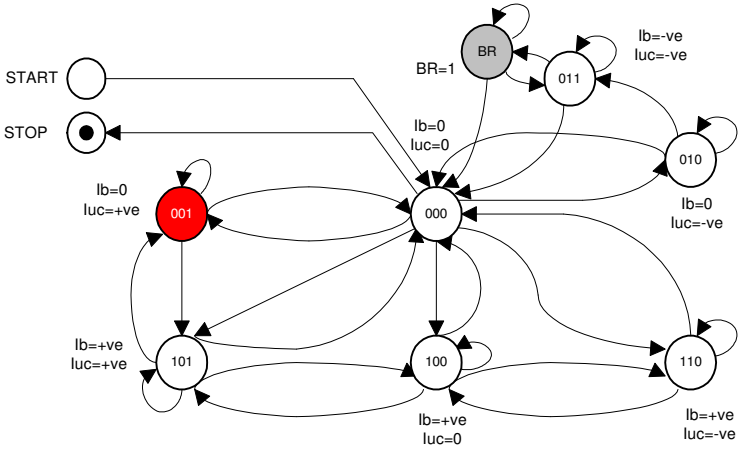

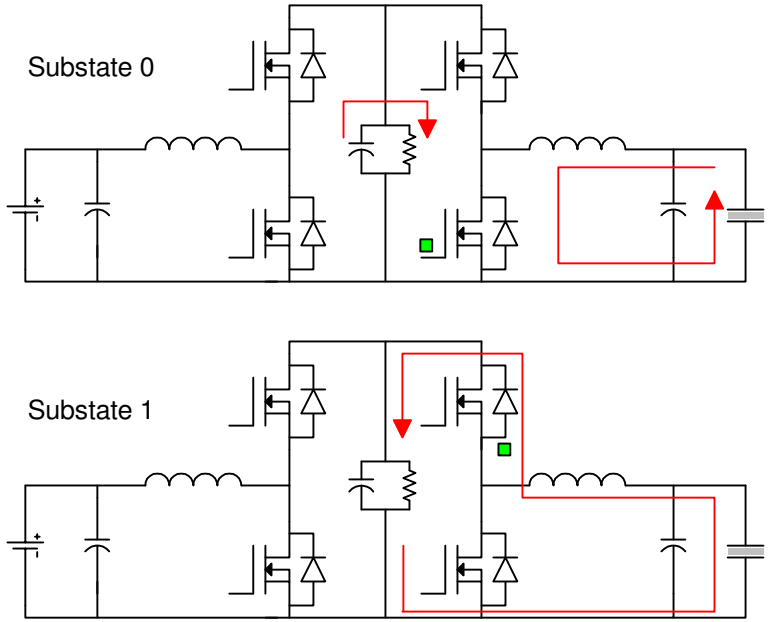

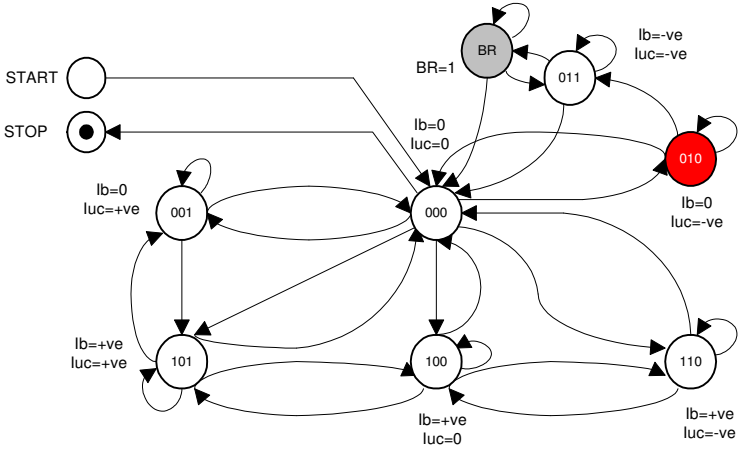

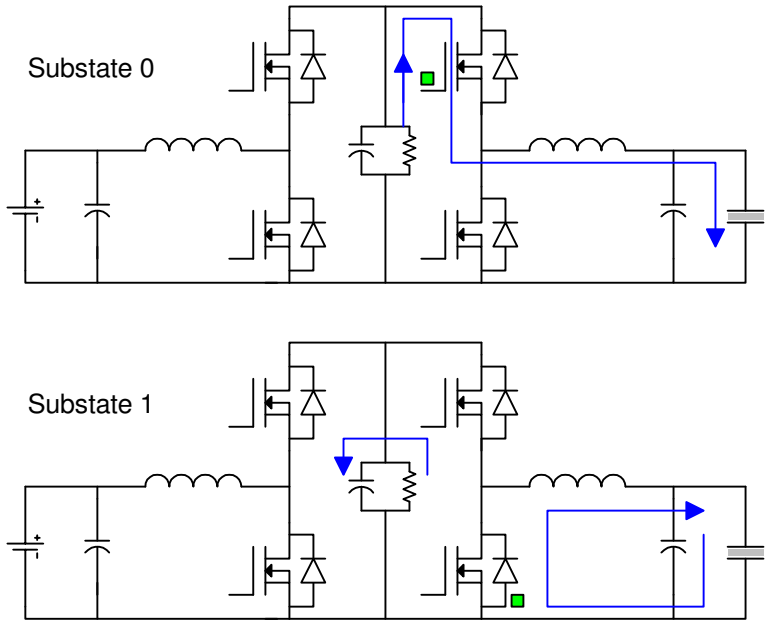

ID	PhD Project	STATE 001 & STATE 010	Rev. Note: NIL		CRANFIELD UNIVERSITY
	LCR		File C:\PhDProject\Dwg\ELE-013_Rev0	REV -0	Drawn LCR 02-05-2006 / CHK / APV / Sheet 1/1 / Drawing No: ELE-013

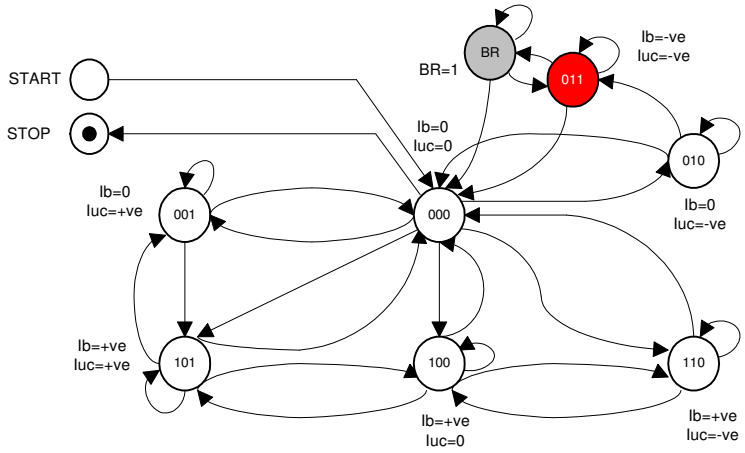

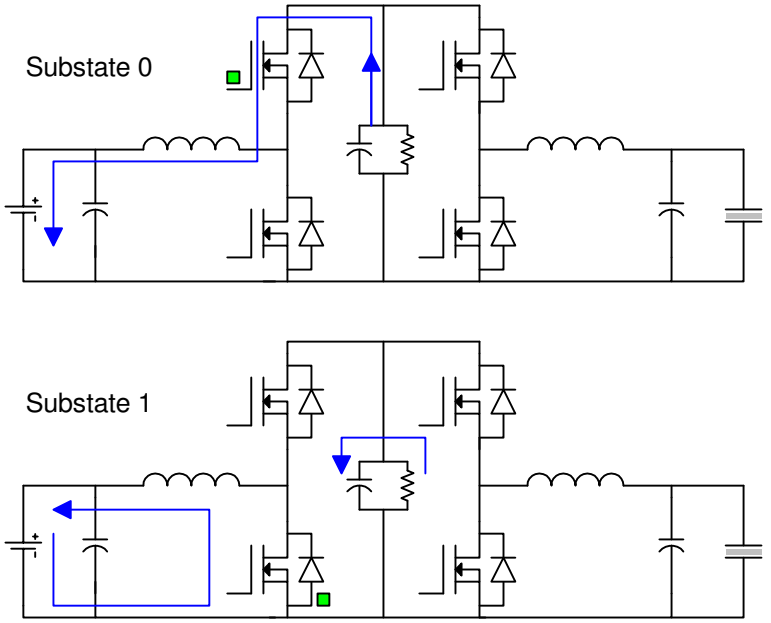

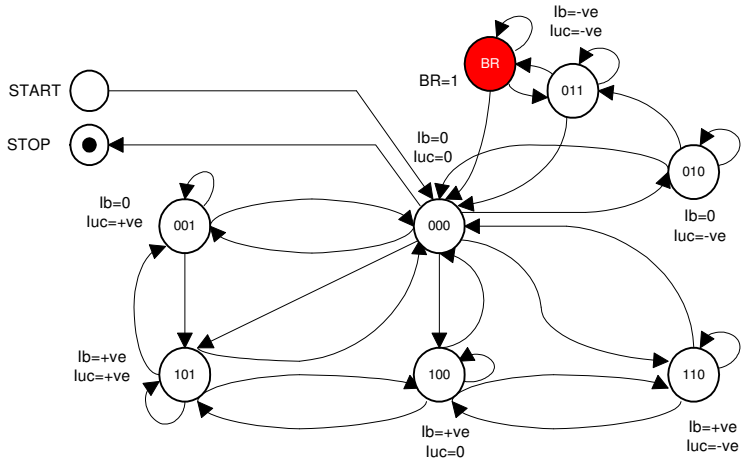

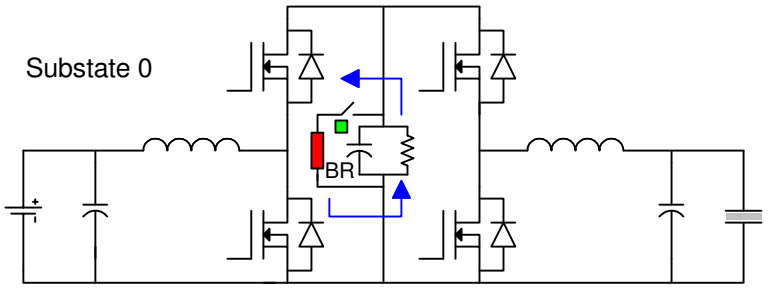

ID	PhD Project	STATE 001 & STATE BR	Rev. Note: NIL		CRANFIELD UNIVERSITY
	LCR		File C:\PhDProject\Dwg\ELE-014_Rev0	REV -0	Drawn LCR 02-05-2006 / CHK / APV / Sheet 1/1 / Drawing No: ELE-014

Type Test- 01

Type tests of the PWM generators used to provide the varying duty cycle PMW signals for switches T1 to T4. Minimum duty cycle at 20Khz is 0.1 and the maximum duty cycle is 0.89.

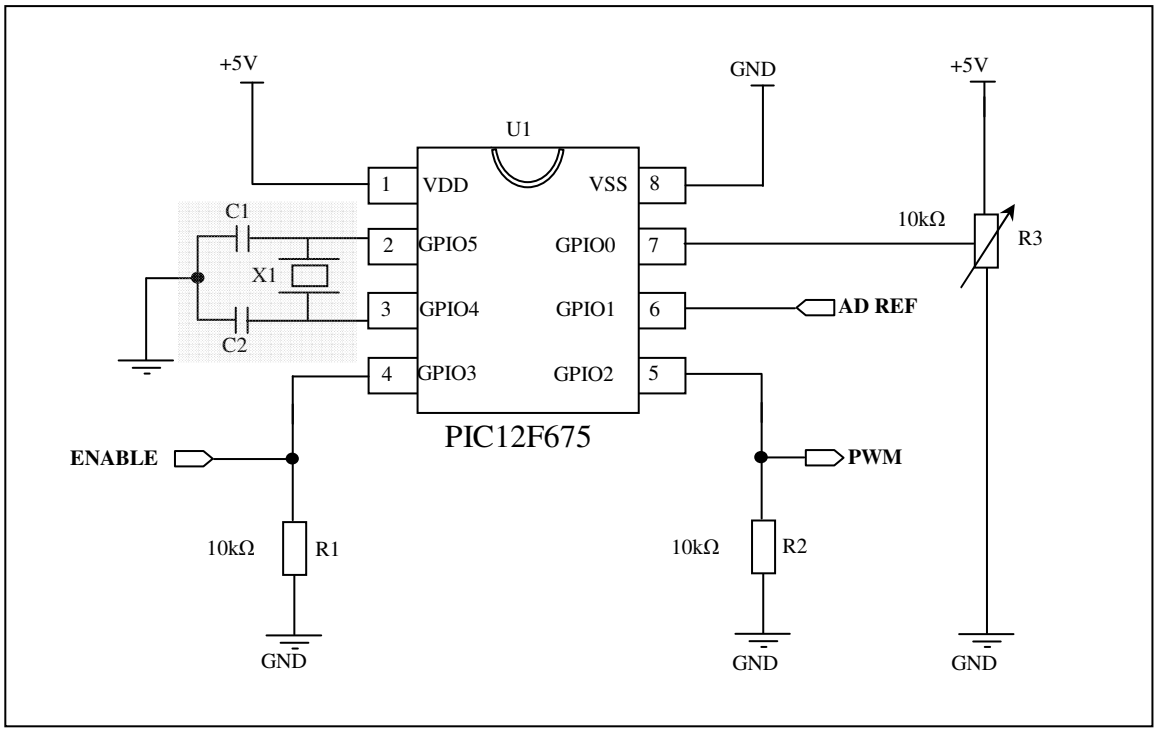

Schematic

PWM output vs Enable signal

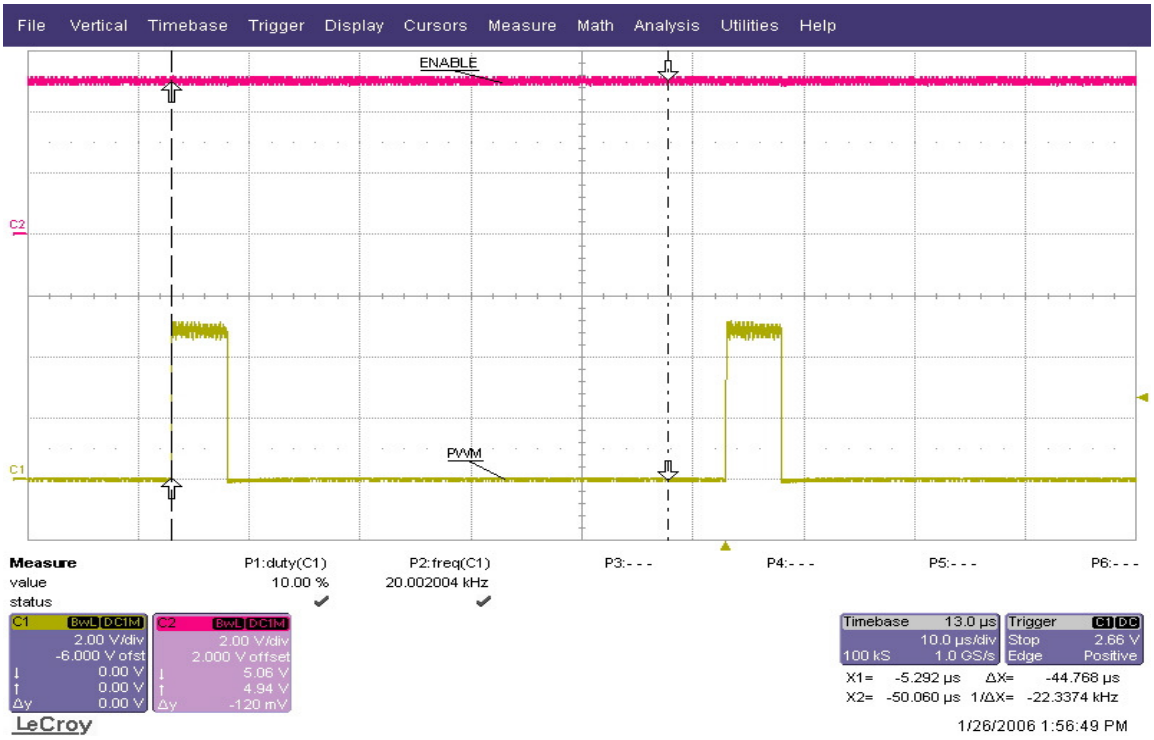

Minimum Duty Cycle

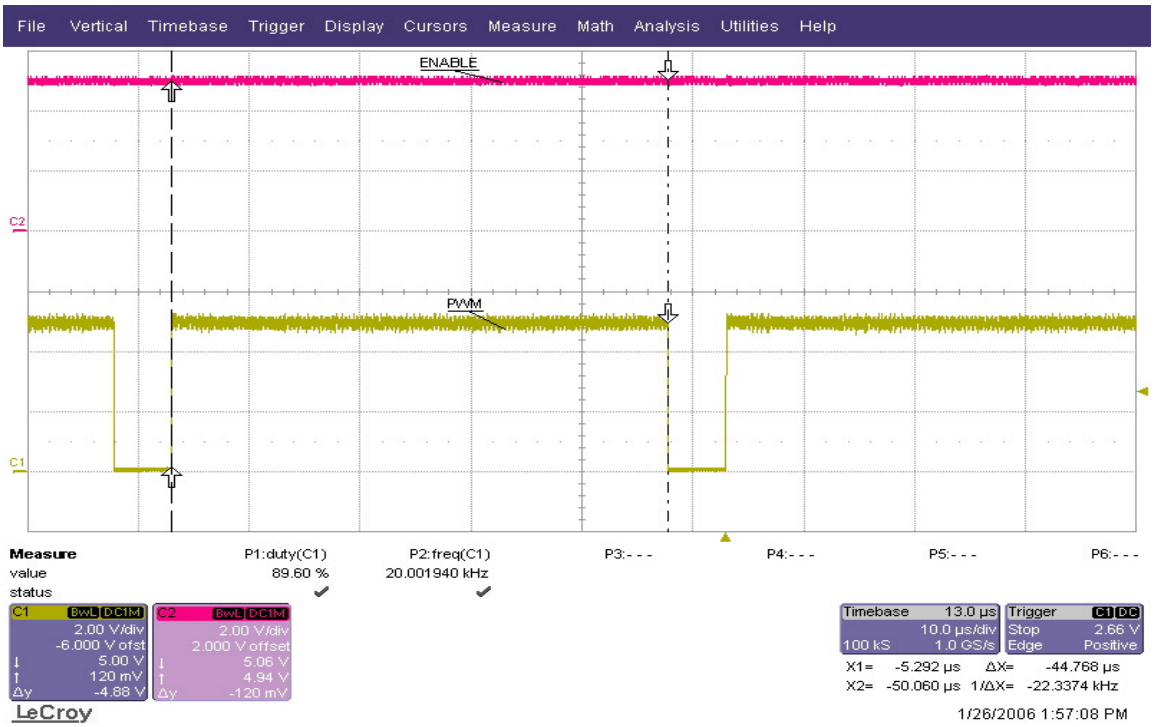

Maximum Duty Cycle

Type Test- 02

Type tests of the RCD Snubber circuits placed on each input section of the converter.

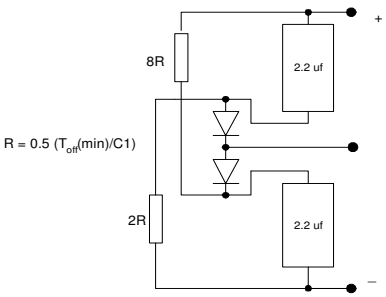

Schematic

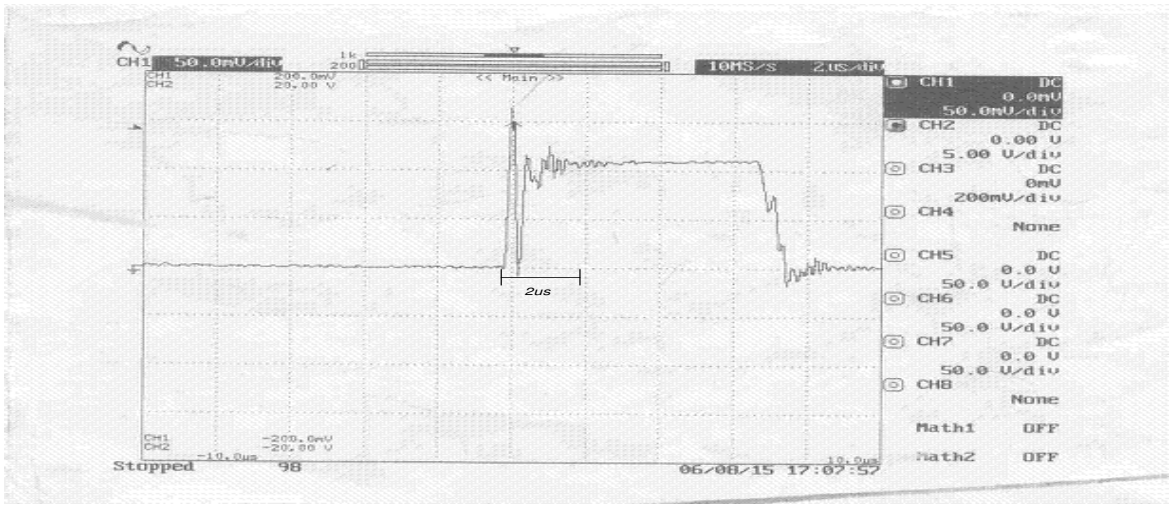

Effect on gate drive without Snubber circuit

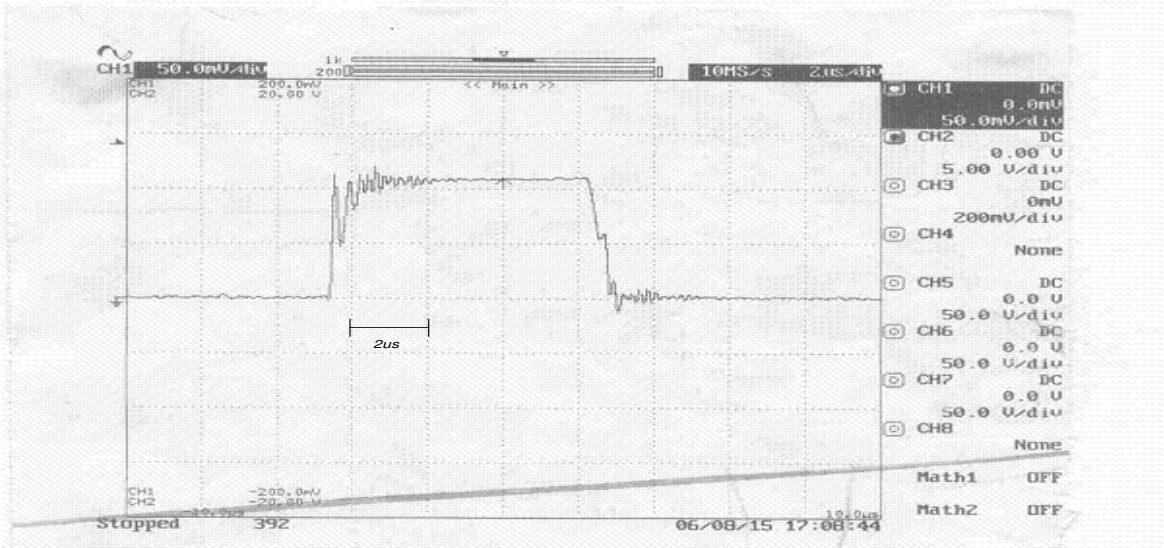

Effect on gate drive with Snubber circuit

Type Test- 03

Type testing of the gate amplifier circuit. The addition of capacitor C_x (2.2uF/25V) is necessary to compensate for the lead inductance between the gate drive circuit and the amplifier.

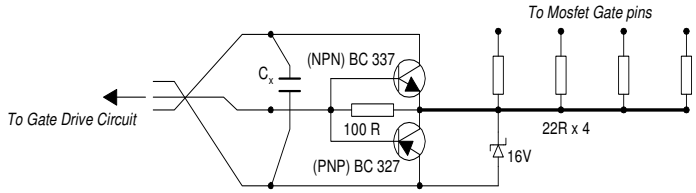

Schematic

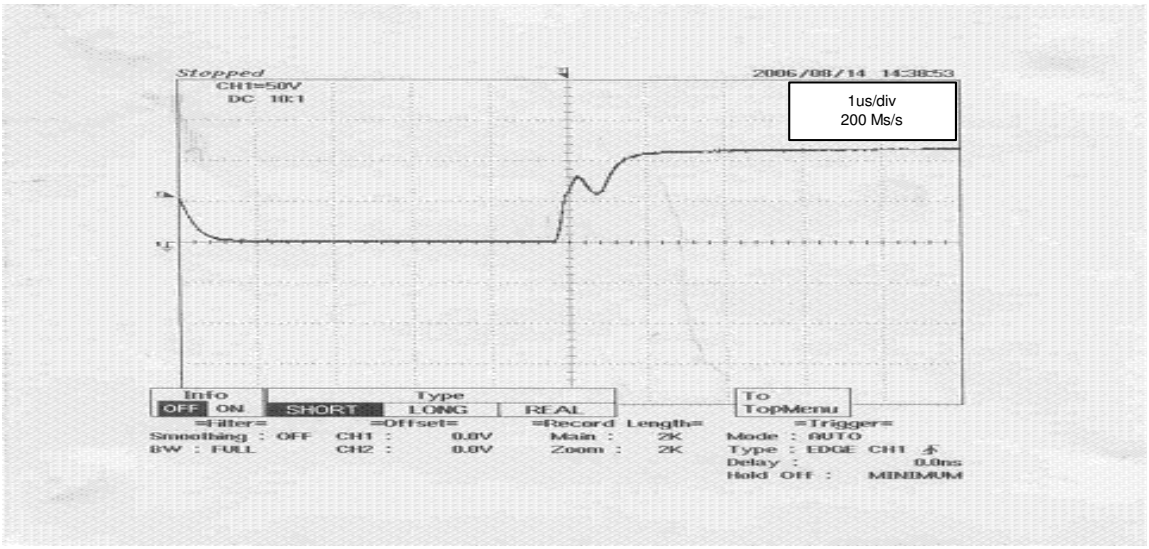

VGS without the inclusion of capacitor C_x

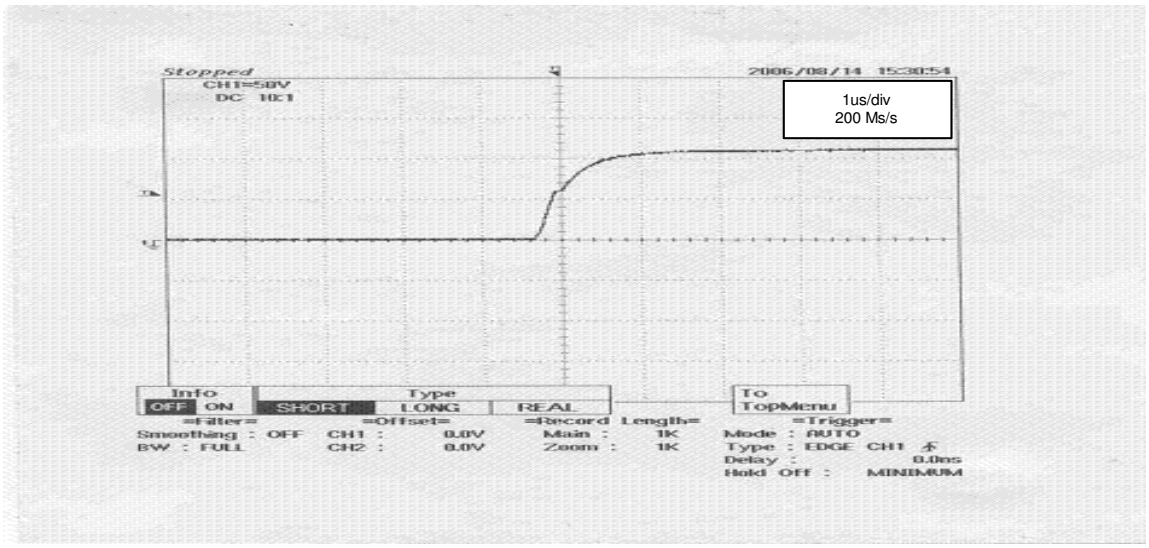

VGS after the addition of capacitor C_x

Power converter section – pre and post assembly

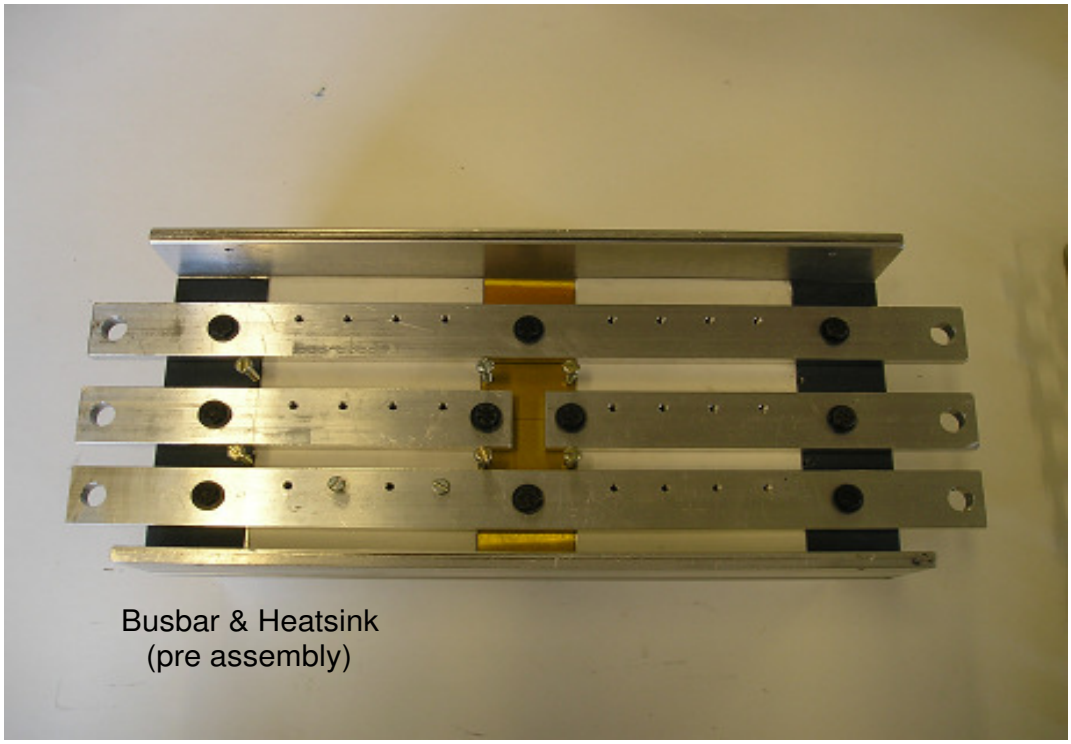

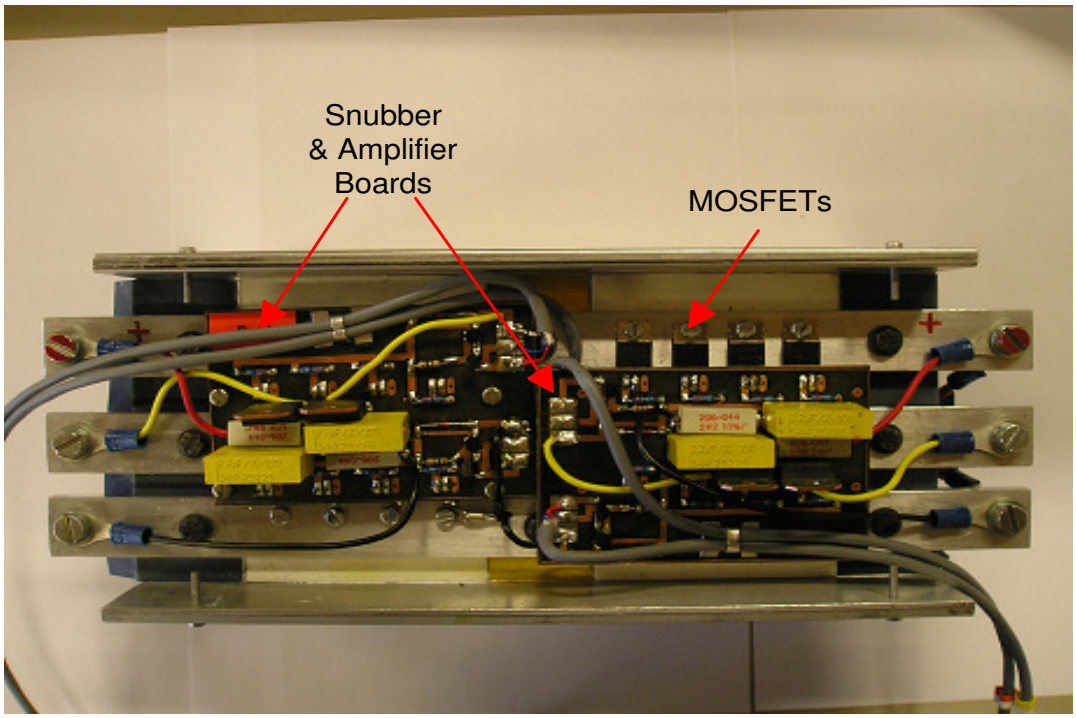

Power, interfacing and sub control board assembly

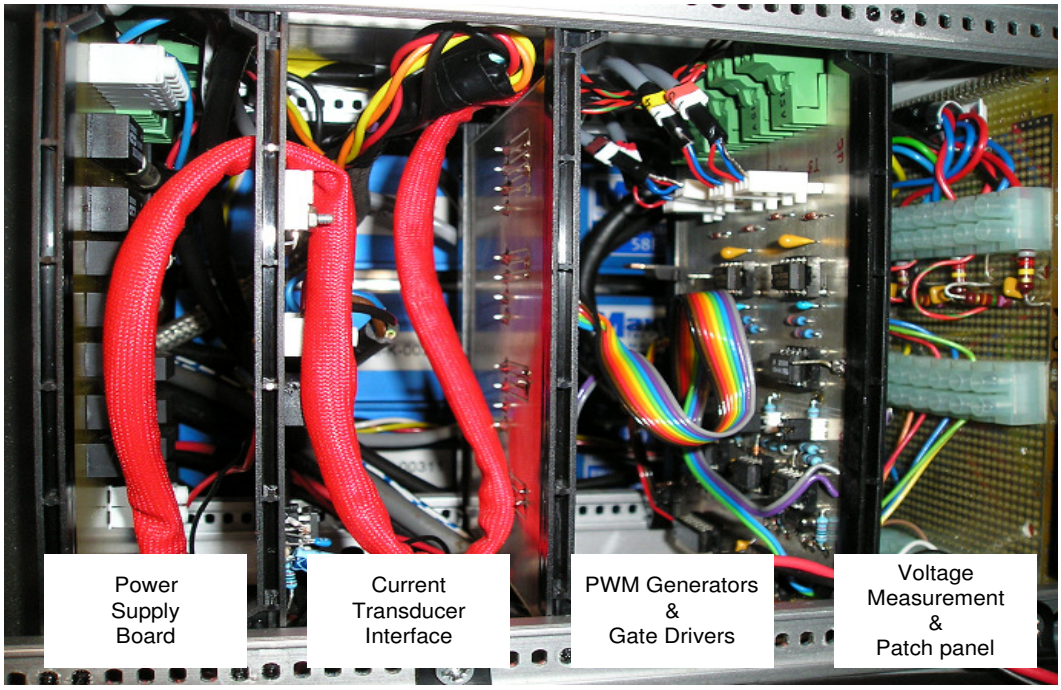

Sub System Layout

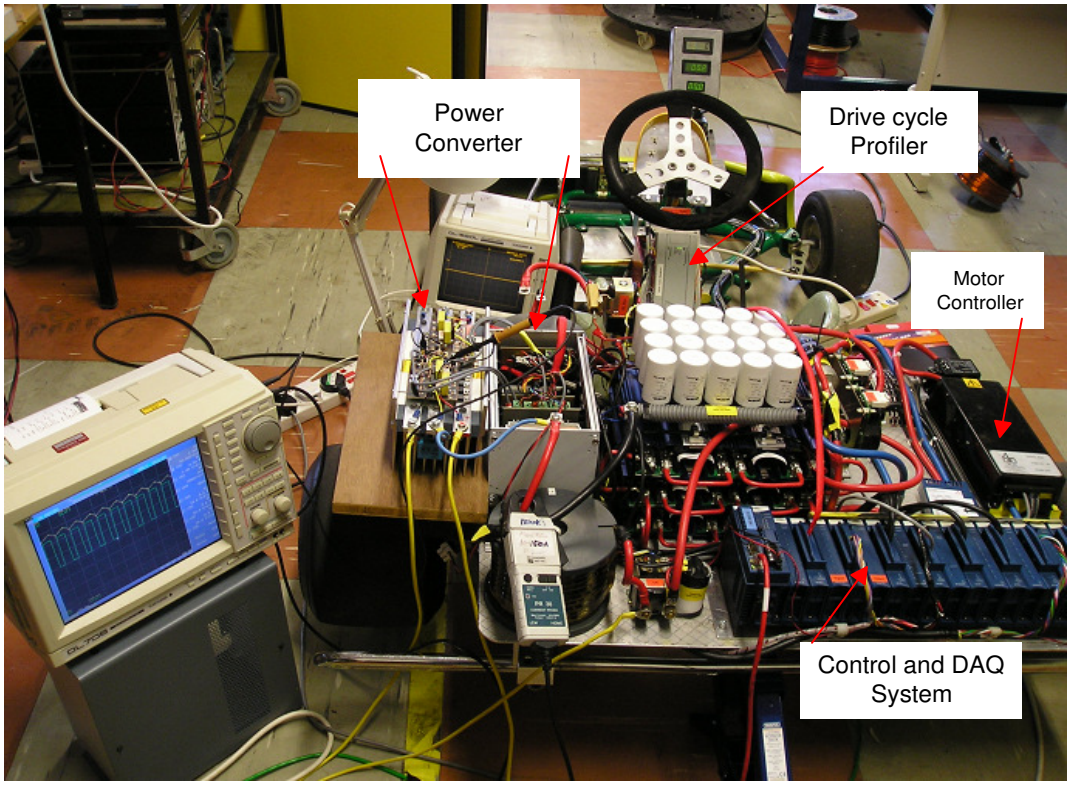

When its all been said and done

All my treasures will mean nothing

Only what I've done for loves reward

Will stand the test of time